Cranfield University

Marco Melega

AUTONOMOUS COLLISION AVOIDANCE FOR UNMANNED AERIAL SYSTEMS

School of Engineering

Department of Engineering Physics
Autonomous and Intelligent Systems Group

Ph.D.Thesis

Supervisors:
Dr. Al Savvaris
Dr. Antonios Tsourdos

2014

Cranfield University

School of Engineering

Department of Engineering Physics
Autonomous and Intelligent Systems Group

Ph.D.Thesis

Marco Melega

AUTONOMOUS COLLISION AVOIDANCE FOR UNMANNED AERIAL SYSTEMS

Supervisors:
Dr. Al Savvaris
Dr. Antonios Tsourdos

2014

This thesis is submitted in partial fulfilment of the requirements for the degree of Ph.D..

Abstract

Unmanned Aerial System (UAS) applications are growing day by day and this will lead *Unmanned Aerial Vehicle (UAV)* in the close future to share the same airspace of manned aircraft.This implies the need for *UAS* to define precise safety standards compatible with operations standards for manned aviation. Among these standards the need for a *Sense And Avoid (S&A)* system to support and, when necessary, substitute the pilot in the detection and avoidance of hazardous situations (e.g. midair collision, controlled flight into terrain, flight path obstacles, and clouds).

This thesis presents the work come out in the development of a *S&A* system taking into account collision risks scenarios with multiple moving and fixed threats. The conflict prediction is based on a straight projection of the threats state in the future. The approximations introduced by this approach have the advantage of high update frequency (1 Hz) of the estimated conflict geometry. This solution allows the algorithm to capture the trajectory changes of the threat or ownship. The resolution manoeuvre evaluation is based on a optimisation approach considering step command applied to the heading and altitude autopilots. The optimisation problem takes into account the *UAV* performances and aims to keep a predefined minimum separation distance between *UAV* and threats during the resolution manouvre. The *Human-Machine Interface (HMI)* of this algorithm is then embedded in a partial *Ground Control Station (GCS)* mock-up with some original concepts for the indication of the flight condition parameters and the indication of the resolution manoeuvre constraints.

Simulations of the *S&A* algorithm in different critical scenarios are moreover included to show the algorithm capabilities. Finally, methodology and results of the tests and interviews with pilots regarding the proposed *GCS* partial layout are covered.

Acknowledgements

The author wishes to express sincere appreciation to Dr. Al Savvaris for the support given in the accomplishment of the work here described. He wants moreover to warmly thanks my family for believing in me and getting behind me in this important part of my life.

List of Contents

List of Figures

List of Tables

Acronyms

ACAD Assured Collision Avoidance Distance

ACAS Airborne Collision Avoidance System

ACS Attitude Control System

ADS-B Automatic Dependent Surveillance-Broadcast

AFSS Automated Flight Service Station

ANS Autonomous Navigation System

ANSD Assured Normal Separation Distance

AoA Angle of Attack

ARD Augmented Reality Display

ASI AirSpeed Indicator

ATC Air Traffic Control

ATV Advanced Tactical Vehicle

BRLOS Broad *RLOS*

BVLOS Beyond *VLOS*

CAA Civil Aviation Authority

CAZ Collision Avoidance Zone

CDTI Cockpit Display on Traffic Information

CDZ Conflict Detection Zone

CFIT Controlled Flight into Terrain

DoF Degree of Freedom

EASA European Aviation Safety Agency

ECAM Electronic Centralised Aircraft Monitor

ECEF Earth Centered Earth Fixed

EGPWS Enhanced Ground Proximity Warning System

EHS EnHanced Surveillance

EICAS Engine-Indicating and Crew-Alerting System

EKF Extended Kalman Filter

ELOS Equivalent Level of Safety

ELS ELementary Surveillance

EO/IR Electro-Optical/InfraRed

ERF Ego-centered Reference Frame

EVS Enhanced Vision System

FAA Federal Aviation Administration

FOV Field Of View

FPCS Flight Path Control System

FSF Flight Safety Foundation

GCNS Ground Control Navigation System

GCS Ground Control Station

GNSS Global Navigation Satellite System

GPS Global Positioning System

GUI Graphical User Interface

HITL Human In The Loop

HMI Human-Machine Interface

HUD Head-Up Display

ICAO International Civil Aviation Authority

IFF Identification Friend or Foe

IFR Instrument Flight Rules

ILS Instrument landing system

IMC Instrument Meteorological Conditions

IMU Inertial Measurement Unit

INS Inertial navigation System

IP Internet Protocol

LCD Liquid-crystal display

LOA Level of Authority

LoS Loss of Separation

LQR Linear-Quadratic Regulator

MAV Micro Air Vehicle

MDT Minimum Detect Time

MRT Minimum Response Time

MSA Minimum Safety Altitude

NASA National Aeronautics and Space Administration

NOAA National Oceanic and Atmospheric Administration

NED North-East-Down Reference Frame

ND Navigation Display

OAT Outside Air Temperature

PACT Pilot Authorisation and Control of Tasks

PCP Proximity Compatibility Principle

PDA Personal Digital Assistant

PF Path Following

PFD Primary Flight Display

PI Proportional-Integral

PUZ Position Uncertainty Zone

RA Resolution Advisory

RLOS Radio *LoS*

RNP Required Navigation Performance

RPV Remotely Piloted Vehicle

RTF Radio Telephone

S&A Sense And Avoid

SAS Stability Augmentation System

SSR Secondary Surveillance Radar

SVS Synthetic Vision System

SZ Safety Zone

TA Traffic Advisory

TAWS Terrain Awareness Warning System

TCAS Traffic alert and Collision Avoidance System

TCS Trim Control System

TTC Time-To-Conflict

UAS Unmanned Aerial System

UAV Unmanned Aerial Vehicle

USAAF US Army Air Forces

VF Visual Field

VFC Visual Field Control

VFI visual Field Information

VFR Visual Flight Rules

VLOS Visual Line Of Sight

VHF Very High Frequency

VMC Visual Meteorological Conditions

VOR *VHF* Omnidirectional Range

VSD Vertical Situation Display

VSI Vertical Speed Indicator

WN Waypoint Navigation

WP W/PWayPoint

WRF World Centered Reference Frame

Nomenclature

d_{D}	required minimum detection range
$d_{\mathrm{h},i}$	horizontal distance between the ownship and the i-th threat after the altitude change imposed by the vertical resolution manoeuvre
$d_{\mathrm{t},i}$	minimum estimated distance between the i-th threat and the ownship during the resolution manoeuvre
$\mathbb{H}_i$	set of the threats altitude
h_{d}	altitude command
$h_{\mathrm{O/S}}$	ownship altitude
$h_{\mathrm{W}\P}$	waypoint altitude
h_i	i-th threat altitude
h_{o}	ownship altitude
h_{s}	safety zone half-height
N_{t}	number of threats
$\vec{P}_i$	threat absolute position
$\vec{P}_{i,r}$	threat relative position
$\vec{P}_o$	ownship absolute position
$\vec{P}_{\mathrm{O/S}}$	ownship geocentric position
$\vec{P}_{\mathrm{W/P}}$	waypoint geocentric position
$\vec{P}_{\mathrm{f},i}$	i-th threat position in the non-rotating reference frame moving with the ownship
$\mathbb{R}(\alpha)$	rotation matrix related to the rotation α in respect with the z-axis
r_{s}	radius of the safety zone
r_{u}	radius of the position uncertainty zone
t	time
t_0	time lag related with the ownship heading angle dynamics estimation
t_{M}	time necessary for the accomplishment of the avoidance manoeuvbre by the system
t_{T}	time necessary for data tansmission
t_{T}	transmission time
$t_{\mathrm{T/C}}$	Time-To-Conflict
$t_{\mathrm{V/T}}$	maximum available veto time
$t_{\mathrm{W/P}}$	elapsed time to next waypoint
t_{c}	vertical manoeuvre rise time
$t_{\max}$	time for which $\frac{\mathrm{d}\,\bar{\psi}_{\mathrm{o}}}{\mathrm{d}\,t}$ has the maximum value
t_{s}	heading angle profile settling time
V_{d}	airspeed command

$\vec{V_i}$	i-th threat airspeed vector
$\vec{V_o}$	ownship airspeed vector
$\vec{V_o}$	ownship airspeed
$V_{\mathrm{O/S}}$	current ownship airspeed
V_{R}	maximum relative velocity between ownship and threat
$\vec{V_r}$	threat relative airspeed vector
$V_{\mathrm{W/P}}$	commanded airspeed on waypoint
V_{z}	ownship vertical speed
$\vec{V}_{\mathrm{f},i}$	i-th threat relative speed in the non-rotating reference frame moving with the ownship
$\vec{V}_{\mathrm{r},i}$	i-th threat speed in the reference frame moving and rotating in the horizontal plane with the ownship
$j\vec{v}\|_h$	horizontal projection modulus of vector $\vec{v}$
$\|\vec{v}\|$	modulus of vector $\vec{v}$
$\|\vec{v}\|_h$	horizontal projection modulus of the vector $\vec{v}$
$\vec{x}_{\mathrm{W/P}}$	waypoint position in the *NED* reference frame centered in the current ownship position
$\alpha(\vec{v})$	azimuth angle of the vector $\vec{v}$
$\alpha(\vec{v})$	azimuth angle of vector $\vec{v}$
$\beta(\vec{v})$	elevation angle of vector $\vec{v}$
γ_o	ownship flight path angle
Δd	horizontal manoeuvre optimisation cost function
$\Delta d_{\mathrm{t},i}$	estimated change in the distance between ownship and intruder after the resolution manoeuvre
ΔH_{res}	range of the altitude step changes suitable to avoid all the potential conflicts
Δh_{res}	altitude step change imposed by the vertical resolution manoeuvre
$\Delta\psi_{\mathrm{f},i}$	estimated change in the ownship heading angle change after the resolution manoeuvre
$\Delta\psi_{\mathrm{o}}$	step command applied to the ownship heading angle
$\Delta\Psi_{\mathrm{res}}$	range of the heading angle step changes suitable to avoid all the potential conflicts
$\Delta\psi_{\mathrm{res}}$	heading angle step change imposed by the horizontal resolution manoeuvre
$\epsilon_{\mathrm{W/P}}$	waypoint threshold considered by path following algorithm
$\lambda_{\mathrm{O/S}}$	ownship longitude
$\lambda_{\mathrm{W/P}}$	waypoint longitude
τ	time constant related with the ownship heading angle dynamics estimation
$\phi_{\mathrm{O/S}}$	ownship latitude
$\phi_{\mathrm{W/P}}$	waypoint latitude
ψ_{d}	heading angle command
ψ_o	ownship heading angle
$\psi_{\mathrm{f},i}$	i-th threat relative heading in the non-rotating reference frame moving with the ownship
$\bar{\psi}_{\mathrm{o}}$	estimated ownship heading angle

CHAPTER 1

Introduction

Initially *Unmanned Aerial System (UAS)* were deployed mainly in surveillance missions, however their use has gradually extended to more complex military missions and nowadays they are finding their ways also in different types of civilian missions. This increase in operations, flight envelope and applications leads to an increasing pressure for *Unmanned Aerial Vehicles (UAVs)* to leave the segregated airspace, in which they were operating currently, and share the same airspace with manned aviation. On the other hand, the loss of sensory cues valuable for situational awareness and flight control caused by the separation between the *UAV* and the operator presents a major challenge for this integration. In fact, this loss causes a degradation in human piloting performance, especially regarding the operator ability to estimate and predict aircraft states in respect to external factors, such as threats, weather, terrain etc. Therefore it is necessary to introduce additional means, usually not used in manned aviation, to provide the operator with complete situational awareness [1].

Among the technologies necessary to meet this requirement, the concept of autonomous *Sense And Avoid (S&A)* system is defined within the proposed regulations, for example in the report *Limitations of the See-and-Avoid Principle* of the *Australian Transport Safety Bureau* [2], as an artificial system equivalent to the human pilot for detecting and avoiding hazardous situations. Those include midair collisions, controlled flight into terrain, flight path obstacles and weather. The development of this system is still an area of open research and involves a number of issues [3]. This thesis presents the results obtained from the design and simulation validations of a *S&A* system concept for *UAS*.

This chapter gives a short introduction regarding *UASs* operations and the challenges related to their deployment in shared airspace. More precisely section 1.1 starts with some general definitions about *UASs*. Section 1.2 continues then with the most interesting examples of their use in current civilian applications. In section 1.3 an overview of recent initiatives regarding *UASs* certification is given. In section 1.4, the human factors issues related with *UAS* operations are introduced. The problem of *UAS* operator situation awareness is analysed in more depth in section 1.5. The requirements defined for safe *UAS* operations are then listed in section 1.6. The presentation of the aims and objectives and the contributions to knowledge of this project is then given in section 1.7. Section 1.8 summarises the methodology used in the work accomplishment. The thesis outline and the list of the publications produced during the work carried out in this project are included in section 1.9 and section 1.10, respectively.

1.1 *UAVs* and *UASs*

According to the publication *CAP 722* issued by the *Civil Aviation Authority* [4] an *UAV* is:

> "An aircraft which is designed to operate with no human pilot on board and which does not carry personnel. Moreover an *UAV*:
>
> - is capable of sustained flight by aerodynamics means;
> - is remotely piloted or automatically flies on a preprogrammed route;
> - is reusable;
> - is not classified as guided weapon or similar one shot device designed for the delivery of munitions."

UAVs are also commonly linked with the word *drone*. Originally this word indicates that male honeybee inside the hive having the only role to mate with the queen and who, differently from worker bees, does not have the task to gather nectar or pollen. As explained in the article *The Flight of 'Drone' From Bees to Planes* of *The Wall Street Journal* [5], the use of this term to indicate *UAVs* is related with the fact that in 1935 U.S. Admiral William H. Standley visited a British demonstration in which a new remote-control aircraft for target practice, identified as *DH 82B Queen Bee*, was exhibited by the *Royal Navy*. When Standley came back to the *US*, he assigned Commander Delmer Fahrney with the task to develop something similar for the Navy. The name *drone* was then used for the aircraft coming from this work in homage to the *Queen Bee* that Standley saw in the *UK*.

It is worth noting here that the expression *Remotely Piloted Vehicle (RPV)* applies to remotely piloted *UAVs* that are. Usually the *UAV* flight operations are controlled and/or monitored by an operator on the ground through the *Ground Control Station (GCS)*. This is defined in [4] as:

> "The *UAV* control station, which is the facility or device from which the *UAV* is controlled and/or monitored for all phases of flight."

Both the *UAV* and the *GCS* are part of a *UAS* defined as follows [4]:

> "An *UAS* comprises individual system elements consisting of the *UAV*, the *GCS* and any other *UAV* system elements necessary to enable flight, such as *communication link* and *launch and recovery elements*. There may be multiple *GCS* or *launch and recovery elements* within a *UAS*."

1.2 Unmanned Aerial System Today

UAS applications are growing day by day thanks to the continuous refinement and price reduction of the technologies used in their development. The new applications of

Table 1.1: list of the suggested civilian applications for *UASs*. Source: [6]

Field	Applications
Agriculture	crops and harvests monitoring and spraying
Air Cargo	short and long distances transport
Border Authorities	ground and maritime borders observation for human and contraband smuggling
Communications	cellular, cable and broadband transmissions support (by providing an antenna in the sky)
Fisheries	fish presence monitoring and illegal fishing activities observation
Forestry	woodlands monitoring for potential fires, poaching
Law Enforcement	traffic and crowds monitoring, pursuit of criminals
Meteorology	weather monitoring and patterns study
Oil Companies	pipelines monitoring and installation
Power Companies	power lines monitoring and installation
Public Authorities	disasters management (e.g. fires, hurricanes, floods, tsunamis, volcanic eruptions, nuclear leaks)
Scientists	remote sensing in heart observation and environmental conditions

UAS have extended from the original military surveillance and monitoring to a large range of civilian uses. Some examples are listed in Table 1.1.

A first attempt in this direction took place in the 2004 when the *National Aeronautics and Space Administration (NASA)*, together with two of the biggest military *UAV* production companies, *Northrop Grumman Corporation* and the *Boeing Company*, started considering the possibility to employ military *UAV* for civilian disasters support and predictive flights, and global warming measurements and surveillance missions [7]. At the same time, *NASA* worked together with the *National Oceanic and Atmospheric Administration (NOAA)* to develop the *RPV Altair*, shown in fig. 1.1. It took-off on the 20$^{\text{th}}$ April 2005 from Palmdale in California [8]. The mission was aimed to fill research and operational data gaps regarding weather, water, climate and ecosystem monitoring and management.

The deployment of the *U.S. Air Force RPV Northrop Grumman RQ-4 Global Hawk* (fig. 1.2) during the rescue mission to Haiti following the 12$^{\text{th}}$ January 2010 earthquake was an example of use of *UAVs* for civilian operations in humanitarian missions. The aircraft provided aerial photographs used for the planning of the relief and recovery missions [9]. Similarly, two *Aerostar UAV*s (fig. 1.3) were loaned from Israel to *Chilean Air Force* to monitor the area struck by the 27$^{\text{th}}$ February 2008 earthquake [10].

The use of *UAV* in civilian applications was also undertaken by other countries around the world: the following are just two examples. In Italy, some research entities are currently developing and testing *UAVs* for the deployment on volcanic activity monitoring missions[1]. At Svalbard, in Norway, *KOLIBRI Geo Services* [12] has already employed *UAVs* (see fig. 1.4) for avalanche and climate research tasks.

[1] An example is reported in the article identified in [13].

Figure 1.1: the *Altair RPV*. Source: [11]

Figure 1.2: the *Northrop Grumman RQ-4 Global Hawk RPV*. Source: [11]

Figure 1.3: the preparation for the flight by technicians of an *Aerostar UAV* on the area struck from the 27th February 2008 earthquake in Chile. Source: [10]

Figure 1.4: an *UAV* used by *KOLIBRI Geo Services* for avalanche and climate research tasks. Source: [12]

1.3 New Rules to Allow *UAVs* to Fly

Most of the current applications *UAS* missions are flown in segregated airspaces. However, as the use of *UASs* is being extended into other areas and applications, it is expected that in the near future *UAVs* will need to operate in non-segregated airspace, that is shared with other aircraft and flying entities. This obviously requires that the *UAV* has to obey the same flight rules of other airspace users in order to avoid dangerous accidents and incidents.

This problem was immediately recognised by both international organisations and research entities. In fact, according to the report of *International Civil Aviation Authority (ICAO)* in reference [14]:

> "On 12 April 2005, the *Air Navigation Commission* requested the *Secretary General* to consult selected States and international organisations with respect to present and foreseen:

- international civilian *UAV* activities in civilian airspace;
- procedures to obviate danger to civilian aircraft posed by *UAVs* operated as *State aircraft*;
- procedures that might be in place for the issuance of *special operating authorisations* for international civilian *UAV* operations."

Before this official act, the *European Commission*, in the scope of the 5^{th} *Framework Program for Research and Technology Development*, had already started a series of projects promoting the utilisation of *UASs* for civilian purposes presented in *Civil UAV Activity within the Framework of European Commission Research* [15]. These background experiences led to the definition by the *European Aviation Safety Agency (EASA)* of the general airworthiness certification requirements for *UAS* reported in the technical report *Policy Statement on Airworthiness Certification of Unmanned Aircraft Systems (UAS)* [16]. Those were developed in more detail by the *UK Civil Aviation Authority (CAA)* in reference [4]. More technical aspects about these requirements, especially regarding the collision avoidance, are further explained in the technical report of *EUROCAE WG-73: Unmanned aircraft systems* [17], and recalled shortly in the next sections.

1.4 *UAS* Human Factors

According to *Design and Evaluation for Situation Awareness Enhancement* [18],

> "A pilot is supported by his visual surveillance of the sky (the See and Avoid principle) prior information (e.g. near-airport behaviours of aircraft), and onboard displays and warnings (e.g. the *Traffic alert and Collision Avoidance System (TCAS)*). A pilot is also constrained by regulations on their reactions, including following *TCAS* instructions, the rules of the air, and may react in unwritten ways designed to increase their safety (e.g. signalling intent by exaggerating turns)."

On the other hand, the *UASs* operations are characterised by greater human factors challenges compared to manned flight, particularly if the aircraft is directly controlled by the operator [1]. The main reason behind this is the fact that the operator and the aircraft are not co-located. This leads to the sensory isolation of the operator from the aircraft due to the loss of sensory cues valuable for flight control. Therefore, the *UASs* operator, rather than using the direct sensory information about the surrounding environment available for manned aviation pilots, receives only the data provided by on-board sensors via datalink [19]. These consist primarily of potentially degraded visual imagery covering a relatively small *Field Of View (FOV)*. Therefore a significant reduction of the human piloting performance is due to difficulty in scanning the visual environment surrounding the vehicle and the delays in control and communications loops.

1.5 Situation Awareness and Equivalent Level of Safety for *UAS*

The issues described in the previous section reduces particularly the *situation awareness* of the *UAS* operator, that is fundamental for proper decision-making and better judgement. According to the paper *Measurement of Situation Awareness in Dynamic Systems* of Mica R. Endsley [20], situation awareness can be defined as "the perception of the elements within a volume of time and space, the comprehension of their meaning, and the projection of their status in the near future". In other words, situation awareness is the mental model of the current and future state of the flight environment, as the same Endsley explains in *Level of Automation Effects on Performance, Situation Awareness and Workload in a Dynamic Control Task* [21]. As stated in [22], the situation awareness is strongly related to the operator workload and performance. Endsley [20] define three levels of situation awareness:

Level 1. **Perception of elements in the environment** that implies the knowledge of the status, attributes and dynamics of relevant elements in the environment;

Level 2. **Comprehension of the current situation** in terms of understanding the significance of those elements in light of one's goals;

Level 3. **Projection of future status** in order to anticipate future actions of the elements in the environment.

Particularly, as stated in [19], the projection time is a fundamental parameter of the situation awareness. In fact, this value should be great enough to provide the pilot with all the necessary information about the future status of the *UAV* without overloading or confusing the operator with an excessive amount of information. A too short prediction time could lead the operator to perform wrong actions when reacting to incoming threats. Therefore the flight plan must be continuously updated during the mission taking into account the following information [23]:

- changes of mission objectives, e.g. new targets and restrictions;
- non-conformance of the current *UAV* state, e.g. position errors or change in *UAV* capabilities due to failures;
- hazardous weather, e.g. clouds or storms in the flight trajectory;
- separation conflicts, e.g. when another manned aircraft or *UAV* exceeds the specified separation criteria;
- integrity conflicts, that are generally related with discrepancies between different information sources.

According to [24], situation awareness is identified as the understanding that the operator has of the:

- current estimation and prediction of:
  - position of *UAV* in respect on the earth surface;

  - position of other aircraft or flying objects;
  - distance from the local ground level;
- weather close to the *UAV*;
- health of the *UAV*, in terms of malfunctions or other deficiencies;
- status of the *UAV*, that include the *UAV*'s operating parameters different from those related to health;
- logic of the *UAV*[2];
- operational threats, like surface-to-air missile batteries;
- *UAV*'s mission
- *UAV*'s progress towards completing the mission
- degree to which the *UAV* can be trusted, in other words knowing the "probability that commands sent to the *UAV* will be correctly executed, and that the data sent back from the *UAV* are accurate" [24]

Further, the *UAS* operator has to be aware from the point of view of the commands in terms of [24]:

Human's commands necessary to direct a *UAV*: the operator needs to specify to the *UAV* the current flight course, altitude and airspeed, which are the sensors and/or weapons to deploy (and when to deploy them), and the degree of autonomy with which to act.

Human-delineated constraints: these may require a modified course of action or command noncompliance: in particular, the operator needs to be aware of any preprogrammed fail-safe modes, such as *return to home*.

On the other hand, to fly safely in a non-segregated airspace, the *UAS* has to operate in compliance with manned aviation regulations and practices [17]. More precisely "the *UAS* operational issues linked to *UAS* specificity must be standardized in a way that makes *UAS* behaviour predictable for other aviation actors such as manned aircraft pilots and Air Traffic Controllers" [17] and guarantee therefore the interoperability between *UAS* operations and manned aircraft operations. From the point of view of the terminology, it is stated that the *UAVs* must operate at an *Equivalent Level of Safety (ELOS)* to manned aviation [25]. From the legal point of view, this implies, in particular, that the *Human In The Loop (HITL)* philosophy used for the *UAV* control gives to the operator the same legal responsibility of the manned aviation pilot for the operational safety of the aircraft. Since both roles are supposed to have the same ultimate authority for operational decisions affecting the aircraft. This approach helps to reduce opposition from the manned aviation activities to *UAV* operations.

[2] As stated in [24], "the operator needs to have a model in his/her mind based on the *UAV*'s internal programming, so that he/she can predict the *UAV*'s responses to various conditions."

1.6 *UAS* Airworthiness

The criteria defined in the previous section lead to requirements in terms of additional systems to be installed on the *UAS* and safety procedures to replace the missing capabilities of the on-board pilot. In chapter 7 of [16] the following airworthiness certification issues have been defined:

Emergency Recovery Capability, in order to mitigate the effects of critical failure conditions (e.g. total loss of command and control link) and to avoid the possibility to create additional hazards to persons or property on the ground.

Command and Control Link, the *UAS* flight crew must be aware of the command and control link signal strength and working state during the whole duration of the flight in order to act effectively in case of any degradation or faults the command and control link might experience.

Human Machine Interface has to display the information about the current operating condition of the *UAV* in a manner that provide the operator with the maximum situation awareness about flight safety and failure conditions and to give indications about the emergency procedures when necessary.

System Safety Assessment has to certify that the risk of uncontrolled crash or critical failures is remote.

***Sense And Avoid* (*S&A*)** is the artificial system employed to substitute the on-board human pilot in the detection and avoidance of hazardous situations (e.g. midair collision, controlled flight into terrain, flight path obstacles, and clouds).

1.7 Contributions to Knowledge of this Project

The aims of this work are the development of a *S&A* algorithm for *UASs* and the definition of a possible approach for integrating its advisories in the *GCS Human-Machine Interface (HMI)*. The algorithm is designed for scenarios including multiple non-cooperative flying threats and ground obstacles. It uses the hypothesis of a threat moving on a final straight trajectory to get a quick evaluation of the advisories about the suggested resolution manoeuvre. These advisories are updated with an high frequency (1 Hz) to track constantly the conflict geometry evolution. The resolution manoeuvres are estimated as step changes in the heading or altitude autopilots, generating a simple horizontal or vertical manoeuvre, respectively. The manoeuvres are evaluated in order to reduce deviation from the original trajectory. More precisely, they are defined as autopilot command step changes. The value of these commands are optimised in order to get respectively a sufficient horizontal and vertical separation between the ownship and all the threats detected during the overall manoeuvre. The separation is evaluated considering a prediction of the future trajectory of ownship and threats. This prediction is derived from an estimation of the performances of the

aircraft based on a fitting model. In the definition of the suggested resolution manoeuvre, the horizontal manoeuvres are preferred to the vertical ones when the required heading variation is inferior to a predefined threshold. The resolution manoeuvres are autonomously performed by the system by enabling the heading or altitude autopilots, when they are disabled, and applying the evaluated step command.

The proposed integration of the *S&A* algorithm is based on an innovative *Primary Flight Display (PFD)* layout to be integrated in the *GCS*. The choice for location and layout of the instruments on display is inspired from the configuration used in manned aviation *PFD*. Among the novelties introduced, it is noticeable the use of a new concept for the original digital displays for the airspeed, altitude, vertical speed and angle of attack indicators integrating red and green bands on their range. These bands identify the allowed or forbidden zones of the flight envelope according to the current condition in terms of conflict risk detected, aerodynamics performances and structural limitations. Some other original solution are the presence on the display of buttons allowing pilot to select the autopilots mode and the choice to integrate the controls for the autopilots settings directly on flight parameters indicators.

The main contributions achieved with this work can therefore be summarised as follows:

1. The developed *S&A* algorithm is based on an optimisation approach. This approach, differently from the other solutions illustrated in section 3.8.2, is able to provide an update of the generated advisories in a very short time step (less than 1 s). The algorithm provides therefore a constant tracking of the evolution of the conflict geometry without the need to use complex models to predict the future trajectory of threats.
2. Another advantage of the proposed algorithm is the ability to take into account unpredictable changes of the detected threats trajectory, if their dynamics is sufficiently slow. In fact, the advisories are continuously updated according to the detected conflict geometry evolution.
3. The proposed approach provides indication on the resolution manoeuvre easy to be implemented by a human operator. In fact, the manoeuvres proposed by the system can be communicated to the *UAS* operator as simple aural "climb", "descent" or "turn" messages similar to those issued by the *TCAS* system.
4. The resolution manoeuvres generated by the algorithm are moreover particularly suitable to be displayed on the conventional altitude, vertical speed and airspeed indicators used both in cockpits and *GCSs*. This supports therefore the *UAS* operator awareness regarding the suggested resolution manoeuvre, and therefore the detected conflict risks, especially when he/she is concentrated on a different task; for example the *UAV*'s control.
5. The developed enhanced *PFD* investigates new and original design possibilities for the conventional flight instruments displayed on the *GCS*. Its design takes into account the different performances and operating environment of *UAVs* in respect with manned aviation. The key driver of the design pro-

cess is the integration of all basic information about the flight condition, the autopilots controls, the advisories about detected threats and suggested avoidance manoeuvre in just one display. The aim is to reduce the *UAS* operator workload caused by the need to search the information on a set of different displays, instead of just one screen, coherently with the guidelines defined in section 4.3.

6. The enhanced *PFD* concept was tested in simulations by pilots flying different mission scenarios. During tests the feedbacks about the layout characteristics improving the display's comfortability for the pilots were collected. A part the suggested design proposal, this work provides therefore useful guidelines for the future works aiming to develop more enhanced displays for *UAS* operators.

1.8 Methodology

The work was accomplished using the following methodology:

step 1: **Review of requirements for *UAV* operations certification** (sections 3.1 to 3.7) including both documents produced by certification autorities, e.g. *CAA*, *EASA* and *EUROCONTROL*, and previous literature in order to define the guidelines for the *S&A* systems development;

step 2: **Review of the previous *S&A* system studies** (sections 3.6 to 3.8) based on the previous literature aiming to identify the main solutions proposed and their advantages and disadvantages;

step 3: **Review of the concepts of *GCS HMI* layout previously developed** (chapter 2) to define issues, guidelines and main solutions proposed;

step 4: **Review of the *GCS* displays trends and guidelines** (chapter 4) based on previous experiences described in literature;

step 5: **Implementation of a simulation environment** (chapter 5) for the *S&A* system's development and testing and including therefore all the elements of its operating scenario (i.e. dynamics of the aircraft involved in the conflict geometry, communications between the aircraft transponders, algorithm computing unit and *HMI*);

step 6: **Development of a *S&A* algorithm architecture** (chapter 6) taking into account the guidelines defined in step 1 and 2;

step 7: **Development of a *GCS* primary display** (chapter 7) for the visualisation of the flight parameters useful for the pilot to monitor the current flight condition and integration of the *S&A* advisories in it and taking into account the guidelines obtained from step 3;

step 8: **Validation of the *S&A* algorithm** (sections 8.1 to 8.4) with simulations of complex test cases in the implemented virtual environment;

step 9: **Validation of the developed *GCS* configuration layout** (sections 8.5 to 8.7) by pilots simulations and interviews.

1.9 Thesis Outline

This section presents the general outline of the next chapters of the thesis. In chapter 2 some general notes about the use of automation in *UAS* are given. It starts with the classifications of different levels of division of responsibility between *UAS* and operator. It goes on then with some considerations about the parameters influenced by this classification. Some notes on the model used for describing the *UAS* operator in the *UAS* operating conditions are moreover illustrated. Finally, the chapter ends with the presentation of the *GCS HMI* concepts proposed in previous literature and *UAS* applications.

Chapter 3 illustrates some general considerations on *S&A* systems. More precisely, it defines performed tasks, functions and operating phases of such a system. The notes on the *Rules of Air* to be considered in the development of such a system and the consequences of the operator involvement in the system are then presented. The previous work both in manned aviation and *UAS* regarding autonomous collision avoidance systems is finally described.

Some notes on the integration of the *S&A* system in the *GCS* are then presented in chapter 4. The chapter starts with some general considerations on requirements in terms of provided information, functions and implementation issues of the *GCS*. The tasks in which the *GCS* supports the operator are then defined, followed by some general guidelines on the *GCS* design. The chapter goes on with the requirements defined by the previous work done on the integration of such a system and the solutions proposed.

The general architecture of the simulation environment integrating the developed *S&A* system is then presented in chapter 5. This chapter includes also the description of the aircraft simulator used and of the *Autonomous Navigation System (ANS)* integrating the *S&A* algorithm developed and the integrated path following algorithm.

Chapter 6 describes the *S&A* algorithm. It includes the definition of its assumptions and of the solutions used for conflict detection, resolution manoeuvre evaluation and autonomous resolution execution.

The *GCS* mock-up used for the pilot tests on the integration of the *S&A* advisories in the *GCS* is then described in chapter 7. More precisely, the *GCS HMI* layout chosen for this project, its components and the layout used for depiction of the information on the displays are defined.

The results of some simulations used to validate the *S&A* algorithm and its integration in the *GCS* are then presented in chapter 8. The criteria used to choose the scenarios presented for the *S&A* algorithm test and the results of the simulations are then described. The description of pilots tests procedure and of feedback obtained is then illustrated. Finally chapter 9 ends with the conclusions drawn by the simulations and the suggested future works.

1.10 Publications

This section lists the papers produced during this research work listed in chronological order. The first prototype of *S&A* algorithm for scenarios considering just a single flying threat was developed in [2]. This solution was further developed in [3] by extending it to multiple threats scenarios and including a *HMI*. The results obtained in these papers were then collected in [1] as a journal paper. An improvement of the algorithm and the application on it of an *Extended Kalman Filter (EKF)* was then proposed in [4]. A further improvement and its extension of the algorithm also to ground obstacles is then presented in [5].

[1] Melega, M., Lazarus, S., Lone, M. and Savvaris, A. [2013], 'Autonomous sense & avoid capabilities based on aircraft performances estimation', *Proceedings of the Institution of Mechanical Engineers, Part G: Journal of Aerospace Engineering* .

[2] Melega, M., Lazarus, S. and Savvaris, A. [2011*a*], Autonomous collision avoidance based on aircraft performances estimation, *in* 'Digital Avionics Systems Conference (DASC), 2011 IEEE/AIAA 30th', pp. 5B4–1–5B4–15.

[3] Melega, M., Lazarus, S. and Savvaris, A. [2011*b*], Sense & avoid algorithm based on aircraft performances estimation, *in* 'CEAS 2011, The international Conference of the European Aerospace societies', pp. 5B4–1–5B4–15.

[4] Melega, M., Lazarus, S., Savvaris, A. and Tsourdos, A. [2013], GPS/INS integration in a s&a algorithm based on aircraft performances estimation, *in* '21st Mediterranean Conference on Control and Automation (MED 2013)'.

[5] Melega, M., Lazarus, S., Savvaris, A. and Tsourdos, A. [2014], 'Multiple threats sense and avoid algorithm for static and dynamic obstacles', *paper under submission* .

CHAPTER 2

Control of *UAVs*

Some of the requirements that were covered in section 1.6 of the previous chapter, and particularly with regards to the *S&A* system, require the use of *automated* and even *autonomous* systems. This chapter provides an introduction to the employment of automation on board of the *UAVs*. It starts with a short summary of the history of *UAS* operations in section 2.1, introducing the approaches used to remotely operate *UAVs* up to now. The discussion continues then in section 2.2 with the classification of modern *UAVs* based on their autonomy and with the definition of some guidelines to be considered in the choice of the level of automation for *UASs*. The model used to describe the role of a human operator on a highly automated *UAV* is then summarised in section 2.3. Finally, in section 2.4 the main solutions proposed in the literature for the operator *GCS HMI* layout are listed and their relationship with the *UAV* level of autonomy is defined. The presentation of the main trends in the solutions used for the *GCS HMI* layout concludes the chapter. The proposed solution used for the development of the *GCS* mock-up used in this thesis is detailed in chapter 7.

2.1 Short History of *UASs* evolution

Remote *UAV* control evolution is strongly related with *UAV*'s technology improvements. This section provides a short summary of *UAS* history. It starts with the first attempts to use unmanned ground, maritime or flying vehicles in military operations on the battlefield in the 19th century till the development of todays complex reconnaissance platforms.

2.1.1 Early Developments

The use of vehicles without an on-board operator historically began in the military field. They offered a distinct advantage; the loss of lives can be avoided in missions in which the risk is extremely high, e.g. bombings or deep aerial observations. The article *Remotely Piloted Aerial Vehicles: An Anthology* [26] states that *UAVs* were first used for war fighting on the 22nd of August 1849. On that date the city of Venice was attacked by the Austrians with unmanned balloons loaded with explosives. Similarly balloons were flown by both Confederate and Union forces in the *US* Civil War in 1862 for reconnaissance and bombing sorties [27].

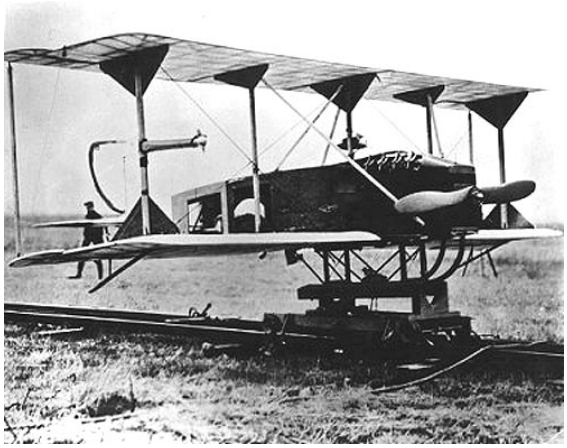

Figure 2.1: the *Hewitt-Sperry Automatic Airplane*. Source: [33]

Figure 2.2: the *Kettering Aerial Torpedo*. Source: [32]

A more refined attempt to implement a remotely piloted vehicle was done by Tesla in 1898 [28]. He operated a radio-controlled motorboat in front of a government representative, demonstrating the potential military application of this technology. Tesla patented a remote-control for unmanned vehicles [29]. He indicated this concept as *teleautomation*, and became one of the founding fathers of the basic principles for today's *UAVs*.

2.1.2 World War I

The use of remotely operated vehicles significantly increased in World War I. On the German side the *FL-7* wire guided motorboat were loaded with explosives and rammed into enemy ships. The drivers were initially placed on towers and then on seaplanes [28]. The wire control method was unwieldy. Therefore in 1916, it was decided to put Tesla's wireless radio-control system into service on the *FL-7*.

Regarding aircraft, the first pilotless model was an aerial target developed in 1916 [30]. At the end of the war it was followed by the *Hewitt-Sperry Automatic Airplane* or *torpedo* (fig. 2.1) [31]. It was a radio-controlled flying bomb integrating the *Elmer Sperrys automatic gyroscopic stabilizer*, used to level out aircraft during flight. This prototype can be considered a first important step in the historical development of *UAVs*. The interest of *US Army* in the project resulted in the successful development of the revolutionary *Kettering Aerial Torpedo* (fig. 2.2). It was nicknamed the *Kettering Bug* and first flew in 1918 [32]. It weighted just 270 kg, including a 135 kg bomb as payload. It was designed to be launched from a trolley with rolling wheels and with detachable wings. Plenty of these aircraft were ordered by the *US* military, however the war ended before they can be used in battle.

Figure 2.3: the *Standard E-1*. Source: [35]

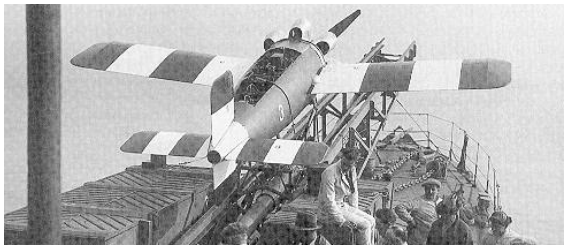

Figure 2.4: the *RAE Larynx*. Source: [36]

Figure 2.5: the *Fairey IIIF* floatplane. Source: [37]

Figure 2.6: the *de Havilland DH.82B Queen Bee*. Source: [38]

2.1.3 Interwar Period

Following World War I, quite a lot of work was done on *UAVs* development [34]. More precisely, three models of the early *US Army* fighter aircraft identified by the name *Standard E-1* (fig. 2.3) were converted as drones. Similarly to the *Kettering Bug*, the *Larynx* (fig. 2.4) was an early cruise missile developed by the *Royal Aircraft Establishment* (*RAE*) from a small monoplane aircraft designed to be launched from a warship and flown by an autopilot. It was tested by the *Royal Navy* between 1927 and 1929.

Following the successes of these first pilotless aircraft, the *UK* and *US* started the development of radio controlled pilotless target aircraft in the 1930s. The *Fairey Queen* radio-controlled target was developed by the British in 1931 starting from the *Fairey IIIF* floatplane (fig. 2.5), building a small batch of three. In 1935, this first experiment was followed by the production of larger numbers of another remotely controlled target, the *de Havilland DH.82B Queen Bee* (fig. 2.6). It was derived from a *de Havilland DH.82 Tiger Moth* biplane trainer. As explained in section 1.2, the term *drone* used for pilotless aircraft is linked with the name of this plane. The *Queen Bee* was also the first *UAV* able to return to the launch point and be reused.

During the same period, the *US Navy* continued developing radio controlled aircraft. The term *drone* was used in 1936 by the head of this research group to indicate radio controlled aerial targets [40]. In 1937 the *Curtiss N2C-2* drone (fig. 2.7) was one

Figure 2.7: the *Curtiss N2C-2*. Source: [36]

Figure 2.8: the *Culver PQ-8*. Source: [39]

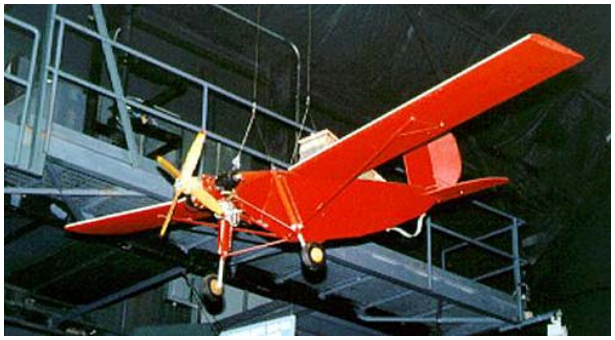

Figure 2.9: the *Radioplane OQ-2*. Source: [26]

of the first outcomes of this research. It was remotely controlled from another aircraft, called the *TG-2* [41].

Another trend in *US Army Air Forces (USAAF)* was to use obsolescent aircraft as anti-aircraft target drones [41]. These *full-sized* targets were identified by the designation *PQ*, in order to be distinguished by the *Attack* aircraft identified by the *A* code. One of the first examples of these target drones was the *Culver PQ-8* target drone (fig. 2.8) a radio-controlled versions of the tidy little *Culver Cadet* two-seat light civil aircraft followed by the improved *Culver PQ-14* derivative of the *PQ-8*.

The first mass-produced *UAV* was the *Radioplane OQ-2* (fig. 2.9), created by the *Radioplane Company* at their southern California-based facility. This company was formed by a team including the british-born actor Reginald Denny. He served in the *Royal Flying Corps* during World War I and developed a fascination with radio-controlled aircraft in the 1930s. During the war, nearly 15,000 of these aircraft were rolled out for the *US Army* and *Navy*, who used the *Radioplanes* as targets for antiaircraft training [28].

2.1.4 World War II

During World War II, on the German side, the first workable cruise missile, the *Fieseler Fi 103*, known as *V1* (fig. 2.10), and the first ballistic missile, the *Aggregat-4 A4*, known as *V2* (fig. 2.12), were developed [28]. The Germans were also the first to deploy aerial drones that were remotely piloted instead of preprogrammed. The *Ruhrstahl SD 1400* or *FX 1400 Fritz X* (fig. 2.11) was a glide bomb with a weight of 3000 pounds and a warhead weighting 700 lb. It was equipped with four small wings, controllable tail

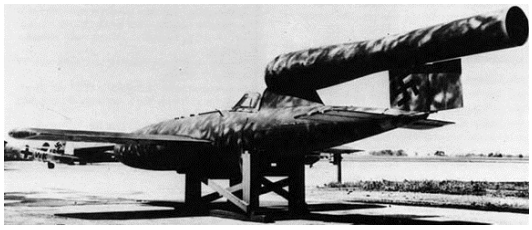

Figure 2.10: the *Fieseler Fi103*. Source: [42]

Figure 2.11: the *Ruhrstahl SD1400*. Source: [26]

Figure 2.12: the *Aggregat-4 A4*. Source: [43]

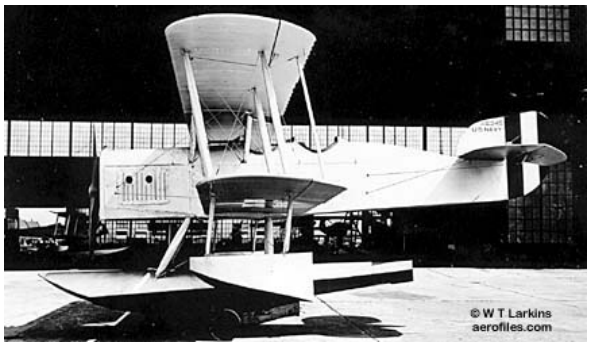

Figure 2.13: the *NAF TG-2*. Source: [44]

surfaces and a rocket motor. The device was dropped from high altitude by a *Dornier Do 217* bomber and then steered by a bombardier via radio link using a joystick.

On the other side of the Atlantic Ocean, the *TG-2* (fig. 2.13) was an assault drone developed in 1941 by *Naval Aircraft Factory* (*NAF*) on which a camera communicating with a television screen was installed [34]. After the first successes of this drone in attack missions, the *Navy Bureau of Aeronautics* proposed a television-assisted remote control assault drone program. This program was based on the use of 162 control planes and 1000 assault drones. However, the risk of revealing the concept to the enemy and allowing development of countermeasures prior to full production left assault drones as an unproven concept in the minds of military planners. Their use was in fact limited to a 4-drone attack on a beached Japanese merchant ship in the Russell Islands at the end of July and the expenditure of 46 drones in the northern Solomon Islands.

The focus on aerial weapons led the *USAAF* and *US Navy* to launch in 1944 *Operations Aphrodite and Anvil*, respectively [28, 45]. These projects were based on the idea to use heavy bombers, including modified *Boeing B-17 Flying Fortress* and *Consolidated B-24 Liberator* bombers. All unnecessary equipment were removed from these aircraft to carry 10 tons of *Torpex*, an explosive more powerful than *TNT*. The plane was controlled in the air by a crew (fig. 2.14), arming the explosives and then bailing

out using parachutes at an altitude of 10 000 ft. The aircraft would then be remotely controlled through radio-controlled actuators from a nearby mother ship, fitted with television receivers and radio control equipment. In this phase, two television cameras mounted in the drone's cockpit (one looking out from the nose of the aircraft, and one aimed at the instruments panel) would have been used to steer the plane into the target. These *UAVs* were meant to attack targets difficult to be approached by manned bombers because of the high level of protection around these targets.

Figure 2.14: a pilot sitting in one of the stripped-down bombers used in Aphrodite project; once airborne the pilot bailed out from the plane. Source: [46]

These programs were however prematurely stopped by a serious accident. One of the converted *B-24* was sent from England by the *US Navy* the 12th of August 1944 to eliminate a suspected German supergun in northern France, supposedly able to hit London, more than 100 miles away. The aircraft was destroyed by a premature detonation of the volatile *Torpex*. The crew, pilot Lieutenant Wilford J. Willy and co-pilot Lieutenant Joseph P. Kennedy Jr., Kennedy's younger brother, was killed in the accident. The *Army* and *Navy* decided therefore to terminate the operations.

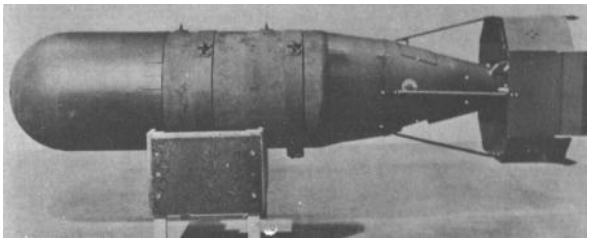

Figure 2.15: the *VB-1 Azons*. Source: [47]

Similarly to the strategy used in the *Operations Aphrodite and Anvil*, since the early 1944, some *B-24*s were used to drop more than 450 *Army*-developed *VB-1 Azons* (fig. 2.15). These were radio remote-control glide bombs with a weight of 1000 lb steered visually by bombardiers, over the Pacific and Burma.

2.1.5 Post-War

Remotely operated weapons, including aircraft, evolved very slowly in the immediate postwar years [28]. Particularly while the *US Army* and the *US Navy* worked on the development of such systems the *US Air Force* did not recognise unmanned aircraft as professional weapons.

Piston engines were normally used for target drones, few pulsejet propulsion drones were built and used as target drones by *US* military in this era [34]. They had the problem of limited speed and range due to the fact that their air intake vanes were self

Figure 2.16: the *McDonnell T2D2-1 Katydid*. Source: [48]

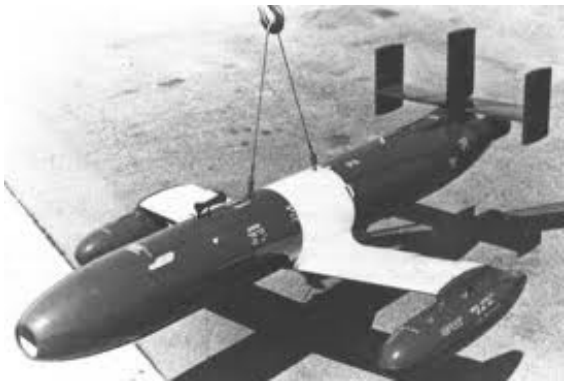

Figure 2.17: the *Curtiss KD2C Skeet*. Source: [49]

destructing. Among these, a pulsejet-powered target, the *T2D2-1 Katydid* (fig. 2.16), later the *KDD-1* and then *KDH-1*, was developed during the war by *McDonnell* for the *US Navy*. This drone was air-launched. Its layout was based on a cigar-shaped fuselage, a straight mid-mounted wing and a V-tail on which the pulsejet engine was placed. Another cigar-shaped drone was the *KD2C Skeet* series (fig. 2.17), a pulsejet-powered target built by *Curtiss*. A small number of these drones were obtained by the Navy after the war. In this configuration the pulsejet was placed inside the fuselage with the intake in the nose. The wings were low-mounted with tip tanks and the tail was a triple-fin.

The *B-17*s were also used as drones in 1946 to collect the radioactive data in *Operation Crossroads* [34]. They were radio-controlled from a jeep during takeoff and landing and from another *B-17* during flight. These planes gathered samples from inside the radioactive cloud on Bikini Atoll. In a test two of them were flown directly above the explosion. Both of them gained height when reached by the shock wave and the lowest was damaged. Similar tests were performed by the *US Navy* with *Grumman F6F Hellcat* drones. A similar use of *B-17* drones was done in *Operation Sandstone* in 1947, and in *Operation Greenhouse* in 1951. In the last operation several *Lockheed P-80 Shooting Star* jets were modified into drones by *Sperry Corporation* and used. Their complexity caused a very high accident rate.

After World War II, *Radioplane* developed another very successful series of piston-powered target drones. They were designed in 1980s as the *Basic Training Target* (*BTT*) family and remained in service for the rest of the 20th century [34]. In this family, the *Northrop Radioplane RP-71 Falconer* (fig. 2.18), designated the *SD-1* by the *US Army*, was the first *US Army* reconnaissance drone [45]. It was produced in 1955 and it was based on a target vehicle design. The Falconer was launched by two rockets and recovered by a parachute. It could transmit crude video recorded by the still film camera with which it was equipped.

Drones were used as decoys at least since the 1950s, when the *Northrop GAM-67 Crossbow* (fig. 2.19) was tested in such a role [34]. The *McDonnell Douglas ADM-20*

Figure 2.18: the *Northrop Radioplane RP-71 Falconer*. Source: [50]

Figure 2.19: the *Northrop GAM-67 Crossbow*. Source: [51]

Figure 2.20: the *McDonnell Douglas ADM-20 Quail*. Source: [52]

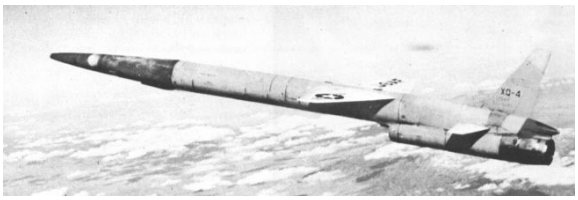

Figure 2.21: the *Northrop Q-4*. Source: [53]

Quail (fig. 2.20) was the first operational decoy drone. They were used on *Boeing B-52 Stratofortress* bombers to make easier the penetration of defended airspace.

Combat aircraft were capable of reaching Mach 2 by the late 1950s. Faster targets became therefore necessary [34]. A turbojet-powered Mach 2 target was designed by *Northrop* in the late 1950s. It was originally designated as the *Q-4* and later as *AQM-35* (fig. 2.21). It had the shape of a slender dart with wedge-shaped stubby wings, swept conventional tail assembly, and a *General Electric J85* turbojet engine.

2.1.6 Vietnam War

UAVs technology sensibly improved its effectiveness during the Vietnam War and their use became extensive [27]. One of the first jet-propelled drones was the *Firebee*, part of the family of drones manufactured by *Ryan Aeronautical Company* (fig. 2.22). The first prototype was created in 1951 and flew for the first time only four years later. It was used primarily by the *US Air Force* for intelligence-gathering missions and radio-communications monitoring.

The *Firebee* was then evolved into the *AQM-34*, an aircraft with roughly the same size of today's *General Atomics RQ-1 Predator UAV*, from which comes the modern concept of unmanned reconnaissance aircraft [45]. The *AQM-34* was used from the mid-1960s to the mid-1970s in tens of thousands of reconnaissance missions at varying altitude levels [27] over North Vietnam, parts of China, and even the Soviet Union in order to reduce the risks related with manned reconnaissance flights. The *Lockheed C-130 Hercules* was used to transport these *UAVs* to the mission target zone. After

Figure 2.22: the family of Teledyne Ryan targets and *RPVs*. Source: [54]

the mission completion they were parachuted for recovery [34].

Figure 2.26: the *D-21* on its *M-21*. Source: [57]

The *M-21* is a variant of the *A-12*, the earliest in the *Blackbird* family developed by *Lockheed*. This aircraft was used to launch the *D-21*, a drone flying at a higher altitude than the *M-21* (fig. 2.26). The *M-21* included a second cockpit for a launch control operator. This concept was developed as part of a project in operation from 1963 until 1968. It was used in four missions between 1969 and 1971 to spy on the Lop Nur nuclear test site. The operations with these aircraft stopped in 1966 after a collision during a launch between a *D-21* drone and the *M-21* mother ship.

Figure 2.23: the *Northrop BQM-74F*. Source: [52]

Figure 2.24: the *BQM-155A* (*RQ-5A*). Source: [55]

Figure 2.25: the *RQ-2A*. Source: [56]

2.1.7 Modern Era

Israel also had interest in developing *UAVs*. More precisely, in the 1970s, Israel started to develop new *UAV* designs based on the modification of existing *UAVs* [45] and continued with as a aggressive development of new *UAV* concepts [27]. Among Israeli *UAVs* operations, particularly ingenious was the mission of a *swarm* of *Northrop BQM-74 Chukar* (fig. 2.23) to the Golan Heights during the Yom Kippur War of October 1973 [45]. The flying fleet was wrongly identified by Syrian military with a massive air attack against its potent *Surface-to-Air Missile* (*SAM*) batteries. Dozens of *SAM*s were therefore launched against the incoming aircraft, causing the depletion of the air defenses. In the following years, Israel became a reference in the world for specific types of *UAVs*, particularly in the 1980s, when lighter and smaller *UAVs* were developed. Among these, the *IAI RQ-5 Hunter* (fig. 2.24) and *AAI RQ-2 Pioneer* (fig. 2.25) *UAVs* extensively used by *US* in the 1991 Gulf War were actually derived from Israeli systems [27].

Israel was also responsible of a radical change of attitude towards *UAVs* [34]. They were considered too unreliable and expensive to be used as weapons, but in 1982 *Israeli Air Force* won against the *Syrian Air Force* by using a strategy based on the coordinated use of *UAVs* alongside manned aircraft. This strategy allowed the quick destruction of dozens of Syrian aircraft with minimal losses. The drones were used in these operations as electronic decoys, electronic jammers as well as for real-time video reconnaissance.

The first flight of the *General Atomics RQ-1 Predator* (fig. 2.27), one of the best-known modern *UAV*, took place in 1994 [45]. This drone comes from a design by Abraham Karem, a former engineering officer for the *Israeli Air Force*. The aircraft was developed for *long loiter* reconnaissance work and is considered by the military

Figure 2.27: the *RQ-1L*. Source: [58]

Figure 2.28: the *RQ-4A*. Source: [59]

Figure 2.29: the *AeroVironment Wasp*: an example of *MAV*. Source: [60]

Figure 2.30: the *AeroVironment RQ-11A*: an example of man-portable *UAV*. Source: [61]

as a medium altitude *UAV*. The *Predator* was used in military operations in the Balkans in 1995 and Iraq in 1996. It showed particularly its effectiveness in *Operation Iraqi Freedom* and in Afghanistan [34]. The original design of the *RQ-1* evolved into different variants that are currently used to patrol the US-Mexico border, collect air samples for scientific research, and destroy ground military targets [45].

Another well-known drone is the *Northrop Grumman RQ-4 Global Hawk*, a high-altitude, long endurance aircraft with impressive performance and sensor capabilities [45]. It was developed from a 1995 request of the *Defense Advanced Research Projects Agency* (*DARPA*). It is able to fly for more than 32 hours at a stretch and loiter at altitudes as high as 65 000 ft. The sensors with which it is equipped are able to see through clouds, dense fog, haze, and dust storms. The data transmission rate is very quick and can provide operators with very high resolution imagery of wide swaths of the ground below.

Another interesting application of *UAVs* in the field are miniature *UAVs*, designed to be carried by infantrymen in the battlefield [34]. They range from *Micro Air Vehicle (MAV)* (e.g., fig. 2.29), which can be launched directly by an infantryman, to man-portable *UAVs* (e.g., fig. 2.30), that can be operated like an infantry anti-aircraft missile.

2.2 *UAV* Level of Autonomy

It was widely demonstrated that the automation of some basic flight and mission tasks on manned aircraft and *UAS* can lead to a reduction of the operator's workload and better piloting performance [23]. The division of responsibility of a task and the support of that task between *UAV* and operator in terms of *Pilot Authorisation and Control of Tasks (PACT)* levels, [18] use the following classification:

Level 0: the operator has full control of the *UAS*;

Level 1: the operator has full control of the *UAS*, but can request advice on actions to the *UAS*;

Level 2: the operator has control of the *UAS*, with advice on actions provided by the *UAS*;

Level 3: the operator controls the *UAS*, and accepts or rejects *UAS*'s proposed actions;

Level 4: *UAS* has full control of each of its actions unless it is revoked by the operator;

Level 5: *UAS* has full control of its actions.

It should be noted that this classification is slightly different in some interpretations. More precisely the levels 4 and 5 may be subdivided to include the idea of operator's approval/veto and variable levels of *UAV* action reporting. These task levels vary according to the environment and the urgency of a task. Regarding flight control mode, reference [4] defines the *UAVs flight control mode* classification as tabulated in Table 2.1.

Generally speaking, reference [23] identifies the following aspects related with the definition of level of automation of a function on a *UAS*:

Time available for replanning: if the function involve time-critical events, the time available might not be enough in order to let the operator understand the problem and take the appropriate decision.

Complexity of the conflict or problem: the reasoning capability of the human mind, based on a wider knowledge than the *UAS*, is necessary for higher level decisions and decisions in unfamiliar situations.

Consequences of a wrong decision: this is closely related to the aspect of liability and responsibility.

Dilemma between controlling and monitoring: it is clear that the operator might become overloaded and fatigued if he/she takes care of all the controlling tasks. On the other hand, if the task of the operator is just monitoring the progress of an automatic system, he/she might become bored and less attentive.

From a general point of view, the main disadvantage of the *HITL* control is the fact that the human behaviour is variable and this produce errors [62]. Moreover, humans are creative and might decide to change their responses, choosing non optimal options.

Table 2.1: *UASs* flight control modes class ratings. Source: Adapted by author from [4, section 4.8].

Control type	Class	Class Name	Description	Examples
On-Board Pilot	0	Manned Aircraft	This is the reference class, that is the same of the manned aircraft.	Airbus A320, EH101
Remote Operator	1	Direct Command	The operator have the direct control on the conventional controls (throttle, ailerons,elevator,rudder).	Jindivik, RMA
	2	Attitude Command	The aircraft is equipped with *SAS*[1] and therefore the operator controls the attitude angles rates.	Mirach
	3	Flight Parameters Command	The *ACS*[2] gives the operator the possibility to set the desired attitude angles.	Global Hawk
Programmed Flight[3]	4	Stored Flight Profile Command	The operator simply set the desired flight profile in the *Navigation, Guidance and Control System* of the aircraft.	BGM-109
	5	Sensor Command	The aircraft route is defined by real-time sensors acquisitions.	
	6	Autonomous Command	The aircraft is completely autonomous.	AI-UAV

[1] *Stability Augmentation Systems*
[2] *Attitude Control Systems*
[3] According to certification criteria, Classes 4, 5 and 6 require command override intervention capability.

On the other hand, on aircraft with preprogrammed fight routes, the high automation of the system prevents the remote operator from managing directly the short-term dynamics of the aircraft [62]. Therefore, he loses awareness of potential imminent dangers. This makes difficult for him/her to produce the corrective actions that are usually performed by the on-board pilot. Moreover, humans have the advantage of being more flexible. More specifically in this context paper Tadema *et al.* [63] identifies the following key points:

- they integrate perceived data with other information to resolve ambiguities and detect contradictions,
- they are able to recognise and exploit advantageous opportunities,
- they adapt more easily to changing environment,
- they take more appropriate decisions than computers when sudden changes happen.

Therefore it could be worthy to include the operator in the control loop by allowing him/her to make strategic decisions on-the-fly, when the effectiveness of predetermined flight plans is reduced as highlighted in *Semi-Autonomous Human-UAV Interfaces for Fixed-Wing Mini-UAVs* [64].

For these reasons, when a fully autonomous control mode is implemented, the following functions must be implemented [62]:

Operator override capability: operator has to be provided with the authority to override the automation when deemed necessary.

Autonomous mode back-up: high-level automation of decision selection and action is justified in highly time-critical situations in which the time is insufficient for a human operator to respond and take appropriate action. Moreover, the ability of the human operators to identify appropriate solutions diminishes when the operator situation awareness is reduced. On the other hand, a computer is able to determine a logic-based appropriate action much faster than a human operator.

2.3 Supervisory Controller

As the autonomy of the *UAV* increases, the operator role involves higher levels of multitasking [23]. More precisely, as vehicle autonomy increases, the role of the operator changes from that of a *manual controller*, using stick and rudder inputs, i.e. class 1 in Table 2.1, to a *supervisory controller*, that provides higher level system inputs such as navigation waypoints and target speeds, i.e. class 4 in Table 2.1, while the automated systems determine the means to achieve the performances required by the inputs.

A *supervisory controller* is defined as that type of operator who is responsible for coordinating human and machine tasks and goals. A successful coordination requires the operator to have a correct understanding of the tasks and goals of the automated

systems and the prediction of how the system will react to environmental perturbations as well as to operator inputs. It is therefore necessary to minimise breakdowns in human-machine coordination in order to make it easier for the operator to understand and predict vehicle behaviour.

The presence of an outer loop control, due to the specification of higher level goals (e.g. navigation waypoints), produces the following two consequences generally related with supervisory control systems. The first one is the time lag between operator input and system response increases. That's why predictive displays are generally recommended in order to overcome the effects of this time delay. Operator awareness of *UAS* performance weakens, i.e. he is taken *out of the loop*. This imply that it is important to ensure a clear view of automation behaviour to the operator in order to support operator mental models and system awareness.

Reference [65] define the supervisory control model sketched in fig. 2.31, in which the system commands are provided by the operator to the *GCS*. In this case, the *GCS* typically consists of a set of displays showing information about the system status, including vehicle attitude, altitude, navigation status, and a set of controls to allow the operator to enter navigation waypoints, airspeed and altitude. The function of the *GCS* is to translate higher level commands into sets of inputs to the actuators producing the desired system performance. *UAS* operator is then in charge of five basic human roles. These are *planning*, *teaching*, *monitoring*, *intervening* and *learning*.

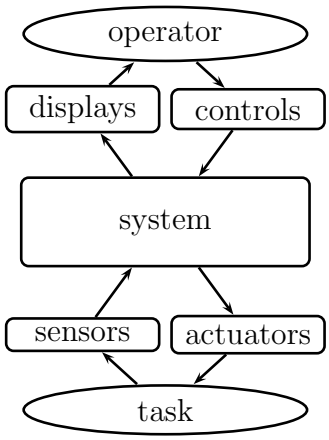

Figure 2.31: flowchart of the supervisory control model. Source: Adapted from [65]

In the planning role, the operator defines the way to implement a desired change in vehicle performance in order to accomplish the vehicle routing alteration. It involves, for example:

- choice of the control variables to manipulate, e.g. to change the vehicle heading or to insert new waypoints,
- development of criteria to assess the system actions, e.g. to decide which are the displays that provide the best feedback on the desired action,
- determination of constraints to be considered for the automated systems activities management, e.g. to define if the new routing is compatible with onboard navigational capabilities such as *Required Navigation Performance (RNP)*.

This role is the base for the subsequent roles including *UAV* activities programming and monitoring of the system behaviour.

When the planning has been defined, the operator must *teach* the *UAV* control systems by providing the *UAS* with the appropriate instructions. The fact that the operator is providing high-level instructions to the system is important because excessively high automation levels could lead to unpredictable or critical situations, in

which automated systems do more than expected. In this conditions, the coupling between control systems could, in fact, lead to unintended consequences[1]. This situations is particularly difficult to be detected. Therefore all projected changes resulting from operator inputs must be highlighted on the *GCS* displays.

After providing the inputs to the control systems, the operator has to monitor the system performance to ensure that it evolves as desired. This role includes those activities necessary to adjust the system performances in response to small deviations (trimming) and to fault detections.

If undesired system performances are detected, an operator intervention is necessary (i.e. the level 4 *PACT* defined in the previous section). Please note that in some highly autonomous *UAV* no possibility is left to the operator to assume manual control[2]. In this case an *intelligent automated detection/intervention system* might be necessary. On the other hand, when the operator have the ability to intervene in system behavior, the operator intervention has to be simplified by the provision of quick and low workload method to re-instruct/re-program the automated systems.

Finally, the operator can learn lessons based on the given plan, system inputs, system behaviour, and interventions (if any) that could be useful for the system control in future situations. To get the most effective learning, the *GCS* must "support an accurate mental model of the system and allow the operator to understand why the system behaved as it did" [65].

2.4 *GCS* Human-Machine Interface Design

The *GCS* architecture depends on the flight control mode of the *UAS*, as per the classification illustrated in section 2.2. The possible solutions range from concepts based on the conventional stick, rudder and throttle for class 1 to more innovative fully automated flight control interfaces for class 4 to 6 [19].

The primary functions performed by *UAS* operators in the *GCS* during a mission are the same as those performed by the flight crew of manned aircraft during a flight. They are classified as follows [66]:

flight management is the primary control and the navigation of the aircraft;

communications management including both communications with air traffic control and with other crew members during the flight;

systems management deals with the management and interaction of *UAS* operator with functions performed by the system: this implies a *GCS* designed to provide the operators all the information regarding system status and potential system failures [19];

[1] E.g. the changes to the horizontal dynamics in conventional aircraft can cause unintended consequences in vertical dynamics

[2] E.g. Global Hawk only provides a limited manual control capability

tasks management is the function that manages all the tasks and the associated resources necessary to mission accomplishment: this is both a supervisory and a supporting function to the previous three functions and involves monitoring, scheduling, and allocating the tasks and their resources.

The chosen solution used for the *GCS* have to be a trade-off between precision of the inputs, intuition and speed of response, in order to get an in-the-loop feel supporting efficient task completion [64]. From this point of view it is fundamental to take into account in design the human factors guidelines already defined for manned aviation [19].

The paper *Vehicle teleoperation interfaces* [67] classifies the *HMI* for vehicle teleoperation proposed in literature into four categories:

direct control interfaces include all traditional systems based on hand-controllers and video feedback;

multimodal/multisensory interfaces based on multiple control modes or the use of fused data displays (e.g. virtual reality);

supervisory control interfaces are designed for high-level command generation and monitoring;

novel interfaces use unconventional input methods or are intended for unusual applications.

A more detailed description about these solutions is presented in the following sections.

2.5 Direct Control Interfaces

Direct control interfaces are the most common control method for vehicle teleoperation. An example about their application in *UAS* is given in fig. 2.32, that shows the *GCS* of the *MQ-1 Predator*. In this type of *HMI*, the *UAV* is controlled directly via hand-controllers (e.g. joysticks, *TrackPoint*™ controllers [64]), and visually supervised by the operator through vehicle mounted cameras. The operator is therefore part of the control loop and he/she depends on real-time video for external environment perception. As explained in [67], this kind of control is often referred to as *inside-out* piloting because the operator feels like being inside the vehicle.

It is particularly suitable when real-time human decision making or control is required and the environment can support high-bandwidth, low latency communications. Outside these conditions, direct interfaces could still be used despite a sub-optimal performance. In particular, this kind of control is difficult and not accurate when there is any kind of delay related with transmission or other causes.

In order to make the training easier, some of the *GCS* based on this concept are designed with a layout and controls similar to that of some aircraft cockpits. In some other cases designers attempt to improve operator performance with the use of a kind of telepresence via head-mounted video, binaural sound, and physical cues.

Figure 2.32: the *MQ-1 Predator GCS*: an example of direct control. Source: [68]

Experimental work on these type of systems [64] have shown that the main advantage of this type of *HMI* is the fact that they allow the operator to have a quick and easy understanding of the physical motion of aircraft attitude. They are therefore characterised by fastest response times. Moreover, these kind of *HMIs* "do not require a focal shift between the onboard camera feed of the *UAV* and the *HMI* itself" [64].

However, this type of *HMI* requires physical components with sizes and power requirements that could make them detrimental or even prohibitive in some circumstances [64]. More precisely, for large vehicle the *UAV* control stations built as a part of system have enough space and a suitable power supply for a physical interface allowing fast and easy control. On the other hand, wilderness search-and-rescue applications based on small vehicle such as *Advanced Tactical Vehicle (ATV)* could not allow a location suitable to host this kind of *HMI*. Moreover, previous research demonstrated that direct interfaces can produce in some istances an inaccurate attitude judgement and inadequate situation awareness, and failure to detect obstacles [67].

2.6 Multimodal/Multisensory Interface

It could be difficult for the operator to have an accurate perception of remote environment and to make quick control decisions, when the *UAV* is in a complex and quickly changing situation, as stated previously in [67]. In these conditions *multi-*

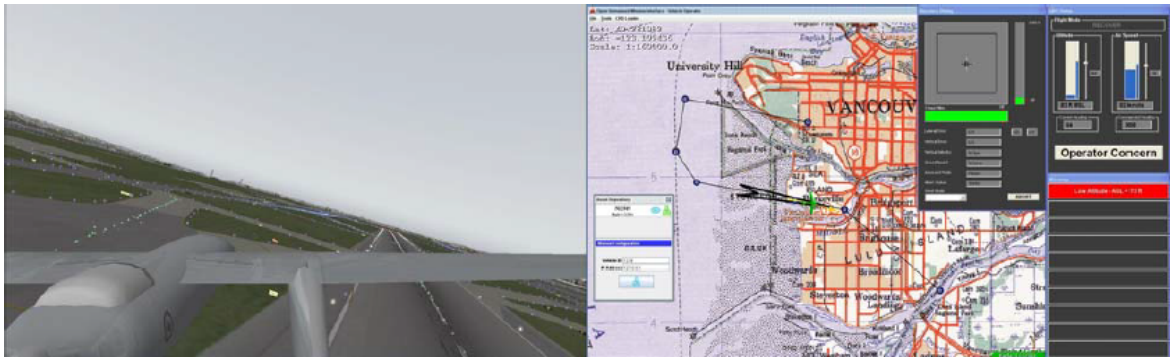

Figure 2.33: example of multimodal interface, the *OmniSense* Sensor Display and Map Display. Source: [69]

modal/multisensory interfaces are more suitable because of their effectiveness in the command generation and of the rich information feedback. This kind of *HMIs* provides a variety of control modes (individual actuator, coordinated motion etc.) and displays (text, visual etc.). They are particularly suitable for applications which demand context specific actions[3].

Multisensory displays provide a single integrated view, also called virtual reality (e.g. in fig. 2.33), derived from the information acquired from several sensors or data sources. Moreover, they offer the advantages of improved situation awareness, facilitate depth judgement and speed decision making [67]. In fact, virtual reality provides to the *UAS* operator with an external point of view that make it possible for him/her to control the aircraft from the *outside*.

2.7 Supervisory Control Interfaces

The name of this type of control, shown in fig. 2.34, means that this type of control acts similarly to a supervisor interacting with subordinates [67]. The mission to be accomplished is divided by the operator in a sequence of subtasks which are executed by the *UAS*. Therefore the *UAS* must have a degree of autonomy to be able to safely accomplish the tasks required by the operator. This kind of *HMI* are designed for high-level command generation, monitoring and diagnosis and are ideal for applications involving low-bandwidth or large delay communications channels. They are currently few in number, but they are expected to grow with the increase of autonomy in *UAS* applications. Supervisory control interfaces simplify navigation despite they still involve many design challenges including display layout, management of human-system interaction and simplification of sharing/trading of control.[4]

[3] i.e. "when it is necessary to select control modes and displays based on situational requirements" [67]

[4] In fact, as stated in [67], "supervisory control interfaces must provide mechanisms for the operator and the robot to exchange information at different levels of detail or abstraction. This is particularly

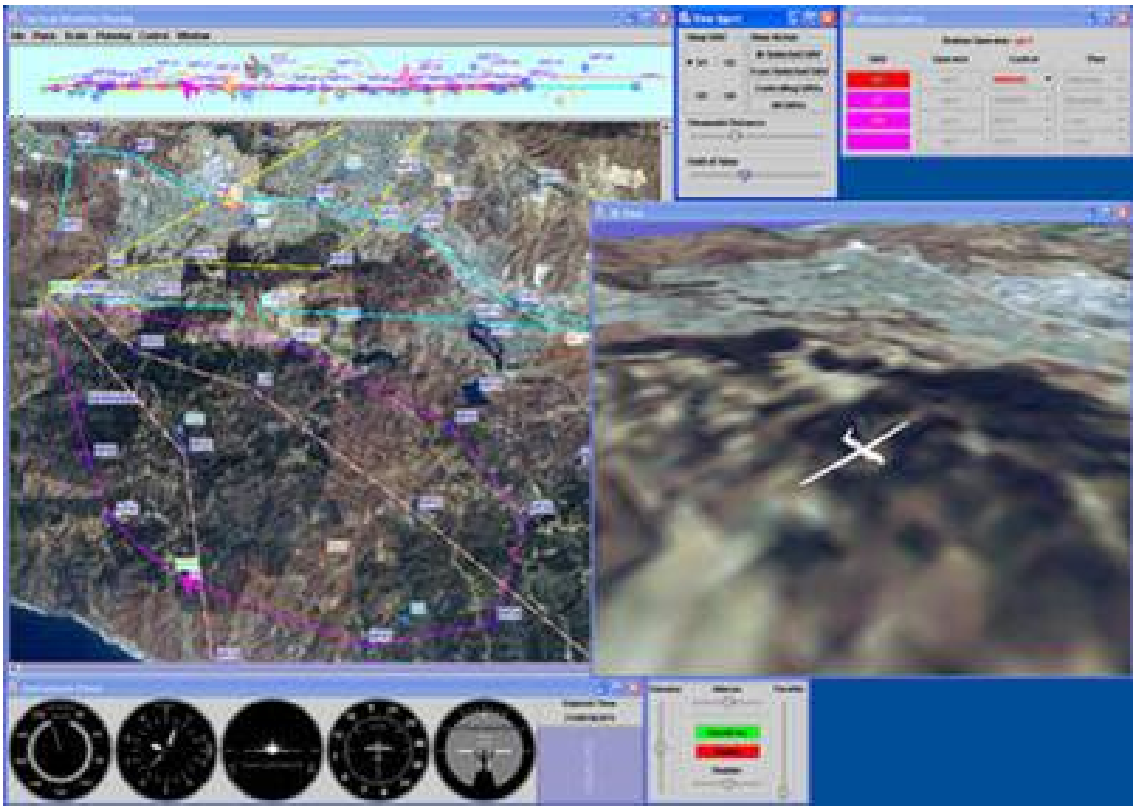

Figure 2.34: an example of supervisory control interface for *UAV*. Source: [70]

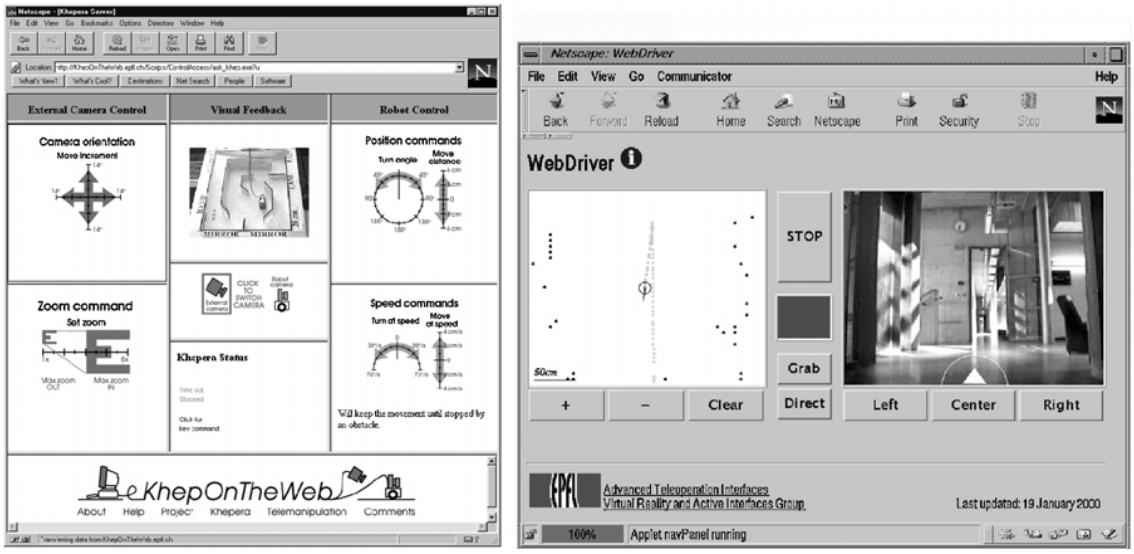

Figure 2.35: web-based interface for remote driving developed from the *Swiss Federal Institute of Technology* in Lausanne). Source: [67]

2.8 Novel Interfaces

Despite the name, this kind of vehicle teleoperation interfaces are now commonplace. Their novelty is sometimes based on unconventional input methods.

An example of *novel interface* are the *Web-based interfaces* described in [67], e.g. fig. 2.35, that are *World Wide Web* based application. This kind of *HMIs* are advantageous from different points of view. Firstly, they can be accessed world-wide. They are moreover highly cost-effective. Finally they requires little (or no) operator training. On the other hand, Web-based teleoperation have different issues from more traditional systems, for example the variable communication bandwidth of the Internet.

Another interesting example is given in [64], where the attitude of a small model airplane (see fig. 2.36) used as a *physical icon* of the real *UAV* is converted by a computer into roll and pitch commands for the real *UAV*. This kind of *HMI* is called *physical icon interface*.

The following sections present in detail some very interesting and quite complete *HMI* based respectively on touch-screens, *Personal Digital Assistant (PDA)* and speech commands.

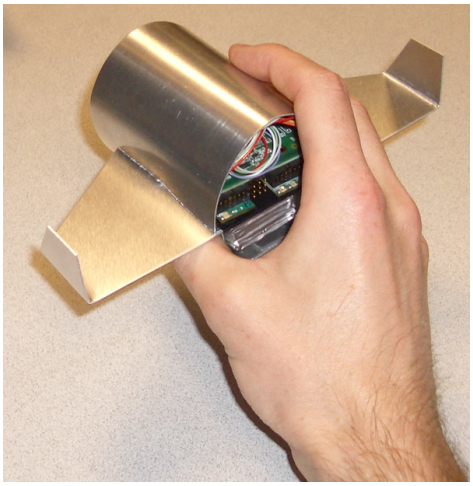

Figure 2.36: physical icon interface. Source: [70]

2.8.1 Soft Controls

In manned aviation the current trend aims to design the displays for aircraft subsystems on multi-functional display screens and controls (switches, knobs etc.) which are mounted on panels in front of the two pilots. The next step, where some of the research projects development is currently in progress, will focus on replacing hardware controls with reconfigurable touch-screen based controls on the display. This type of controls are called in *soft controls* [71].

However, despite the interest in the topic, many issues regarding the design of these displays and control are still left unanswered and makes it difficult to implement them in a cockpit environment. Some of these issues include:

1. ease of using *soft* controls as compared to *hard* controls,
2. absence of tactile and aural feedback,
3. loss of dedicated, *geographical*, location of controls,
4. limited display *real estate*,

---

important when the robot has problems performing a task and the operator needs to ascertain what has happened".

5. *navigation* between displays during configuration tasks and emergency situations,
6. accuracy in mapping between the display schematic and sub-system components,
7. response time and display update rate of complex systems,
8. reliability of *soft* controls[5] for high-risk domains, and
9. several environmental effects (e.g. vibration, glare).

More precisely, it was identified that it is necessary to redesign the input modality of the *HMI* taking into account the following guidelines. The touch logic for activating the touch areas must be improved. An effective design must be based on a *lift-off* touch logic. In fact, in this logic the action related with soft control selection is executed only after the finger lifted off from the soft control touch area. This solution make possible for the user to select the control even if he fails to hit it on initial contact by simply dragging his/her finger into the touchable area. In the same way, if the control is accidentally touched, the user can avoid the selection by simply dragging his/her finger out. This is an important feature, particularly when the control has a very limited extension on the screen.

Moreover, synoptic displays (buttons and icons) must be enhanced and based on graphical solutions to distinguish between touchable and non-touchable areas. (e.g. giving to touch areas a 3-D button shape and making them opaque and using 2-D transparent boxes with rounded corners for non-touchable areas). Furthermore, the visual feedback about the position of the operator finger in respect with the control has to be provided to the operator (e.g. by making the buttons depressed into its slot, when the operator's finger is in the touch area, and making it come out of its lot when the operator lift-off the finger). It would be possible to reproduce the tactile and aural feedback associated with *hard* switches that is missing with soft controls, by using a *click-clack* recorder sound to be played when activating and releasing a button.

Regarding the integration of alerts, procedures, displays, and controls, the computer-based displays have the advantage of enabling the integration with other systems in the cockpit, like alerting systems and electronic checklist system, making it possible to efficiently *navigate* between displays, especially during abnormal situations. The pilots feedback collected in [71] showed a good appreciation of the pilots for this proposed approach.

This thesis describes in chapter 7 an example of partial *GCS* mock-up derived from the concept of a *GCS* based on soft controls.

[5] In the previous experiments reported in [71], "the pilots stated that it was sometimes difficult to activate a touch area".

2.8.2 *PDA* Based Interface

In some cases, conventional control stations could be impractical (or impossible) due to monetary, technical or other constraints in some applications. An interesting alternative is the *PDA*, like the one shown in fig. 2.37, having the advantage of being lightweight, shirt-pocket portable, and have touch-sensitive displays [64].

In particular, its small size and light weight make it perfect to be used in highly mobile environments like the one often associated with mini-*UAVs*. Of course, cause of the reduced dimension of the screen, the few instrument displayed do not require a high mental workload. Moreover, the trackpad characteristic of the laptop-based interface could be more difficult to use for novice users rather than a mouse. More precisely the movement of the cursor with a trackpad to drag a control could be more difficult to perform for the users if they also must hold down a trackpad button than using single- or double-clicks to select new parameter values.

On the other hand, a *PDA* implementation of the *GCS* is for sure characterised by much lower network and graphics performances than the laptop implementation. Moreover the reduced size of the screen allows only the visualisation of a very restricted set of instruments.

Figure 2.37: an example of *PDA* based interface. Source [64]

2.8.3 Speech-Based Input

Conventional manual input requires the operator to choose and click through several menu items producing therefore an "extensive "head-down time" and error-prone button selections" [72]. Speech-based input is a natural and intuitive communication method and therefore allows a more efficient information management by the operators and have different advantages [72]. More precisely this type of *HMI* reduces resource competition by freeing operator's hands from operating some controls and allowing head-up control. Moreover, they offer a potential reduction of the error caused by the simplification of complex strings of control actions that is necessary to implement *voice macros*. Simulations demonstrated the presence of these advantages for manned aviation. In particular, this type of control gives improved performances and simplified operations for certain tasks, compared to switches and keyboards. In the case of command and control applications, the speech inputs reduce the task completion time in respect with conventional mouse and keyboard input method. The speech input could allow the operator simply to specify the end menu item, while the system take care of selecting it and/or filling it with the appropriate information. Therefore, according to the experimental results presented in [72], despite the additional *processing time* for elaborating each individual voice command, the operators' performance is improved

for speech input than manual input in a simulated teleoperated *UAV* control station environment, both for the flight/navigation task and data entry tasks. However, as with any of the new technologies, there are other challenges which are necessary to consider. For example, in some conditions the speech input could conflict with intercom operations and intra-crew verbal communications.

2.9 Chapter Summary

The solutions used to remotely operate the various *UAV* classes nowadays are based on standard models derived from previous experiences gained from developing and operating *UASs*. The ancestors of *UAVs* were the aerial targets and radio-controlled flying bombs firstly employed by the *US* during World War I. In their evolution the first concepts of assault drones appeared during World War II. The first use of *UAVs* for scientific analysis was recorded in 1946, when some remotely operated *B-17*s collected radioactive data. The main application of *UAVs* from that time onwards was intelligence gathering. It started with the *AQM-34* of *Ryan Aeronautical Company* employed in tens of thousand of reconnaissance missions from the mid-1960s to the mid-1970s. The great effectiveness of drones on the battlefield was demonstrated in the 1980s, when *Israeli Air Force* won against the *Sirian Air Force* with a strategy based on the coordinated use of *UAVs* alongside manned aircraft. Nowadays *UAVs* classes range from miniature *UAVs* carried on the battlefield by infantrymen, to bigger aircraft, such as the *General Atomics RQ-1 Predator* used in military and civilian application.

UASs can be characterised by different flight control modes according to the environment and the urgency of the task in which they are employed. The level of autonomy ranges from the case in which the operator has full control of the *UAV* to that in which the *UAV* is autonomous. Generally speaking the choice of the level of autonomy for every *UAS* function include different aspects. Main factors include the time available for replanning, complexity of the function, consequences of a wrong decision and differences in terms of performance for a human operator controlling or monitoring the *UAS*. The behaviour of human operators is in fact variable and this could lead the operator not selecting the optimal options. On the other hand, humans have the advantage of being more flexible than computers and make therefore more appropriate decisions when sudden changes occurs. For these reasons, when the *UAV* navigate autonomously, an *operator override capability* should always be provided. Similarly, when a function is manually controlled, an *autonomous mode back-up* should be implemented. This is necessary for highly time-critical situations, in which the time is insufficient for a human operator to respond and take appropriate action.

When the *UAV* is autonomous the operator acts as a supervisory controller providing to the *UAS* high level inputs such as navigation waypoints. The supervisory controller is therefore responsible for coordinating human and machine tasks and goals. He needs so to have a correct understanding of the vehicle behaviour in order to easily

predict it. This implies that the model of the supervisory controller have to include the communication with the the *GCS*. The operator derives from it the information about system status, including vehicle attitude, altitude, navigation status, a part setting the navigation waypoints and parameters. In this model the operator take care of five basic roles; first of all he/she plans the change in vehicle performance necessary to get the desired change in the vehicle routing. Then he/she teaches the *UAV* control systems how to get the planned change in the vehicle routing by providing it with appropriate instructions. He/she monitors then the system performance to ensure that it evolves as desired. He/she has moreover to intervene if undesired system performances are detected. Finally he/she learns from the experience gained from the previous roles.

The *GCS* has therefore an important role in supporting the operator regardless of the level of autonomy of the *UAV* may be. More precisely the *GCS* structure depends on the flight control mode of the *UAV* operating in. Generally speaking the *GCS* supports the primary functions performed by the operator that include: flight, communication, systems and mission task management. The final design of the *GCS* is therefore a trade-off between precision for intuition and speed of response. Its layout has in fact to allow the pilot to efficiently complete these functions. The design of the *GCS* should therefore take into account the human factors guidelines defined for manned aviation. Different solutions were proposed in literature for vehicle teleoperation. The most common method for vehicle teleoperation is the *direct control*. The *UAV* is controlled directly via hand-controllers, such as joysticks, and visually supervised by the operator through vehicle mounted cameras. *Multimodal/multisensory Interfaces* are more complex and characterised by a variety of control modes (individual actuators, coordinated motions, etc.) and displays (text, visual, etc.). In *supervisory control interfaces* the operator provides to the *UAS* high-level command generation, monitoring and diagnosis. The related subtasks are then executed by the *UAS* that should have therefore a suitable degree of autonomy. Moreover, there are different new vehicle teleoperation interface concepts, currently classified as *novel interfaces*, that are spreading in the world of *UAS*. Among these, a promising option are solutions based on reconfigurable touch-screens integrating controls on the display, which will be covered in more detail in chapter 7 of this thesis. Another interesting concept are *PDA* based solutions. Finally some studies can be found in the literature also regarding *GCS* using speech based inputs.

CHAPTER 3

Sense and Avoid Literature Review

A lot of previous work has already been done in the development of *S&A* systems for *UAS*. A part the research done both in univerties and companies, aviation autorithies, such as *Federal Aviation Administration (FAA)* and *EASA*, already started working on proposals regarding *S&A* systems requirements and standards. Among these, much work was done based on the standards defined for the *Airborne Collision Avoidance System (ACAS)* developed for manned commercial aviation.

This chapter illustrates guidelines and previous works found in the literature regarding the development of *S&A* systems. It starts with section 3.1, that covers some general considerations of the *S&A* system. The *S&A* system functions are then defined in section 3.2. Section 3.3 describes the typical operating phases. The *Rules of Air* that have to be considered by the system in the avoidance manoevre execution are then identified in section 3.4. The topic of the operator involvement in the operations of the system is discussed in section 3.5. Section 3.6 summarises the work previously carried on in manned aviation for developing collision avoidance systems for both airborne and ground threats. A standard for the alerting logic is proposed in section 3.7. Finally section 3.8 illustrates the design factors and the different solutions proposed in iterature for *S&A* systems.

3.1 General Considerations

The *UASs airworthiness requirements* regarding *S&A* capabilities depend strongly on the aircraft *operating mode*, that can be [73]:

Visual Line Of Sight (VLOS), that is, according to the *ICAO* definition:

> "A mode of *UAS* operation in which the flight crew monitors the flight path in relation to other aircraft, persons, vehicles or structures through direct and unaided visual contact with the aircraft, in order to maintain *separation* and *collision avoidance*."

Beyond VLOS (BVLOS), also called *Radio LoS (RLOS)*, and when a communication relay (e.g. a satellite) is employed, it is referred to as *Broad RLOS (BRLOS)*. In this mode the aircraft is controlled from a *GCS* equipped with the necessary instruments and displays.

In *VLOS* flight conditions, *UAVs* are constrained to fly at very low altitude in order to be visible and therefore controllable by the operator. *ICAO* rules prescribe

that, except for take-off and landing flight phases, the minimum flight altitude has to be above 500 ft. Moreover, flying threats, terrain and obstacles are detected and avoided by the *UAS* operator using his/her eyes. Therefore the *S&A* system is not compulsory for *VLOS UAV* operations.

The situation is different in *BVLOS*/*BRLOS*, where the *S&A* system is necessary to support the *UAS* operator in the accomplishment of the following tasks [17]:

1. maintaining appropriate *separation distance*[1] from other airspace users;
2. avoidance of collision with terrain and obstacles;
3. avoidance of severe/adverse weather;
4. maintaining appropriate flight visibilities and distance from clouds;
5. *visual observation* of lighting and markings;
6. *visual observation* of in-flight interception signals;
7. *visual observation* of the landing/departure runway;
8. *visual observation* of next aircraft where reduced separation is approved[2].

3.2 Functions

According to the classification that was given in section 2.2, *S&A* usually operates at *PACT* level 3 [18]. In fact, the system communicate to the *UAS* operator the potenzial hazards detected and the suggested resolution and allow him/her to decide whether or not to execute those solutions. However, in the case of an imminent collision situation, if the operator is unresponsive or do not react in time, *S&A* operates at *PACT* level 5 and autonomously executes the hazard avoidance actions.

Taking into account all the considerations proposed by Hutchings *et al.* [18], Coulter [74] and Albaker *et al.* [75], the following functions are therefore performed by the *S&A* system:

Environment sensing, in which the system monitors the airspace using sensors to detect and identify every potential hazard for the *UAV*. The aim is to get a synthetic description of the airspace in terms of of the current state of the threats including their position and, if they are airborne then also their velocity and heading.

Conflicts detection, where the informations collected in the previous phase are elaborated to determine which of the objects detected are "real threats".

Resolution estimation defines the necessary resolution manoeuvre if an imminent conflict risk is detected.

Advisories communication, where the advisories about conflict risks and the suggested resolution manoeuvre estimated in the previous two tasks are re-

[1] The *separation distance* is defined as "the minimum distance between an aircraft and an hazard that maintain the risk of collision to an acceptable level of safety" [17].

[2] For example, the vicinity of an aerodrome or in *Visual Meteorological Conditions (VMC)* climbs and descents.

ported to the *UAS* operator. The operator task is then to accept, reject or ignore the suggested route changes or ignore them. In fact, even tough the system is capable of operating autonomously, a *S&A* system must normally report to and share the responsibility for its tasks (including safety) with the *UAS* operator. He/she is therefore a part of a *S&A* system, linked to the *UAV* via a low-bandwidth communications link.

Autonomous resolution is the autonomus execution of the calculated resolution manoeuvre and it is executed if the operator does not react to the advisory of the *minimum safe time before impact*[3].

3.3 Operating Phases

The functions defined in the previous section are performed in three distinct phases [18]:

strategic conflict management: long range potential conflicts are assessed using all available information sources to take early measures to prevent conflict;

conflict resolution advisory: the system communicates to the *UAS* operator the estimated avoidance manoeuvre and the operator can accept or refuse the advisory;

autonomous resolution execution: when the *minimum safe time before impact* is imminent, and there is no input from the *UAS* operator the system execute the resolution manoeuvre in order to avoid the imminent collision.

Regarding the *strategic conflict management*, automation is a fundamental tool to compensate for the limitation in human performance in predicting the aircrafts future status [76]. It acts as supporting tool to the human operator in the conflict risks detection. This part of the system is designed to sense the proximity of potential threats, involving airspace users, ground and terrain obstacles risks and assess the encounter geometry in case of other flying agents. Generally, the prediction algorithms used in automated conflict detection provides an automatic evaluation of the conflict risks detected over a certain temporal span [77]. It indicates therefore when and where the conflict will happen and which aircraft or threats are involved.

In the case where a conflict risk is detected, the *conflict resolution advisory* phase performs the following tasks:

define the escape trajectory necessary to maintain separation and avoid collision with all threats taking into account *Rules of Air* (that will be covered in the next section, section 3.4), aircraft performances limitations and operator response delay;

[3]This parameter is defined as the "time before impact, after which, due to latencies in the system, a successful collision avoidance manoeuvre is impossible" [18].

monitor the evolution of the encounter geometry during the resolution manoeuvre in order to ensure its effectiveness and update it if necessary;

communicate to the *UAS* operator the suggested manoeuvre.

The *autonomous resolution execution* is engaged when the *UAS* operator does not react timely to an imminent threat[4]. This function is an example of the *autonomous mode back-up* defined in section 2.2. This element must be implemented in order to enable the *UAS* operator the possibility to override any collision avoidance manoeuvre, if the situation demands this. This is the *command override capability* described previously in section 2.2 and it is also engaged in the event of a loss of the data link.

3.4 Rules of Air and *S&A*

As stated in section 1.6, a *S&A* system has to take into account the same collision avoidance requirements of *Rules of Air* for manned aviation, delineated in the *ICAO Annex 2* [78], in order to guarantee the *ELOS*, defined in section 1.5. This section identifies the subset of *Rules of Air* to be considered for *S&A* systems.

Regarding the *minimum flight altitude*, all the aircraft, apart the ones involved in particular types of missions, have to take into account the following low flying prohibitions:

failure of power unit: in case of power unit failure, the aircraft shall not fly below the altitude necessary to make an emergency landing without causing dangers to persons or property on the surface;

the 500 ft **rule:** the aircraft shall not be flown closer than 500 ft to any person, vessel, vehicle or structure;

the 1000 ft **rule:** when flying over a congested area of a city town or settlement, the aircraft shall fly at an vertical distance of at least 1000 ft above the highest obstacle on ground within a horizontal radius of 600 m of the aircraft;

the land clear rule: when flying over a congested area of a city, town or settlement, the aircraft shall not fly below the altitude necessary to make a landing out of the congested area in the event of a power unit failure;

flying over open air assemblies: when flying over an organised open-air assembly of more than 1000 persons, the aircraft shall fly above the higher of the following values:

- 1000 ft,
- such altitude to permit a landing out of the assembly in the event of a power unit failure.

Whenever an aircraft is flying in circumstances in which more than one of the low flying rules apply, it shall fly at the highest altitude required by any of them.

[4] See section A2.1 of reference [17].

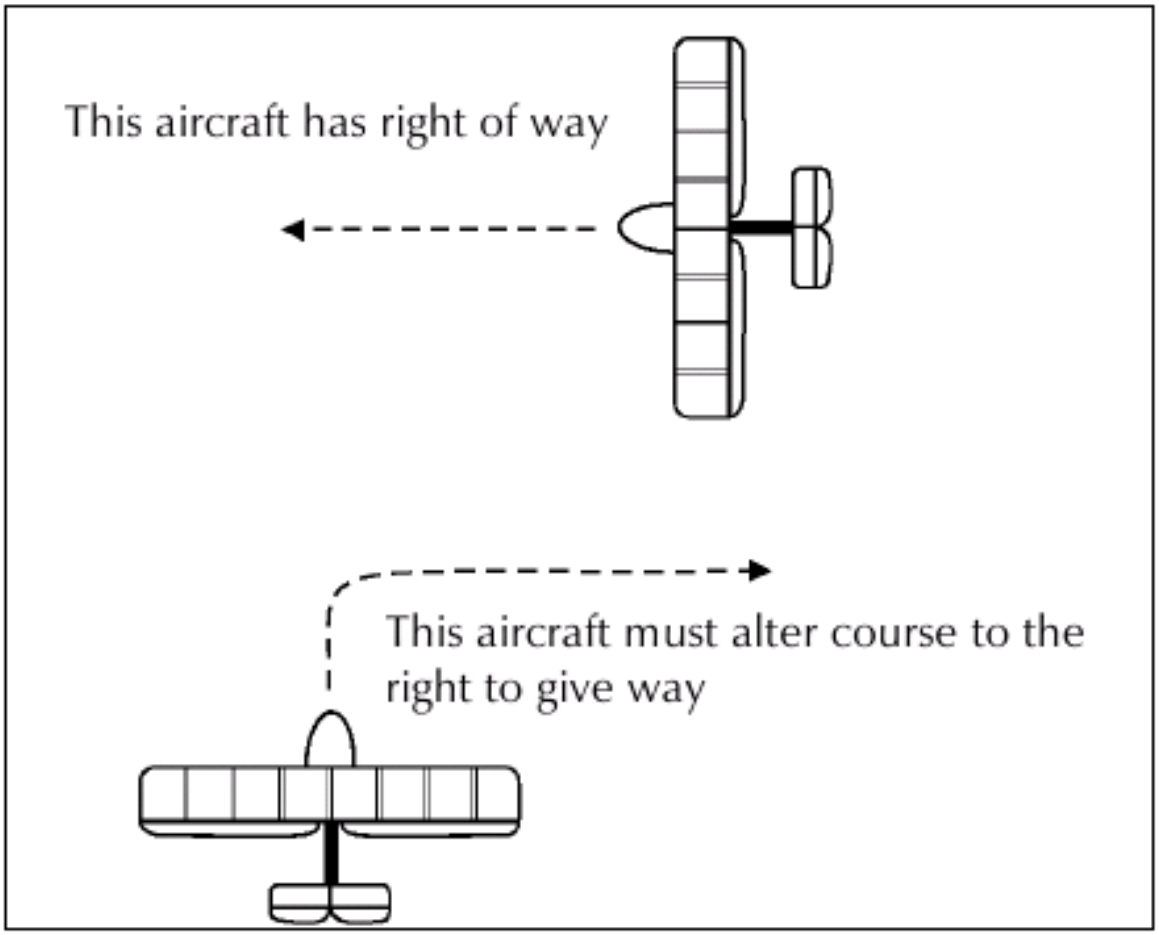

Figure 3.1: converging encounter geometry: all aircraft shall apply the right hand rule, except that power driven aircraft shall give way to gliders or aircraft towing objects. Source: [79]

Collision risks between aircraft must be generally managed considering the *Right of Way Rules* here shortly summarised:

converging encounters (fig. 3.1): both aircraft have to follow these rules:

- flying machines shall give way to airships, gliders and balloons.
- airships shall give way to gliders and balloons,
- gliders shall give way to balloons,
- mechanically driven aircraft shall give way to aircraft which are towing other aircraft or objects.
- when two aircraft are converging in the air at approximately the same altitude, the aircraft which has the other on its right shall give way;

head-on encounters (fig. 3.2): each aircraft shall modify its course to the right;

overtaking encounters (fig. 3.3): when an aircraft is being overtaken in the air, this aircraft shall have the right-of-way and the overtaking aircraft, whether

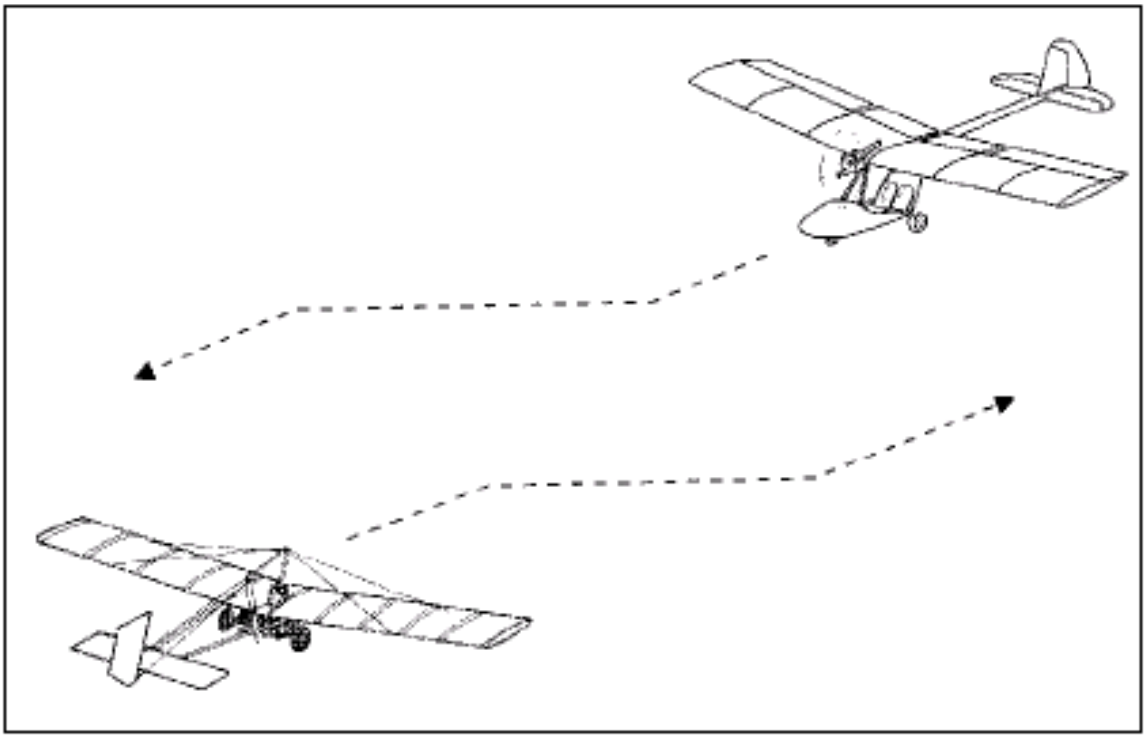

Figure 3.2: head on encounter geometry: both the aircraft shall turn right. Source: [79]

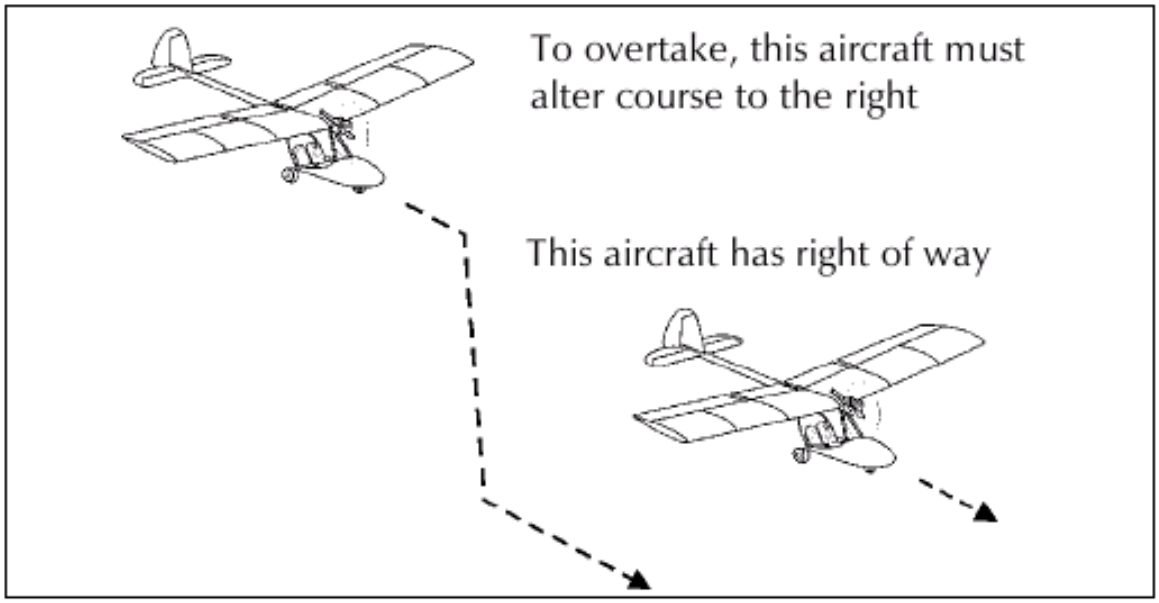

Figure 3.3: overtaking encounter geometry: the slower aircraft has the right of way. If overtaking, it shall alter course to the right. Source: [79]

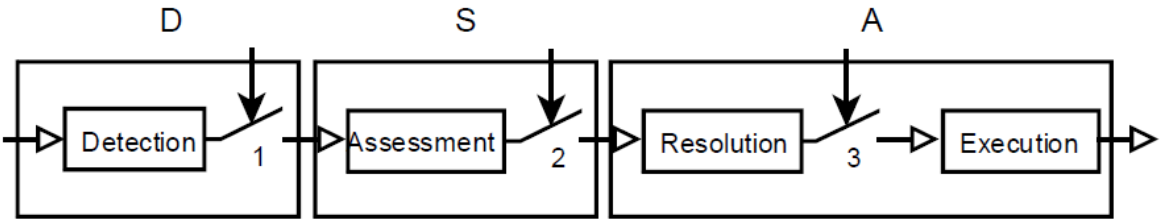

Figure 3.4: depiction of the operator involvement in the *S&A* system by use of switches. Source: [81]

> climbing, descending or in horizontal flight, shall keep out of the way of the other aircraft by altering course to the right. When there is no collision risk the overtaking aircraft has to keep out of the way of the other aircraft until that other aircraft has been passed, notwithstanding any change in the relative positions of the two aircraft. Finally, a glider overtaking another glider may alter its course to the right or to the left.

3.5 Operator Involvement in *S&A* Systems

It is recognised in [80] that, in conditions in which the time to conflict is long enough, the involvement of the operator in the *S&A* system can mitigate the following issues:

- falsely identified threats, resulting in unnecessary avoidance manoeuvres;
- critical information, e.g. changes in mission targets and/or tasks, flight re-planning due to *Air Traffic Control (ATC)* or detection of threats in the environment, that cannot be considered by the *S&A* system when computing the avoidance manoeuvre.

The level of operator involvement or *Level of Authority (LOA)* of a *S&A* depends on the allocation of the authority between the operator and the system in the tasks performed by the system [80] illustrated in fig. 3.4 as follows [81]:

Block D: detection of the potential threats,
Block S: assessment of the conflict risks,
Block A: evaluation and execution of the avoidance manoeuvre.

The involvement of the operator in the system can be seen as a switch between two subsequent tasks. When the switch is closed, it implies that the system needs the operator consent, and therefore his/her involvement, to close the switch and perform the passage between the tasks. Otherwise the operator is not involved in that passage.

More precisely, the first switch is related with the judgement of the nature of detection (true or false alarm). When the system requires to the operator to confirm detected traffic in order to proceed with the assessment of the resolution manoeuvre, this switch is open by default. The switch is then closed by the operator's confirma-

tion. Another possible approach is that in which the default status of the detection is defined as *correct* and therefore the switch is closed. In this case, the system can be programmed to let the operator open the switch when a false alarm is detected.

The second switch determines whether the operator consent is necessary to provide the assessed conflict risks information to the block A, evaluating the resolution.

The third switch is meant to enable the resolution manoeuvre execution. The case in which the operator consent for the resolution manoeuvre execution is required is represented by a switch open by default. Since the operator can assess the manoeuvre only in a limited time before its autonomous execution, a timer controls the switch together with the operator. Alternatively, when the resolution manoeuvre evaluated by the *S&A* system is directly executed by the system, that is the case of the fully automatic resolution, the switch is closed by default.

The configuration of the switches in the figure defines therefore the *LOA*. These switches can be used to define the system autonomy classification in Table 3.1. A fully autonomous system would have LOA[D]=8, LOA[S]=8 and LOA[A]=8. When the *LOA* is equal to 6 or 7, the operator can only intervene on an already initiated action by declaring a false alert or canceling the execution [81]. The modes characterised by LOA[D]=5 provide the operator a predefined amount of time in which the operator can assess the validity of the detection. When LOA[D]=6, LOA[S]=6 and LOA[A]=5, the system provides the operator the time to assess the avoidance manoeuvre, that can also be used to assess the validity of the conflict detection. It is also interesting to note that for all combinations for which LOA[D]>4, LOA[S]>4 and LOA[A]>4 the system is operative also in case of a control-link failure [80].

3.5.1 Effect of Link Latency and Criticality

Operator involvement introduces in *S&A* systems a latency caused by the time necessary to accomplish the following operations [81]:

1. downlink data for depiction to the operator,
2. allow the operator to assess data and decide,
3. uplink the decision.

Morever, when the *S&A* system does not have a sufficient authority to execute the conflict resolution, the datalink is a critical element for the conflict avoidance. A *S&A* system has therefore to be designed in order to ensure autonomous operations in the following conditions [82]:

1. loss of data link situation.
2. when the latency of the communication between the *UAV* and the operator would cause a situation in which the *UAV* response is too late to avoid the collision.

Table 3.1: characterisation of the *LOAs* for *S&A* systems in terms of potential threats detection (D), conflict risks sensing (S) and conflict avoidance (A):*HO* stands for *human operator*, *SS* stands for *system*. Source: [82]

LOA	**Computer**	**Human**	**D**	**S**	**A**
1	-Offers no assistance -Switch always open	Does all	*HO* uses sensor view to look for traffic	*HO* determines whether a loss of separation exist and predicts whether a future loss of separation is likely to occur	*HO* determines desired flight path and inputs the required control actions
2	-Suggests options -Switch always open	Chooses			-Manoeuvre options depicted to *HO* -*HO* chooses from options
3	-Selects way to do task -Switch always open	Schedules function			-*SS* presents option to *HO* -*HO* determines moment of execution
4	-Selects and executes -Switch open	Must approve		-Sensors perform detection task -*HO* must confirm result -*SS* presents option to *HO* -*HO* needs to provide approval to *SS*	
5	-Executes unless vetoed -Switch open until veto time	Has limited veto time		-Sensors perform detection task -*HO* has limited time to either confirm result or declare a false alarm -*SS* presents option to *HO* -*HO* assesses the manoeuvre and vetoes if deemed unsuitable	
6	-Executes immediately -Switch closed	Informed upon execution	-Sensors perform detection task -Video of suspected target shown to *HO*	-*SS* determines whether a loss of separation exists or current state will lead to a loss of separation -Results depicted to *HO* -*SS* takes action to avoid loss of separation if needed -*SS* shows target flight path	
7	-Executes immediately -Switch always closed	Informed if asked	No default video	As 6, but results only depicted upon request	As 6, but target flight path only shown on request
8	-Executes immediately -Switch always closed	Ignored by computer	No video	As 6 without depiction of results	As 6, but no depiction of flight path target

The loss of data link can be addressed by implementing a function that reconfigures the system in order to operate autonomously.

Regarding the second issue, a mode of operation based on *operator consent with a limited veto time* should be used [81] in those cases where the time necessary to the operator to assess the situation and the *Time-To-Conflict (TTC)* sufficient for a successful avoidance manoeuvre can be estimated. The maximum available *veto time*, here identified as $t_{V/T}$, is, in fact, defined with the following relationship:

$$t_{V/T} = t_{T/C} - t_M - t_T \tag{3.1}$$

where $t_{T/C}$ is the *TTC*, t_M is the time necessary to the system to accomplish the avoidance manoeuvre and t_T is the time necessary to transmit the data, including the downlink of data to the operator *GCS* and uplink of the chosen avoidance manoeuvre to the system. It is then possible to estimate a minimum time span, that is function of conflict geometry and of ownship and flying threats speeds, below which any delay between detection and resolution significantly increases the collision risk likelihood. Prior to this time span, the involvement of the operator in the conflict detection process is useful to assess the information on which the conflict detection is based, and therefore identify false alarms and assess the manoeuvre generated by *S&A* system. According to this definition, the required *minimum detection range* d_D necessary for a fully autonomous system is given by the following formula:

$$d_D = V_R * (t_{V/T} + t_T) \tag{3.2}$$

where V_R is the maximum relative velocity between ownship and threat, $t_{V/T}$ is the maximum allowed veto time and t_T the transmission time. This information can be used to evaluate in which the time the autonomous manoeuvre has to be initiated in those cases in which time is not sufficient to allow the operator to assess the situation [82]. Therefore the benefits of operator involvement can be pursued with the following conditions [81]:

- an authority level of 5,
- a specified maximum veto time $t_{V/T}$, defined as in relationship given in eq. (3.1),
- a detection range, that is the sum of d_D defined in eq. (3.2) and of the minimum detection range for a fully autonomous system.

3.6 Automatic Collision Detection in Manned Aviation

An *ACAS* was introduced in commercial aviation in 1999. It was initially called *TCAS* and is currently developed in bosom of the *ACAS* project of *Eurocontrol*.[5] In the latest version of *ACAS*, when a collision risk is detected an alert and suggests

[5] More information in reference [83].

a potential resolution manoeuvre is given to the pilot. However the system is able to track only aircraft equipped with a *mode S transponder* [6] and can partially detect *mode A/C transponders*. The *ACAS* is not able to locate aircraft without transponder or equipped with old types of transponders, listed in Table 3.2.

Differently from *S&A* system, it does not include any *autonomous resolution execution* function, as defined in section 3.3, that executes the suggested manoeuvre when the pilot is not reacting. In fact, as explained in [85], *ACAS* has characteristics and performances different from those required by a *S&A* system for *UAS*. One of the main reasons is that the differences in the climb performance of the various *UAVs* are not compatible with current *TCAS* requirements. More precisely the limitations on the climb performance could make impossible for the operator or the *S&A* system to execute the suggested manoeuvre by *TCAS* advisories. Moreover, most of small general aviation aircraft and all aerostatic balloons are not fitted with a *mode S transponder*. Therefore this system is not able to track all potential flying threats. Finally the *ACAS* is designed such as that it suggests to the pilot only last-minute avoidance manoeuvres in order to provide minimal separation to avert a collision [3]. Extended the use of this system to *UAS*, then such a functionality would typically lead the aircraft to come into close proximity to the other aircraft before initiating its avoidance action. This behaviour is not compatible with normal safe airspace operations. In manned aircraft, this is avoided because the *S&A* functions are accomplished by either using *ATC* or *Visual Flight Rules (VFR)* to manoeuvre, before any *ACAS* resolution advisories are deemed necessary. However, in *UAVs* the *S&A* system would substitute the manned aircraft counterpart.

Also a *Terrain Awareness Warning System (TAWS)* has been already developed and certified for manned aviation.[7] Differently from a complete *S&A* system, it simply alerts the *UAS* operator about the ground collision risks without providing *conflict resolution advisory* function as defined in section 3.3 ofthis thesis.

3.7 Alerting System Design

As it was stated in section 3.2, *S&A* system communication to the operator is based on two types of advisories. They are usually in the following two types that are the same used for *ACAS* advisories [87]:

Traffic Advisory (TA) supports the operator in detecting potential conflicting threats by alerting him/her;

Resolution Advisory (RA) communicates to the operator the recommended avoidance manoeuvres.

As shown in fig. 3.5, in an *ACAS* they are issued according to the following procedure [77].

[6] More information in reference [84].
[7] More information in reference [86].

Table 3.2: transponder interrogation modes

mode	usage field	identification code	altitude	operative condition and position data	flight condition parameters
1	military	2-digits 5-bits code			
2	military	4-digits octal unit code			
3/A	military civilian	4-digits octal unit code assigned by air traffic control			
4	military	3 pulse reply to cripto coded interrogation			
C	military civilian	4-digits octal unit code assigned by air traffic control	barometric measure		
S ***ELS***	military civilian	24-bit address assigned to the aircraft during its national registration and never changed	reported in 25 ft intervals	-flight status (airborne/on the ground) indicator; -surveillance identifier code capability (mode S indicator);	
S ***EHS***	military civilian	24-bit address assigned to the aircraft during its national registration and never changed	value selected on the airplane *GCNS*	-flight status (airborne/on the ground) indicator; -surveillance identifier code capability (mode S indicator);	-roll angle; -track angle rate or, if not available, true airspeed; true track angle; ground speed; magnetic heading; indicated airspeed/Mach number -vertical rate (barometric or baro-inertial measure)
ADS-B	military civilian	24-bit address assigned to the aircraft during its national registration and never changed or periodic identification utilising either the *RTF* Callsign or the aircraft registration	barometric measure	-horizontal position (latitude, longitude) derived from *GNSS*; -aircraft position quality indicator -emergency status indicators selected by the flight crew on the control boxes;	optional

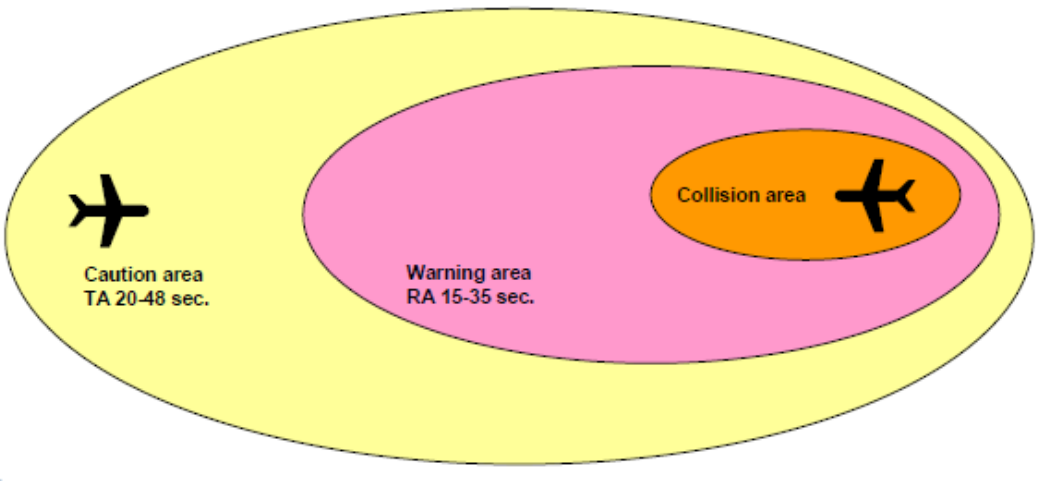

(a)

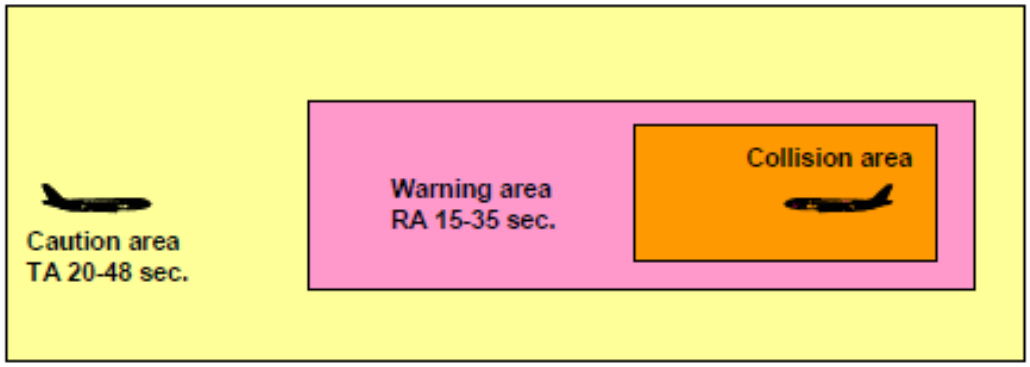

(b)

Figure 3.5: relationship between *TCAS* II advisories and protected volume: (a) horizontal view, (b) vertical view. Source: [87]

When colliding threat is within 50 s of loss of separation with the ownship, the verbal warning *Traffic Traffic* is used to communicate the *TA* and the color of the colliding threat icon on the display is changed to yellow. If traffic reaches a loss of separation that is less than 25 s, the color of the threat icon becomes red and the *RA* indicating the required avoidance manoeuvre is issued verbally.

As suggested by Xu *et al.* in [77], The sequence used for the alerts levels can be the same three-levels scheme used by the *ACAS* system. This scheme is preferable to a two-level or dichotomous one (conflict vs. no-conflict) because of its grater accuracy. More precisely, the presence of imperfections in a multiple-level alerting system is less prone to errors than in a two-level system. As explained in [88], this logic was inherited from the *McDonnell Douglas MD-11* aircraft system alerting convention where three alert levels are identified. A first level alert is used for information that must be communicated to the operator but do not require the operator to intervene, like when a long range potential conflict is detected. The alert function is just to *point out* the detected

traffic. The second level alert requires operator's initiative. In *S&A* systems this alert can be used when a conflict is detected and operator has the responsibility to avoid the collision. A third level alert is an alert requiring immediate action by the operator. It can be used for the case of the actual loss of separation, that happens when the minimum legal separation is reached by the aircraft.

Moreover, a *S&A* system can be based on the notions of two spatial zones, indicated as *Collision Avoidance Zone (CAZ)* and *CDZ*, and the three alerts related with their thresholds defined by the *RTCAs Airborne Conflict Management (ACM) committee* [90]. An example is shown in fig. 3.6.

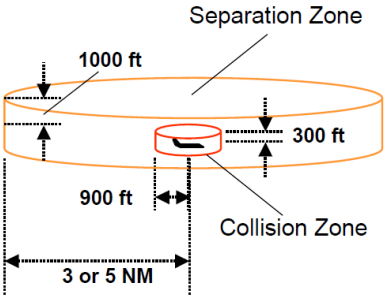

Figure 3.6: example of separation and collision zones proposed for a *S&A* prototype. Source [89].

The *CAZ*is the smallest and therefore most critical zone around each aircraft. The penetration of this zone causes a *near miss* or actual collision between aircraft. This zone includes the three different components shown:

Assured Collision Avoidance Distance (ACAD) is the declared near miss distance;

Position Uncertainty is the accuracy limit of the aircraft's position determination;

Trajectory Uncertainty is a measure of the aircrafts ability to maintain a desired trajectory.

The sum of trajectory uncertainty and position uncertainty of each aircraft with the *ACAD* defines therefore the minimum measured separation distance necessary to maintain the true separation distance equal to the *ACAD* despite position measurement and/or technical flight error.

The *CDZ* is a bigger zone around each aircraft.As soon as this zone is penetrated a loss of legally required separation between the aircraft occurs. The only difference between *CDZ* and *CAZ* is that, as displayed in figures, the *Assured Normal Separation Distance (ANSD)* is typically much larger than the *ACAD*.

The related alert levels are listed below in order of decreasing level of criticality [90]:

***CAZ* violation** is the alert produced by an imminent penetration of the *CAZ* to inform the operator about the necessity of an immediate and aggressive manoeuvres to avoid the penetration of the *CAZ*;

***CDZ* violation** is issued when a penetration of the *CDZ* occurs and it requires the *UAS* operator to carefully decide and accomplish a manoeuvre to avoid the loss of separation;

low level is an optional advisory level that can be activated before the *CDZ violation* alert to provide the *UAS* operator with the opportunity to monitor

and/or resolve detected conflict risk with minimal manoeuvreing.

It is worth noting that alert boundaries have shapes and sizes that are not fixed but are function of relative trajectory orientation, rate of closure, position and trajectory uncertainty values. Among the defined alert levels, *low level*, if enabled, and *CDZ violation* alerts can be considered secondary alerts that could happen frequently in flight operations. Differently, a *CAZ violation* alert is a critical alert related to an exceptional and urgent condition which should only arise when:

- the operator ignores/misunderstands airborne conflict management guidance following a *CDZ* alert or
- one or more aircraft manoeuvre creates a conflict with an aircraft in close proximity.

3.8 Design Factors

Different approaches for the *S&A* algorithm development have been suggested in the literature. The following sections summarises the main design factors sketched in fig. 3.7 and identified in reference [75]. More precisely, section 3.8.1 identifies the sensors configurations proposed for the environment sensing of *S&A* systems and the choices involved in the detection of conflict risks. In section 3.8.2 the solutions proposed for the avoidance manoeuvre planning are analised. Section 3.8.3 finally discuss some considerations on the general design of the system.

3.8.1 Conflict Detection

Detection of conflict risks requires the identification of potential threats in the airspace proximity close to the ownship and continuous data update and collection recording. Therefore it is necessary to provide the system with the tools to enable the detection and identification of specific type of threats. These tools can be simple databases, e.g. for detecting ground threats in fixed position, or sensors set for the detection of moving threats, e.g. traffic, or obstacles not considered in databases.

Sensors used can be classified as *cooperative* or *non-cooperative*. The *cooperative sensors* are sensors that enable exchange of information like position, heading, speed and waypoints, e.g. transponder mode S and *ADS-B*[8]. These sensors can be used to greatly improve improve the detection/identification of all airborne aircraft/ground moving threats[9]. *Non-cooperative sensors* do not have any exchange of information with potential threats. Example of such sensors are: laser range finders, optical flow

[8] See example in [91].

[9] In the case of the transponders, both the ownship and the potential threat must be equipped with a transponder with certain characteristics.

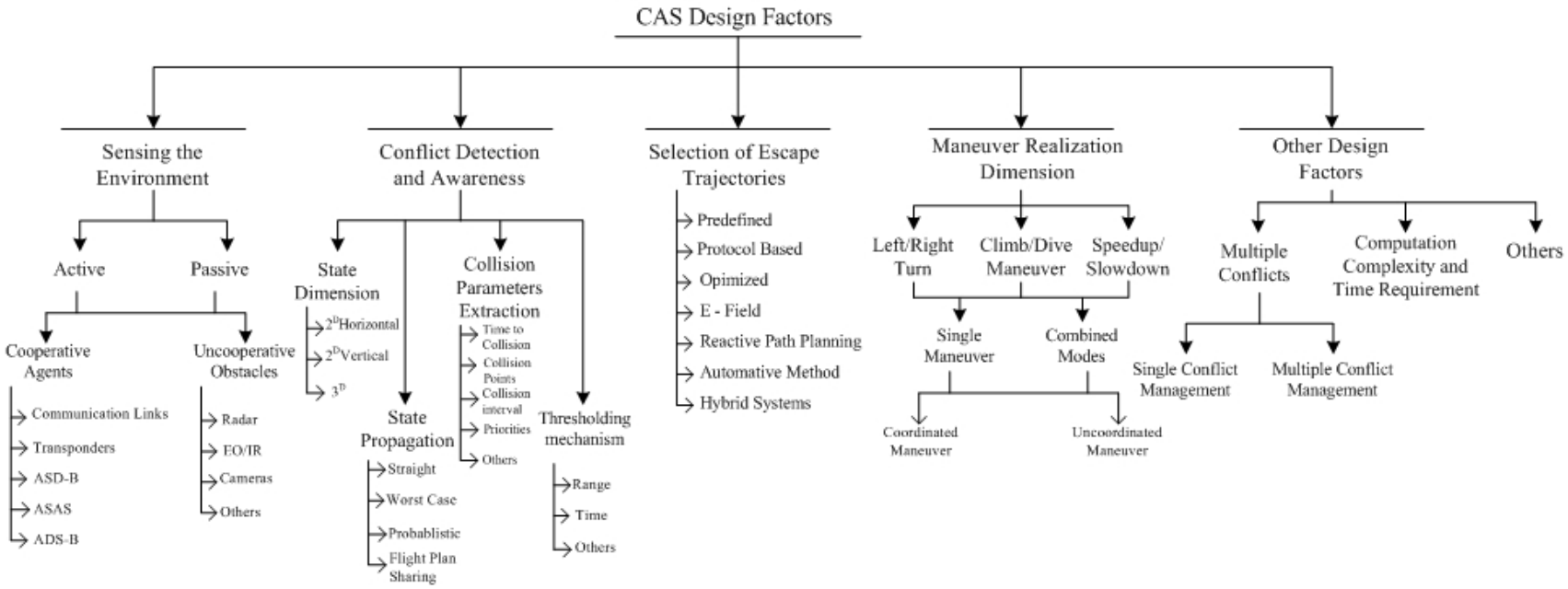

Figure 3.7: *S&A* design factors classification. Source [75]

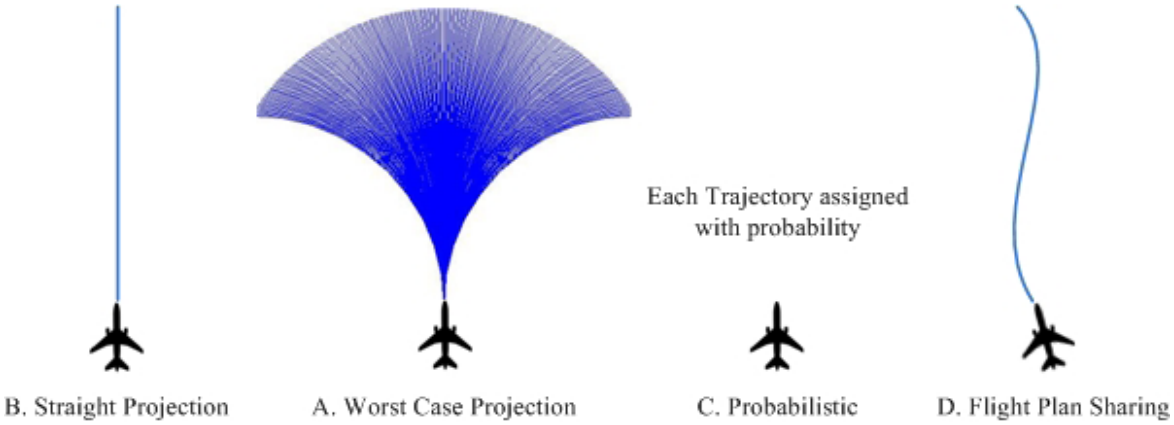

Figure 3.8: trajectory projection methods. Source [75]

sensors *Electro-Optical/Infrared EO/IR*, radar systems,[10] stereo camera pairs or moving single camera[11] or mixed configuration of sensors of both types[12].

According to the performances and the configuration used to install the sensor set, it is possible to obtain different *encounter sensing dimension*. This design factor is defined as the *extension of space surveilled for the conflict risks monitoring*. The algorithm can consider one of the following three options:

two dimensional horizontal plane (*2D-H*), when just a region of the space close to the horizontal plane crossing the position of the aircraft is monitored;

two dimensional vertical plane (*2D-V*), when just a part of the airspace close to the vertical plane is monitored;

three dimensional state information (*3D*) , when a region or all the close airspace is monitored.

The *encounter current information projection* is the *solution used for the dynamical projection of state variables of UAV and threat into near future* for the collision risk detection. The fundamental projection methods identified in reference [75] are sketched in fig. 3.8 and identified as *straight projection*, *worst case projection*, *probabilistic methods* and *path plan sharing*.

In the *straight projection*, the states are projected into the future along a single trajectory, without considering directly uncertainties.[13] This simplifies the problem but can only be applied in situations in which aircraft trajectories are easily predictable and for short periods of time. In fact, this approach does not take into account the possibility that the intruder aircraft can do any manoeuvre during the time range considered.

[10] See examples in [92–94].
[11] See examples in [95–99].
[12] See an example in [100].
[13] See an example in [101].

The *worst case projection* on the other hand assumes that the intruder aircraft could perform any range of manoeuvres. If any of these trajectories causes a conflict, then the related alert is produced.[14] It has to be limited to a short projection time in order to limit the computation requirement.

Probabilistic methods model the uncertainties to describe risk variation in the future trajectory of aircraft. This requires the development of a complete set of possible future trajectories, each weighted by a probability of occurrence, producing a probability density function.[15] A positive characteristic of this method is that the decisions can be taken on the fundamental likelihood of the conflict. In particular, safety and false alarm rate can be assessed and considered directly. The disadvantage is that the logic behind this method may be difficult to model the probabilities of the future trajectories.

Finally, *path plan sharing* provides path trajectory and aircraft specific informations (such as position, heading and velocity) to all other aircraft in the vicinity. More precisely, data from each aircraft are sent to monitoring ground stations and all neighbouring aircraft as a broadcast. This approach gives all aircraft a 3D picture of neighbouring aircraft movements, precise projection of encounters states trajectories and exact collision parameters estimation.

Another important design factor is the approach of the *S&A* system to the detection and accordingly the resolution of conflicts in multiple encounters scenarios. The system can handle traffic situations with multiple aircraft with two approaches:

single conflict management, where the conflicts are avoided sequentially in pairs in multiple conflict secenarios;

multiple conflict management, if all threats are handled simultaneously.

3.8.2 Avoidance manoeuvre Planning

Different design factors are identified in [106] regarding the evaluation of the resolution manoeuvre. First of all, the constraints imposed by hazards, e.g. vehicle manoeuvreing capabilities and right of way rules, should be considered in order to get a reliable conflict resolution. Also the latency in the remote operator receiving the manoeuvre advice, acting upon it and then commanding the aircraft should be taken into account [3].

Moreover, the allowed type of manoeuvres considered by the algorithm are strongly related with the avoidance manoeuvre choice. These could include speed changes (speed up/slow down commands), lateral (turn left/right) and vertical manoeuvres (climb/dive). These actions may be issued separately or in a combined way. Furthermore, when an avoidance manoeuvre is combined, it can be performed simultaneously or in sequence.

[14] See an example in [102].
[15] See examples in [103–105].

Also the coordination among ownship and flying threats influences the manoeuvre choice. The manoeuvre obtained can be therefore *coordinated* or *uncoordinated*. *Coordinated manoeuvres* are accomplished when there are more alternative versions of the escape action and the system choose the options for the ownship and intruder aircraft, respectively, in order to avoid the generation of new conflicts[16]. *Uncoordinated manoeuvres* refers to the worst case scenario, in which the intruder does not respond to the critical situation and only the ownship execute the resolution manoeuvre.

Considering the computational implementation of this part of the system, several approaches have been proposed in the literature. The main categories are *predefined collision avoidance*, *protocol based decentralised collision avoidance*, *optimised escape trajectory approaches* and *e-field methods* [75].

Predefined collision avoidance is based on a fixed set of predefined rules. It does not perform any additional computation to determine the escape trajectory[17]. The advantage is to reduce the response time to avoid the conflict. On the other hand the manoeuvres are less optimal than those computed in real-time.

Protocol based decentralised collision avoidance defines a solution for a team of aircraft based on inter-agent communication including sharing position, velocities, waypoints and heading. Aircraft take decisions based on a common set of rules decided a priori.[18] This method is decentralised and guarantees safety. However, the trade off is that unnecessary long trajectories can be generated.

The *optimised escape trajectory approaches* involve an optimisation problem that can be defined in a lot of different ways. These approaches generally combine a kinematic model with a set of constraints.[19] An optimal resolution strategy is then computed based on most desired optimisation constraint.

E-field methods are based on the use of a force field to map the volume between aircraft in terms of a potential field. Each aircraft is considered as a charged particle and repulsive forces between aircraft are used to generate manoeuvreing trajectories[20]. The advantage of this method is that conflict avoidance is continuously available using simple electrostatic equations. On the other hand, the algorithms presented have limited relevance because sharp discontinuities may occurs in the commanded manoeuvres. Furthermore, it requires a high level of flight guidance, leading to increase in complexity beyond issuing simple manoeuvreing commands.

In *hybrid S&A systems* continuous and discrete states are combined[21]. In particular, the vehicle and its manoeuvre are modelled as a hybrid system. Its reachable sets of states are filtered based on safety specifications to get a safe subset of the reach

[16] An example is the criteria used for *TCAS*, in which, if aircraft A is diving on a route that leads to a conflict with airplane B climbing, the manoeuvre chosen for A is the climb while a descent is suggested to B.

[17] See an example in [107]

[18] See examples in [108–111].

[19] See an example in [112, 113].

[20] See examples in [90, 114–118].

[21] See an example in [119].

set. Then Hamilton-Jacobi equations are employed to calculate control commands that guarantee *UAV* staying in its safe set. Although this method is decentralised and assures safety, it scales poorly for large *UAVs*.

Finally, also the trade-off between the complex computations performed by an approach versus the time requirement to resolve the conflict has to be considered in the definition of the system algorithm. The final choice has to ensure that the definition of the conflict resolution happens in a time short enough to guarantee effectiveness to the system. Therefore the complexity of the calculation needs to be bounded to provide an approach that is effective and robust but also reasonably simple.

3.8.3 General notes

Further work is also necessary in developing and defining the type and the layout of *HMI* assuring an easy and effective interaction between the system and the *UAS* operator [19, 106]. The performance of the operator in assessing the situation depends in fact on the *HMI* layout. This topic is discussed in more detail in section 4.5 of the next chapter.

The interactions and the trade-offs between all the aforementioned issues must be defined considering certification requirements, limitations and performances of technology. The effects of the human operator involvement in the system management when it is not completely autonomous, should also be taken into account. Finally the *level of autonomy*, that was classified in Table 2.1 and spreading from manual operator in the loop to fully autonomous, influences both the resolution manoeuvres estimated by the algorithm and the *HMI* design [106].

As explained in reference [3], the presence of so many important aspects in the design leaves an open question. It deals with the possibility to define a single *S&A* standard algorithm or several different algorithms to meet the varying capabilities of different *UAVs*. Strongly related with this aspect is the assumption that performances of all aircraft in the avoidance manoeuvres are interoperable. As explained in section 3.6, this is a basic assumption in the *ACAS* development. This hypothesis is the base for making possible the explicit coordination of manoeuvres between aircraft equipped with *S&A* systems in order to assure compatibility.

3.9 Chapter Summary

The requirements of *S&A* capabilities for *UAS* depend strongly on the aircraft operating mode. This is defined *VLOS* when the operator monitors the separation of the *UAV* in respect to other aircraft, persons, vehicles or structures through direct and unaided visual contact with the aircraft. In this case the operator have to visually detect and avoid flying threats, terrain and obstacles and the minimum flight altitude is 500 ft. *BVLOS* or *RLOS* are acronyms used when the communication between op-

erator and *UAV* passes through a communication relay (e.g. a satellite). It is finally indicated as *BRLOS* the case in which the *GCS* includes instruments and displays to communicate with the operator. Both *BVLOS* and *BRLOS* require a dedicated *S&A* for separation assurance and collision avoidance.

A *S&A* system has to perform a precise set of tasks to effectively perform its function. First of all, it has to monitor the surrounding environment to detect potential hazards (*environment sensing*). The real threats have then to be identified from the information collected in the previous task (*conflicts detection*). If necessary, a resolution manoeuvre has then to be estimated (*resolution estimation*). The information of the detected conflict risks and suggested resolution have then to be communicated to the *UAS* operator on the *GCS*, in order to allow him/her to accept or reject the suggested manouevre (*advisories communication*). The resolution has then to be autonomously executed if the operator does not react in time (*autonomous resolution*).

These tasks are executed in three distinct phases. In the first phase, the *strategic conflict management*, the potential conflicts are assessed at long range and early precautions are taken for avoiding the collision. If necessary, the resolution manoeuvre is then evaluated and communicated to the operator in the *conflict resolution advisory* phase, in order to allow him/her to accept or reject it. Finally the system override the operator in controlling the *UAV* in order to avoid the conflict risk, when the collision is imminent; this is the *autonomous resolution execution*.

Many factors should moreover be considered in the design of the *S&A* system algorithm. First of all, a *S&A* system has of course to take into account the collision avoidance requirements already defined in the *Rules of Air* for manned aviation. This is necessary in order to guarantee compatibility with manned aviation operations in the non-segregated airspace. These requirements regard both the *minimum flight altitude* and the *right of way rules*.

Despite the autonomous nature of *UAS* operations, the involvement of the operator in the *S&A* can be very beneficial to the system peroformance. It is useful to mitigate the problems related with falsely identified threats and critical information, such as mission and flight replanning or undetected threats. Of course the *UAS* operator's involvement introduces in the system the latency caused by the time necessary for the communication with the operator. Moreover, the communication datalink between the *UAS* and operator, becomes a critical element of the system. Therefore the *S&A* system has to be designed in order to ensure autonomous operations in those critical conditions in which the delay related with latency caused by the operator activity could lead to dangerous situations, such as collisions, or when the datalink is lost.

In manned aviation flights, collision and conflict risk alerting systems have already been developed and deployed. These include *TCAS* or *ACAS*, mainly used in commercial aviation to detect conflict risks with aircraft equipped with mode S transponders. Another system is the *TAWS* for monitoring terrain collision risks. The advisories issued by a *S&A* system follow a procedure and a levels scheme very similar to that of the *ACAS* system. These advisories include both *TA*, alerting the pilot about con-

flict risks, and *RA*, communicating the resolution manoeuvres when issued. The alert criticality is defined according to a three levels scheme where two concentric zones are centered around the current position of the ownship (*CDZ* and *CAZ*). These zones are used to define the alert criticality and change the advisory accordingly.

The *S&A* algorithms proposed in the literature differs depending on different design factors. First of all, the sensors used to detect the potential threats could be *cooperative*, when they enable exchange of information between the ownship and other aircraft (e.g., transponders mode *S* and *ADS-B*) and *non-cooperative* when they detect the threat without any form of communication with it (such as radar and cameras). The airspace zone in which the collision risk is searched could be a bidimensional plane, such as the horizontal (*2D-H*) and the vertical (*2D-V*) one, or a threedimensional (*3D*). Different models are moreover used for projecting the threat state in the future and detecting the conflict risks (*straight projection*, *worst case projection*, *probabilistic methods* and *path plan sharing*). The situations in which more conflict risks are detected can be moreover solved sequentially in pairs, as in *single conflict management*, or handled simultaneously, i.e. *multiple conflict management*.

The *S&A* algorithms differs also regarding the constraints considered in the resolution maneouvre evaluation, such as vehicle manoeuvering capabilities, right of way rules and latency caused by the operator involvement. Finally, the type of resolution manoeuvre (speed changes, lateral and/or vertical manoeuvres) and the method used for its evaluation are design factors of the *S&A* system. The final solution should be chosen as a trade-off between the complexity of computations performed by the algorithm and the time available to safely resolve the conflict. It is also very important to define the layout of the *GCS* in order to allow an easier and more effective understanding of the *S&A* advisories by the operator. The final design of the *S&A* system should also take into account certification requirements, limitations and performances of the technologies employed. It should moreover take into account the level of autonomy of the *UAS*. All these factors might make it impossible to develop just one *S&A* system standard and hence require different implementations might be required for different *UAVs*.

CHAPTER 4

Previous Works on *GCS* and *S&A* Integration

The sensory isolation of the operator from the *UAV* results in a reduction in his/her situation awareness (see sections 1.4 and 1.5 in chapter 1). The *GCS* plays a significant role in supporting and carrying out the mission successfully. It should therefore be designed to increase the effectiveness of communications between *UAS* and operator, minimize the operator workload and the mental load to extract and process the information.

This chapter covers some general considerations about the design of information displays on *GCS* and main solutions proposed in the literature. More precisely, section 4.1 defines the requirements in terms of information provided for a *GCS* display set. In section 4.2, the issues related with the design of the *GCS* taking into account the human operator nature are identified. Some guidelines to reduce the operator workload are then defined in section 4.3. The description of the *PFD*, a standard instrument commonly used in manned and unmanned aviation to display the flight condition information is given in section 4.4. Section 4.5 defines some useful guidelines to be considered in the design of the *S&A* system displays to be integrated in the *GCS*. The last sections describes then the *HMI* solutions proposed in literature to increase the operator situation awareness in *GCSs*.

4.1 *GCS* and situation awareness

One of the main tasks of *GCS* is to support the operator situation awareness, as defined in section 1.5. In *UASs* the level 1 of situation awareness deals with the knowledge about:

mission, including flight plan and targets;
hazards, including terrain, obstacles, threats, airspace restrictions, traffic and weather;
performances, including datalink coverage and sensor capabilities.

The level 2 of situation awareness requires the integration of these aspects to allow the operator to perform the following functions necessary for mission accomplishment [120]:

- monitor/assure conformance with timing constraints in the air tasking order

and the airspace control order;
- monitor/assure conformance with vehicle endurance constraints;
- monitor/assure separation with terrain;
- comply with datalink constraints (coverage and link availability);
- assure planning within payload parameter constraints;
- monitor/assure deconfliction with traffic and restricted areas;
- monitor/assure deconfliction with known threat areas and adverse weather;
- comply with contingency plans for system failures and degradations.

The *GCS* must moreover support the operator in understanding the effects of changes in the expected environment on the future situation, that is the level 3 situation awareness [120]. This imply that, when new information become available and/or the mission changes[1], the *GCS* must support the operator in the accomplishment of the following tasks:

- analyse the options, determine the overall impact of the choices or information, and assemble the required changes to the plan;
- decide on the choices;
- execute the re-planning.

From this point of view, automated prediction functions have to substitute the operator in the cognitive task related with the projection of the current status into the future. This is necessary because the high mental workload required from the operator required by this task. More precisely, these prediction functions are necessary to support the operator in evaluating:

- proximity of planned route to static constraints (terrain, obstacles, threat areas or restricted areas);
- conflict risk prediction with other traffic;
- the effect of plan changes on mission success during interactive re-planning, particularly regarding:
  - impact of changes on the time needed to reach the target,
  - impact of changes on assigned time slots in the area of interest,
  - impact of changes on loiter time and endurance.

Finally it is necessary to consider that the introduction of the automation in flight management tasks typical in civilian aviation is related with a number of further situation awareness related challenges [23]. This implies that the introduction of automation must be supported by a suitable design of the *GCS HMI*. From this point of view, it was pointed out in section 2.3 that the requirements in terms of information are different for a supervisory controller and for a manual controller [65]. More precisely, in a system based on manual control, the operator has direct control on the deviation from the performance, that he/she set on the *GCS*. In fact, he/she monitors directly the information regarding any deviation, particularly in terms of vehicle

[1] Generally speaking, the events requiring a reassessment of the plan and a possible operator action include [120] re-tasking required from mission controllers, *ATC* instructions, new threats, weather.

attitude, altitude, airspeed, and provides to the system the input necessary to return to the desired state. On the other hand, a supervisory control system, i.e. an *UAV* with a high level of autonomy, requires the operator to understand:

- the goals the automated systems are attempting to achieve,
- the control methods used to achieve those goals,
- the extent to which system performance matches operator expectations.

In fact, in this case the same automated system performs the inner loop control functions, i.e. control surface activation. Therefore the information regarding the automated systems operations are more important than the aircraft attitude and airspeed [65]. These include information about:

- automated system status, i.e. its operating mode,
- system goals, i.e. the performance targets,
- flight control computer functions, such as controls operating range limitation according to flight envelope limits.

4.2 *UAS* and Operator

The development of a *GCS* integrating all the functionalities defined in the previous section includes several *HMI* aspects [121]. First of all, as stated in [122], it is necessary to take into account the performances of the sources used to feed its indicators[2]. Moreover, also the bandwidth and the latency time of the communications link between the *UAV* and the *GCS* influences the quality of visual sensor information[3] communicated to the *UAS* operator.

The guiding principles derived from airworthiness criteria must aim to minimise human error and workload both in normal and adverse operating conditions. From this point of view, the number, the type and the layout of displays are important parameters. Moreover, the warning indications must be properly included. Handling of emergency procedures has also to be taken into account. The colour coding used in the displays should be based on relevant existing criteria of manned aircraft. In the *GCS* design, it is necessary to define also the minimum number of *UAS* operators necessary for safe operations. Finally, it is fundamental to identify the parameters related to flight safety that need to be displayed, including also those related to specific *UAS* features such as communication link status [121].

Table 2.1 (see chapter 2, page 25 defines the *UAVs* flight control mode classification in which the various levels identified are shades varying between the two following extremes:

[2]E.g. spatial and temporal resolutions provided from the sensors, field of view provided from the cameras etc.

[3]E.g. temporal and spatial resolution, color capabilities and field of view of visual displays, data transmission delays

- the operator acts as a pilot and flies the *UAV* and navigates from waypoint to waypoint [123];
- the operator is simply a supervisor (see description in section 2.3 of chapter 2), who monitors the *UAS* while it performs its mission as per the flight plan previously set by the operator.

As described in section 4.1, it should be noted that the second case too could lead to conditions in which the operator has to take over control of the system and replan the flight route.

In such a condition the presence of the human operator as agent inside of the *UAS* introduces significant issues. These are related to the multiple tasks delegated to the human operator[4]. The multiple tasks are based on all four stages of the human information processing system including sensory input, perception/cognition, selection of action and execution of action [123]. These stages compete for the same attentional resources when they are performed concurrently. In fact, according to Dixon [123]:

> "For example, while on a reconnaissance mission, an *UAS* operator must scan a map (stage 1) in order to determine where the ownship is and where the next waypoint is located (stage 2), determine which direction to fly to (stage 3), and then proceed towards the next waypoint (stage 4). These four stages must be repeated constantly throughout all mission requirements, whether occurring serially or simultaneously."

Therefore, considering that many of these tasks are based on the same overlapping information processing resources, the operator capability is often unable to satisfy the resource demand. This causes task interference and performance degradation. Furthermore, monitoring aircraft parameters requires a significant amount of mental resources. The operator has to monitor constantly the system gauges for possible problems or failures[5]. Once a problem is detected, the operator has to perform the appropriate diagnosis, and then undertake the necessary action to address the the fault and protect the aircraft and the mission integrity.

4.3 *GCS* Design Guidelines

The operator workload described in the previous section can be reduced by implementing *GCS* displays supporting both display salience and easy extraction of critical information [65]. Previous research showed that automated system complexity and autonomy are difficult to be understood by operators. This lack of knowledge about the automated system performance makes difficult for him/her to identify relevant displays and/or interpret correctly system information. As a result the performance

[4] Some issues also applies to *UAS* manually flown, *i.e.* *UAS* with low-level automation.

[5] *e.g. icing on the wings, low fuel levels, etc* [123]

Figure 4.1: the *GCS C4I System*, a generic *GCS* for controlling various unmanned vehicle missions in real-time developed by *Aeronautics*. Source: [124]

of the operator in monitoring the complete system is reduced. Therefore *GCS* displays has to be designed in such a way as to guide the operator attention to critical information.

Generally a *GCS* includes a set of computer display screens, similar to those shown in fig. 4.1. They display most of the information available in a conventional aircraft cockpit together with some *UAS* specific information such as communication links and systems status. This large amount of information competes for display space. Therefore intelligent display technology or cueing techniques are necessary to direct operator attention to divergent information[6]. It is moreover important to define the information that must always be visible due to their importance[7].

Moreover, a *GCS* must also be designed in order to minimise the workload re-

[6]Branching menu structure are a widespread example of these techniques. They offer the advantage of having much of the information not visible. In fact, high volume of information available previously demonstrated to make difficult for the operator to retrieve important information in *GCSs* (keyhole effect).

[7]E.g. the attitude of the aircraft is such a critical information that it is required from the certification to be standby display information.

quired to extract the relevant information, usually called *information access cost*[8]. The information access costs can be minimised by [65]:

- automatically indicating relevant information,
- integrating dimensions,
- ensuring display methods compatible with the type of information displayed.

Reconfigurable displays offer the advantage to allow the operator to change the display elements according to his/her preferences. This allows the operator to adapt the displays in order to optimise the display control strategy. On the other hand, too much control of the display elements may produce configurations which are not optimal for some tasks[9]. Therefore it is also necessary to identify the displays that can be reconfigured without jeopardising system performance or safety [65].

4.4 Primary Flight Display

A component that is always present both in manned aircraft cockpits and *UAS GCS* is the *Primary Flight Display (PFD)* (see fig. 4.2). It provides in one integrated display the data provided by primary flight instruments, navigation instruments and status of flight [125]. In some cases it includes also powerplant information and other systems information.

The layout of *PFDs* is quite standardised nowadays in available commercial models and include:

attitude indicator is placed on central upper position and characterised by the conventional round-dial presentation used for artificial horizon;

airspeed/altitude indicators are given by vertical tape displays placed on the left and right sides of the attitude indicator;

vertical speed indicator is usually placed on the right of the altitude indicator with the classic analog presentation;

turn coordination is shown on a round-dial instrument using a segmented triangle near the top of the attitude indicator;

heading indicator is based on the round-dial gauge conventionally used for directional gyros displaying also some navigation informations and is placed on the bottom of the attitude indicator;

[8] From this point of view, multi-menu displays are affected by additional data management demands because the operator must determine [65]:

- what information is desired,
- where the information is located and
- how to access that information.

[9] E.g. the caution or warning information should not in any condition be moved out of the operators primary field of view in order to allow a timely operator intervention [65].

Figure 4.2: typical layout of a *PFD*. Source: [125]

rate-of-turn indicator is implemented by a curved line display on top of the heading indicator.

The *PFD* aims to provide the pilot the same information given by the conventional instruments in terms of ease and understanding of aircraft behaviour. This task is accomplished without changing the standardised way in which the pilot scans the instruments[10] during flight phases based on attitude instruments. However, some training is still required for the pilots to find the information on the *PFD* and to interpret them correctly.

A common problem for experienced pilots used to conventional flight instruments is that *PFD* induce deviations from assigned altitudes when they have their first experiences with the tape display presentation of altitude information typical of *PFD*. Another common problem for pilots operating with *PFD* is the fact that they tend to fixate and attempt to correct small deviations, with the risk of allowing significant deviations of other parameters.

On the other hand *PFDs* offer some enhancements when compared with conven-

[10]This is defined in the document *Instrument Flying Handbook* issued by *FAA* in the advisory circularAC 61-27c.

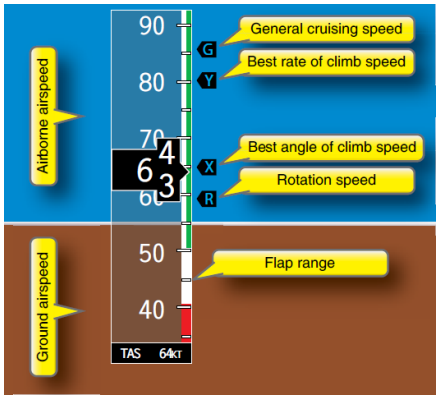

Figure 4.3: vertical airspeed indicator on a *PFD* with reference speeds and operating ranges visualisation. Source: [125]

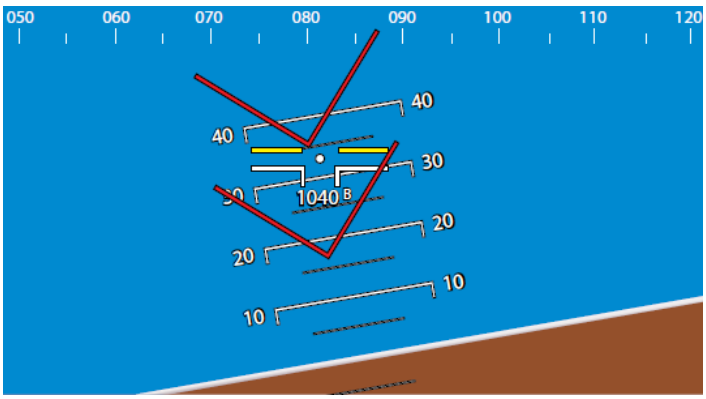

Figure 4.4: symbols implemented on the attitude indicator of a *PFD* to assist in recovery from unusual attitude. Source: [125]

tional primary flight instruments. As shown in fig. 4.3, some *PFDs* include an airspeed indicator displaying reference speeds and operating ranges for the aircraft. Depiction of operating ranges is based on the usual red-green color coding. Moreover, the attitude indicator of a *PFD* can depict red symbols to assist in recovery from unusual attitudes, as shown in fig. 4.4. In this figure, the symbols on the display advising the pilot to lower the pitch attitude.

Trend indicators, which process data to predict and display future performance, are valuable enhancements that can be included in *PFD*. For example, some *PFD* are characterised by *trend vectors*, predicting aircrafts airspeed, altitude, and bank angle up to several seconds into the future.

Morever, *PFDs* offers the advantage of combining "several navigation instruments into a single presentation" [125]. As can be seen in fig. 4.2, these instrument are included in the heading indicator by means of two navigation indicators: a course deviation indicator and a bearing pointer. Those indicators can be linked to many navigation systems available in the aircraft, including *Global Positioning System (GPS)*, *Instrument landing system (ILS)* and *VHF Omnidirectional Range (VOR)*.

Finally a very important feature of the *PFD* is the possibility of displaying to the pilot the information collected from other aircraft systems in a single integrated display. An example is given in fig. 4.5 where the the next waypoint in the planned flight route, the distance and bearing to the waypoint, and the current ground track are shown in the bar on top of the attitude indicator. Moreover, the value of the *Outside Air Temperature (OAT)* is also given in the lower left corner of the display. The transponder code and status are displayed with current time in the lower right corner. The *PFD* in fig. 4.5 enables the pilot to set the communication and navigation radio frequencies on upper zone of the display.

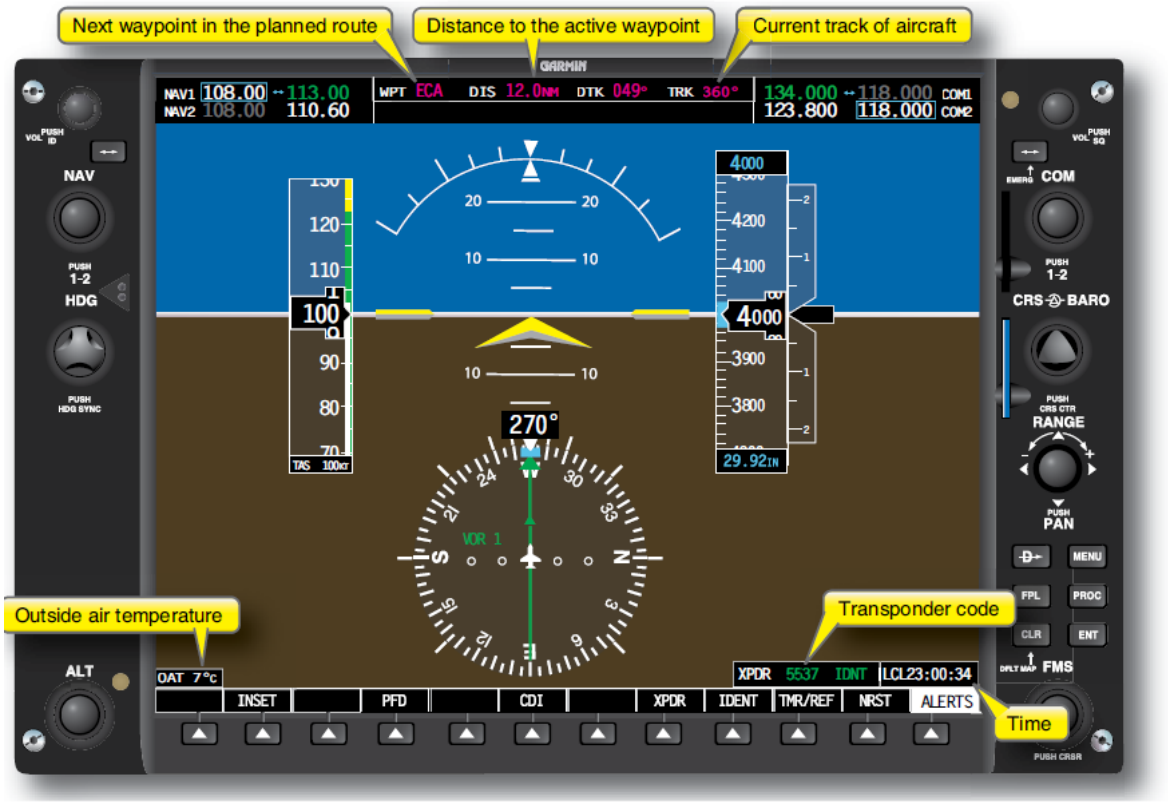

Figure 4.5: identification of the items used in *PFD* for communication of flight status information. Source: [125]

4.5 *S&A* Display Design Guidelines

Among the information requirements for the *GCS* as defined in section 4.1 and which is of paramount importance is communicating to the operator of any advisories produced by the *S&A* system. The most common way to implement this is by means of a graphical display. Generally speaking a *HMI* integrating the *S&A* system advisories should support all the tasks defined in chapter 3, section 3.1.

In fact, as stated in [126], the use of separate alerting and display philosophies for warnings about time-critical external conditions, such as terrain, traffic, wind shear, clear air turbulence and wake vortices bring two main issues both in unmanned and manned aviation:

lack of integration among the alerting systems, giving rise to alert proliferation and potential conflicting and contradictory information;

lack of strategic information about the alerts, that fails on providing operators with resources, i.e. predictive situation awareness and planning ahead, and time to prepare for or avoid emerging situations

In the particular case of manned aviation, the availability of strategic information for

look-ahead prediction, planning, and situation awareness is noticeably absent among the abundance of information provided on the flight deck. More precisely, even though pilots are briefed about an hour prior to their planned departure concerning forecasts, advisories, and expected delays, they operate in a dynamic environment in which conditions are continuosly changing. Pilots generally have access to real-time tactical weather information via their weather radar systems and by looking out the windscreen. For up-to-date strategic information, pilots rely on supplemental information from the *Automated Flight Service Station (AFSS)* briefing facilities, communications with *ATC*, dispatch, and the *party line*, by which pilots overhear other airspace users reporting current conditions. However, these information are presented verbally or textually and need to be processed, integrated, and visualised by the crew to understand the relevance to their current flight plan. This increases therefore the pilot workload.

On the other hand, if the pilot/*UAV* operator is updated about developing conditions it might be possible that potential cautions and warnings can be avoided. Despite today's manned aircraft having integrated alerting systems for conditions inside the aircraft, e.g. *Electronic Centralised Aircraft Monitor (ECAM)*, *Engine-Indicating and Crew-Alerting System (EICAS)*, there is no comparable fully integrated alerting system for conditions detected outside of the aircraft. An integrated alerting system have to deconflict alerts, and present information in an integrated manner. This concept have to be based on the application of human-centered guidelines and on the development of a consistent philosophy for designing the components of an aural and visual alerting system. Key aspects of this concept are:

- ability to de-conflict currently separate alerts such as *TCAS* and *TAWS*;
- categorisation (weather, traffic, ground, other) and prioritisation (time-critical, tactical and strategic) of alerts to reduce operator information processing requirements;
- directional, multidimensional aural cueing to allow quick *pre-processing* of the condition[11];
- integrated graphical presentation of conditions external to the aircraft to support better situation awareness: the system have to merge information from independent alerting systems enabling multiple alerts of external conditions to be prioritised and de-conflicted before presenting them to the crew.

The goal of this approach is to support prompt, appropriate responses to adverse conditions based on good situation awareness.

In the following sections some general notes about the main solutions proposed in literature for displays supporting operator situation awareness and integrating *S&A* advisories are presented. From the point of view of general layout, two possible implementation of the *S&A* system *HMI* are described in [106]. The first is obtained by the conformal integration of the *S&A* probing data in the *Navigation Display (ND)*, with a

[11]This characteristics is effective in supporting the operator in time-critical responses and in deciding the priority of the alerted condition relative to the on-going task

solution similar to that proposed in section 4.7, and the *Head-Up Display (HUD)*, that will be described in section 4.9. The latter is based on a dedicated probing display that continuosly supports level 3 traffic awareness, showing to the operator the potential effects of manoeuvres in terms of conflict risks. This is a more refined solution than the conventional *Cockpit Display on Traffic Information (CDTI)*, described in section 4.6. Section 4.10 of this chapter covers then *Augmented Reality Displays (ARDs)*, an evolution of *Synthetic Vision System (SVS)* integrating *HUD* advantages. Some notes on the cognitive tunneling are outlined in section 4.11. Finally a short discussion about the multimodal displays concept is presented in section 4.12.

4.6 *CDTI*

The *CDTI*, first introduced in manned aviation, displays the horizontal and vertical positions relative to the ownship of nearby traffic (e.g. in fig. 4.6). It moreover shows the traffic information status related to proximity of traffic, *TAs* and *RAs* [87]. As explained in [87, 127], the *CDTI* has the primary purpose of *attention cue* and as a secondary purpose *tactical guidance display*. It is an *attention cue*, because it supports the pilot in visually acquiring the transponder equipped aircraft in the surrounding airspace. In fact, it informs the pilot about the region of the surrounding airspace within which to look for other aircraft. It supports therefore a faster and more accurate detection. The *tactical guidance display* is related with the capability of the *CDTI* to display to the pilot the proper system operation, and to inform him/her on time to prepare to manoeuvre the aircraft if a *RA* is issued.

Both colours and shapes are used to assist the pilot in the information interpretation. On the dark background the ownship is a white or cyan (light blue) aircraft-like symbol. Its location on the display depend on the display implementation. The symbols used for the other detected aircraft are displayed according to relative positions in respect with the ownship and symbology depends on the threat status as shown in fig. 4.7 [87]:

- solid red square for threats (i.e. aircraft which trigger an RA).
- solid yellow or amber circle for intruding aircraft (i.e. aircraft which trigger a *TA*).
- solid cyan (light blue) or white diamond for proximate traffic.
- hollow cyan (light blue) or white diamond (the colour is distinct from the ownship symbol, i.e. if one is cyan the other is white, and vice versa) for other traffic.

The solid white or cyan (light blue) diamond used for proximate traffic identified as non-intruding aircraft within 6 NM and 1200 ft from the ownship has a particular function. If an advisory is issued, it indicates that the aircraft is not the intruding aircraft generating the advisory, considering that the closest traffic might not necessarily be the most threatening. When the transponder of the detected aircraft is able

Figure 4.6: *CDTI* example. Source: [87]

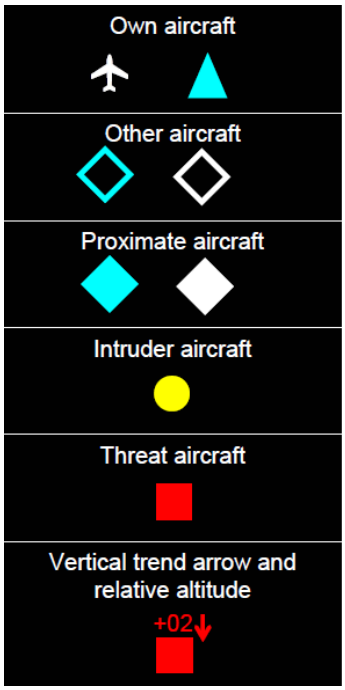

Figure 4.7: standardised *CDTI* traffic symbology. Source: [87]

to report altitude, the relative altitude or flight level of this aircraft is displayed in hundreds of feet. This value is placed above the detected aircraft symbol if this is at an higher altitude than the ownship and below the symbol in the opposite case. Moreover an arrow shows when the detected aircraft is climbing or descending with a vertical speed greater or equal to 500 ft min^{-1}.

4.7 2D Planner Display

According to the experimental work done in [120], a planner touch screen displaying a map with the current *UAV* position and the flightplan, if it integrates the layers of information considered in the previous section (traffic, terrain, available airspace and weather layers), then it might be suitable for providing level 1 and level 2 situation awareness to the operator [128].

Traffic depiction must provide real-time information about type of aircraft (e.g. *Identification Friend or Foe (IFF)*, manned or unmanned aircraft), its position and the flight parameters, including altitude, airspeed and heading. A symbology and advisories syntax consistent with *TCAS* systems must be used for this layer [19]. In fact, even though *TCAS* symbology, described in section 4.6, does not provide all the information required for adequate *UAV* operators situation awareness, *TCAS* symbols and colours provides an useful benchmark that is familiar to *UAS* operators/pilots and

hence it is less confusing.

An user-activated terrain overlay is necessary for terrain awareness. Indeed, terrain morphology has to be always taken into account during re-routing. A good example, cited in [128], is the case in which the weather conditions reduce the flight ceiling so much that makes it difficult to avoid the terrain). More precisely, as explained in [129], terrain presentation on a *GCS* display is useful to increase the awareness of operators regarding the surrounding terrain. It allow him/her moreover to use terrain data for navigation and guidance purposes. From this point of view, understanding the overall shape of the terrain is important to ensure collision avoidance in all flight conditions with or without the presence of any other factors (e.g. weather conditions). The knowledge of this information is necessary to recognise and execute avoidance manoeuvres when the related advisory is not provided by on-board systems. A widespread solution to this issue is to display terrain separation violations by means of a color coding of the map, in order to distiguinsh terrain below, close or above current flight level. It was experimentally found in [120] that this approach, similarly to the convention used in *TAWS* as described in section 3.6, provides an effective indication of terrain clearance. Furthermore for *UAS* operations, this layer should include [128]:

- a *Loss of Separation (LoS)* indicator to show terrain that could mask the control signal if the *UAV* is below a certain altitude;
- a pop-up display to show areas where the terrain could mask the control signal given the *UAV*'s present altitude;
- a 3-D display with a variable viewing angle, or a separate top-down display with a corresponding profile view.

An user-activated overlay have to be provided to indicate the airspace areas that can be used by the *UAV* for accomplishing its mission. Finally, another selective overlay displaying current radar and satellite information about weather hazards, such as thunderstorms, rain, dust, cloud layers, and freezing temperature boundaries should be provided.

This planar display has the advantage of allowing easier and more precise horizontal and vertical judgments than 3D displays, (that will be covered more in detail in section 4.8). This is due to the faithful axis representation [130] and to the fact that the bearing information for threats [19] are easy to extract.

On the other hand, there is the risk that such a display, so similar to a *CDTI*, behaves as a head down *attention sink*. They divert *UAS* operator from controlling the outside world view [131]. More precisely, it was shown in the experiments described in [132] that pilots flying in a cockpit equipped with *CDTI* miss a significant part of the visible traffic and important outside events. This is caused by the added workload and the resulting *head-down* time related to the use of *CDTI*, that could be of substantial concern particularly for single operator operations.

4.8 Synthetic Vision System

The planner described in section 4.7, allows the operator to assess just two-dimensional manoeuvre given by a combination of track and flight path angle commands [133]. It does not show the vertical dimension integrated in the display. This was a reason for the development of perspective flight path displays, such as *SVSs*, as a supporting tool for flight guidance in manned aviation. This solution is highly valued by pilots [134]. It provides the pilot/*UAV* operator with a clear computer-generated perspective depiction of the out-of-cockpit view of the external environment ahead. It includes both physical (e.g. terrain and obstacles) and non-physical objects (e.g. flight path and airspace constraints, such as prohibited airspace) [19, 23] (see fig. 4.8). The information are taken from high-resolution terrain databases, advanced sensors for database integrity and object detection, *ADS-B* traffic broadcasting systems, and satellite navigational systems, e.g. *GPS* [130]. The result of this solution is a clear view of the forward view equivalent to that of a bright, clear, sunny day, regardless of the outside weather conditions [135]. It includes various types of data, such as [23]:

- ownship state and status in a format similar to the *PFD* described in section 4.4;
- 4D navigation plan and task/payload plan;
- digital charts and maps;
- terrain elevation data;
- obstacle data;
- other traffic, enabling the possibility to see and avoid other aircraft;
- weather data;
- *ATC*-instructions;
- temporary changes and restrictions;
- real-time sensor data (e.g. radar, video/IR), providing up-to-date information about areas of interest and danger zones.

Moreover *SVS* usually includes a depiction of planned trajectory from a 3D perspective to support guidance and control [130]. This predictive display, with both aircraft prediction and flight path preview information, reduces pilot mental workload [136].

Furthermore, as explained in [137], *SVS* is designed in order to get enough redundancy of informations to prevent the pilots from misinterpreting the presented data. Considering altitude, a first clue is provided by the size of the terrain surface grid allowing an estimation of the altitude above the ground at a first glance. Moreover the glide slope channel provides a very precise graphical estimation of the required altitude for precision approach. Finally a digital readout of the exact value is provided for both altitude and airspeed in their scale. Similarly to altitude, the visual flow field (especially the grid) gives to the pilot an indication of the actual speed change. A spatial flight path predictor and a predetermined flight path indicator are included to support the pilot in understanding situation and provide a complete situation awareness. The quick situation awareness produced by this system increases pilot's reaction

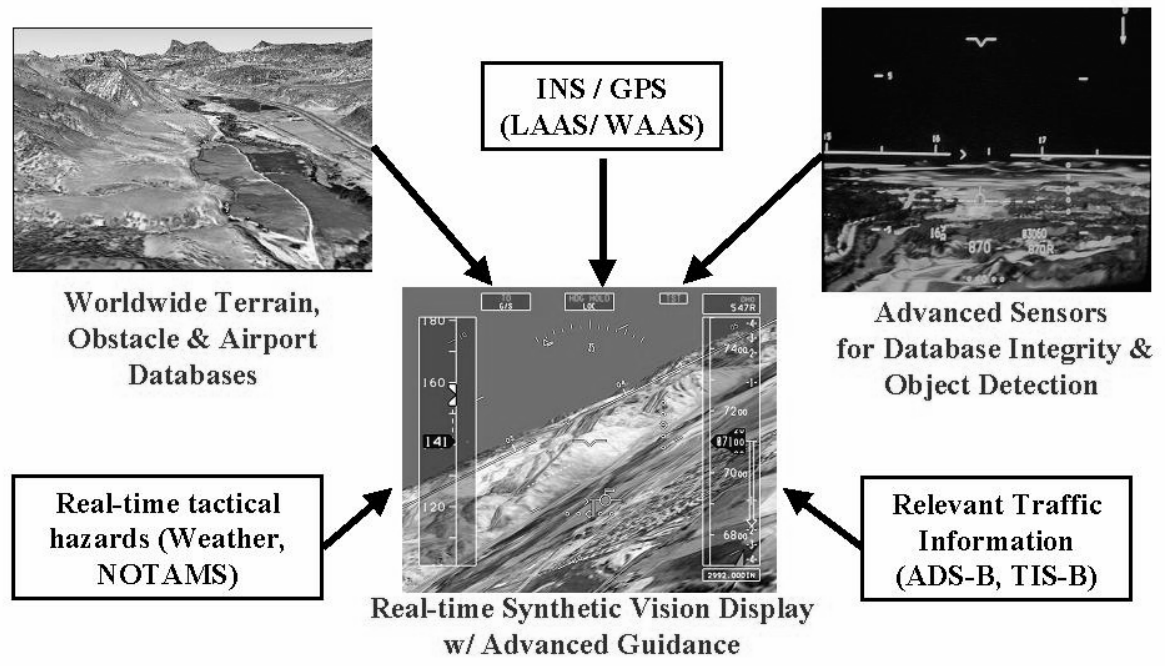

Figure 4.8: identification of the information layers included in a *SVS* display. Source: [130]

promptness allowing precision approaches and landings in adverse weather conditions. Finally, the predictor length and color change as function of aircraft speed in order to provide an additional *continuous feedback*.

4.8.1 *SVSs* in *UASs*

The *SVS* main advantage is the compatibility with the pilot view. In fact, 3D perspective display are closer to the pilot's *world view* rather than 2D planar displays [136]. For this reason 3D displays exhibit improved tracking performance, better situation awareness and lower workload particularly for complex paths in respect with conventional display formats [134, 138]. Moreover, this advantage is particularly perceivable regarding outside world traffic – and, of course terrain conflict risks – detection [120, 127]. Moreover, the situation awareness is better improved with a 3D display than 2D coplanar displays for pilot tasks involving comparisons between the display and the outside view.

Just to summarise, in manned aviation, *SVSs* were introduced to:

- increase situation awareness [23, 120, 135],
- support the pilot during limited visibility conditions [23, 130, 135, 139],
- increase terrain awareness and reduce therefore the likelihood of *Controlled Flight into Terrain (CFIT)* accidents [130, 134, 140],
- enhance aircraft operational capabilities [139].

Moreover, information requirements for navigation, guidance and control of manned aircraft and *UAV* are the main reasons for using *SVSs* for *UAS* operator support [63]. Key characteristics for an effective implementation of *SVSs* concepts to *UAVs* is the use of integrated data presentation to support the operator in obtaining level 2 situation awareness in addition to the immediate feedback on expected future effects of changes to the situation to support level 3 situation awareness.

In the domain of information presentation, *SVSs* offers advantages for *UAS* in terms of *augmentation of the sensor view* and *visualisation of non-physical constraints*. *Augmentation of the sensor view* is related with the anticipation of environment features and the compensation for the effects of sensor limitations such as field of view, effective range and occlusion[12]. It can be obtained by:

- increasing field of view,
- adding symbology to support enhanced visual acquisition,
- depiction of elements not (yet) available in the sensor image,
- guidance augmentation,
- integration of *Enhanced Vision System (EVS)* sensor image,
- integrated depiction of the planned path to improve manual control with a representation based on a virtual tunnel,

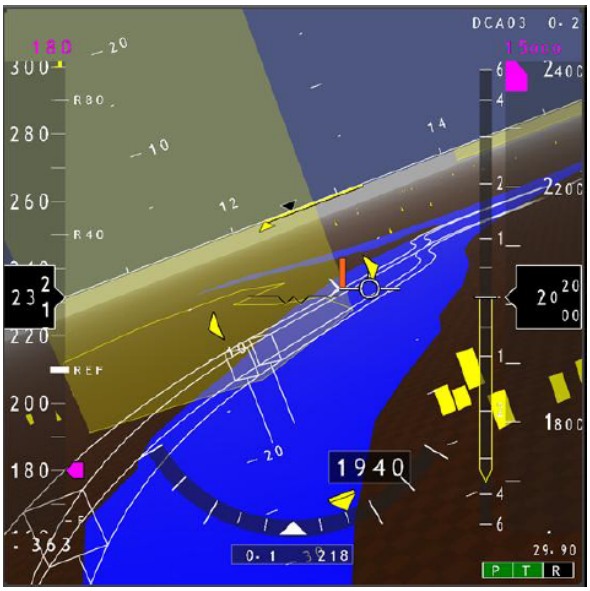

Figure 4.9: *SVS* display with integrated depiction of airspace constraints: the yellow cylinders show their location. Source: [63]

The *visualisation of non-physical constraints* is the the graphical depiction of *SVS* terrain and obstacles in an ego-centered reference frame (e.g. threat volume depiction). It has the advantage of producing a mental spatial picture of the situation more accurate than non-physical constraints (e.g. restricted airspace) specified as textual messages. Therefore a spatially integrated presentation of physical constraints in *SVSs* through the depiction of 3D volumetric objects could be used for non-physical constraints such as the boundaries of exclusionary airspace. The integration of information regarding special-use airspace into the guidance and the navigation displays has already been used in commercial aviation to increase operator's situation awareness during approaches in which he/she flies close to prohibited airspace (see fig. 4.9).

In the domain of functionalities, *SVSs* provide *flight path de-confliction with terrain during planning* and *predictive look-ahead terrain alerting capability* [63]. The first

[12] caused, e.g. by clouds, precipitation, smoke or terrain

functionality consists in the use of the terrain elevation database to detect separation violations of the desired path in the planning phase and correct them during the planning process. The latter is useful to increase safety during off-path flight phases. This function can provide a timely warning for terrain separation violations when the aircraft has to deviate from a conflict-free planned path based on future path prediction and terrain elevation database.

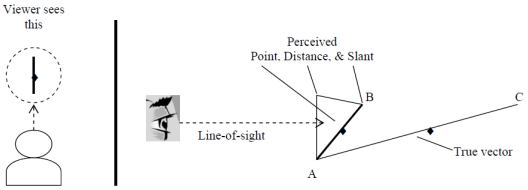

Figure 4.10: depiction of the slant underestimation effect. Source: [130]

4.8.2 *SVS* ambiguities

On the other hand, the 3D displays have also some drawbacks and limitations. More precisely, they are characterised by the following ambiguities [130]:

- slant underestimation,
- compression effect,
- line-of-sight ambiguity effect.

As displayed in fig. 4.10, the *slant underestimation* is related with the human tendency "to perceive a slanted surface within a 3D display to have a smaller angle (relative to the vertical) than it actually does" [130]. It is thought that this bias is the cause for pilots tendency to select descending manoeuvres when avoiding conflicts within a 3D display, similar to that shown in fig. 4.11. The effect of this bias might be decreased by adding depth cues to the display.

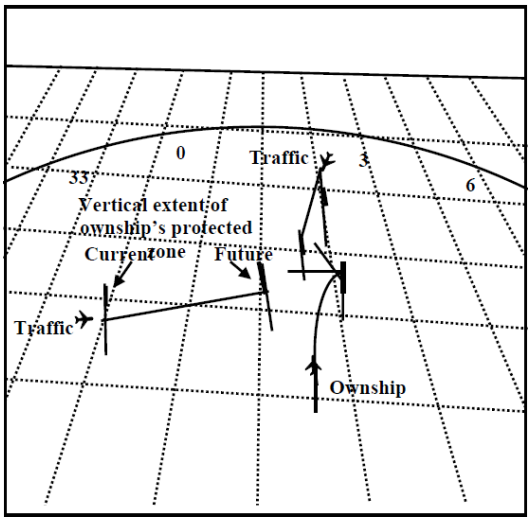

Figure 4.11: schematic representation of a 3D traffic display. Source: [130]

Compression effect is sketched in fig. 4.12. It is the compression of at least two or three axes of a 3D world that is necessary when displayed on a 2D screen. The resolution of position along an axis is a decreasing function of its amount of compression. This reduction in resolution usually produces bias in estimating distances along the compressed axis because of the small number of pixels and of the small visual angle. Therefore it might be necessary to spend more cognitive effort to get an accurate estimation of distances and positions along this compressed axis (possibly to

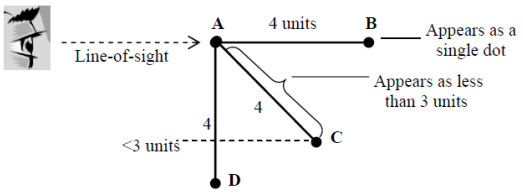

Figure 4.12: effect of compression: three line segments of equal length but at different orientations appear with different lengths. Source: [130]

mentally *stretch* it to its uncompressed state). Of course, the accuracy of estimation obtained from the *mental stretching* depends on the accuracy of the transformation of the compressed axis to its uncompressed state.

The *line-of-sight ambiguity effect* is the reduction of "the amount of linear information available within a visible vector as that vector approaches the line-of-sight viewing axis" [130], as illustrated in fig. 4.13. This ambiguity degrades the estimation of the distance and the absolute position orthogonal to the viewing plane of objects in the display. It makes it more difficult to judge the location of traffic, weather, terrain hazards and to determine the future position of traffic with respect to ownship.

From a general point of view, it might be more difficult for the pilot to judge the precise location and trajectory of aircraft based on a 3D display [141, 142]. Moreover, 3D displays seem to produce higher mental workload for the pilots than 2d coplanar displays [141] This is probably caused by the mental demand required by the rotations of vectors between ownship and traffic, that the pilots need to compensate for in 3D displays. Considering all these challenges, in order to communicate all this information about terrain, obstacles and adjacent air traffic, a *PFD* had to be complemented with a *ND* [120, 137]. In fact, the navigational awareness of a pilot or *UAS* operator is strongly influenced by "the ability to make a cognitive coupling between the *World Centered Reference Frame (WRF)* and the *Ego-centered Reference Frame (ERF)*" [23]. In particular, *ERF* displays are aligned with the vehicle movement and therefore no mental rotations of the presented information have to be made by the operator. This leads to a reduction in the probability of control reversal. However, *WRF* displays provide a stable reference frame in which the coordination between different vehicles or units can be monitored more easily. Therefore the *ERF* displays are more beneficial in situations demanding quick resolutions or manoeuvreing, while planning and other higher-level decision making are more effective on *WRF* displays.

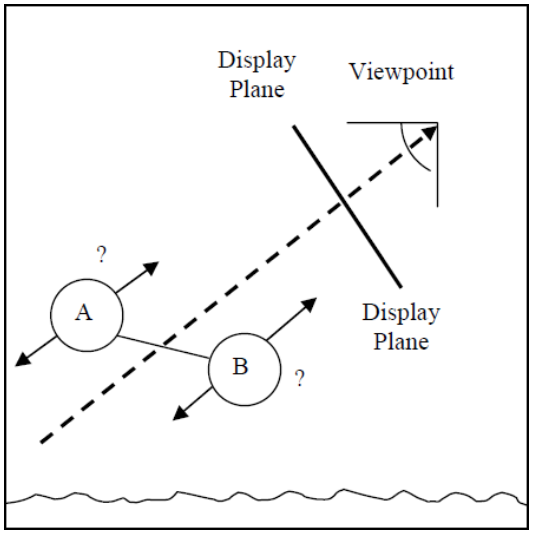

Figure 4.13: line-of-sight ambiguity effect: this side-view schematic shows the 3D display viewpoint, the line-of-sight viewing axis (dashed line) and two objects A and B. Their location along the viewing axis (distance), as well as orthogonal to the display plane (altitude), will be ambiguous to the viewer, as reflected by the "?". Source: [130]

4.9 Head-Up Display

In manned aviation, the *HUD*, such as that displayed in fig. 4.14, is a small see-through screen positioned just in front of pilot's line of sight looking ahead out of the aircraft. Precisely key flight instruments data are projected in a format similar to the *PFD* [143] previously described in section 4.4. In *UAS GCS* the same operating principle can be obtained simply by superposing on a transparent layer these data on the forward camera view. In manned aviation, it was developed for fighter jets in order to reduce the need for the pilot to monitor his/her instrument panel especially during complex manoeuvres [144], hence enabling the pilot to maintain an external lookout without losing access to key aircraft instrumentation [143]. This also enahnces situation awareness in limited (or night) visibility and in proximity of visible terrain, water, ground-based obstacles or other aircraft.

In civilian manned aviation this advantage is therefore most useful in the initial climb after take-off and also for the approach and landing phases of flight [143]. These are the flight manoeuvres involving the majority of all aircraft accidents [143]. These are also the conditions in which *HUD* visualize more effectively to the pilot any gaps between the required aircraft trajectory for a safe landing and the projection of the aircraft current status in the future [143, 145]. This conclusion is supported by a *Flight Safety Foundation (FSF)* study [146] that concluded that if a *HUD* had been fitted and operated by properly trained flight crew, it might have prevented or positively influenced 31% of total loss accidents and 29% of *major partial loss* accidents.

In *UAS* operations, this feature is particularly suitable for *RPVs*, which are usually employed in flight mission at much lower altitudes than manned aircraft. The benefits of *HUDs* compared to the usual cockpit instruments in manned aircraft are several and classified in the following three general categories [147] that applies also to *UAS*.

HUDs are usually collimated at optical infinity. This usually reduces, and sometimes removes, the problems related with visual re-accommodation and attention switching [149] between the instrument view and the out of cockpit view, necessary for tasks like traffic monitoring or to confirm cleared runway.

Since *HUDs are superimposed over the outside world*, they reduce the amount of visual scanning necessary to monitor both instruments and outside world domain for events that might occur, therefore reducing the risk that an event may occur in one domain (instrument panel or outside world), while the pilot is monitoring the other. This risk would therefore leave the event to be detected by peripheral vision, then unproperly detected, or to be undetected until the pilot takes a look to the previously unattended domain. *HUD* can reduce this problem, although it cannot eliminate it. The "simultaneous viewing of two overlaid scenes does not guarantee simultaneous detection of events in both scenes" [147].

HUD information can be configured such that it overlays its far domain counterpart. This could be useful for piloting tasks requiring specific integration of information between the two domains. When this configuration is used for the *HUD*, its imagery

Figure 4.14: example of a typical *HUD* display. Source: [148]

is identified as *conformal imagery*, since it conforms to features of the outside world [149]. Examples of this are:

- the horizon line that overlays the true horizon [147],
- a flight path velocity vector in the forward view [149],
- the depiction of the planned trajectory with a virtual tunnel [149],
- the runway overlay that superposing the trapezoid formed by a true runway [147].

The advantages of conformal symbology affect not only the tasks of focusing attention on both near and far domain events (e.g. airspeed monitoring, traffic monitoring) but flight path control also [149]. The use of conformal symbology may moreover reinforce other motion cues and benefit information retrieval [150].

On the other hand, these benefits are obtained at the cost of cluttering the view with overlapping images. These could mask events or relevant information (e.g. critical hazards on forward flight path in the far domain could be obscured by *HUD* imagery, or the processing of that imagery itself might be corrupted by the view of the far domain beyond the aircraft, such as terrain or clouds [149]). This phenomenon could also be due to perceptual or cognitive masking, that cause some objects in a visual scene with many overlapping images to become difficult to detect despite they are not totally obscured [147].

However, as stated in [149], in the comparisons of head-up versus head-down presentation of identically formatted instrumentation the costs of scanning (head down) are greater than the costs of the clutter from overlapping imagery (head up). The implementation and use of *HUD* technology produces therefore an overall benefit for most tasks. This is particularly true for confomal *HUDs*.

4.10 Augmented Reality Display

The video imagery from various cameras mounted on the *UAV* is particularly valuable for the *UAS* operator situation awareness, mainly regarding tasks such as [150]:

- verify clear path for taxi/runway operations,
- scan for other air traffic in the area,
- identify navigational landmarks and potential obstructions,
- perform a wide variety of intelligence, surveillance and reconnaissance activities, in the case of gimbal-mounted cameras.

However, the quality of the video imagery can be compromised by factors such as [150]:

- narrow camera field-of-view,
- datalink degradations,
- poor environmental conditions (e.g. dawn/dusk/night, adverse weather, variable clouds),
- bandwidth limitations,
- highly cluttered visual scene (e.g. in urban areas or mountainous terrain).

Hence it could be reasoned that the *UAV* mission effectiveness should increase if the imagery interpretation is enhanced and made more robust under various operating conditions.

In *ARD* (see example in fig. 4.15), similarly to the *SVS*, spatially-relevant information are derived from databases (e.g. terrain, cultural features, maps etc.) and real-time information are updated by fusing other sources (e.g. intelligence assets, C2 sources etc.) and overlaid as conformal imagery onto the camera image [150]. The result is a set of computer-generated overlays *co-existing* with real objects viewed by the camera and highlight those points and regions of interest to the operator.

The idea of overlaying a synthetic vision system on a sensor image can have both a positive and negative impact. As stated in [150], previous studies demonstrated that the presentation of information generated from a computer in a conformal manner with sensor imagery on an unified display has the following advantages:

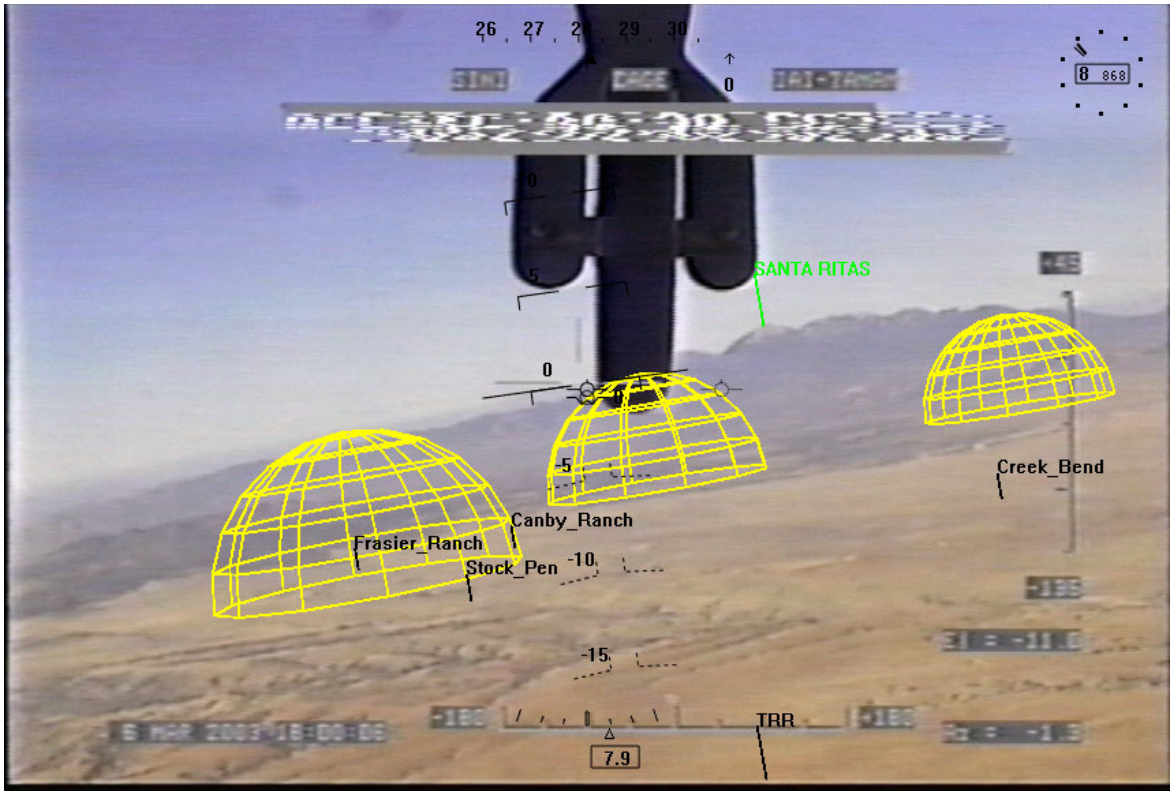

Figure 4.15: example of *ARD*. Source: [150]

- reduction of scanning time and effort required to access and monitor all the elements,
- reduction of need to mentally integrate spatial information from different sources,
- decrease of the workload related with attentional focus and management.

Generally speaking, *ARDs* are expected to have the following benefits both in manned and unmanned aviation [150]. They improve operator's situation awareness, by highlighting elements of interest on the camera image. They enhance therefore *UAS* operator interpretation of imagery, like location of threats, targets, landmarks, emergency airfields and position of friendly forces. By reducing negative video characteristics, they maintain the operator's situation awareness of the environment, if the video datalink is temporarily degraded or lost or the visibility is limited. Moreover *ARD* can include in *UAV* operations [150]:

- information unrelated with actual sensor imagery, such as threat lethality envelopes and indicators for ground target search and identification tasks associated with many *UAV* missions,
- self-motion cues and depth cues,
- flight guidance symbology, similar to the symbology of *HUDs* described in section 4.9, for reduced visibility conditions, especially during terminal flight

operations (*i.e.* landings).

Among others, the following two issues regarding *ARDs* must be considered [150]. The cluttering of information overlay may reduce the accuracy of sensor imagery processing. The data about objects not visible in real sensor imagery provided by synthetic vision overlays can increase the clutter (e.g. a threat that is hidden behind a mountain might be visible on the display, causing the operator's loss of the occlusion cues, which are important for depth perception).

However, from a general point of view, as stated in [150], previous work showed that the use of a separate display is related with a longer scanning time. This is a greater disadvantage than the additional clutter related with the imposition of the augmented reality layers onto existing camera view imagery.

4.11 Cognitive Tunneling

The *attentional tunneling* or *cognitive tunneling* is defined as the pilot tendency to focus his/her attention on the the near domain instrumentation, even if important signals appear in the far world domain [147]. Its direct consequence is the reduction of pilot's ability to detect unexpected events. In the particular case of *UAVs*, it could moreover involve the missed detection of unexpected, high-interest targets [150].

Some studies brought to evidence that this effect is stronger with *HUD* than head-down displays [140]. In the case of *HUDs*, it was suggested that the cognitive tunneling may be produced by the fact that the *HUD* symbology superimposed over the outside world view has a compelling nature, regardless its relevance to the flight task. Moreover, it was observed that the cognitive tunneling effect causes the pilot to focus his/her attention for an exceptionally long time on the near-domain information (*HUD* symbology). On the other hand, not even the minimal amount of attention was given to the far-domain (outside world), despite the unexpected events included in this domain. However, the effect is not limited to attention focusing and is typical of a variety of situations where one source of information with highly compelling information makes the pilot ignore other information sources, causing therefore a non-optimal information sampling pattern.

As stated in [149, 150], conformal symbology may cause a reduction of the incidence of the cognitive tunneling in *SVS*. In fact, conformal symbology makes it possible to integrate rather than superimpose augmented information into the visual scene. Moreover, it was suggested that a conformal *SVS* in which synthetic and real sensor information are grouped into one perceptual group should reduce the problems associated with attentional allocation and therefore cognitive tunneling [150][13]. On the other hand, an increase of the amount of information presented via synthetic vision

[13] According to [150]: "This is based on object-based models of visual attention that postulate that complex scenes are parsed into groups of objects, with attention focused on only one object at a time, with object groups defined by contours, color etc."

overlays could produce an increase of the cognitive tunneling risk by the operator.

4.12 Multimodal Display

When a *GCS* is equipped with visual displays presenting sensor information beyond those provided from a vehicle-mounted camera, the UAV operator may not be able to choose the optimal visual scanning strategy in order to compensate for the absence of multisensory cues [19]. In that case, the use of of *multimodal* (e.g. tactile or auditory) information displays could be more effective.

Multimodal systems have the advantage of providing the users with better expressive power, naturalness, flexibility and portability than conventional visual displays [151]. They are based on a set of communication channels. The use of different communication channels allows the simulataneous integration of various modalities, like visual display, audio, and tactile feedback. This enables the understanding of the display information by engaging the human perceptual, cognitive, and communication skills.

Previous studies showed that some aspects of flight control and system monitoring are improved by auditory and tactile displays [19]. Furthermore, the use of auditory information reduces the workload related with the visual scanning similar to that achieved with *HUD* overlay. On the other hand, contrarily to *HUD*, it is not characterised by any cost produced by the clutter and the use of peripheral vision to process both the *HUD* and the outside world layers of information [152]. This reduction of the visual scanning workload gives the pilot the possibility to allocate more attention to the complex visual tasks related to flight control (aviating) and traffic awareness (navigating) [127].

Generally speaking, multimodal displays reduce cognitive-perceptual workload levels [19]. This could be linked to the fact that the distribution of the total load across the auditory and visual channels makes easier the parallel processing than when the processing is concentrated within the visual system [127].

Moreover, the following advantages were found in previous studies [151]. The use of multimodal interfaces lead to an increase in the overall efficiency of interaction. More precisely, the amount of task-critical errors is reduced in multimodal interaction. Therefore the use of multimodal techniques is particularly suitable in highly interactive environments, such as the aircraft cockpit. Moreover, multimodal interfaces are flexible and can therefore be easily used by a wide range of users, to accomplish different tasks and in various environments. These include also adverse surroundings (aircraft cockpit, for example). It should be observed also that users prefer multimodal interactions, particularly when describing spatial information about location, number, orientation or shape of an object (spatial domain systems). Finally, the learning process for using multimodal interfaces is simplified by their greater naturalness and flexibility of interaction. This characteristic is particularly useful for flight simulator training.

Of course the message comprehension requires the operator to use an amount of working memory and the comprehension load increases with the length of the message [127]. This might causes some recall errors on long messages and thereby decreasing the readback accuracy in some instances. Therefore short message lengths need to be used to avoid an overload of the subject short-term memory [153].

According to previous research findings, short verbal and linguistic messages are inherently more compatibly delivered in the auditory, as aural messages, rather than in the visual channel, as written text messages [127]. This compatibility is related with the use of fewer resources which is a distinct advantage, particularly in multi-task situations. On the other hand, spatial information, such as those involved in target cueing, are less suited for the auditory channel. In fact, the auditory channel "is fundamentally temporal, not spatial in its characteristic" [127]. Therefore the auditory modality is not effective in providing target search and cueing information. This makes the use of separate resources not advantageous for the *CDTI*.

Moreover, a disadvantage of the auditory delivery of information is the *pre-emption*. The auditory modality behaves as an *attention sink* and has the intrinsic characteristic to capture the user attention and distract him/her from ongoing visual tasks [127]. This is the reason why the auditory modality is chosen for high priority alerts. A previous research shows moreover that "the auditory delivery of discrete information is more disruptive of ongoing visual tasks (e.g. tracking, visual monitoring or flight control), than is the visual delivery of the same information" [127]. For this reason previous studies found that in multi-task environment the performance obtained by the auditory delivery of information is not always superior to the visual delivery. Especially when considering the case of ongoing navigation and aviation tasks, it is inferior.

In particular in the case of traffic detection [127], it should be noted that the redundancy produced from the presence of both the auditory and visual information delivery channels does not lead to an improvement in communication to include all the advantages of the two communication channels. More precisely, the availability of the *echo* of the visual information channel provided by the *CDTI* avoids that communications are disrupted when the messages are too long. On the other hand, the availability of the auditory channel does not prevent the disruption of vertical flight path tracking when the traffic is detected. Moreover, it does not reduce the amount of looking at the data link display. It seems that the pilots feel the need "to cross check the visual display with the auditory message when the latter arrives" [127]. Therefore, the pilots have to be instructed or trained to avoid diverting their gaze due to the arrival of an auditory information, except if the retention of longer messages is considered not accurate.

4.13 Chapter Summary

The function of the *GCS* in a *UAS* operations is to support the operator situation awareness. This includes three levels. The first is the communication of mission data, hazards and *UAS* vehicle performance to the operator. The second level requires the operator to monitor the constraints regarding mission timing, airspace, vehicle endurance, terrain separation, datalink, payload, traffic restricted areas and weather. Finally, level 3 situation awareness requires the operator to understand the future effect of changes in the flight plan due to new information and changes in mission objectives. The *GCS* should moreover provide the operator with all the information necessary to effectively accomplish his/her task as a supervisory controller, when the *UAV* level of autonomy is very high. The design of the *GCS* layout have moreover to consider different *HMI* aspects. These include the information sources constraints such as sensors performances and datalink latency. Airworthiness criteria defined for manned aviation have to be considered to define the warning indications, the displays configuration and the information displayed.

The presence of a human operator in the *UAS* loop introduces the issues related to delegation of multiple tasks to him/her. These involve all four stages of human information processing system (sensory input, perception/cognition, selection of action, and execution of action), competing for the same attentional resources when performed concurrently. Because of this overlapping in information processing resources, the operator capability is often not sufficient to meet all this resource demand. This results in task interference and loss in performance.

The *GCS* operator workload described in the previous paragraph have to be minimised by implementing *GCS* displays supporting both display salience and the ease of extraction of critical information. Currently, the *GCS* includes in fact a set of displays showing most of the information available in a conventional aircraft cockpit, in addition to *UAS* specific information such as communication links and system status. This results in a large amount of information competing for display space. Intelligent display technologies, such as reconfigurable displays, or cueing techniques are therefore necessary to direct the operator attention to divergent information.

If a *S&A* system is implemented in the *UAS*, the related operator interface have to be included in the *GCS*. Given that generally this is based on a display, its design should take into account all the hazards considered by the system such as terrain impact, traffic, wind shear, clear air turbulence and wake vortices. This is necessary to avoid the lack of integration between advisories and to provide the operator with strategic information. The *CDTI* is the simplest example of *S&A GCS* interface. It graphically displays the horizontal position of the ownship in respect with nearby traffic and provides a numerical estimation of the vertical separation. A direct evolution of the *CDTI* is the *2D planner display*. This is a touch-screen display showing to the operator a map displaying the current *UAV* position and the flightplan while integrating also the layers of information regarding traffic, terrain, available airspace and weather. A significant step forward is given by the perspective flight path dis-

plays such as *SVS* that integrate the vertical dimension in the display. They provide a clear computer-generated perspective depiction of the out-of-cockpit view of the external environment ahead, integrating also non-physical objects, such as flight path and airspace constraints. *ARDs* are an enhancement of *SVSs* in which spatially relevant information are updated with other sources (e.g. intelligence assets, C2 sources etc.) and overlaid as conformal imagery onto the camera image. Finally *Multimodal displays*, including tactile or auditory feedbacks, have the advantage of providing the users with greater expressive power, naturalness and portability compared to conventional visual displays.

CHAPTER 5

Simulation Environment

The testing of the developed algorithm were carried-out in *Matlab/Simulink®* simulation environment. The simulations were designed to model the typical operating environment of the *S&A* algorithm. They include therefore the dynamic model of all components of this environment, such as ownship and threat aircraft dynamics, sensors, transponders and control systems. The *S&A* algorithm is integrated with a *Path Following (PF)* algorithm in an *ANS* to provide the *UAS* with autonomous navigation capabilities. This is necessary to enable the *S&A* algorithm testing both in modes 1 and 4 of Table 2.1 (remotely piloted to fully autonomous) and validate therefore the applicability of proposed *S&A* algorithm to both these *UAVs* flight control modes.

The simulation environment general architecture will be described in the following section 5.1. Aircraft dynamics used for both ownship and threat aircraft is described in section 5.2. Section 5.3 describes the *Graphical User Interface (GUI)* for setting the simulation parameters of the ownship *UAV* prior to starting the simulation. The *ANS* architecture is then defined in section 5.4. A more detailed depiction of the *PF* algorithm used for the autonomous navigation is then illustrated in section 5.5.

5.1 System Architecture

Basic structure of the simulation environment used to develop and test the *ANS* system is sketched in fig. 5.1. Both ownship and threat aircraft blocks are the *Piper J3 Cub 40* model aircraft (see section 5.2). The ownship is a *BRLOS UAV*. In this simulation environment it is controlled/supervised by the operator from the *GCS* mock-up described in section 7.3. It is moreover supposed that ownship and threat aircraft are equipped with mode S *ADS-B* transponders, that are *cooperative sensors* described in section 3.8.1. The ownship *ANS* received inputs are the on-board sensors data and the received threats transponders data. The output of the *ANS* are the

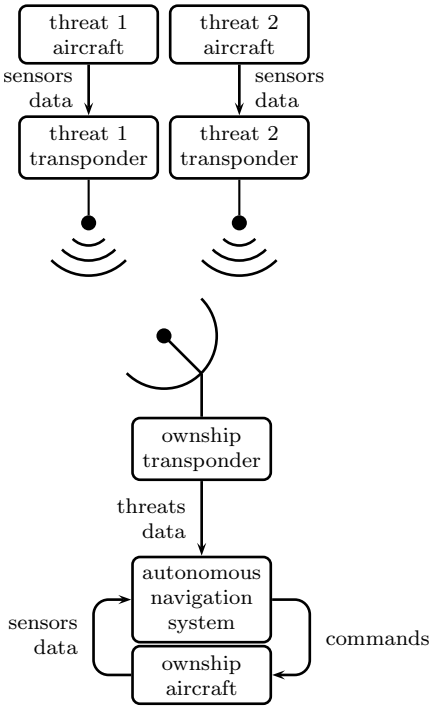

Figure 5.1: basic structure of the simulation environment used to test the *ANS*

autopilots commands sent for execution.

According to Table 3.2, the mode S *ADS-B* transponders output includes the following on-board sensors data:

identification code, that, to simplify the implementation in this simulation environment, is an integer number different for each aircraft;

barometric altitude;

horizontal *Global Positioning System (GPS)* position;

***GPS* position estimation quality indicator,** set to 1 in order to simulate optimal reception of the position estimated by *GPS*.

emergency status indicator, set to 0 because the aircraft considered are not in an emergency condition;

roll angle, derived from magnetometers measurements;

true airspeed, taken from conventional differential barometric airspeed measurements;

ground speed, obtained from *GPS* acquisitions;

true track angle, extracted also from *GPS* data;

magnetic heading, obtained from magnetometers;

indicated airspeed, measured from air data system;

barometric vertical rate, once more derived by air data system.

As in real operating environment, data exchange between transponders is enabled only when the horizontal relative distance between aircraft is within the reception range of ownship transponder. This distance is computed by transforming the *GPS* position of threat from the geocentric reference frame to the *North-East-Down Reference Frame (NED)*[1] which is centered on the current ownship position and estimating the length of the resulting vector.

The collisions between the ownship and a flying threat or a ground obstacle are identified in the simulation environment by a switch. It stops the simulation when the horizontal or vertical separation between the ownship and any of the hazards is smaller than the radius or half-height, respectively, of the *CAZ* defined in section 3.7. This switch was implemented in a first development stage to allow the identification of those conditions causing a real collision and detect therefore the conditions in which the algorithm was failing.

5.2 Aircraft Simulator

A *Piper J3 Cub 40* aircraft model, shown in fig. 5.2, is considered for both ownship and flying threats. Its configuration parameters are given in Table 5.1. The structure of

[1]This is a reference frame in which the axis are pointing respectively towards North, East and down direction in respect with the local point of earth surface considered and the origin is exactly in that point.

Figure 5.2: Piper J3 Cub 40 model aircraft

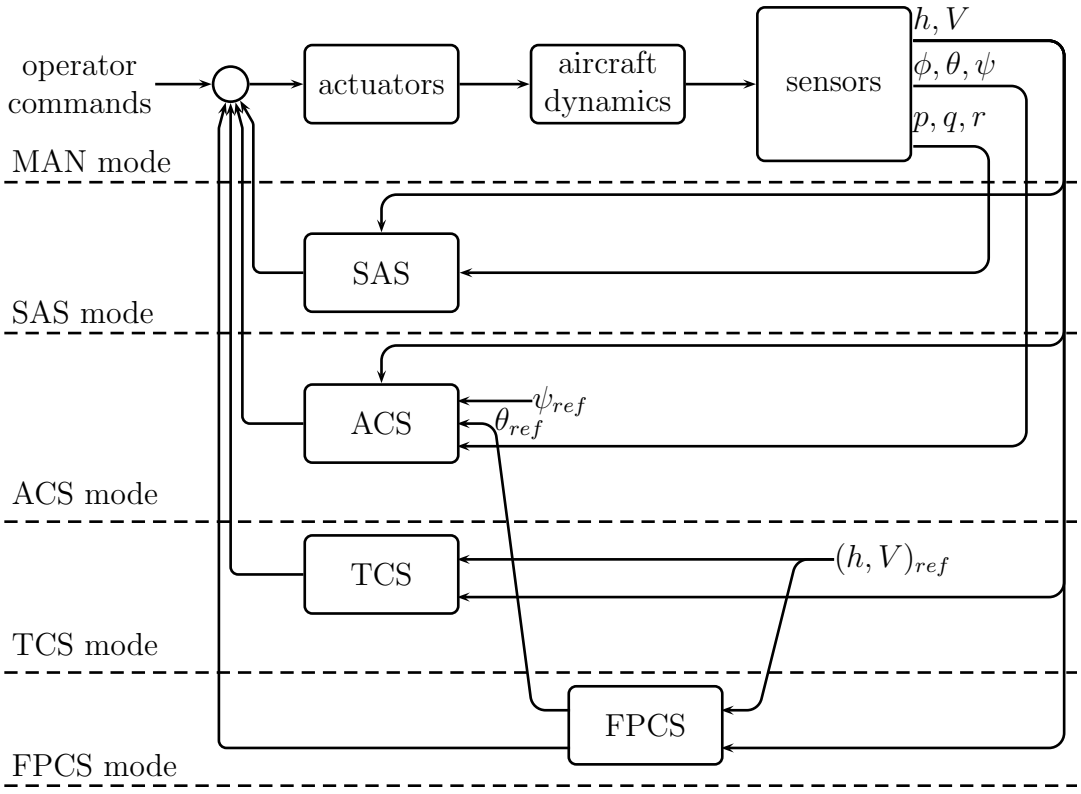

Figure 5.3: block diagram of the aircraft simulator: p, q, r are the roll, pitch and heading angle rates, ϕ, θ, ψ are the roll,pitch and heading attitude angles, h, V are the altitude and airspeed; the subscript ref indicates the reference values used in the autopilots

Table 5.1: Piper J3 Cub 40 configuration parameters

parameters	value
mass	5.3 kg
wing span	2032 mm
wing chord	307 mm
CG position[1]	345 mm
CP position[1]	320.2 mm
propeller radius	175 mm

[1] horizontal position referred to the propeller position

Table 5.2: performance parameters considered for the actuators simulators

actuator	lag	saturation limit	max change rate
ailerons	0.02 s	[-20,20]°	$20\,^\circ\,s^{-1}$
elevator	0.02 s	[-15,15]°	$15\,^\circ\,s^{-1}$
rudder	0.02 s	[-30,30]°	$30\,^\circ\,s^{-1}$

Table 5.3: values of the sensors performance parameters

sensor	range	resolution	f_s [Hz]	bandwidth [Hz]
accelerometers[1]	$[-50\,m\,s^{-2},50\,m\,s^{-2}]$	$0.5\,m\,s^{-2}$	50	-
gyroscope[1]	$[-1200\,^\circ\,s^{-1},1200\,^\circ\,s^{-1}]$	$0.01\,^\circ\,s^{-1}$	50	10.95,12.18,10.95
magnetometers[1]	[−360°,360°]	0.05°	50	0.2,0.63,0.2
attack angle	[−45°,45°]	0.1°	50	29.59
sideslip angle	[−90°,90°]	0.1°	50	12.55
anemometer	$[0\,m\,s^{-1},50\,m\,s^{-1}]$	$0.2\,m\,s^{-1}$	50	40
barometer	[0 m,500 m]	2 m	50	40
vertical rates	$[-3\,m\,s^{-1},3\,m\,s^{-1}]$	$0.005\,m\,s^{-1}$	50	40

[1] The values of every cell of this row are valid for roll, pitch and heading axes except for the bandwidth in which are displayed separately the values for every axis separated by a comma.

the simulator is sketched in fig. 5.3. The *GUI* that will be described in the next section enables the user to set the initial flight condition and the simulation parameters.

The **aircraft dynamics** is the non-linear 6*Degree of Freedom (DoF)* model described in [154]. The **actuators** are simulated by the block *Simple Actuator* of the *Aerosim* blockset in *Simulink*®. This is a first order dynamics model taking into account time constant, saturation and rate limits as listed in Table 5.2. No dynamics is considered for the throttle. This choice is supported by the fact that the engine is electrical and related delays are very small. The **sensors** specifications are tabulated in Table 5.3. The *GPS* receiver considers an accuracy for the position of 10 m in the horizontal plane and 30 m for the vertical position with an update frequency of 5 Hz.

The aircraft is equipped with *Stability Augmentation System (SAS)*, *Attitude Control System (ACS)* and *Trim Control System (TCS)* described in the next paragraphs. The *SAS* includes three proportional controllers. They feedback roll, pitch and heading angular rates measured by means of aircraft sensors to ailerons, elevator and rudder

commands. The aim of these autopilots is to improve the handling qualities of the aircraft.

ACS includes three *Proportional-Integral (PI)* controllers. These feedback the difference between measured attitude angles, i.e. roll, pitch and heading angles, and a set of reference values to the ailerons, elevator and rudder commands. This control system holds a set of commanded attitude angle values, the reference values. These are defined by operator or an outer-loop control system, such as the *Flight Path Control System (FPCS)*.

Table 5.4: specifications used for the autopilots tuning

autopilot		max control input	max output change
SAS	roll	30%	$15\,^\circ\,s^{-1}$
	pitch	30%	$15\,^\circ\,s^{-1}$
	yaw	20%	$10\,^\circ\,s^{-1}$
ACS	roll	70%	20°
	pitch	70%	15°
	yaw	80%	15°
FPCS	airspeed	100%	$0.5\,m\,s^{-1}$
	altitude	70%	5 m

The *TCS* is the control system trimming the aircraft at a reference altitude and airspeed. This system adds to the elevator and throttle commands the inputs necessary to hold the reference altitude and airspeed, as specified by the operator or an outer-loop control system, like the *FPCS*.

The *FPCS* includes *altitude autopilot* and *airspeed autopilot*. The *altitude autopilot* is a *PI* controller feeding back the difference between measured altitude and a reference value to the *ACS* pitch autopilot. The aim is to get an autopilot that holds aircraft's altitude to a commanded value, *i.e.* the reference value. This is defined by the pilot or by an outer-loop control system, such as the *PF* algorithm that will be described in section 5.5.

The *airspeed autopilot* is a *PI* controller feeding back the difference between measured airspeed and a reference value to throttle command. This control system implements therefore an autopilot holding the aircraft's airspeed to a commanded value, the reference value. This can be defined by the pilot or by an outer-loop control system.

The *FPCS* is therefore a control system holding target heading, altitude and airspeed as specified by an operator or by any other outer-loop control system, like the *PF* system (see section 5.5). The *FPCS* altitude and airspeed autopilots are designed as *acquire & hold* autopilots. In order to take into account the wide range of variations of the altitude command, they include a logic to limit the flight path angle in order to avoid the aircraft from entering a stall condition when steep variations of altitude command are imposed to the autopilot. This logic is obtained by defining the pitch angle command $\theta_c(t)$ with the following relationship:

$$\theta_c(t) = \begin{cases} \alpha + \gamma_u & \text{if} \quad h_c(t) - h_m(t) < h_l \\ \alpha & \text{if} \quad h_l < h_c(t) - h_m(t) < h_u \\ \alpha + \gamma_l & \text{if} \quad h_c(t) - h_m(t) > h_u \end{cases} \tag{5.1}$$

where:

- $h_m(t)$ and $h_c(t)$ are respectively the current measured and commanded altitude,

- α is the angle of attack value to hold the trim condition defined by the current airspeed and altitude,
- $h_{\text{l}} = -5m$ and $h_{\text{u}} = 5m$ are the boundaries outside which the flight path angle limiter is necessary to avoid the stall,
- $\gamma_{\text{l}} = -25°$ and $\gamma_{\text{u}} = 25°$ are the minimum and maximum allowed flight path angles, respectively.

The control systems are based on *gain scheduling*. The proportional and integral gains are scheduled according to the flight condition, defined in terms of altitude and airspeed. For every flight condition, the autopilots are tuned with the *Linear-Quadratic Regulator (LQR)* design techniques by using the following functions of the *Control System Toolbox* of *Matlab*®:

- `lqry` for the simple proportional *LQR*,
- `lqi` function for the *PI LQR*.

The specifications used for the autopilots tuning are shown in Table 5.4.

5.3 Simulator Settings

The window to allow the user to set the simulation parameters of the aircraft model includes the following three tabs:

- Initial Conditions
- Control Mode
- Camera View

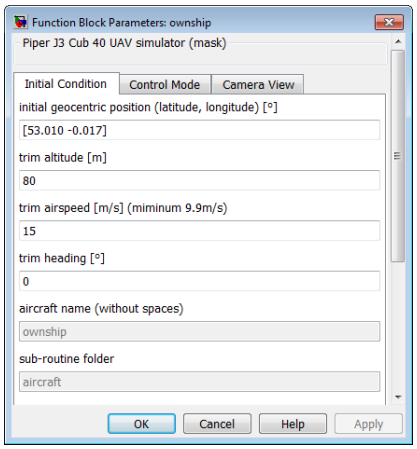

Figure 5.4: snapshot of the *Initial Condition* pane

The *Initial Conditions* tab shows the initial conditions of the aircraft dynamics considered at the beginning of the simulation. As can be seen in fig. 5.4, it includes the following parameters. **Initial geocentric position (latitude, longitude)** [°] is the initial aircraft horizontal position expressed in geocentric latitude and longitude in degrees. The value of these two parameters is inserted in this field according to *Matlab*® syntax for vectors. They are inserted and displayed in the textfield as a vector of two elements separated by a comma or a space and enclosed in square brackets. The value used for latitude can be a decimal number ranging between -90 and 90. The longitude accepts both values from $-180°$ to $180°$ and from $0°$ to $360°$ so it is compatible with both these standards. **Trim altitude** [m] is the initial aircraft altitude expressed in meters. A callback was implemented in the *GUI* to constrain the user

to insert a value inside the range for which the autopilots where tuned. **Trim airspeed** [$\mathrm{m\,s^{-1}}$] (**minimum** $9.9\,\mathrm{m\,s^{-1}}$) is the initial aircraft airspeed expressed in meters per second. The stall value is displayed and another callback is implemented to avoid the user inserting an airspeed value inferior lower than the minimum allowed value. **Trim heading** [°] is the initial aircraft heading angle expressed in degrees. The accepted values are inside the range 0 and 360. **Aircraft name** is the name of the data structure used in the model workspace to store the aircraft model parameters and settings. The value of this parameter is displayed on a gray background because it cannot be modified. **Subroutines folder** is the name of the folder containing the aircraft model callbacks and subroutines. This parameter is also on a gray background because this name is defined only once. Its value is used just when the aircraft model is added in the *Simulink*® model to copy its content in a folder in the model directory.

The *Control Mode* tab specifies the settings of the *UAV* control systems. In particular, the following controls are displayed in fig. 5.5. If the check-box **enable control systems** is ticked, the user can select one of the control systems configuration defined in the menu displayed below in the figure. Otherwise all the control systems are switched off and the aircraft is controlled with the conventional flight controls (ailerons, elevator, rudder and throttle) that is the *MAN mode* sketched in fig. 5.3. The pop-up menu **control mode** allows the user to define the configuration of the activated control systems that are the other modes defined in fig. 5.3. More precisely, the following modes can be chosen:

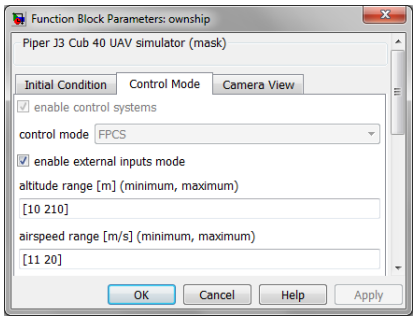

Figure 5.5: snapshot of the *Control Mode* pane

SAS is the configuration in which only *SAS* control systems are operating and operator uses conventional flight controls (ailerons, elevator, rudder and throttle commands) to control the aircraft;

ACS is the configuration in which both *SAS* and *ACS* are switched on and operator sets desired attitude angles values in real-time;

TCS is the configuration in which both *SAS* and *TCS* are switched on and operator sets the desired altitude and airspeed: the aileron, elevator, rudder and throttle commands coming from the operator through the conventional controls are summed to the trim values defined by *TCS*;

FPCS is the configuration in which all control systems (*SAS*, *TCS*, *ACS* and *FPCS*) are enabled and operator sets desired altitude, airspeed and heading angles in real-time.

The check-box **enable external inputs mode** enables a simulation mode in which the operator commands in real-time all controls (conventional controls, autopilots commands and autopilots switches) and the input of the model are the following:

conventional commands including ailerons, elevator, rudder and throttle commands;

autopilots switch that enables switching between *SAS* and *FPCS* modes as defined previously; when this control is switched off the only inputs considered by the system are conventional commands otherwise all the inputs as specified below will be considered;

altitude, airspeed and heading commands are the reference flight parameters for *FPCS*;

climb/descent switch is the control to allow the aircraft to start a climb, when its value is set to 1, or descent manouevre, when its value is -1, with predefined flight path angles (25° and −25°, respectively), or to stay in a cruise condition, when its value is 0;

climb/descent flight path angle commands gives the operator the possibility to set the value of the flight path angle in real-time to start a climb/descent flight phase.

Altitude range [m] **(minimum, maximum)** defines the altitude range considered for autopilots gains scheduling. **Airspeed range** [$\mathrm{m\,s^{-1}}$] **(minimum, maximum)** defines the airspeed range considered for autopilots gains scheduling.

Finally, the *Camera View* tab gives the user the possibility to set the parameters of the forward camera view. This is obtained with a real-time link between the *Simulink*® simulation environment and the *FlightGear* [155] open-source flight simulator. As can be seen in fig. 5.6, the parameters displayed in the window are the following. The control **Enable FlightGear interface** switches on/off the visualisation of the camera view during simulation. **Use network computer** gives the possibility to the user to run *FlightGear* and show the external view in real-time on a slave computer on the network. **Computer name** is the name of that computer and ***Internet Protocol (IP)*** **address** contains its *IP* address. If necessary, **User name** defines the user name of the computer account used on the slave computer and **Password** contains its password. **FlightGear Path** defines the directory of the *FlightGear* software. **Update frequency** [Hz] is the frequency used to update the forward camera view. ***HUD*** enables the *HUD* layer in *FlightGear*. **Enable FlightGear recording** enables the user to record an ".avi" file of the forward camera view during simulation. **Sampling frequency** specifies the frequency used for recording.

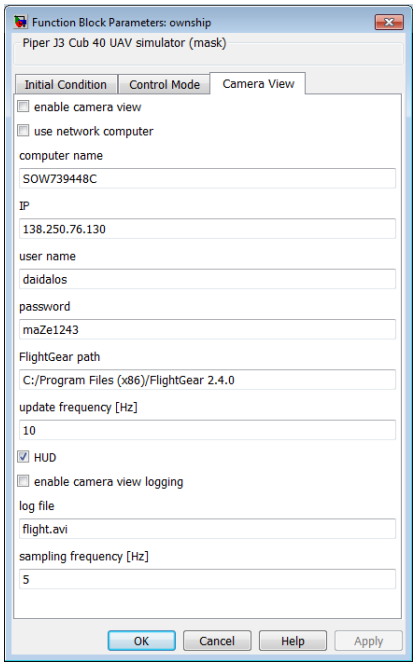

Figure 5.6: snapshot of the flight simulator pane

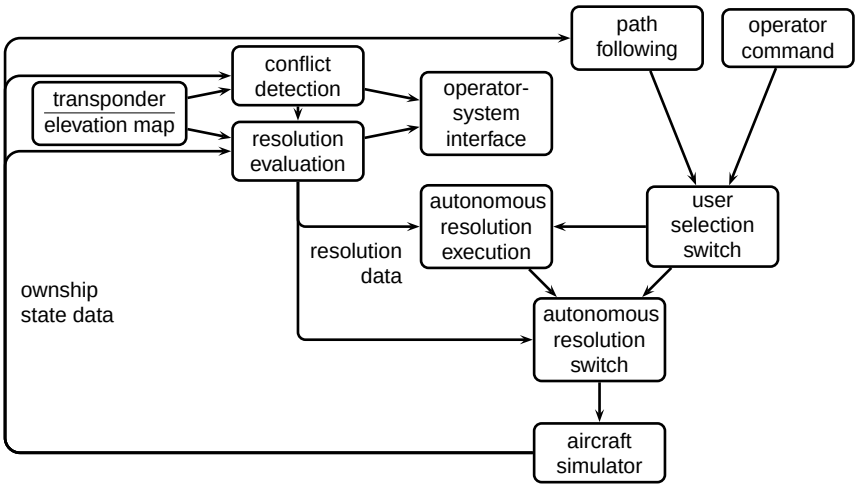

Figure 5.7: block diagram of the *ANS* system

5.4 *ANS* Structure

The block diagram of the *ANS* is shown in fig. 5.7. The switch with the label **user selection** selects the modes between the two operating modes:

manual navigation mode where the system input is the operator command;

autonomous navigation mode, where the inputs are given by the path following;

The **manual navigation mode** enables the flight control mode 1, as defined in section 2.2. In this mode, *UAS* operator can directly control the aircraft dynamics using conventional controls. Moreover, operator can set in real-time altitude, airspeed and heading angle autopilot commands, such as in the *FPCS* mode described in section 5.3. This option was included to allow manual modes simulations in which it is not necessary an operator to pilot the *UAV*.

In the **autonomous navigation mode**, that is the flight control mode 4, as defined in section 2.2, the *FPCS* commands are defined by the *PF* system. The operator is therefore just a supervisory controller, as this is described in section 2.3, with the role of setting the waypoints considered by the *PF* algorithm for the flight plan.

The five functions of the *S&A* system introduced in section 3.2 (that are *environment sensing*, *conflicts detection*, *resolution estimation*, *advisories communication*, *autonomous resolution*) are performed as follows. Regarding the *environment sensing*, the flying threats detection is based on their aircraft transponder. The operating principle of the simulated transponders is described in section 5.1. The detection of collision risks with ground terrain is based on the ground obstacles detected using the system elevation map database. This map is based on the *ASTER Global Digital Elevation Model* [156]. The conflict detection algorithm, which will be described

in section 6.3, evaluates the collision risks and generates the associated alerts. If one or more potential conflicts are detected, the resolution estimation algorithm (see sections 6.4 to 6.7) estimates the resolution manoeuvre. The *GCS* through which the *advisories communication* is performed is then described in chapter 7. The autonomous resolution block takes over and executes a collision avoidance manoeuvre "if" an imminent conflict is detected "and" the *UAV* operator does not react to the advisory; hence breaching the *minimum safe time before impact*, defined in section 3.2 of chapter 3.

5.5 Path Following Algorithm

The *path following algorithm* navigates the aircraft through a given set of predefined waypoints. Those ones are defined in geocentric coordinates as:

$$\vec{P}_{\mathrm{W/P}} \triangleq \left(\phi_{\mathrm{W/P}}, \lambda_{\mathrm{W/P}}, h_{\mathrm{W/P}}\right) \tag{5.2}$$

where $\phi_{W/P}$, $\lambda_{W/P}$ and $h_{W/P}$ are latitude, longitude and altitude, respectively. The airspeed $V_{\mathrm{W/P}}$ is controlled between each of the waypoints and it is maintained to be a constant one. If it is assumed that the ownship position is:

$$\vec{P}_{\mathrm{O/S}}(t) \triangleq \left(\phi_{\mathrm{O/S}}(t), \lambda_{\mathrm{O/S}}(t), h_{\mathrm{O/S}}(t)\right) \tag{5.3}$$

Then the waypoint can be represented in the *NED* reference frame which is centered in $\vec{P}_{\mathrm{O/S}}(t)$. Therefore, the heading angle command $\psi_{\mathrm{d}}(t)$ and the airspeed command $V_d(t)$ are:

$$\psi_{\mathrm{d}}(t) = \arctan \frac{\vec{x}_{\mathrm{W/P},2}}{\vec{x}_{\mathrm{W/P},1}}(t) \tag{5.4}$$

$$V_{\mathrm{d}}(t) = V_{\mathrm{W/P}} \tag{5.5}$$

where $\vec{x}_{\mathrm{W/P}}$ is the waypoint position in the *NED* reference frame centered in the current ownship position $\vec{P}_{\mathrm{O/S}}(t)$. The altitude command $h_d(t)$ is defined as a linear variation in the altitude during the flight between each of the waypoints. In order to accomplish this, the vertical speed $V_z(t)$ is maintained constant and it is estimated as:

$$V_{\mathrm{z}}(t) = \frac{h_{\mathrm{d}}(t) + x_{\mathrm{W/P},3}}{t_{\mathrm{W/P}}} \tag{5.6}$$

where $t_{\mathrm{W/P}}$ is the elapsed time to reach the waypoint calculated as follows:

$$t_{\mathrm{W/P}} = \frac{\left|\vec{x}_{\mathrm{W/P}}\right|}{V_{\mathrm{O/S}}} \tag{5.7}$$

where $V_{\mathrm{O/S}}(t)$ is the current ownship airspeed. Therefore, the mathematical expression of the altitude command $h_d(t)$ is:

$$h_{\mathrm{d}}(t) = \int_0^t V_{\mathrm{z}}(t)\,\mathrm{d}\,t \tag{5.8}$$

Due to the uncertainties in the aircraft position, the aircraft might not exactly reach the desired waypoint. Therefore the aircraft is assumed to reach the desired waypoints if the following condition is satisfied:

$$\left|\vec{x}_{W/P}\right| < \epsilon_{\mathrm{W/P}} \tag{5.9}$$

where $\epsilon_{W/P}$ is a threshold value defined based on the aircraft position accuracy. If the above defined condition is fulfilled, then the next waypoint is considered for the next iteration algorithm iteration.

CHAPTER 6

Proposed *S&A* Algorithm

This chapter covers some considerations on the parts of the *S&A* algorithm presented in previous chapter in section 5.4. Section 6.1 starts with some notes regarding the assumptions used for the development of the algorithm. Section 6.2 introduces then some preliminary definitions used in the algorithm development. The criteria used for the conflict risks detection is described in section 6.3. The model used for the estimation of the aircraft dynamics during the resolution manoeuvre is defined in section 6.4. In section 6.5 this model is applied for the estimation of the horizontal resolution manoeuvre. Section 6.6 describes then the approach used for the vertical resolution manoeuvres. The logic used for the suggested manoeuvre selection and the autonomous resolution execution is presented in section 6.7. Finally, section 6.8 provides a short comparison between the proposed algorithm and previous works presented in the literature.

6.1 Assumptions

The following assumptions were used in respect with the implementation issues defined in section 3.8. As explained in chapter 5, the system was designed to operate with the levels of autonomy ranging from *manual navigation mode* to fully *autonomous navigation mode* as defined in section 5.4. The algorithm was developed with a *multiple conflict management* approach[1] considering both airborne and ground threats. The aircraft performance and *Rules of Air* are both considered in the resolution manoeuvre evaluation (see section 3.8.2). The allowed types of manoeuvre are horizontal, *i.e.* changes of the heading autopilot command; and vertical, *i.e.* changes of the altitude autopilot command. The conflict avoidance is based on *uncoordinated manoeuvres*[2]. The resolution manoeuvre is updated at 1 Hz, to take into account changes of the conflict geometry caused by unpredictable trajectory changes of the threats.

6.2 Preliminary Definitions

The Cartesian reference frame used for the development of the algorithm is shown in fig. 6.1 and is so defined:

origin in current ownship position

[1] More information can be found in section 3.8.1.
[2] More information can be found in section 3.8.2.

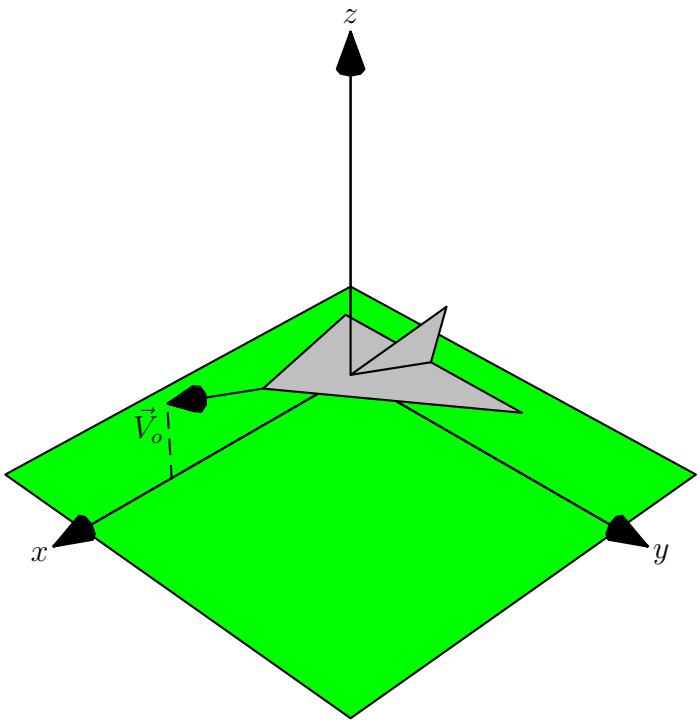

Figure 6.1: Cartesian reference frame

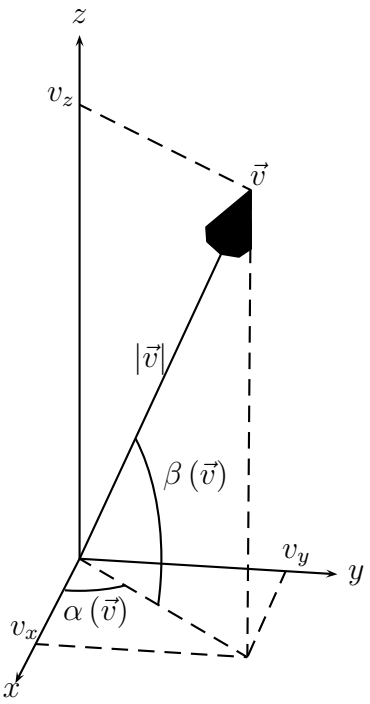

Figure 6.2: graphical representation of the spherical coordinates used for vectors parametrisation

axes x on the direction of the projection of the ownship airspeed vector $\vec{V}_o$ in the local horizontal plane,

axes y perpendicular to x on its left side and lying in the local horizontal plane,

axes z perpendicular to the xy plane and pointing upwards.

As can be seen in fig. 6.2, in this reference frame an arbitrary vector $\vec{v}$ can be defined through its Cartesian components according to the relationship:

$$\vec{v} \triangleq (v_x, v_y, v_z) \tag{6.1}$$

but also through spherical coordinates in terms of modulus $|\vec{v}|$, azimuth and elevation angles $\alpha(\vec{v})$ and $\beta(\vec{v})$ defined by the following relationships:

$$|\vec{v}| = \triangleq \sqrt{v_x^2 + v_y^2 + v_z^2} \tag{6.2}$$

$$\alpha(\vec{v}) \triangleq \arctan \frac{v_y}{v_x} \tag{6.3}$$

$$\beta(\vec{v}) \triangleq \arctan \frac{v_z}{\sqrt{v_x^2 + v_y^2}} \tag{6.4}$$

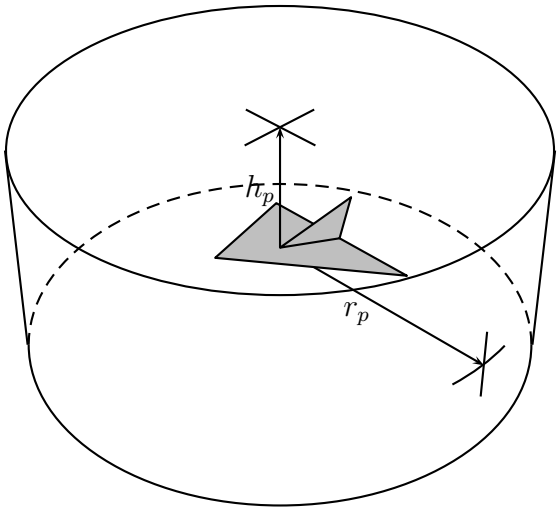

Figure 6.3: extension and geometric parameters of the position uncertainty zone

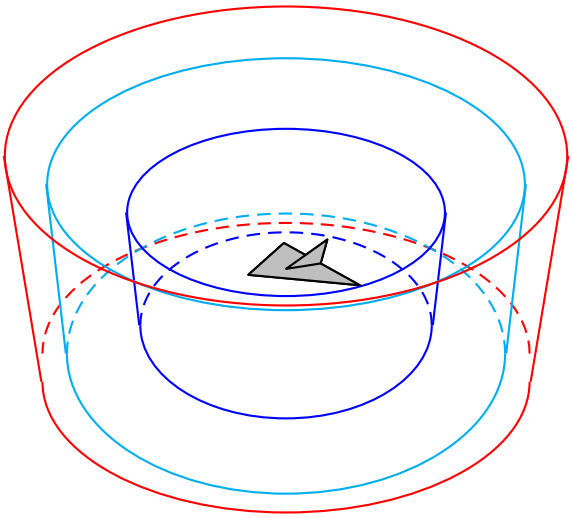

Figure 6.4: position uncertainty zone (red), safety zone (cyan) and separation (blue) zone

Another useful parameter is the horizontal projection modulus $|\vec{v}|_h$ defined as:

$$|\vec{v}|_h \triangleq \sqrt{v_x^2 + v_y^2} \tag{6.5}$$

Assuming that the ownship position estimation comes from the *GPS* receiver, it is necessary to take into account the uncertainty related with position estimation accuracy of both ownship and threats. This leads to the definition of a *PUZ* as the locus in which the true aircraft position lies. According to the conventional format used to express the accuracy of the *GPS* position estimation, a cylindrical region is considered. It is centered on the aircraft position with a radius of r_p and a half-height of h_p, respectively, equal to the horizontal and the vertical position estimation accuracy, as shown in fig. 6.3.

In addition to this, a cylindrical *SZ* region is defined a cylindrical zone with dimensions given by the *PUZ* dimensions increased by a safety factor in order to take into account the approximations introduced in the resolution manoeuvre estimation.

Similarly, it is defined by *ATC* as the *separation zone* the *cylindrical region centered on the current position of the aircraft, the horizontal and vertical extension of which are set by the regulation or ATC according to the class of the airspace and operational conditions* [17]. All other aircraft have to stay outside the *separation zone* in order to avoid any collision risks. As sketched in fig. 6.4, for safety reasons the safety zone has to be wider than the position uncertainty zone and smaller than the separation zone.

The *CDZ* and *CAZ* dimensions that were defined previously in section 3.7 were set to a fixed value. This value was fixed in order to get conservative results for the scenarios considered. It takes therefore into account the dynamics of ownship and threats aircraft considered. In this work, the *CAZ* was identified with the *separation*

zone.

6.3 Conflicts Detection

According to the aforementioned definition in section 6.2, the ownship remains in the origin of the reference frame for the whole duration of the mission. Based on the straight projection hypothesis, introduced in section 3.8.1, all aircraft in the close proximity airspace moves in a straight line. This line passes through the current position of the threat and is parallel to its relative airspeed $\vec{V}_r$, defined as the sum of the ownship's airspeed vector $\vec{V}_o$ and the threat's airspeed vector $\vec{V}_i$, as shown in fig. 6.5 and given by the following relationship:

$$\vec{V}_r \triangleq \vec{V}_o + \vec{V}_i \tag{6.6}$$

If the threat trajectory intersects the position uncertainty zone, a collision risk is therefore being detected.

When a collision risk is detected, a resolution manoeuvre has to be generated in order to keep the threats outside the safety zone during the overall manoeuvre. Moreover, the control input variation has to be minimized so that to reduce the deviation distance between the resolution manoeuvre and the aircraft original trajectory.

6.4 General Approach for Estimating the Resolution Manoeuvre

A safe resolution manoeuvre always guarantees that, during the overall manoeuvre, the threat is kept outside the safety zone. In order to accomplish this, it is necessary to estimate the threat's trajectory $\vec{P}_{i,r}(t)$ in the reference frame as:

$$\vec{P}_{i,r}(t) = \vec{P}_i(t) - \vec{P}_o(t) \tag{6.7}$$

where $\vec{P}_i(t)$ and $\vec{P}_o(t)$ are threat's and ownship's positions, respectively. Their general expression can be defined as:

$$\vec{P}(t) \triangleq \vec{P}(0) + \int_0^t \vec{V}(\tau)\,\mathrm{d}\,\tau \tag{6.8}$$

where $\vec{P}(0)$ is the *initial position* and $\vec{V}(t)$ is the speed of the aircraft in a fixed reference frame.

In the moving reference frame considered, it can be imposed:

$$\vec{P}_{i,r}(0) \triangleq \vec{P}_i(0) - \vec{P}_o(0) \tag{6.9}$$

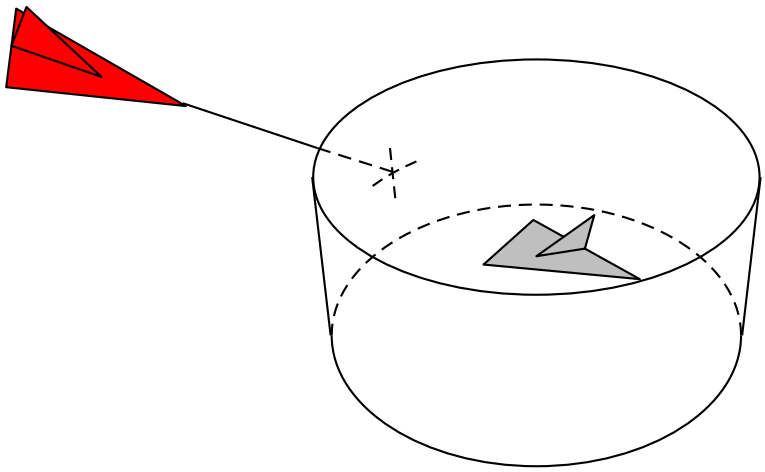

(a)

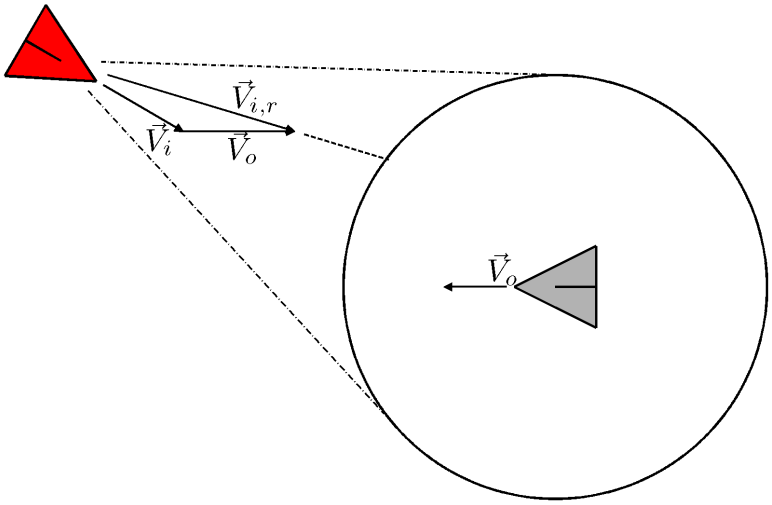

(b)

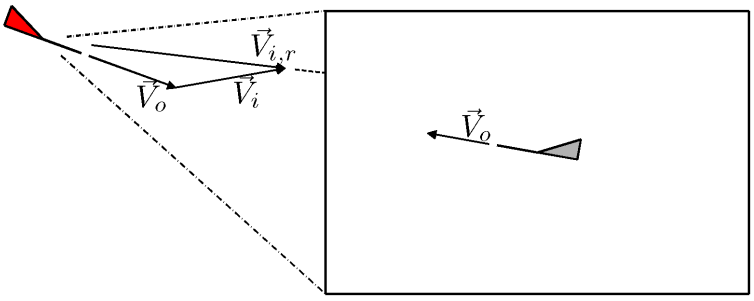

(c)

Figure 6.5: conflict detection approach: (a)three dimensional space, (b)horizontal plane and (c)vertical plane. The aircraft outside the position uncertainty cylinder is the threat (red colour) approaching from the left and the one inside is the ownship.

According to the hypothesis of straight projection, the threat's airspeed is assumed to be constant:

$$\vec{V}_i(t) = \vec{V}_i = \text{const} \tag{6.10}$$

Therefore eq. (6.7) can be re-written as:

$$\vec{P}_{i,r}(t) = \vec{P}_{i,r}(0) + \vec{V}_i t - \int_0^t \vec{V}_o(\tau)\,\mathrm{d}\,\tau \tag{6.11}$$

and for the ownship:

$$\vec{V}_o(t) = V_o(t) \begin{pmatrix} \cos\psi_o(t)\cos\gamma_o(t) \\ \sin\psi_o(t)\cos\gamma_o(t) \\ \sin\gamma_0(t) \end{pmatrix} \tag{6.12}$$

where $V_o(t), \psi_o(t), \gamma_o(t)$ are the ownship airspeed, heading angle and flight path angle, respectively.

If the ownship is assumed to be equipped and controlled with *FPCS*, the interactions between the longitudinal and lateral-directional dynamics during manoeuvres are negligible, and aircraft's airspeed $V_o(t)$ is not significantly affected by manoeuvres. This implies that it is possible to define the resolution manoeuvre in which we assume that the aircrafts airspeed $V_o(t)$ is constant:

$$V_o(t) \cong V_o = \text{const} \qquad \forall t \tag{6.13}$$

6.5 Horizontal Resolution Estimation

Moreover, a simple turn in the horizontal plane will not cause a significant change in the flight path angle $\gamma_o(t)$, that entail:

$$\gamma_o(t) \cong 0 \qquad \forall t \tag{6.14}$$

Therefore eqs. (6.11) and (6.12) can be rewritten as:

$$\vec{V}_o(t) = V_o \begin{pmatrix} \cos\psi_o(t) \\ \sin\psi_o(t) \\ 0 \end{pmatrix} \tag{6.15}$$

$$\vec{P}_{i,r}(t) = \vec{P}_{i,r}(0) + \vec{V}_i t - V_o \int_0^t \begin{pmatrix} \cos\psi_o(\tau) \\ \sin\psi_o(\tau) \\ 0 \end{pmatrix} \mathrm{d}\,\tau \tag{6.16}$$

This implies that the change in the heading angle $\psi_o(t)$ will significantly affect the threat trajectory, $\vec{P}_{i,r}(t)$. Therefore the heading angle profile $\psi_o(t)$ needs to be estimated in order to obtain the threat's trajectory.

Furthermore, a safe resolution manoeuvre has to be defined in order to keep all the detected threats outside the safety zone during the overall manoeuvre. To test if this condition is verified, it is necessary to estimate the threats trajectories. In particular, during a simple turn in the horizontal plane performed by the ownship, the trajectory $\vec{P}_{\mathrm{r},i}(t)$ of the i-th threat can be expressed with the following relationship [157]:

$$\vec{P}_{\mathrm{r},i}(t) = \mathbb{R}\left(-\psi_{\mathrm{o}}(t)\right)\left(\vec{P}_{\mathrm{r},i}(0) + \vec{V}_i t - V_{\mathrm{o}}\int_0^t \begin{pmatrix}\cos\psi_{\mathrm{o}}(\tau)\\ \sin\psi_{\mathrm{o}}(\tau)\\ 0\end{pmatrix}\mathrm{d}\,\tau\right) \tag{6.17}$$

where:

- the rotation matrix $\mathbf{R}(-\psi_o(t))$ takes into account the reference frame rotation caused by the heading attitude $\psi_o(t)$ changes of the ownship,
- $\vec{P}_{r,i}(0)$ is the initial threat position in the reference frame considered,
- $\vec{V}_i$ is the threat speed in a fixed reference frame, that is obviously 'zero' if the threat is a point of the contour of a ground obstacle,
- V_o is the ownship airspeed.

Therefore, the threat trajectory $\vec{P}_{r,i}(t)$ is a function of the dynamics of the heading angle $\psi_o(t)$.

Among the different heading command profiles, the step command is the more demanding for aircraft's control systems. Such a command profile, makes it easier to display the resolution manoeuvre to the operator, since the only information that needs to be communicated is the heading angle variation. Therefore, if it is used a procedure such as that defined in section 6.5.2, a conservative estimation of the related heading angle profile $\psi_{\mathrm{o}}(t)$ can be obtained from the first order dynamics $\bar{\psi}_{\mathrm{o}}(t)$ expressed by the following relationship (see fig. 6.6):

$$\bar{\psi}_{\mathrm{o}}(t) = \begin{cases}\psi_{\mathrm{o}}(0) & \text{if} \quad 0 < t < t_0\\ \psi_{\mathrm{o}}(0) + \Delta\psi_{\mathrm{o}}\left(1 - \mathrm{e}^{-\frac{t-t_0}{\tau}}\right) & \text{if} \quad t > t_0\end{cases} \tag{6.18}$$

where $\Delta\psi$ is the chosen heading angle command and t_0 and τ are the fitting parameters.

6.5.1 Conditions for a Conservative Trajectory Estimation

A conservative estimation of these fitting parameters for head-on encounters is obtained if the following condition is satisfied for the rise phase of the heading angle profile:

$$|\psi_{\mathrm{o}}(t) - \psi_{\mathrm{o}}(0)| \geq \left|\bar{\psi}_{\mathrm{o}}(t) - \psi_{\mathrm{o}}(0)\right| \qquad \forall t > 0 \tag{6.19}$$

As can be seen in fig. 6.7, an avoidance manoeuvre in the horizontal plane will leads to one or both of the following effects:

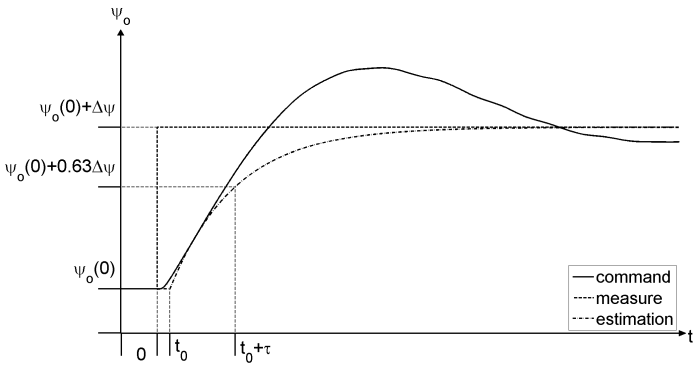

Figure 6.6: parametrisation of the aircraft heading angle response to a step variation of the heading angle autopilot command

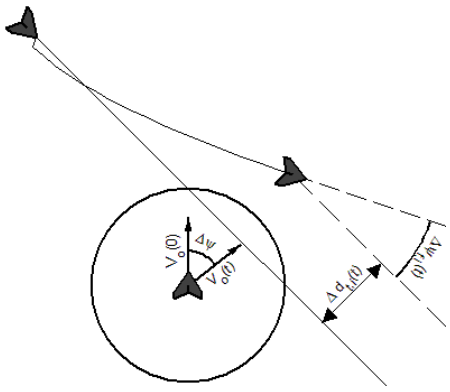

Figure 6.7: parameters considered for the resolution manoeuvre optimisation

1. the smallest distance $\Delta d_{\mathrm{t},i}(t)$ between the ownship position and the threat trajectory increases to a value greater than the radius of the collision risk zone r_{p};
2. the direction of motion $\Delta\psi_{\mathrm{f},i}(t)$ of the threat changes from its initial value to avoid an intersection with the collision risk zone.

Let us consider a reference frame moving with the ownship where its position coincides with the frame origin. It can be assumed moreover that the axes have a fixed orientation in which the x-axis points to the direction of the initial heading of the ownship. In this reference frame the equation of threat's motion becomes, according to (6.17):

$$\vec{P}_{\mathrm{f},i}(t) = \vec{P}_{\mathrm{r},i}(0) + \vec{V}_i t - V_{\mathrm{o}} \int_0^t \begin{pmatrix} \cos\psi_{\mathrm{o}}(\tau) \\ \sin\psi_{\mathrm{o}}(\tau) \\ 0 \end{pmatrix} \mathrm{d}\,\tau \tag{6.20}$$

from which the following expression of the threat heading $\psi_{\mathrm{f},i}(t)$ is derived:

$$\psi_{\mathrm{f},i}(t) \triangleq \arctan \frac{\partial V_{\mathrm{f},i,y}}{\partial V_{\mathrm{f},i,x}}(t) \tag{6.21}$$

where $\vec{V}_{\mathrm{f},i}$ is the threat speed expressed in the reference frame moving with the ownship and non-rotating in the horizontal plane defined by the classical relationship:

$$\vec{V}_{\mathrm{f},i}(t) \triangleq \frac{\mathrm{d}\,\vec{P}_{\mathrm{f},i}}{\mathrm{d}\,t}(t) = \vec{V}_i - V_{\mathrm{o}} \begin{pmatrix} \cos\psi_{\mathrm{o}}(t) \\ \sin\psi_{\mathrm{o}}(t) \\ 0 \end{pmatrix} \tag{6.22}$$

Therefore (6.21) becomes:

$$\psi_{\mathrm{f},i}(t) = \arctan \frac{V_{i,y} - V_{\mathrm{o}} \sin\psi_{\mathrm{o}}(t)}{V_{i,x} - V_{\mathrm{o}} \cos\psi_{\mathrm{o}}(t)} \tag{6.23}$$

Considering that for the angles α and β:

$$\arctan\alpha - \arctan\beta = \arctan\frac{\alpha-\beta}{1+\alpha\beta} \tag{6.24}$$

and imposing $\psi_{\mathrm{o}}(0) \triangleq 0$ and $\psi_{\mathrm{o}}(t) \triangleq \Delta\psi$, $\Delta\psi_{\mathrm{f},i}$ can be expressed as:

$$\begin{aligned}
\Delta\psi_{\mathrm{f},i} &\triangleq |\psi_{\mathrm{f},i}(t) - \psi_{\mathrm{f},i}(0)| = \\
&= \left|\arctan\frac{V_{i,y} - V_{\mathrm{o}}\sin\Delta\psi}{V_{i,x} - V_{\mathrm{o}}\cos\Delta\psi} - \arctan\frac{V_{i,y}}{V_{i,x}-V_{\mathrm{o}}}\right| = \\
&= \left|\arctan\frac{\frac{V_{i,y}-V_{\mathrm{o}}\sin\Delta\psi}{V_{i,x}-V_{\mathrm{o}}\cos\Delta\psi} - \frac{V_{i,y}}{V_{i,x}-V_{\mathrm{o}}}}{1+\frac{V_{i,y}-V_{\mathrm{o}}\sin\Delta\psi}{V_{i,x}-V_{\mathrm{o}}\cos\Delta\psi}\frac{V_{i,y}}{V_{i,x}-V_{\mathrm{o}}}}\right| = \\
&= \left|\arctan\frac{V_{\mathrm{o}}V_{i,y}\left(\cos\Delta\psi - 1\right) - V_{\mathrm{o}}V_{i,x}\sin\Delta\psi + V_{\mathrm{o}}^2\sin\Delta\psi}{(V_{i,x}^2+V_{i,y}^2) - V_{\mathrm{o}}V_{i,x}(\cos\Delta\psi+1) - V_{\mathrm{o}}V_{i,y}\sin\Delta\psi + V_{\mathrm{o}}^2\cos\Delta\psi}\right|
\end{aligned} \tag{6.25}$$

in which, considering a small time step of the manoeuvre, $\Delta\psi$ is small and $\Delta\psi_{\mathrm{f},i}$ can be therefore approximated as:

$$\Delta\psi_{\mathrm{f},i} \cong \left|\arctan\left(\frac{-V_{\mathrm{o}}V_{i,x} + V_{\mathrm{o}}^2}{(V_{i,x}^2+V_{i,y}^2) - 2V_{\mathrm{o}}V_{i,x} - V_{\mathrm{o}}V_{i,y}\Delta\psi + V_{\mathrm{o}}^2}\Delta\psi\right)\right| \tag{6.26}$$

Therefore $\Delta\psi_{\mathrm{f},i}$ increases with the value of $\Delta\psi$. This implies that the estimated change in the motion direction in the reference frame considered is an increasing function of $\Delta\psi$. On the other hand, a greater change in motion direction generally produces a bigger distance from the collision route. Therefore a smaller and consequently conservative estimation of the parameter $\Delta\psi_{\mathrm{f},i}$ is obtained with a smaller value of $\Delta\psi$.

Regarding distance $\Delta d_{\mathrm{t}}(t)$ and according to fig. 6.7, a raw approximation can be obtained from the following formula, if $\Delta\psi$ is small enough:

$$\Delta d_{\mathrm{t},i}(t) \cong \sin\Delta\psi_{\mathrm{f},i}\left|\vec{P}_{\mathrm{f},i}(t) - \vec{P}_{\mathrm{r},i}(0)\right|_{\mathrm{h}} \tag{6.27}$$

where the expression $|\vec{v}|_{\mathrm{h}}$ indicate the projection on the horizontal plane of the vector $\vec{v}$.

From (6.27), based on (6.20), the following formula is obtained:

$$\begin{aligned}
\Delta d_{\mathrm{t},i}(t) &\cong \sin\Delta\psi_{\mathrm{f},i}\left|\vec{V}_i t - V_o\int_0^t\begin{pmatrix}\cos\psi_{\mathrm{o}}(\tau)\\ \sin\psi_{\mathrm{o}}(\tau)\\ 0\end{pmatrix}\mathrm{d}\,\tau\right|_{\mathrm{h}} = \\
&= \sin\Delta\psi_{\mathrm{f},i}\left|\begin{pmatrix}\vec{V}_{i,x}t - V_{\mathrm{o}}\int_0^t\cos\psi_{\mathrm{o}}(\tau)\,\mathrm{d}\,\tau\\ \vec{V}_{i,y}t - V_{\mathrm{o}}\int_0^t\sin\psi_{\mathrm{o}}(\tau)\,\mathrm{d}\,\tau\\ \vec{V}_{i,z}t\end{pmatrix}\right|_{\mathrm{h}} = \\
&= \sin\Delta\psi_{\mathrm{t}}(t)\sqrt{(\vec{V}_{i,x}t - V_{\mathrm{o}}[\sin\psi_{\mathrm{o}}(\tau)]_0^t)^2 + (\vec{V}_{i,y}t - V_{\mathrm{o}}[-\cos\psi_{\mathrm{o}}(\tau)]_0^t)^2} = \\
&= \sin\Delta\psi_{\mathrm{t}}(t)\sqrt{(\vec{V}_{i,x}t - V_o\sin\Delta\psi)^2 + (\vec{V}_{i,y}t - V_{\mathrm{o}}(1-\cos\Delta\psi))^2}
\end{aligned} \tag{6.28}$$

Considering the results previously obtained for $\Delta\psi_{\mathrm{t}}(t)$, it can be seen that $\Delta d_{\mathrm{t}}(t)$ increases with $\Delta\psi$. Therefore, since the heading manoeuvre change $\Delta\psi$ is underestimated in respect with the real value, a more conservative estimation is obtained, being the smaller estimated distance $\Delta d_{\mathrm{t}}(t)$.

6.5.2 Heading Angle Profile Fitting

It is well known from calculus that the exponential function and all its derivatives (first, second and superior degrees derivatives) are monotonically increasing functions. Therefore the maximum value of $\frac{\mathrm{d}\,\bar{\psi}_{\mathrm{o}}}{\mathrm{d}\,t}$ is obtained for $t = t_0$, while the maximum $\max\left(\frac{\mathrm{d}\,\psi_{\mathrm{o}}}{\mathrm{d}\,t}\right)$ is obtained for a value of t lying inside the rise phase of $\psi_{\mathrm{o}}(t)$ (see fig. 6.6). Therefore, indicating with $t_{\max}$ the value of t for which:

$$\frac{\mathrm{d}\,\psi_o}{\mathrm{d}\,t}(t_{\max}) = \max\left(\frac{\mathrm{d}\,\psi_o}{\mathrm{d}\,t}\right) \tag{6.29}$$

A conservative estimation of ψ_{o} for the rise phase is obtained if:

$$\begin{cases} \psi_{\mathrm{o}}(t_{\max}) = \bar{\psi}_{\mathrm{o}}(t_{\max}) \\ \frac{\mathrm{d}\,\psi_{\mathrm{o}}}{\mathrm{d}\,t}(t_{\max}) = \frac{\mathrm{d}\,\bar{\psi}_{\mathrm{o}}}{\mathrm{d}\,t}(t_{\max}) \end{cases} \tag{6.30}$$

In fact, during the rise phase, for $t < t_{\max}$ it holds:

$$\frac{\mathrm{d}\,\psi_{\mathrm{o}}}{\mathrm{d}\,t}(t) < \frac{\mathrm{d}\,\bar{\psi}_{\mathrm{o}}}{\mathrm{d}\,t}(t) \tag{6.31}$$

and for $\Delta t > 0$:

$$\psi_{\mathrm{o}}(t_{\max}) - \frac{\mathrm{d}\,\psi_{\mathrm{o}}}{\mathrm{d}\,t}(t)\Delta t > \bar{\psi}_{\mathrm{o}}(t_{\max}) - \frac{\mathrm{d}\,\bar{\psi}_{\mathrm{o}}}{\mathrm{d}\,t}(t)\Delta t \tag{6.32}$$

Considering now that for small Δt holds:

$$\psi_{\mathrm{o}}(t + \Delta t) \cong \psi_{\mathrm{o}}(t) + \frac{\mathrm{d}\,\psi_{\mathrm{o}}}{\mathrm{d}\,t}(t)\Delta t \tag{6.33}$$

that imply:

$$\psi_{\mathrm{o}}(t) \cong \psi_{\mathrm{o}}(t + \Delta t) - \frac{\mathrm{d}\,\psi_{\mathrm{o}}}{\mathrm{d}\,t}(t)\Delta t \tag{6.34}$$

So (6.32) becomes:

$$\psi_{\mathrm{o}}(t) > \bar{\psi}_{\mathrm{o}}(t) \tag{6.35}$$

Similarly for $t > t_{max}$:

$$\frac{\mathrm{d}\,\psi_{\mathrm{o}}}{\mathrm{d}\,t}(t) > \frac{\mathrm{d}\,\bar{\psi}_{\mathrm{o}}}{\mathrm{d}\,t}(t) \tag{6.36}$$

that imply:

$$\psi_{\mathrm{o}}(t_{\max}) + \frac{\mathrm{d}\,\psi_{\mathrm{o}}}{\mathrm{d}\,t}(t)\Delta t > \bar{\psi}_{\mathrm{o}}(t_{\max}) + \frac{\mathrm{d}\,\bar{\psi}_{\mathrm{o}}}{\mathrm{d}\,t}(t)\Delta t \tag{6.37}$$

If Δt is substituted with $-\Delta t$ in (6.34) it is obtained:

$$\psi_o(t) \cong \psi_o(t - \Delta t) + \frac{d\,\psi_o}{d\,t}(t)\Delta t \tag{6.38}$$

that implies therefore (6.37) to become:

$$\psi_o(t) > \bar{\psi}_o(t) \tag{6.39}$$

From the mathematical point of view the two conditions expressed in (6.30) produce the following set of equations:

$$\begin{cases} \psi_o(t_{max}) = \psi_o(0) + \Delta\psi_o \left(1 - e^{\frac{t_{max}-t_0}{\tau}}\right) \\ \frac{d\,\psi_o}{d\,t}(t_{max}) = \Delta\psi_o\, e^{-\frac{t_{max}-t_0}{\tau}} \end{cases} \tag{6.40}$$

from which it is obtained:

$$\begin{cases} \tau = \frac{\psi_o(0) - \bar{\psi}_o(t_{max}) + \Delta\psi_o}{\frac{d\,\bar{\psi}_o}{d\,t}(t_{max})} \\ t_0 = \tau \log\left(\frac{1}{\Delta\psi_o}\frac{d\,\bar{\psi}_o}{d\,t}(t_{max})\right) + t_{max} \end{cases} \tag{6.41}$$

Therefore it is possible to get an estimation of t_0 and τ as a function of $\Delta\psi_o$ by solving the set of equations (6.41) for a discrete set of heading changes $\Delta\psi_o$. The values of t_0 and τ obtained with this approach depend on the trim condition considered and are therefore function of altitude h_o and airspeed V_o.

It is therefore possible to estimate the heading angle dynamics $\psi_o(t)$ by running the simulator described in [157] with a step heading angle command with intensity $\Delta\psi_o$. The evolution with thime of the variable $\psi_o(t)$ obtained from the simulation can be then used to estimate the values of the parameters t_0 and τ can be obtained according to the previous formula. If this operation is then repeated for a discrete set of heading angle command values $\Delta\psi_o$, it is possible to obtain the related set of values t_0 and τ as shown in fig. 6.8. From these sets, the following conservative polynomial approximations of t_0 and τ can be defined:

$$\tau = 0.0327\Delta\psi_o^2 - 0.0018\Delta\psi_o + 1.3789 \tag{6.42}$$

$$\begin{aligned} t_0 = &-0.0002\Delta\psi_o^9 + 0.0009\Delta\psi_o^8 + 0.0039\Delta\psi_o^7 - 0.0125\Delta\psi_o^6 - 0.0290\Delta\psi_o^5 + \\ &+ 0.0549\Delta\psi_o^4 + 0.0928\Delta\psi_o^3 - 0.0710\Delta\psi_o^2 - 0.1110\Delta\psi_o + 7.5833 \end{aligned} \tag{6.43}$$

6.5.3 Horizontal Manoeuvre Optimisation

When a conflict risk is detected, an avoidance manoeuvre should be executed. This could be achieved in the horizontal plane by applying a step change $\Delta\psi_o$ to the heading angle autopilot command. As can be seen in fig. 6.9, the resulting heading angle response $\psi_o(t)$ is characterised by a settling phase followed by a steady state condition.

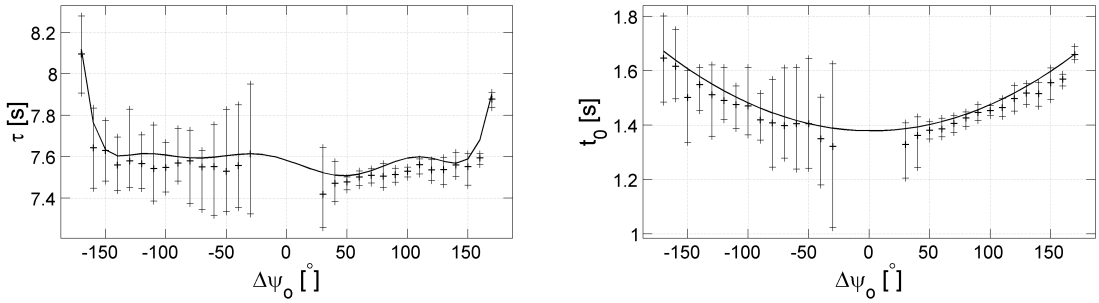

(a) (b)

Figure 6.8: estimation of the heading angle response parameters for a discrete grid of heading angle commands $\Delta\psi_\mathrm{o}$ and comparison with the linear segments approximation in cruise condition at an altitude of 80 m and an airspeed of 15 m s^{-1}: (a) τ, (b) t_0

This includes the time range elapsed before the settling time t_s that is identified in the figure.

During the settling phase it is difficult to estimate the true ownship's heading angle $\psi_\mathrm{o}(t)$ and the trajectory of the i-th threat $\vec{P}_{\mathrm{r},i}(t)$ in the real flight. This is due to the interaction effects between longitudinal and lateral-directional dynamics and the environmental disturbances such as turbulence and gusts. However, a conservative estimation of the i-th threat's trajectory $\vec{P}_{\mathrm{r},i}(t_\mathrm{s})$ can be obtained from (6.17).

During the steady state phase, the threat's trajectory is approximately a straight line passing through the point $\vec{P}_{\mathrm{r},i}(t_\mathrm{s})$ of the trajectory. Hence, during this phase, the smallest distance d_i between the i-th threat and the ownship can be estimated with the following relationship derived from vectorial geometry considerations:

$$d_{\mathrm{t},i} = \left| \vec{P}_{\mathrm{r},i}(t_\mathrm{s}) \times \frac{\vec{V}_{\mathrm{r},i}(t_\mathrm{s})}{\left|\vec{V}_{\mathrm{r},i}(t_\mathrm{s})\right|} \right| \tag{6.44}$$

where $\vec{V}_{\mathrm{r},i}(t)$ is the threat speed expressed in the reference frame moving with the ownship defined with the usual relationship as follow:

$$\vec{V}_{\mathrm{r},i}(t) = \frac{\mathrm{d}\,\vec{P}_{\mathrm{r},i}}{\mathrm{d}\,t}(t) \tag{6.45}$$

Therefore the cost function Δd to optimise the resolution manoeuvre can be defined by the following formula:

$$\Delta d = \begin{cases} \sum_{i=1}^{N_\mathrm{t}} \left(d_{\mathrm{t},i} - r_\mathrm{s} - r_\mathrm{u}\right) & \text{if} \quad \forall i | i \in \{1,2,...,N_\mathrm{t}\} \\ & \quad d_{\mathrm{t},i} \geq r_\mathrm{s} + r_\mathrm{u} \wedge \vec{P}_{\mathrm{t},i}(t_\mathrm{s}) \cdot \vec{V}_{\mathrm{t},i}(t_\mathrm{s}) \leq 0 \\ 5 \left| \sum_{i=1}^{N_\mathrm{t}} \left(d_{\mathrm{t},i} - r_\mathrm{s} - r_\mathrm{u}\right) \right| & \text{if} \quad \exists i | i \in \{1,2,...,N_\mathrm{t}\} \\ & \quad d_{\mathrm{t},i} \geq r_\mathrm{s} + r_\mathrm{u} \vee \vec{P}_{\mathrm{t},i}(t_\mathrm{s}) \cdot \vec{V}_{\mathrm{t},i}(t_\mathrm{s}) > 0 \end{cases} \tag{6.46}$$

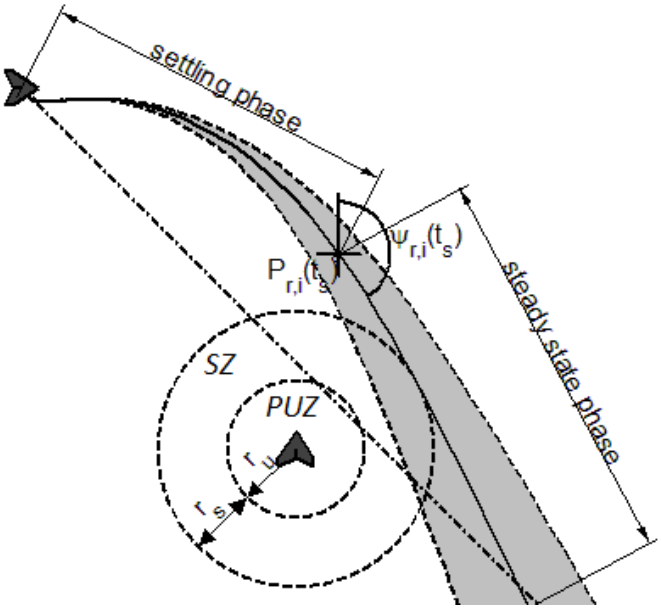

Figure 6.9: resolution manouevre phases and uncertainties related with its estimation: the gray strip is the uncertainties of the threat trajectory estimation in the ownship reference frame, the circle with the label *PUZ* is the position uncertainty zone and the locus *SZ* is the safety zone

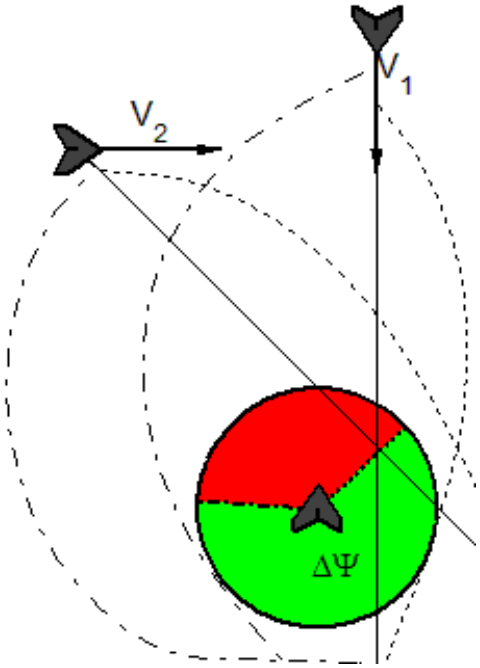

Figure 6.10: graphical representation of the safe resolution heading range $\Delta\Psi_{\text{res}}$ and the trajectory produced by the two extremes of the range defined.

where the vectorial condition $\vec{P}_{t,i}(t_s) \cdot \vec{V}_{t,i}(t_s) \leq 0$ is imposed to avoid solutions in which the steady state phase is reached after the ownship enters the *SZ*. The above optimisation problem can be solved using the `fmincon` function of the *Optimization Toolbox* of *Matlab*®. The solution of the problem defines in the range $[-\pi, \pi]$ a set $\Delta\Psi_{\text{res}}$, (see example in fig. 6.10) of the heading angle commands $\Delta\psi_{\text{res}}$ that includes the heading angle command changes suitable to avoid all the conflicts. This range includes all the values of $\Delta\psi_{\text{res}}$ for which the first condition of the system (6.46) holds, that is, in the case of head-on encounters, the range not including the value $\Delta\psi_{\text{res}} = 0$.

It is worth mentioning that this optimisation problem could be characterised by two, one or none solution in the range $[-\pi, \pi]$ for a multiple head-on encounters scenario. In the first case the algorithm used for the resolution manoeuvre selection, described in section 6.7, selects the option with the lowest absolute value for the proposed horizontal resolution manoeuvre. In the second case the only available solution is the proposed horizontal resolution manoeuvre. In the third one the range $\Delta\psi_{\text{res}}$ is empty and the algorithm does not consider any possible horizontal resolution. In this case the algorithm considers only the vertical manoeuvres according to the procedure defined in the next section.

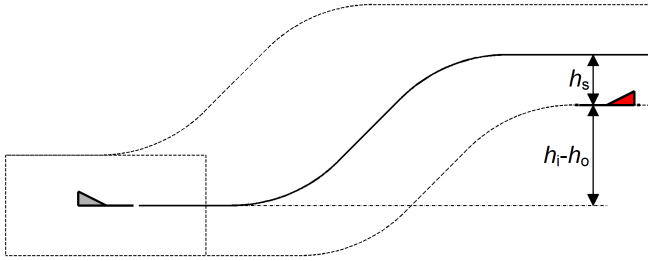

Figure 6.11: approach used for the vertical resolution evaluation: the red aircraft on the right-hand side is considered as the threat and the gray one to the left is the ownship

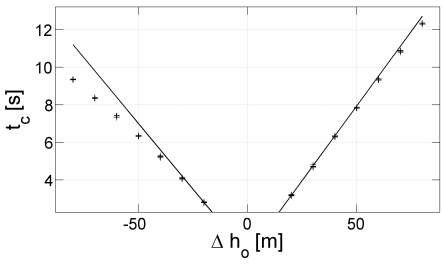

Figure 6.12: estimation of the t_c values for a discrete grid of Δh value and comparison with the approximation (vertical view)

6.6 Vertical Resolution Manoeuvre Definition

As fig. 6.11 shows, a safe resolution manoeuvre in the vertical plane can be produced by a suitable altitude change Δh_{res}. This should place the ownship in a final condition in which the vertical distance from threats is equal or greater than the half-height h_s of the safety zone. Therefore the range ΔH_{res} of the altitude changes suitable for a safe resolution manoeuvre is:

$$\begin{aligned}\Delta H_{\text{res}} = [-\infty, h_{\text{o}}(t) - (\min(\mathbb{H}_i(t)) + h_{\text{s}})] \cup \\ \cup [h_{\text{o}}(t) + (\max(\mathbb{H}_i(t)) + h_{\text{s}}), +\infty]\end{aligned} \tag{6.47}$$

where $\mathbb{H}_i(t)$ is defined as the set of the current altitude values $h_i(t)$ of the detected threats or:

$$\mathbb{H}_i(t) = \{h_i(t) | i = 1, \ldots, n\} \tag{6.48}$$

For each of the two finite extremes obtained, the safety of the related resolution manoeuvre has to be evaluated. It can be accomplished by verifying that the horizontal distance necessary for the aircraft to reach the new commanded altitude is low enough to avoid all the threats of entering the ownship safety zone. In order to verify if this condition is true, it is necessary to estimate the rise time t_{c}, which is the time taken by the aircraft to move from the current altitude to the new commanded altitude. The rise time can be estimated from the response of the aircraft based on a discrete set of altitude variations Δh, which starts from the same initial cruise condition. These values can be used to get a linear segment regression as given in the equation below and shown in fig. 6.12:

$$t_{\text{c}} = \begin{cases} 0.16\Delta h_{\text{res}} & \Delta h_{\text{res}} \geq 0 \\ -0.14\Delta h_{\text{res}} & \Delta h_{\text{res}} < 0 \end{cases} \tag{6.49}$$

Once t_{c} is estimated, the horizontal distance $d_{\text{h},i}$ between the ownship and the i-th threat after which the ownship reached the new altitude can be calculated as:

$$d_{\text{h},i} = \left|\vec{P}_{\text{r},i}(0)\right|_{\text{h}} - \left|\vec{V}_{\text{r},i}(0)\right|_{\text{h}} \cos\left(\alpha\left(\vec{V}_{\text{r},i}(0)\right) - \alpha\left(\vec{P}_{\text{r},i}(0)\right)\right) t_{\text{c}} \tag{6.50}$$

where $\vec{V}_{\mathrm{r},i}(0)$ is:

$$\vec{V}_{\mathrm{r},i}(0) = \vec{V}_i(0) + \begin{pmatrix} V_o \\ 0 \\ 0 \end{pmatrix} \tag{6.51}$$

and, for an arbitrary vector $\vec{v}$, the azimuth angle $\alpha(\vec{v})$ is defined by the following relationship:

$$\alpha(\vec{v}) \triangleq \arctan \frac{v_y}{v_x} \tag{6.52}$$

Therefore the vertical manoeuvre is safe if the following condition holds:

$$d_{\mathrm{h},i} \geq r_{\mathrm{s}} + r_{\mathrm{u}} \qquad \forall i | i \in \{1, 2, ..., N_{\mathrm{t}}\} \tag{6.53}$$

If this condition is not valid for one of the two ranges considered in (6.47), the related range needs to be removed from the set ΔH_{res}. Similarly to the horizontal case, the selected solution used for the resolution manoeuvre is still the option with the lowest absolute value among the range boundaries with a finite value.

6.7 Manoeuvre Selection and Autonomous Resolution

The two ranges $\Delta\Psi_{\mathrm{res}}$ and ΔH_{res} produced respectively for the horizontal and vertical manoeuvres, as described in sections 6.5.3 and 6.6, could be easily displayed on *GCS HMI* interface. Moreover, it gives the *UAV* operator a wide range of selectable resolution options. This in turn allows more freedom with regards to the resolution manoeuvre planning and execution.

Among the resulting horizontal and the vertical resolution manoeuvres, the first one is preferred when the required variation in heading angle change is less than a certain threshold (in our case 60°). When this condition is not verified or when the algorithm does not provide an empty set $\Delta\Psi_{\mathrm{res}}$ of feasible horizontal manoeuvres, then the vertical manoeuvre is selected.

In *manual navigation mode*, as the two feasible solutions defined in sections 6.5.3 and 6.6 decrease to one, then the resolution manoeuvre is autonomously performed. In *autonomous navigation mode*, an optimal navigation is obtained where the resolution manoeuvre is initiated as soon as the collision risk is detected. In both modes, the resolution manoeuvre is concluded when the threat passes the current ownship position and is outside of the safety zone.

6.8 Comparison of the algorithm with previous approaches

Section 3.8 covered the main design factors considered in previous research on *S&A* system by other researchers. The algorithm described in this chapter is characterised by many novelties and advantages regarding these factors when compared with other proposed solutions.

First of all, the approach used for the future threats state projection, described in section 3.8.1, is one of the main aspects. More precisely, despite the algorithm is based on the *straight projection* hypothesis, this approach offers more refined predictions than this hypothesis. It is based, in fact, on a frequent update of the information on the motion state of detected threats. The prediction keeps itself therefore very close to the real evolution of the threat's state, cause of the reduced time span of prediction. Moreover, despite this reduced error in the prediction, this solution avoids the higher computational requirements on which more refined approaches are based, such as *worst case projection* and *probabilistic methods*.

These results are furthermore obtained avoiding the complexity in terms of communication hardware necessary for solutions such as *path plan sharing*. The *path plan sharing* requires different aircraft in the workspace to communicate detailed information about their current motion state. This implies that *path plan sharing* is able to avoid conflicts only between aircraft equipped with *cooperative sensors*, as defined in section 3.8.1. Differently, the approach described in this chapter could be based on the horizontal and vertical speed, and heading information derived by simpler *non-cooperative sensors* (see section 3.8.1).

The proposed algorithm is advantageous also regarding the definition of the avoidance manoeuvre. Firstly, the computational requirement of such an approach is for sure lower in respect with *optimised escape trajectory approaches*, *e-field methods* and *hybrid S&A systems* (see section 3.8.2). From the point of view of sensors configuration requirements, this solution does not require the detailed exchange of information about flight plan that characterises *protocol based decentralised collision avoidance*.

The advantage in terms of sensors requirements are clear also in respect with *predefined collision avoidance* and *optimised escape trajectory approaches*. This is supported by the following example, which assumes to use the same radar model to detect the ground obstacles for the algorithm here proposed and these two approaches. For clarity, the solutions based on *predefined collision avoidance* and *optimised escape trajectory* are indicated in this paragraph with the acronyms *PCA* and *OETA*, respectively. In this case, it can be considered the evolution of the encounter geometry sketched in the sequence of figures displayed in fig. 6.13. In this scenario, despite the detected impact risk with the terrain, it is supposed that the *UAV* keeps moving on a straight trajectory controlled by the autopilots. The angle α displayed in the figures is the minimum track angle change required to avoid the conflict risk. It can be evaluated as a function of the

profile of the ground obstacles detected and the *UAV* dynamics. The profile of the ground obstacle detected is that included inside the circle representing the *UAV* radar range. Generally speaking, α increases when the *UAV* gets closer to the ground obstacle.

In this scenario, for $t = t_1$ (fig. 6.13(a)), all the algorithms are equivalent if they are designed in order to suggest a track angle change equal to α_1. For $t = t_2$ (fig. 6.13(b)), where $\alpha_2 > \alpha_1$,it would be necessary for *PCA* to impose a track angle variation equal to α_2 both for $t = t_1$ and $t = t_2$. This implies to consider a sub-optimal result for *PCA* for $t = t_1$, due to the higher deviation from the original trajectory. Regarding *OETA*, the change in track angle variation is captured only if this algorithm is sufficiently quick.

On the other hand, optimised escape trajectory approaches are generally characterised by high computation times necessary for the optimisation problem solution. Therefore there is the risk for *OETA* to be an unreliable solution in this scenario. Considering finally $t = t_3$ (fig. 6.13(c)), it is clear the advantage of designing the algorithm in order to allow switching between horizontal and vertical avoidance manoeuvres, as that described in section 6.7. This ability is particularly useful, e.g., when suggested track angle variation α_3 is superior to a threshold indicating the maximum allowed horizontal deviation from planned track. In this case, the option to switch to a vertical manoeuvre could be of paramount importance in reducing the deviation of the avoidance manoeuvre from the planned route. The implementation of this option makes the *PCA* structure more complex. Similarly it can

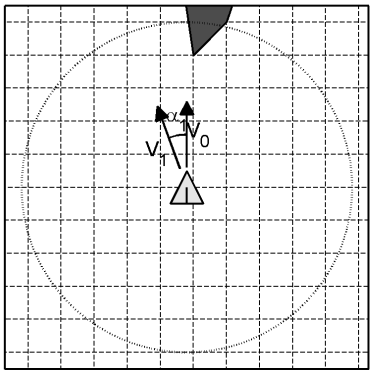

(a)

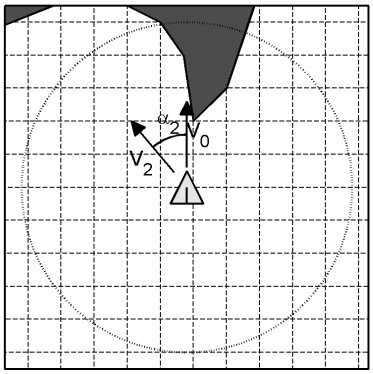

(b)

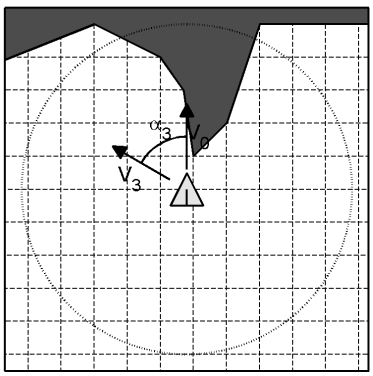

(c)

Figure 6.13: evolution of suggested avoidance manoeuvre in a scenario including a terrain impact: (a)$t = t_1$, (b)$t = t_2$ and (c)$t = t_3$.

be implemented on a *OETA* algorithm, but at the cost of a significant algorithm's complexity increase.

6.9 Chapter Summary

This chapter describes the *S&A* algorithm developed in this project. It is designed to operate with the levels of autonomy ranging from *manual navigation mode* to fully *autonomous navigation mode*. It is based on a *multiple conflict management* approach considering both airborne and ground threats. The *UAV* flight performances and *Rules of Air* are both considered in the resolution manoeuvre evaluation. Regarding the moving threats, the algorithm uses the hypothesis of a threat moving on a straight trajectory to get a quick evaluation of the advisories about the suggested resolution manoeuvre. The value of these commands are optimised in order to get respectively a sufficient horizontal and vertical separation between the ownship and all the threats detected during the overall manoeuvre. In the definition of the suggested resolution manoeuvre, the horizontal manoeuvres are preferred to the vertical ones when the required heading variation is inferior to a predefined threshold of 60°. The evaluated conflict geometry and the related resolution manoeuvre are updated at 1 Hz, to take into account changes of the conflict geometry caused by unpredictable trajectory changes of the threats.

As explained in the previous section, the frequent update of the evaluated conflict geometry allows to get a prediction very close to the real evolution, cause of the reduced time span of prediction. Moreover, the algorithm is characterised by a lower computational requirements in respect with more refined approaches, such as *worst case projection* and *probabilistic methods*. The algorithm avoids moreover the complexity in terms of communication hardware necessary for solutions such as *path plan sharing* and *protocol based decentralised collision avoidance*. More precisely, the solution can be based in fact on *non-cooperative sensors* instead of the *cooperative sensors* necessary for *path plan sharing*. Regarding the definition of the avoidance manoeuvre, the computational requirement of such an approach is finally lower in respect with *optimised escape trajectory approaches*, *e-field methods* and *hybrid S&A systems*.

CHAPTER 7

GCS Mock-Up

This chapter describes the *GCS* mock-up implemented to test the algorithm performances and study the integration of *S&A* systems functions in the *GCS*. This mock-up was moreover used in simulations and pilots interviews to test the effectiveness of the proposed solutions. This set of information display and the related input devices were chosen to support the pilot in the *flight management* task defined in section 2.4. The pilot's interactions with the parts related with other tasks (*communications*, *systems* and *tasks management*) are not relevant for the simulation scenarios chosen for this preliminary validation of the concept.

The configuration selected for the *HMI* is defined in section 7.1. The information display configuration is then illustrated in section 7.2. Section 7.3 includes some notes on the implementation from the point of view of hardware employed. Section 7.4 continues with the description of the solution used for the *S&A* system advisories integration in the *GCS*. The *ND* is illustrated in section 7.5. The layout of the *PFD* integrating the *S&A* advisories is given in section 7.6. The chapter concludes then with a quick illustration of the simulation controller, described in section 7.7, implemented to allow the supervisor to control the simulations during the pilots test.

7.1 Control Interface

The mock-up used for pilots tests is displayed in fig. 7.1. As already stated in section 5.4, the *ANS* system is designed in order to allow operations in both *manual navigation mode* and *autonomous navigation mode*. For this reason, it was necessary to include in the mock-up a mixed solution integrating both a direct and a supervisor control interface. The *direct control interface* (as previously described in section 2.5) is based on joystick and throttle controllers for *UAV* real-time direct control by the pilot. The *supervisory controller interface* (see section 2.3) is based on the integration of some *soft controls* (see section 2.8.1). The aim of these controls is to provide the *operator override function* prescribed in section 2.2 and *S&A* autonomous resolution function switching.

The joystick used is the *Microsoft Sidewinder Joystick* identified by label **3** in fig. 7.1. It provides conventional aircraft ailerons and elevator controls and also trim controls. The trim controls are programmed on the joystick buttons highlighted in fig. 7.2 according to the following convention, defined in order to be as close as possible to the manned aviation standard and pilot preferences:

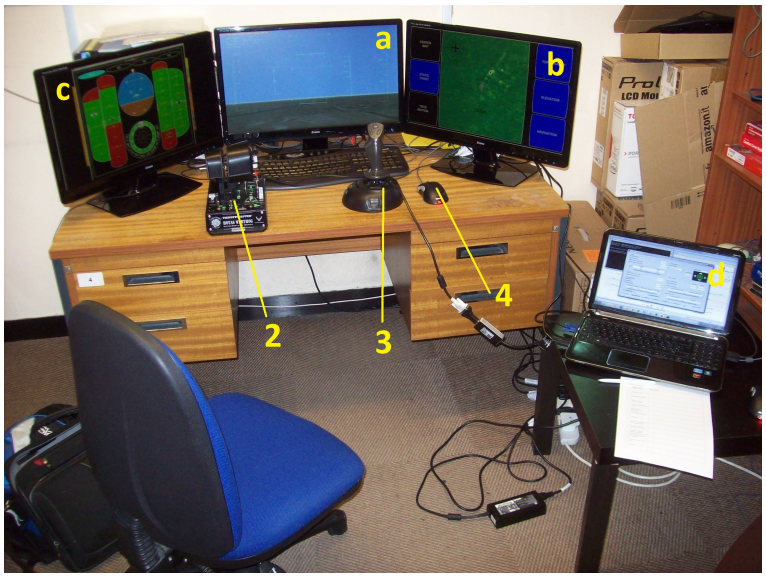

Figure 7.1: *GCS* mock-up used for pilots tests which includes the following elements: a)forward camera view display, b)*ND*, c)*PFD*, d)simulation controller display, 2)throttle, 3)joystick, 4)mouse.

Figure 7.2: identification of the buttons functions on the *Microsoft Sidewinder Joystick*: a)elevator trim-up control, b)elevator trim-down control, c)rudder trim-right control, d)rudder trim-left control

a) elevator trim-up control
b) elevator trim-down control
c) rudder trim-right control
d) rudder trim-left control

The *Thrustmaster® HOTAS Warthog™*, identified by label **2** in fig. 7.1, is used to provide the throttle input. All displays used are not touch-screen and therefore the soft controls are controlled by mouse-clicks. The mouse, identified by **4**, is the *Microsoft Intellimouse Optical 1.1* model in fig. 7.2.

7.2 Information Display Configuration

As will further be explained in next sections of this chapter, the information display set was designed in order to provide the operator an adequate level of situation awareness for real-time control of the *UAV*, when it is operating in the *manual navigation mode*. Moreover, the requirements on display layout optimisation described in sections 4.2 and 4.3 were taken into account. As shown in fig. 7.1 three displays were used and their function is described in the following list:

a. Forward Camera View (fig. 7.3) provides the *UAV* operator a real-time glance of the external environment and includes an *HUD* layer for supporting the operator and increasing his/her situation awareness with regards to flight condition and conflict avoidance manoeuvres;

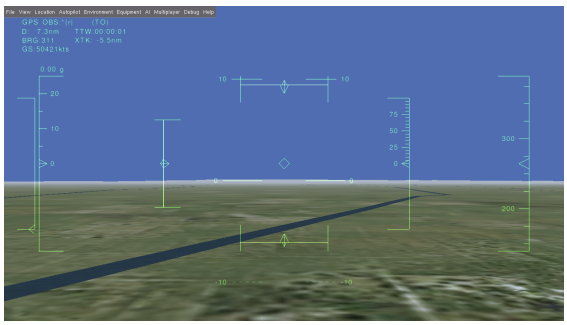

Figure 7.3: snapshot of the forward camera view

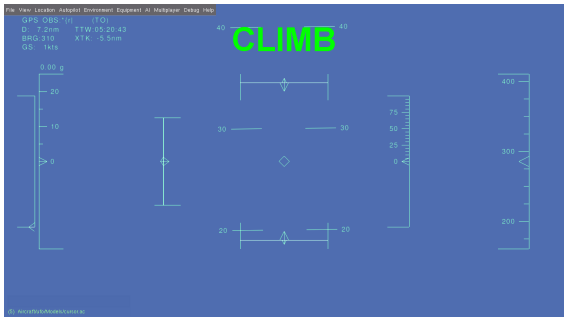

Figure 7.4: snapshot of the forward camera view while a *CLIMB* advisory is issued

b. Navigation Display supports the operator in the accomplishment of the tactical navigation task of the *UAV* mission (see section 7.5);

c. Primary Flight Display gives the operator real-time information about current flight conditions, detected conflict risks and related computed avoidance manoeuvre: it moreover includes an innovative autopilots control interface (further details can be found in section 7.6);

d. Simulation Controller to allow the operator to start/stop and set the simulation parameters during simulations (more details in section 7.7).

The camera view was simulated by running a *FlightGear* session linked with the *Simulink*® environment during simulation. The *HUD* includes two information layers. The first one has a conventional layout such as that described in section 4.9 providing the information about the current flight conditions. An additional layer, of which is given an example in fig. 7.4, replicates as textual message the resolution advisories of the *S&A* system.

7.3 Hardware Structure

This section describes the *GCS* mock-up general structure. The flowchart is displayed in fig. 7.5 and will be shortly described here. As can be seen in the chart, the architecture includes a set of controllers, including the **joystick**, the **throttle** and the **mouse**, connected to the master computer. This is a *HP Pavillion dv6 Notebook PC*, running the *Simulink*® simulation environment and elaborating the inputs for the *GCS* model implemented in *Matlab*®. The master computer controls the *FlightGear* session running on the slave computer, and displays the enhanced *PFD* and the navigation map. Finally, the slave computer, a *RM DESKTOP 310*, displays the *FlightGear* session on the related screen.

It was necessary to use two computers because of the high computational load. More precisely, it was decided to run on the desktop computer the session of *FlightGear* due to its higher computational load requirements. The laptop run the *Matlab/Simulink*® simulation environment and the *GCS* displays.

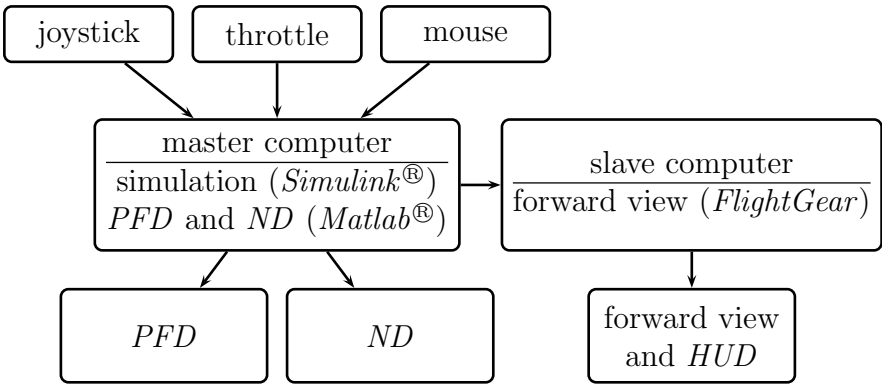

Figure 7.5: *GCS* mock-up flowchart

7.4 *S&A* System Integration

Regarding the integration of the *S&A* system interface, the solution used was based on an enhanced *CDTI* layout (described in section 7.6) and the replication of the *RA* on the *HUD*, a mixed implementation of options presented in [106] and recalled in section 4.5. It was chosen to avoid *SVS* and 3D display solutions for the following reasons: first, a planar display like *CDTI* provide the operator in just one display a depiction of conflict risks detected in all the 3D airspace. It provides the possibility to integrate the information about altitude with labels, such as those described in section 4.6. On the other hand, 3D displays provide just the vision of a part the space close to the forward view direction. Moreover, the planar displays avoid spatial judgements ambiguities (see section 4.8, usually related with 3D displays, leading to wrong judgements both in terms of bearing and distance. This kind of errors can be critical in collision avoidance. For this reason, it was decided to employ a display inspired by commercial aviation *CDTI* layout to take advantage of the easier and more precise position judgments than 3D displays. Finally, this implementation offered the advantage of a mature alerting logic and symbology inspired by *TCAS* (as detailed in section 3.7), together with the advantages of *HUDs*.

The mock-up included also the communication by aural messages of the *S&A* system advisories. The alerts syntax is defined in Table 7.1. When an intruder enters the *CDZ*, if a collision risk is detected a *RA* is directly issued with the calculated resolution manoeuvre. Otherwise, if no conflict risk is detected, the *TA* defined as in Table 7.1 is issued. The *clear of conflict* advisory is issued as soon as all the current conflict risks are resolved.

7.5 Navigation Display

The *ND* is shown in fig. 7.6. This component of the *GCS* information display is meant to support the operator situation awareness and management of the mission

Aural Advisory	Condition
turn right/left	this message, imposing a right/left turn manoeuvre, is issued whenever an horizontal resolution advisory is defined by the system
climb/descent	this message is related with the climb/descent advisories produced by the *S&A* system
autonomous resolution in progress	this message is produced when the *S&A* system start an autonomous resolution execution
clear of conflict	this is the advisory informing the pilot that all the conflict risks previously detetected were resolved
terrain	this advisory is produced in case the aircraft is too close to terrain according to the ground separation requirements set on the system
traffic	this advisory is the only *TA* produced when one or more aircraft violate the ownship separation zone

Table 7.1: aural advisories scheme

tasks defined in section 4.1 and includes navigation (flight plan execution) and mission objectives (targets). In the center a navigation map is displayed designed in order to be a tactical navigation map on which the *S&A* system advisories are not displayed to avoid confusion.

It includes different layers of information controlled by related buttons on the right. More precisely, *TOPOGRAPHY* is the button related with the topography layer visualisation/hiding. The data of this layer are taken from the dataset *OS VectorMap*™ *District* [158]. The *ELEVATION* button is used to switch on/off the elevation layer of the map derived from *ASTER Global Digital Elevation Model* [156]. *NAVIGATION* is finally a layer that was included just for future developments and that should include the typical cues useful for navigation planning (e.g. radio beacons, airports, targets).

The three buttons on the left are for the control of the view modality of the map. The button labelled *CENTER MAP* is related with static map modality of the map and centers the map on the current aircraft position. The *TRUE MOTION* switch controls the moving map mode in which the map moves according to aircraft's horizontal motion in order to keep it in its center. On the other hand, *STATIC CHART* enables the static map mode where the map does not move together with the ownship. This mode is meant to be used for strategic replanning during the flight.

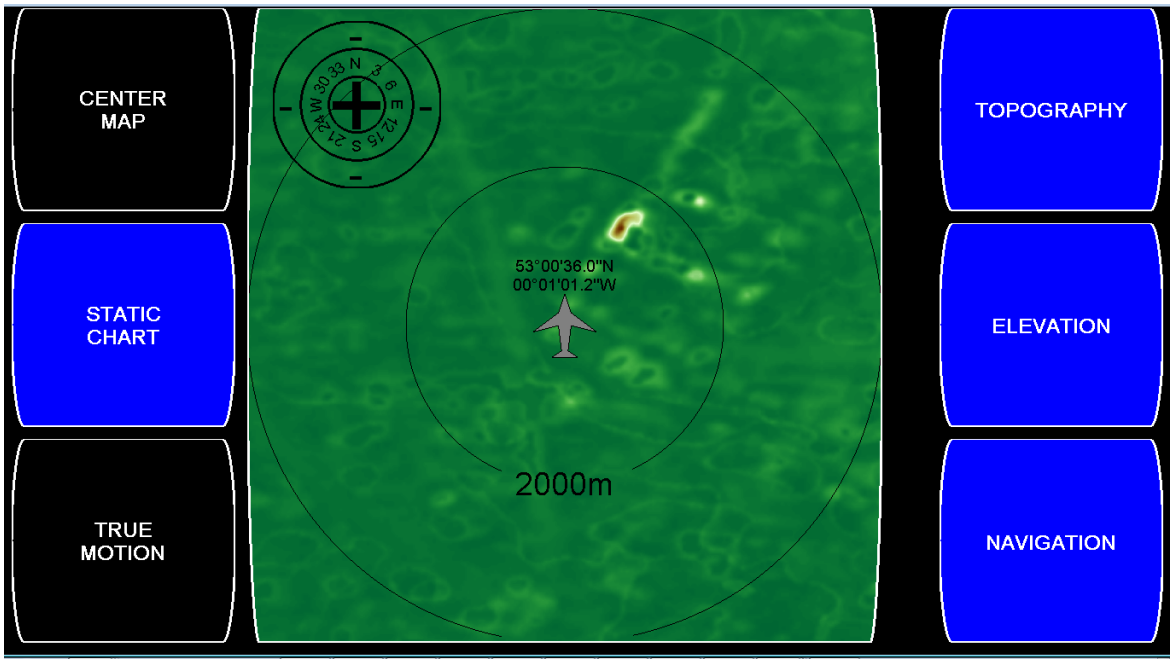

Figure 7.6: navigation display

As can be seen in the figures all the buttons described in this section except *CENTER MAP* does not perform only the function to allow the operator to select the related mode. In fact, they also communicate to the operator their state by changing their color according to the operating state of mode (blue for "on", black for "off"). This approach aims to maximise the number of functions performed by every *GUI* control in order to reduce the number of components on the display. This design philosophy was chosen in order to avoid the operator to spread its attention in a crowd of controls on the display and to minimise related workload.

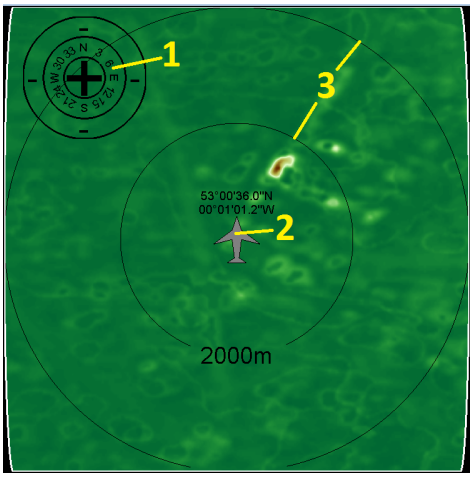

Figure 7.7: navigation map layout: 1)view controller, 2)ownship, 3) reference circles

7.5.1 Navigation Map

Figure 7.7 identify the components of the *navigation map* layout. The number 1 is the controller displayed in fig. 7.8. It allows the operator to perform the following functions:

1. when the mouse moves on the external circular sector, a "zoom-out" action is performed on the map;
2. when the mouse moves on the central circular sector, the map shifts in the

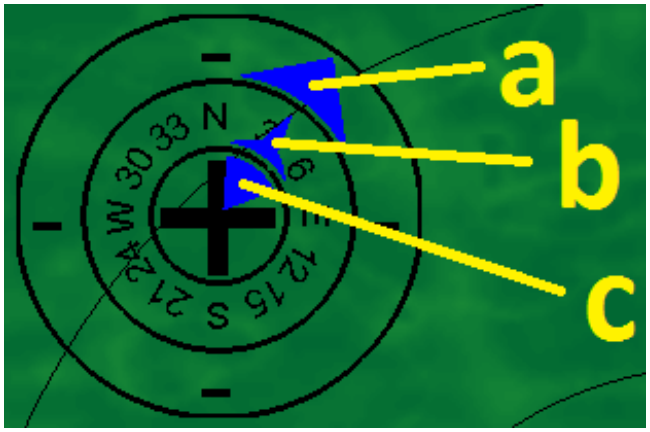

Figure 7.8: navigation map controller:
a)zoom-out control,
b)move control,
c)zoom-in control

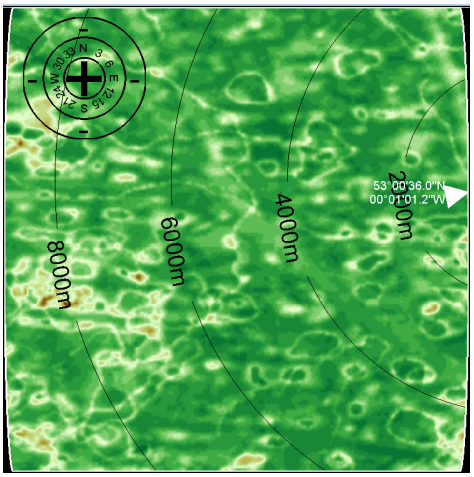

Figure 7.9: snapshot of the navigation map when the ownship is out of range

direction laying onto the segment connecting the pointer and the center of circular sector;

3. when the mouse moves on the internal circular sector the map zoom in;

This implementation was chosen to have all map range controls integrated in the same zone of the display. Moreover, it was designed in order to make easier for the operator to explore the map during tactical navigation planning. It was decided to avoid the implementation of controls activated by touching the map itself. This design philosophy was chosen in order to make possible a future development in which the operator can interact with the map, e.g. by directly selecting waypoints. This operating mode should allow easier tactical trajectory replanning.

The aircraft symbol represents current position and heading of ownship on the map. Over this symbol the current latitude and longitude are shown. In *STATIC CHART* mode, when the operator moves the map in a range in which the ownship is not visible, the simbology displayed in fig. 7.9 is used to provide the operator the direction in which the ownship is currently located. This symbology includes a triangular shape and the current position of the aircraft portrayed on the border of map in the direction where the aircraft is currently located.

Concentric circles centered in the current ownship position represent zones with diameters increasing with a step of 2000 m. They are displayed to make easier for the pilot the visual judgement of distance from map ground cues. Moreover, they can be used for tactical navigation purposes.

7.6 Primary Flight Display

Regarding flight condition monitoring and hazards situation awareness, described in section 4.1, it was decided to fuse these functions into the same display in order to reduce the operator's workload. The resulting display is meant as a testing/development environment tool that could need further testing and improvements for employment in real operating environment. It is a concept of enhanced *PFD*, inspired from the conventional *PFD* described in section 4.4, but with many novelties and integrating the following functions:

- visualisation of flight condition parameters, like conventional manned aviation *PFD*;
- visualisation of *S&A* advisories;
- visualisation and control of *FPCS* autopilots operating mode parameters;

The configuration of instruments/controls depends on the flight control mode, identified by the highlighted indicator/button displayed on the top of the panel as in the following list:

MAN is the **SAS** mode defined in section 5.3, part of the *manual navigation mode* described in section 5.1;

A/P is the **FPCS** mode defined in section 5.3, implemented to enable flight tests without operators in the *manual navigation mode* described in section 5.1;

P/F is the **autonomous navigation mode** defined in section 5.1;

A/R is the switch that can be used in all three overmentioned modes to enable or disable the *autonomous resolution* function described in section 5.1.

Colors were minimised according to guidelines defined in section 4.2. The choice of colors and fonts size used in the different display's elements was based on guidelines and tools provided in [159] and on current standards for manned aviation *PFD*. The following perceptual layers were identified:

Background, Terrain and Sky: culturally conventional coding (black, brown, sky);

Measures, Indicators and Labels: white color, size standard, weight normal;

Commands: high contrast chromatic color with culturally conventional coding, size standard, weight normal (magenta);

Limitations: high contrast chromatic color with culturally conventional coding, size standard, weight normal (red);

Active States Buttons: high contrast chromatic color with culturally conventional coding, size standard, weight normal (cian);

Selections: same color of commands but different symbology, size standard, weight normal (magenta);

Unactive States Buttons and Selection Buttons: background color (black), size normal, weight normal;

Markings: white color, size small, weight normal.

7.6.1 Flight Condition Parameters

A snapshot of the *PFD* in the *MAN* mode is displayed in fig. 7.10. Its general layout is very similar to the *PFD*, as it is described in section 4.4. This configuration was chosen in order to get a display easy to read for an operator used to manned aviation standards. Below flight control buttons, on the central upper position, the artificial horizon is displayed. On its top a roll attitude indicator is depicted in a configuration similar to that described in section 4.4. Figure 7.11 shows an indicator of the roll rate included in the roll angle indicator. This is a wedge moving with roll angle indicator and with an height proportional to the roll rate. At the bottom of the attitude indicator, as in the conventional *PFD* layout (described in section 4.4), a heading indicator is displayed. On its center it is placed the *CDTI* described in section 7.6.2.

The concept used for the *Vertical Speed Indicator (VSI)*, *AirSpeed Indicator (ASI)*, *Altitude Indicator* (*ALT*), and *Angle of Attack (AoA) indicator* (*AoA*) implementation are different from those used in the *PFD* layout. The *AoA* indicator itself is an indicator not present on conventional *PFD* and suggested by experienced pilots. The representation of these indicators is similar to the commercial solution proposed by *Belite Aircraft* [161] for ultralight aircraft. Their operating principle is different from instruments based on non-precision steam gauges instruments (e.g. fig. 7.12), typical of old generation cockpits, where a cursor pointing to the current value of the parameter moves on an angular range. They are also different from more recent linear displays (e.g. fig. 7.13), like those used in *PFD*, whose range slides and the current value of the parameter is magnified on a central fixed position. Differently, the concept here proposed considers a fixed range on which the current value magnified slides. This solution merges some advantages of both these solutions and try to reduce some of their limitations. More precisely:

- The digital representation of the measured value, similarly to linear displays, provides a more precise indication than steam gauges instruments.
- This display depicts the current value inside the range of the allowed values, that is typically small for small *UAVs*, like that considered in this project. This gives to the operator the possibility to judge the position of the current value inside that range and to take into account the allowed range in the short term (tactical) trajectory planning. This advantage is also given by some steam gauge instruments. The same characteristics is absent in linear sliding displays.
- This representation provide moreover the possibility to integrate in the display the restrictions derived by real-time information acquisition (*S&A*, no-fly zones, weather, ...) in order to further support the operator in short term planning. This is possible for linear displays and unappliable to steam gauges instruments.

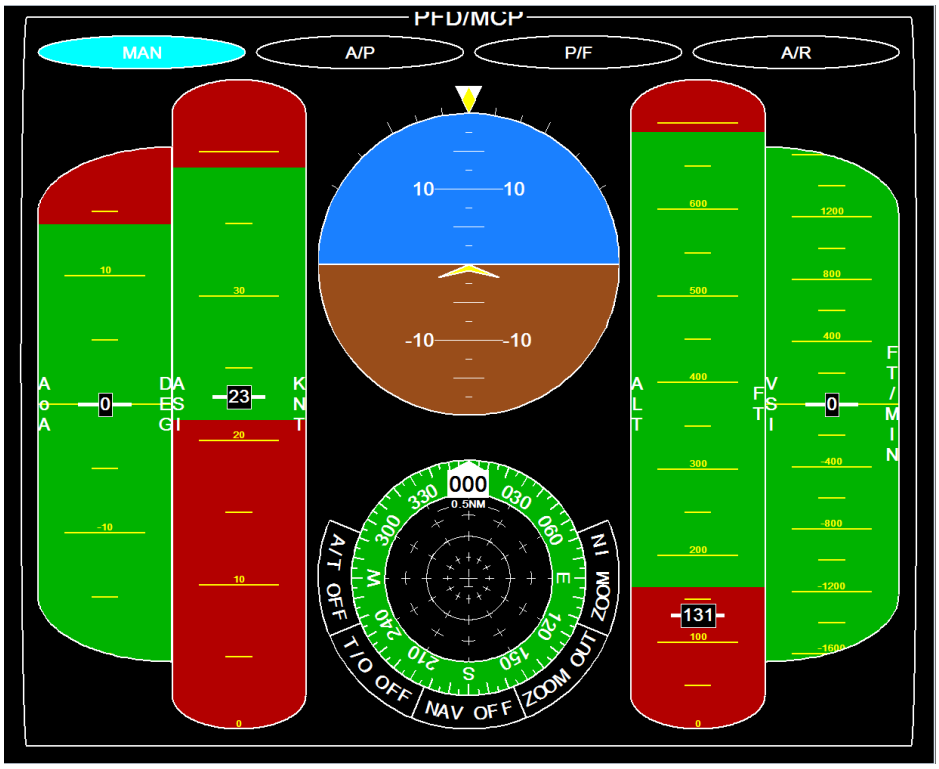

Figure 7.10: snapshot of enhanced *PFD* in the *MAN* mode

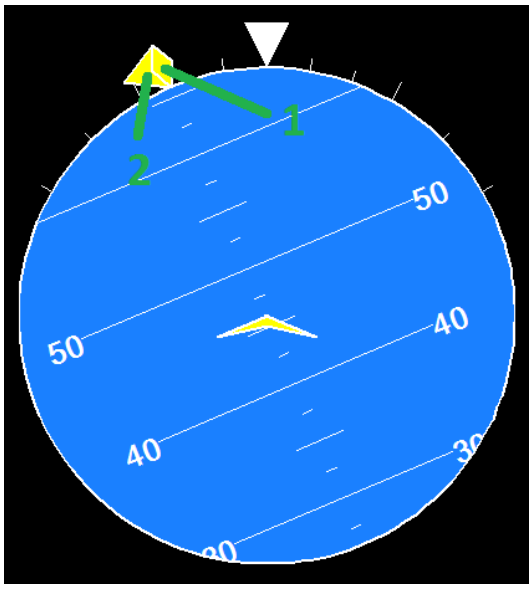

Figure 7.11: snapshot of the attitude indicator during a turn: 1)roll angle indicator, 2)roll rate indicator

Figure 7.12: example of conventional steam gauge *ASI* [160]

During tests, the pilots suggested to include the trend indicators like those of details 1 and 2 of fig. 7.14 to display the trend of variation of the variable. Another pilots suggestion required to display the indicators indicated by details 3 and 4 of fig. 7.14 close to the field displaying the current value. This suggestion was proposed to highlight to pilot the positive or negative value in the *AoA* indicator and the *VSI*.

7.6.2 *S&A* System *HMI*

A polar grid and a circle with the radius equal to the separation distance are added to the layout described in section 4.6. They are meant to support the pilot in the identification of the distance of potential threats. Moreover the *CDTI* range is displayed on the upper part of the grid, as reference for the pilot. The controls for "zoom in/out" functions are implemented with *ZOOM IN* and *ZOOM OUT* buttons. A terrain awareness and a navigation layer are included together with the traffic awareness and they can be enabled/disabled on *CDTI* with the following buttons:

NAV OFF/ON controls the navigation layer, enabling depiction on *CDTI* of the navigation weaypoints

A/T OFF/ON is related with the airborne awareness layer visibility,

T/O OFF/ON is the layer to enable the terrain awareness visibility.

The operating principles of the traffic awareness layer is the same as that described in section 4.6 with the following novelties, pointed out in fig. 7.15.

1. An additional line starting from the intruder position and extending to the direction opposite to that on which the intruder aircraft symbol moves is used to display the direction of movement. The line length is proportional to the intruder aircraft approaching speed.
2. An additional line starting from the intruder position and with a "T" end extending in the direction of aircraft's movement is used to provide an estimation of the *TTC*. The length of this line is proportional to the *TTC*.

Moreover a layer for the ground impact avoidance was included (see fig. 7.16). This layer depicts in an amber color the zones of local elevation map for which the distance between the current aircraft altitude and the elevation is inferior to the prescribed ground separation. Similarly, a red color is used for those zones in which this distance is less than the *PUZ*. In this layer too the line with the "T" end is used in case of impact risks.

The *S&A* system *HMI* includes the calculated safe ranges on the altitude indicator, *VSI*, attitude indicator, *ASI* and heading indicator, as displayed in fig. 7.17. Moreover the suggested resolution manoeuvre is visualised with a cyan line on the instrument for horizontal manoeuvres and on the *VSI*, altitude indicator and attitude indicator for vertical manoeuvres.

Figure 7.13: example of conventional *PFD* with linear displays [162]

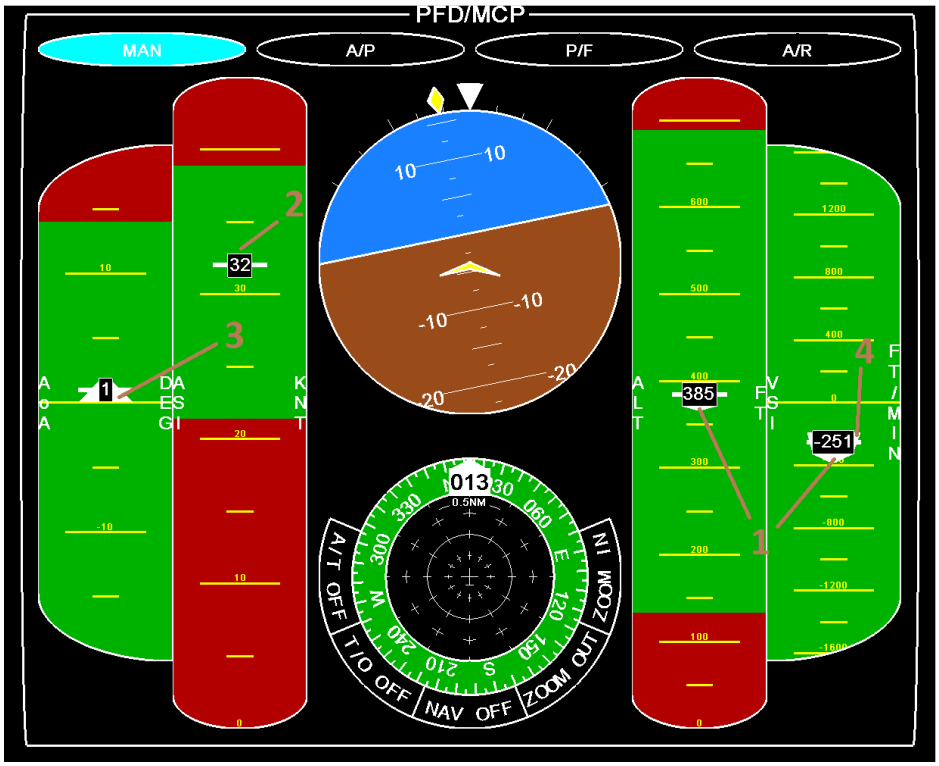

Figure 7.14: snapshot of enhanced *PFD* highlighting the trend and side indicators implemented in linear displays

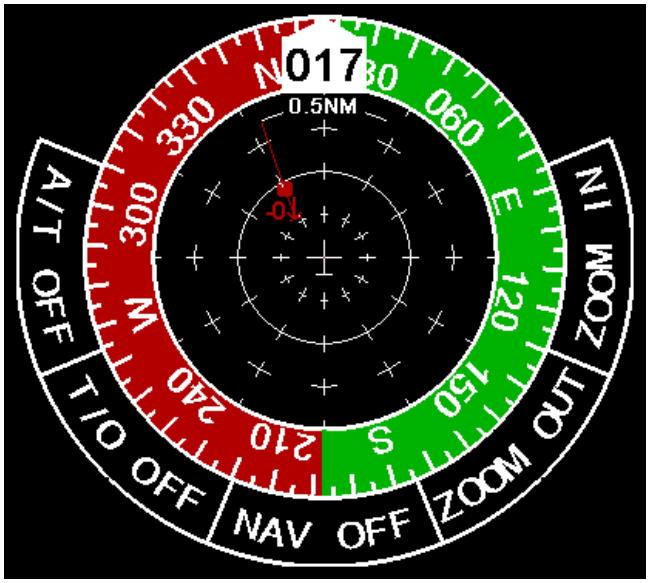

Figure 7.15: snapshot of the *CDTI*

Figure 7.16: snapshot of the *CDTI* as soon as a terrain separation violation is detected

7.6.3 Autopilots Modes

In the **A/P** mode the layout of the *PFD* changes as shown in fig. 7.18. The operator changes the *UAVs* autopilot parameters settings directly on the related instrument. The procedure used for this action is defined in the following list according to the sequence sketched in fig. 7.19:

1. press the side bar on the instrument on a point close to the new value;
2. adjust this value by using the up and down buttons marked with arrows;
3. confirm the new value by pressing the bar where the current value is displayed or the central button on the compass.

Finally, the layout of display in the **W/N** mode, shown in fig. 7.20, does not include any control for the autopilots but just the visualisation of the value currently setted for the autopilot setting.

7.7 Simulation Controller

The window displayed in fig. 7.21 was designed to support the operator during tests execution. It allows to set the simulations parameters at the start and control the simulation execution. The *Display* panel includes the parameters related with general *ANS* system operations. These are:

- horizontal and vertical ranges considered in the display,
- update frequency used for the overall *ANS* commands and advisories,

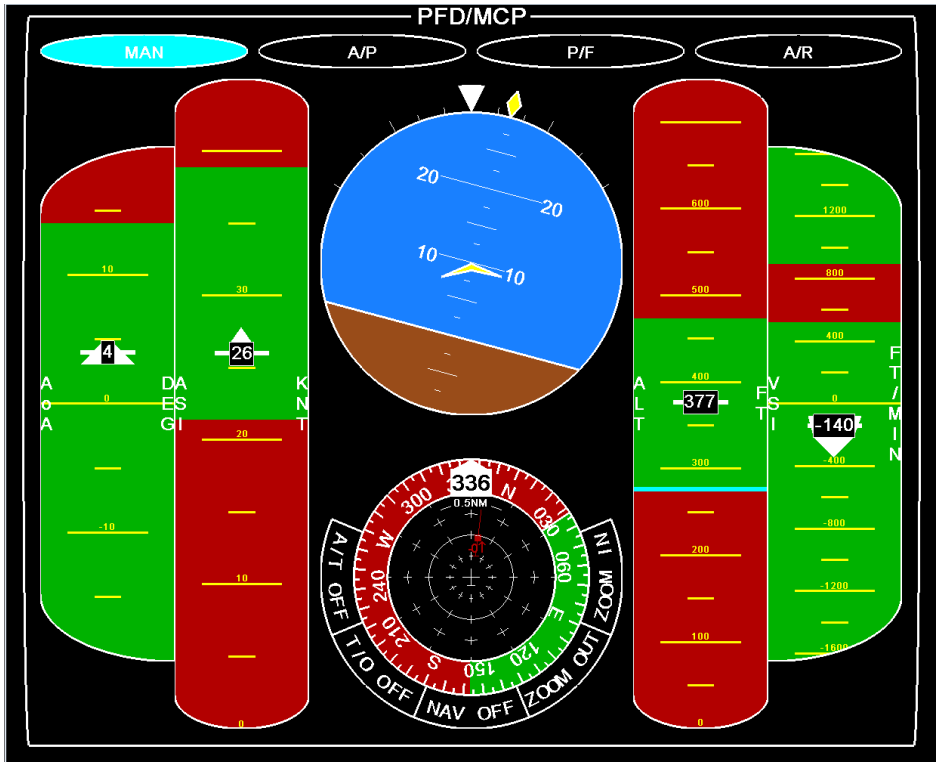

Figure 7.17: snapshot of enhanced *PFD* when a resolution advisory is issued

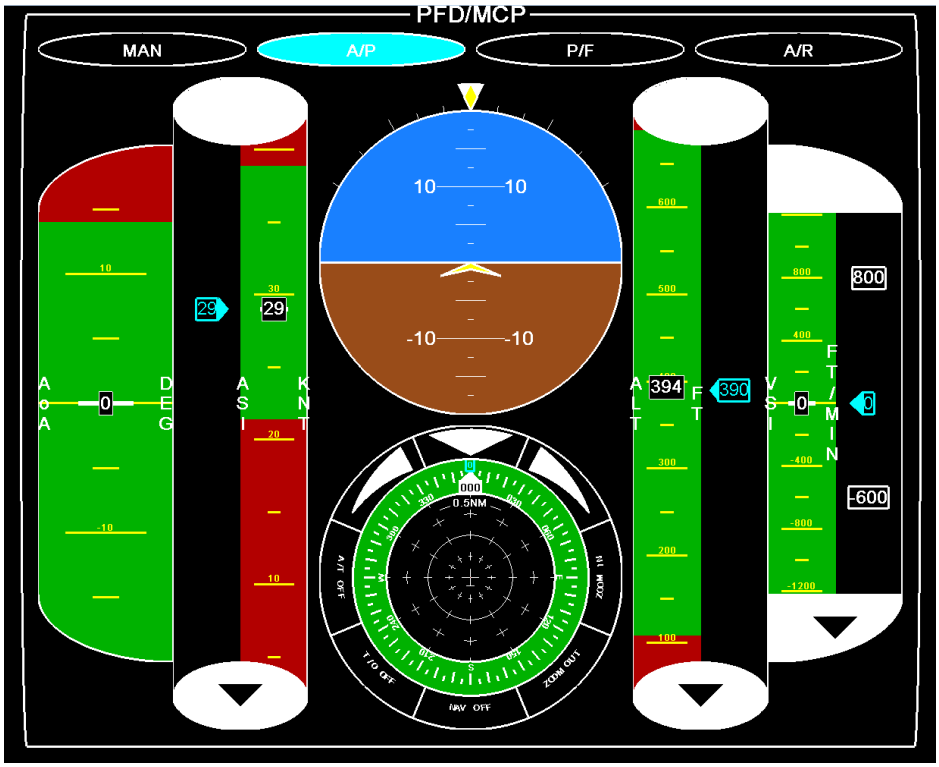

Figure 7.18: snapshot of enhanced *PFD* in the *A/P* mode

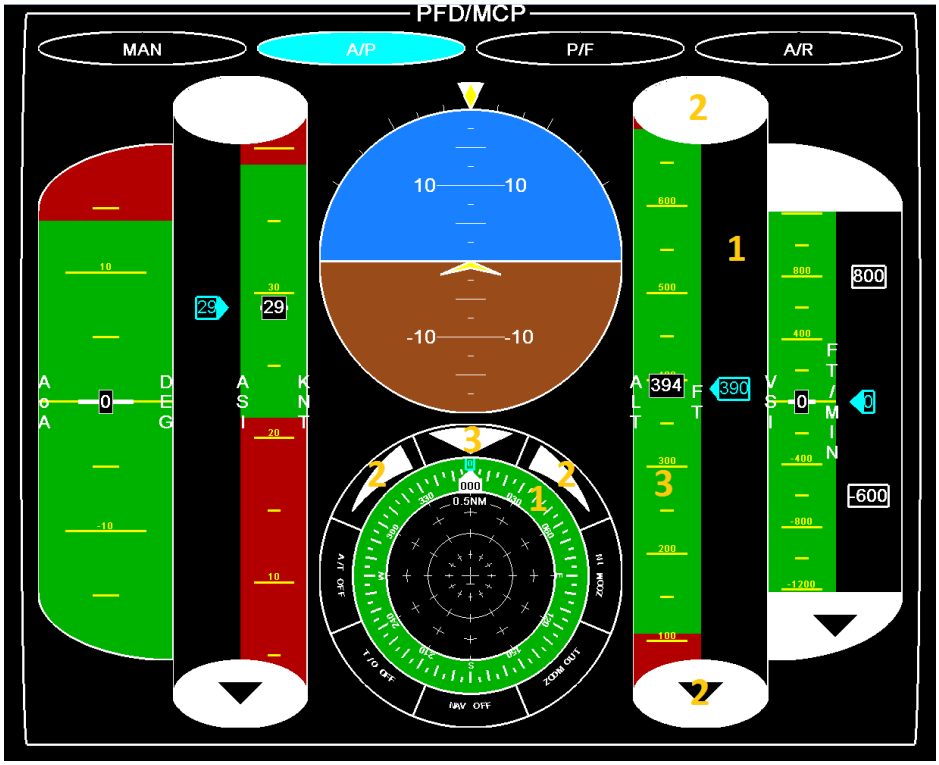

Figure 7.19: depiction of the procedure for the autopilots commands selection in the *A/P* mode

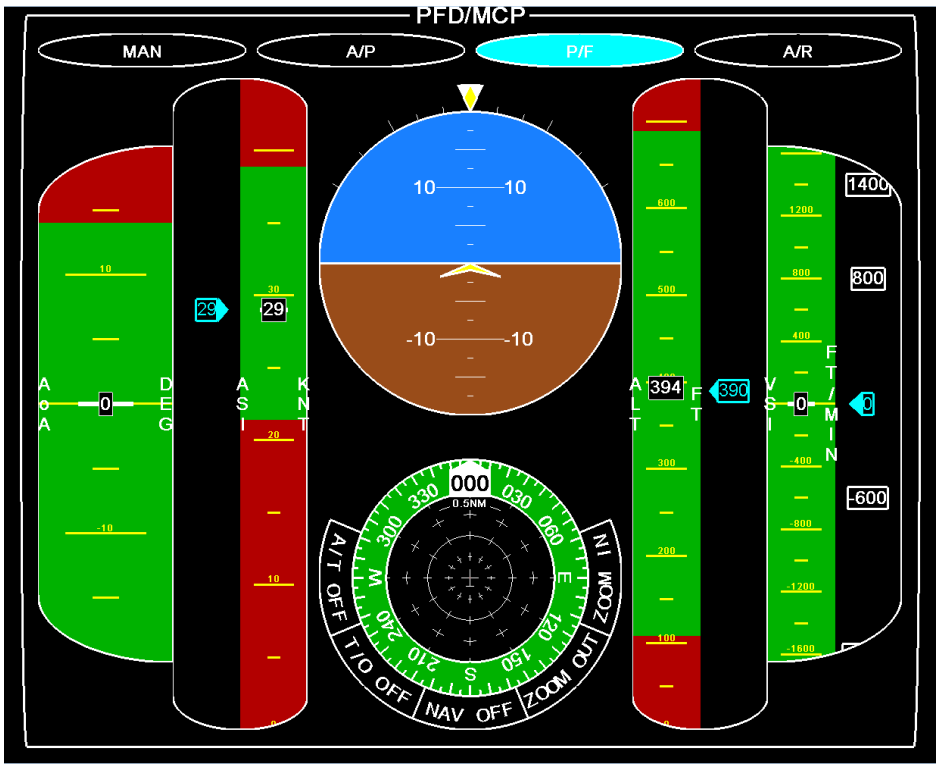

Figure 7.20: Snapshot of enhanced *PFD* in the *W/N* mode

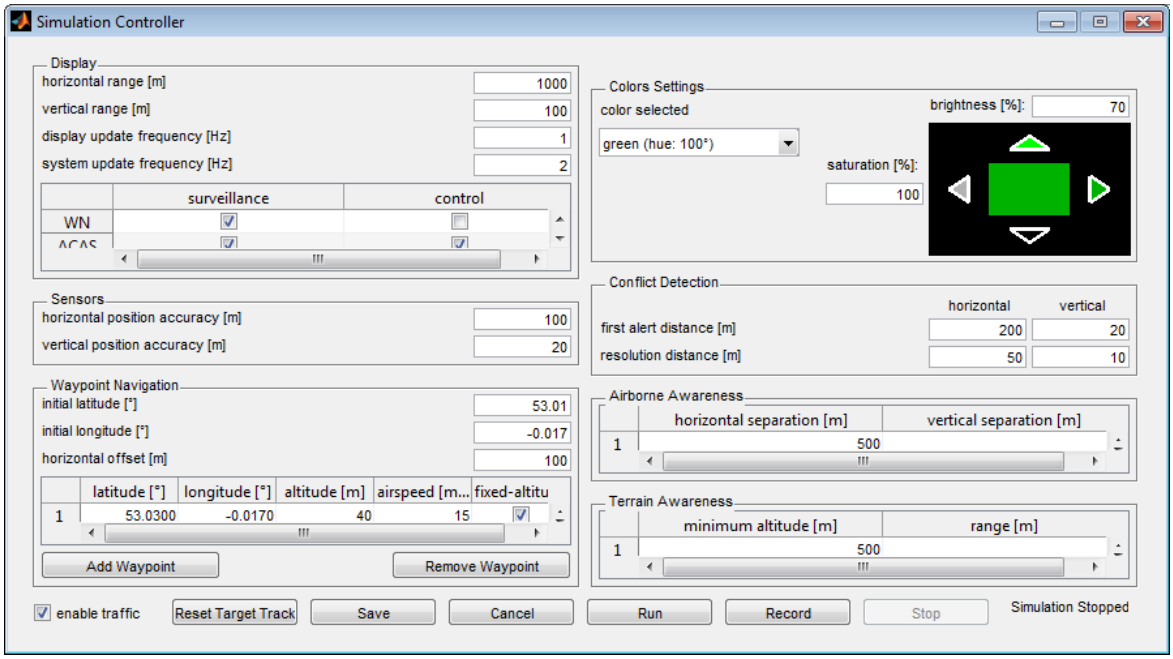

Figure 7.21: Snapshot of the simulation controller

- display's update prequency
- switches to set the operating modes of the various system functions (e.g. autonomous navigation, traffic awareness, ground awareness).

Collision zone is the panel by which the horizontal and vertical position accuracies considered from the conflict detection module of the *S&A* algorithm are set. In *Waypoint Navigation* the operator sets the initial position and the waypoints considered when the **P/F** mode is enabled.

Colors settings gives the user the possibility to change in real-time the brightness and saturation of the colors used for the different parts of the enhanced *PFD*. As portrayed in fig. 7.22, the user can select the color from a popup menu and specify the numeric values of brightness and saturation on related text fields. Otherwise he/she can adjust them by pressing the triangular buttons placed close to the edges of the square sample displayed at the right of the tab. The filling of the buttons is the color of the sample if the user maximise or minimise the related parameter;

The *Conflict Detection* panel defines the values considered for first-alert and collision distances. *Airborne Awareness* is the panel in which the user can set the separation zone dimensions to be considered in different flight segments. Terrain avoidance requirements are specified in *Terrain Awareness*.

Among the buttons displayed in the lower edge, the *enable traffic* checkbox and the *Reset Target Tracks* button allow the simulation supervisor to enable, disable or reset the predefined traffic scenario. The *Save* and *Cancel* buttons are used to save/reset the current settings defined in the panels previously introduced. The *Run* and *Stop*

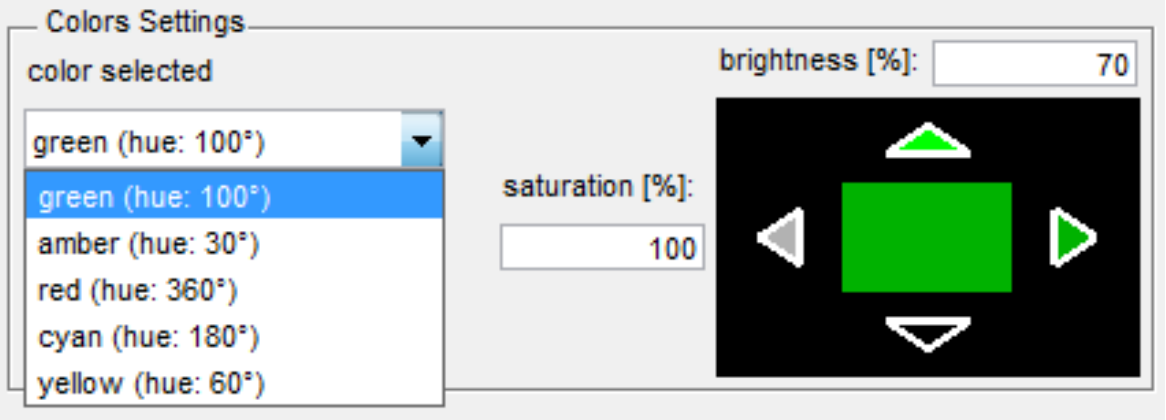

Figure 7.22: Zoom of the Colors Settings Panel with pop-up menu of the colors

buttons run/pause or stop the current simulation. *Record* is the button that allows to save videos and plots of the simulation in a user defined folder. Finally the text on the left-bottom corner of the window indicate the current state of the simulation and can be:

Simulation stopped appears when the simulation is paused or stopped;

Initialisation indicates that the simulation environment is currently initialising a new simulation;

Running 30s indicates that the simulation ran for 30 s

7.8 Chapter Summary

This chapter described the mock-up implemented for integrating *S&A* system in *GCS* and testing it with pilots. Its architecture was designed to allow operations in both *manual navigation mode* and *autonomous navigation mode*. It is therefore a mixed solution integrating both direct and supervisor control interfaces. The *direct control interface* is based on joystick and throttle for *UAV* real-time control by the pilot. The *supervisory controller interface* is based on the integration of some *soft controls*, allowing the *operator override function* prescribed in section 2.2 and the *S&A* autonomous resolution function switching.

The mock-up includes also a set of information displays set designed for supporting the operator particularly during *manual navigation mode* phases. Among these displays the *Forward Camera View* provides the *UAV* operator a real-time glance of the external environment and includes an *HUD* layer for supporting the operator and increasing his/her situation awareness with regards to flight condition and conflict avoidance manoeuvres. Another display is the *Navigation Display*, visualising an interactive map supporting the operator in the accomplishment of the tactical navigation task of the *UAV* mission. Regarding flight control, a fundamental component is the *Primary Flight Display* providing the operator real-time information about current

flight conditions, detected conflict risks and related computed avoidance manoeuvre with a layout optimised for *UAS* operations and including an innovative autopilots control interface. Finally, a *Simulation Controller* allows the operator to start/stop the simulation and set its parameters during simulations. The *S&A* system interface, the solution used is based on a redundant solution including an enhanced *CDTI* layout, the replication of the *RA* on the *HUD* and communication by aural messages of the *S&A* system advisories.

The *PFD* layout is inspired from the configuration used in manned aviation *PFD*, but includes also some novelties. In fact, its design takes into account the different performances and operating environment of *UAVs* in respect with manned aviation. The concept obtained integrates of all basic information about the flight condition, the autopilots controls, the advisories about detected threats and suggested avoidance manoeuvre in just one display. The benefit obtained is the reduction of the *UAS* operator workload caused by the need to search the information on a set of different displays. Among the novelties, a new concept is used for the airspeed, altitude, vertical speed and angle of attack indicators integrating red and green bands on their range. These bands identify the allowed or forbidden zones of the flight envelope according to the current condition in terms of conflict risk detected, aerodynamics performances and structural limitations. The display also includes the buttons allowing pilot to select the autopilots mode and the controls for the autopilots settings are integrated directly on flight parameters indicators.

CHAPTER 8

Simulations

Simulations were used to show capabilities in critical conditions of the *S&A* algorithm covered in chapter 6. Moreover, the *GCS* mock-up described in chapter 7 was used to collect feedbacks from potential *UAS* operators about their impressions on *GCS* concept itself, when operating it.

This chapter includes a selection of simulations aiming to show the *S&A* algorithm capabilities and the pilots interviews regarding the *GCS* mock-up functions and layout. The chapter starts with section 8.1 defining the test cases considered. Section 8.2 shows then some simulations involving a single flying threat mirroring the ownship during the conflict resolution. In these simulations the *UAS* is in the *P/F* control mode defined in section 7.6. The chapter continues then with the description in section 8.3 of a multiple flying and ground threats scenario with *UAS* in the *P/F* mode. Section 8.4 presents a multiple flying and ground threats scenario in *MAN* mode in which the last-resort autonomous resolution capability of the algorithm is tested. The chapter continues then with section 8.5 including some notes about the selection of pilots used for this part of the project. Tests methodology is then described in section 8.6. Finally section 8.7 summarises the findings.

8.1 Simulations Selection

The simulations sets used for the validation of this *S&A* algorithm was defined in order to verify its applicability to the three layers defined in section 3.1, namely: *strategic conflict management*, *conflict resolution advisory*, *autonomous resolution*. The *strategic conflict management* is strongly related with the capability of the algorithm to:

- timely detect the conflict risk when it is still not imminent,
- track its evolution,
- generate safe small corrections of the aircraft trajectory avoiding the conflict risk.

The *conflict resolution advisory* defines the capability of the algorithm to:

- generate a safe resolution manoeuvre,
- promptly update it when required by the evolution of the conflict scenario.

The *autonomous resolution* capability requires the algorithm to:

- be able to recognise the *minimum safe time before impact* defined in section 3.2,
- autonomously initiate the manoeuvre, when the *minimum safe time before impact* is reached and there is no pilot's input to avoid the conflict.

All these performances are related with the algorithm's capability to monitor the conflict geometry evolution and accordingly update the resolution manoeuvre. This can be produced by an unpredicted trajectory change of the detected threats and/or the appearance in the conflict scenario of new threats. The chosen simulations set aims therefore to cover all these aspects and takes into account both factors identified in this paragraph. The included simulations were implemented in the *Matlab/Simulink®* environment covered in chapter 5 and are described in more details in next sections.

More precisely, section 8.2 illustrates a set of simulations where a flying threat comes from different directions and tries to follow the ownship manoeuvres causing a conflict. In these simulations, the *UAS* is controlled in the *P/F* mode defined in section 7.6 with *A/R* switched on. This set of tests investigates the algorithm performance regarding *strategic conflict management* and *conflict resolution advisory*. Namely, it takes into account dangerous trajectory changes of the threat.

Differently from the previous section, section 8.3 considers a conflict geometry including two flying threats and a ground obstacle. These entities cause conflict risks, detected by the *S&A* system in different simulation time steps. The aim of this simulation is to test the performances in the autonomous mode of the algorithm till resolution of all detected conflict risks. The *UAS* is controlled in the *P/F* mode defined in section 7.6 with *A/R* switched on. This simulation tests the algorithm's performances in terms of *strategic conflict management* and *conflict resolution advisory*. This test includes, in fact, a conflict scenario including the appearance of new threats during simulation.

Finally, section 8.4 presents a similar situation with two flying threats and a ground obstacle. In this case, it is supposed the *UAS* operating in the *MAN* mode defined in section 7.6 with *A/R* switched on. The *UAV* moves on a straight levelled trajectory maintained by the *UAV* altitude and airspeed autopilots. The *UAS* operator does not intervene with the *UAV* control during the whole simulation. The *S&A* system starts resolution manoeuvre autonomously at the *minimum safe time before impact*. This simulation tests the algorithm performance in terms of last-resort autonomous resolution. It considers therefore the *strategic conflict management* and *autonomous resolution* performances for multiple threats scenarios.

8.2 Mirroring Simulations

A very interesting test case for *S&A* algorithms is that of a single flying threat which changes its trajectory in orded to be on the collision route with the ownship. This case is very close to a mirroring scenario, where threat and ownship implement the same

avoidance manoeuvre to escape the collision. This is therefore a very critical case to be taken into account in a *S&A* system and that was addressed in the *ACAS* system described in section 3.6. The following subsections describe the results for some cases in which the threat aircraft is coming from different directions.

In all simulations it is supposed that the ownship is moving in the *W/N* mode with *A/R* switched on starting from the initial position latitude 53.010° N, longitude 0.017° W and altitude 80 m and moving towards North with airspeed of 15 m s^{-1}. All simulations consider just one waypoint placed exactly Northwards of the ownship at the latitude 53.030° N, longitude 0.017° W and altitude 80 m. The flying threat moves in the *A/P* mode with autopilots altitude and heading commands continuosly updated in order to point every second towords the ownship. These commands remain fixed until the threat reaches a minimum distance of 250 m. The dimensions chosen for zones introduced in section 6.2 are defined in Table 8.1. The prescribed ground separation considered by *S&A* algorithm is 50 m.

Table 8.1: Dimensions of the *CDZ*, *SZ* and *PUZ* considered in the mirroring simulations

zone	**radius** [m]	**half-height** [m]
CDZ	500	50
SZ	150	40
PUZ	100	20

8.2.1 Head-on Conflict Risk

In the first simulation of this set, a flying threat at the same altitude of the ownship is considered. It moves on the same straight trajectory as the ownship, but in the opposite direction. It is therefore on a collision route with it and therefore leading to a conflict risk during the simulation. More precisely, the threat starts from the initial position with latitude 53.025° N, longitude 0.017° W and altitude 80 m flying at an airspeed of 15 m s^{-1} and initially heads Southwards. The results of the simulation are plotted in figs. 8.1 and 8.2.

The ownship's and threat's trajectories in three dimensional space are displayed in fig. 8.1(a). The projection of these trajectories on horizontal and vertical planes are shown in fig. 8.1(b) and fig. 8.1(c), respectively. The plot depicts the threat initially trying to follow the ownship during its resolution manoeuvre. The threat continues then in the last estimated direction of motion after reaching the threshold of 250 m from the ownship. In the meanwhile, it can be noticed that the ownship keeps on evaluating the resolution manoeuvre till the conflict resolution. When the conflict risk is resolved, the ownship changes its heading and flies towards the original assigned waypoint.

Figures 8.2(a) and 8.2(b) display the evolution of the horizontal and vertical separation distances during the simulation, respectively. Figure 8.2(c) shows that the distance between the two aircraft are both greater than the *CDZ* and *CAZ* dimensions during the whole simulation run. The optimisation time used to monitor the conflict scenario evolution and define the resolution manoeuvre at every simulation time step is displayed in fig. 8.2(d). It is displayed only the period in which the conflict risk

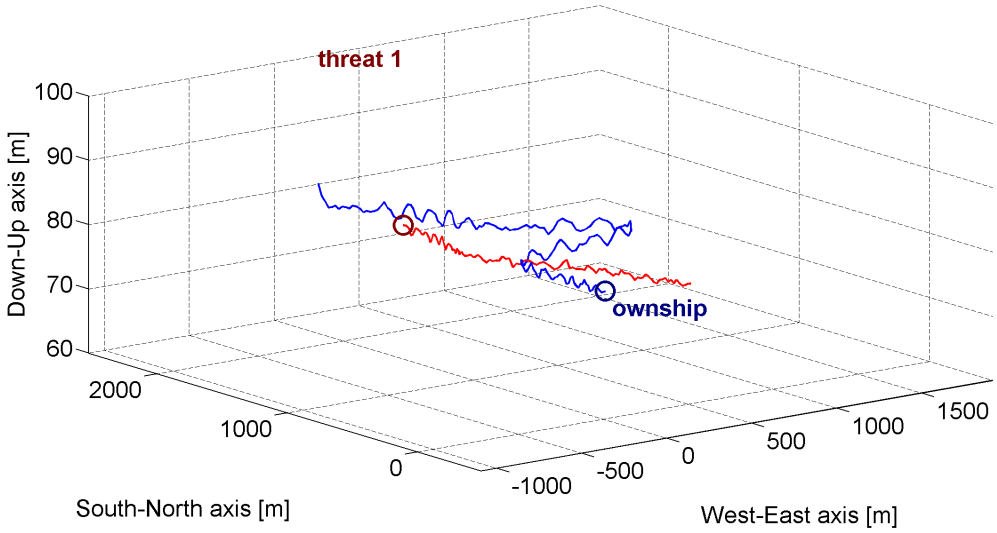

(a)

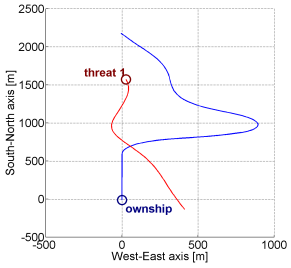

(b)

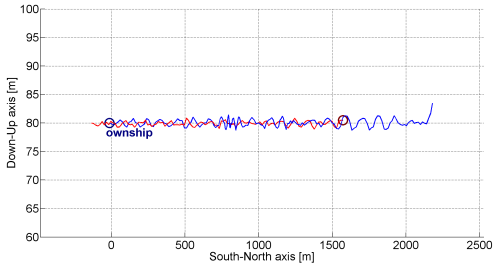

(c)

Figure 8.1: graphs of the head-on conflict simulation (part I): (a) 3D trajectories of ownship and threat, (b) horizontal view of ownship and threat trajectories, (c) vertical view of ownship and threat trajectories

resolution is in progress. The figure also shows that this time reach its maximum, almost 0.05 s, for just few seconds after the detection of the conflict risk. The value of this time is smaller than the threshold of 0.01 s during the whole simulation run, except for a tight peak close to the end of the resolution manoeuvre execution.

Figure 8.2(e) and fig. 8.2(f) show the evolution of computed safe heading and altitude ranges, and threat's position. This position is displayed in terms of bearing and vertical distance, respectively, in respect with the ownship. The threat position is plotted just for the time range where the conflict risk resolution is in progress. The parameter displayed in the horizontal axis is the distance to the point in which the manoeuvre is concluded. It substitutes the simulation time in order to show how the command evolves while the ownship approaches the potential collision point.

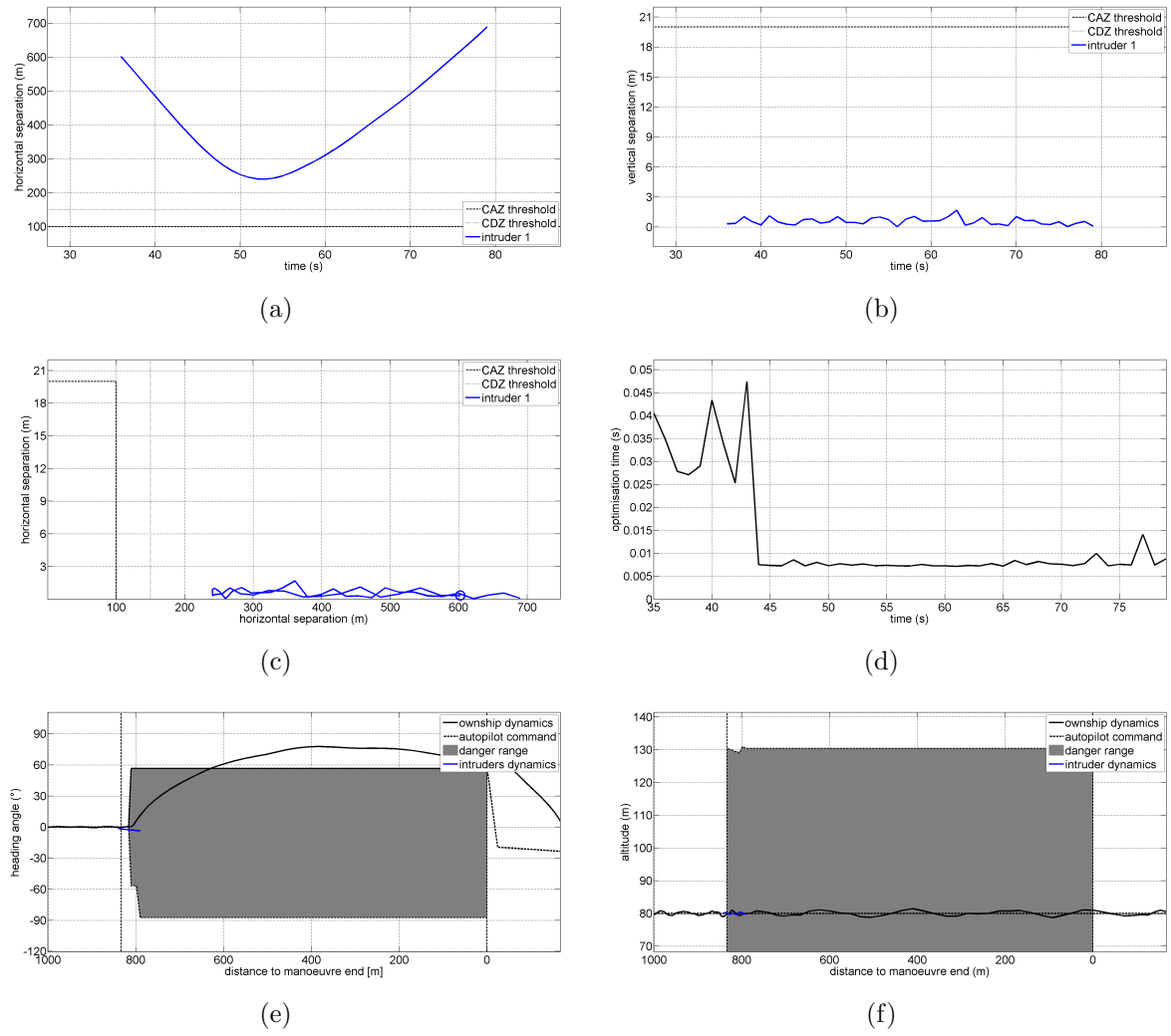

Figure 8.2: graphs of the head-on conflict simulation (part II): (a) evolution of the horizontal separation distance between ownship and threat and comparison with the *CDZ* and *CAZ* thresholds, (b) evolution of the vertical separation distance between ownship and threat and comparison with the *CDZ* and *CAZ* thresholds, (c) horizontal/vertical separation between ownship and threat plot, (d) computational time employed by the algorithm for advisories update, (e) evolution of ownship heading angle, autopilot command and computed safe range during simulation and comparison with threat bearing in those time ranges in which a conflict risk is detected, (f) evolution of ownship altitude, autopilot command and computed safe range during simulation and comparison with threat vertical position in those time ranges in which a conflict risk is detected

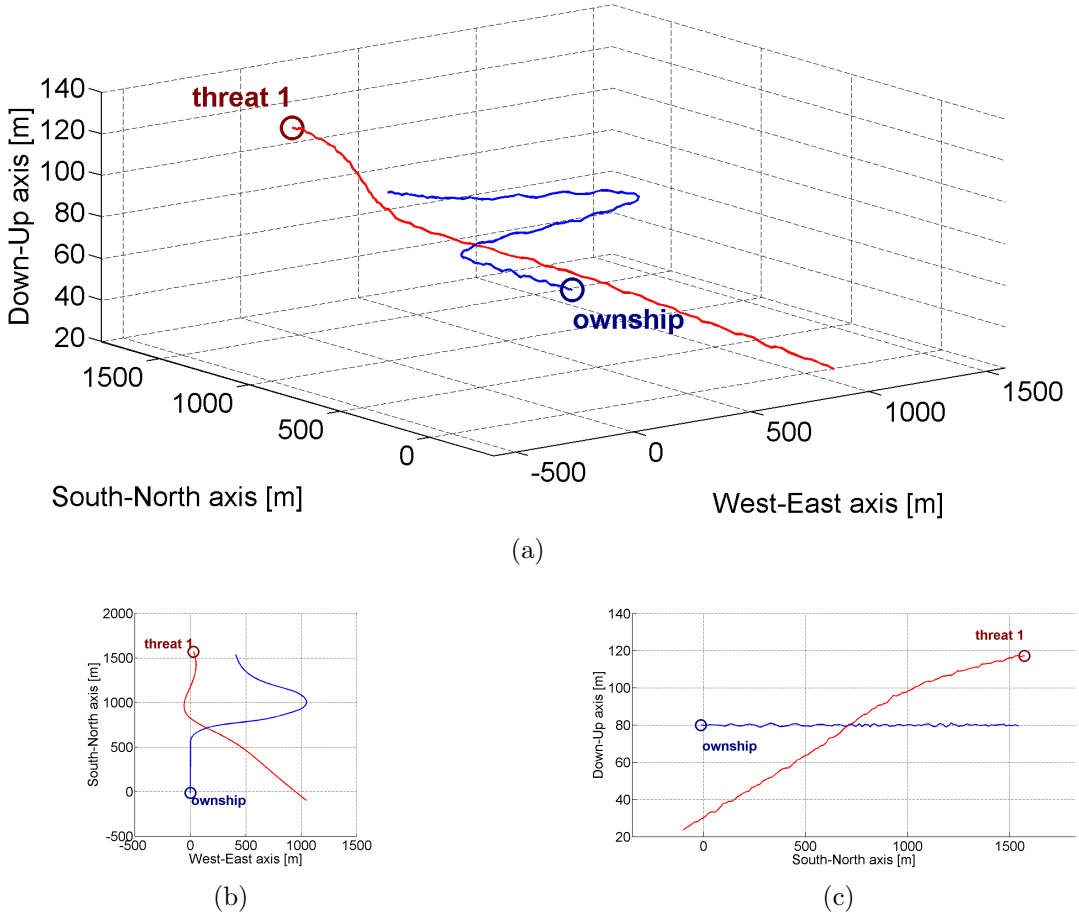

Figure 8.3: simulation graphs of descending threat scenario (part I): (a) 3D trajectories of ownship and threat, (b) horizontal view of ownship and threat trajectories, (c) vertical view of ownship and threat trajectories

8.2.2 Descending Threat

Another interesting simulation considers a threat on a descending route causing a potential conflict with the ownship. In this case the threat starts from the initial position with latitude 53.025° N, longitude 0.017° W and altitude 120 m. It moves with an airspeed of 15 m s^{-1} and initially heads Southwards. The simulation's results are plotted in figs. 8.3 and 8.4.

The ownship's and threat's trajectories in three dimensional space are displayed in fig. 8.3(a). The projection of these trajectories on horizontal and vertical planes are shown in fig. 8.3(b) and fig. 8.3(c), respectively. The plots clearly depict the threat initially trying to follow the ownship with both manoeuvres in horizontal and vertical plane. In fact, it tries to intercept it with a left turn during the resolution manoeuvre execution. Moreover, the threat descends in the vertical plane in order to follow the ownship. In the meanwhile, the ownship keeps on following the computed

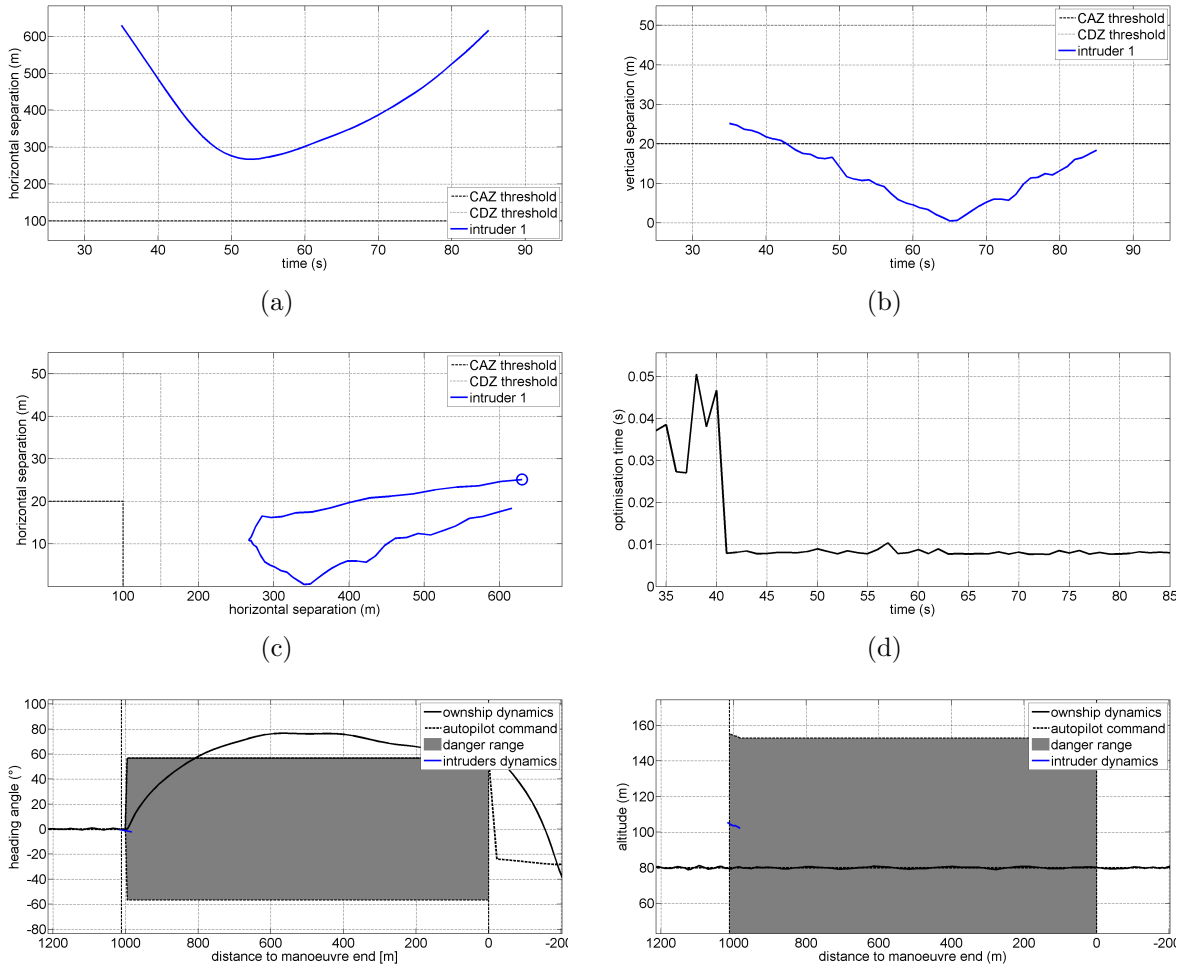

Figure 8.4: simulation graphs of descending threat scenario (part II): (a) evolution of the horizontal separation distance between ownship and threat and comparison with the *CDZ* and *CAZ* thresholds, (b) evolution of the vertical separation distance between ownship and threat and comparison with *CDZ* and *CAZ* thresholds, (c) horizontal/vertical separation between ownship and threat plot, (d) computational time employed by the algorithm for advisories update, (e) evolution of ownship heading angle, autopilot command and computed safe range during simulation and comparison with threat bearing in those time ranges in which a conflict risk is detected, (f) evolution of ownship altitude, autopilot command and computed safe range during simulation and comparison with threat vertical position in those time ranges in which a conflict risk is detected

resolution manoeuvre. This manoeuvre is not modified by the *S&A* algorithm during the simulation. In fact, the *CDZ* is wide enough to take into account the change of trajectory. The same plots show also that, as soon as the conflict risk is resolved, the ownship heads back to the assigned waypoint.

Figures 8.4(a) and 8.4(b) display the evolution of the horizontal and vertical separation distances during the simulation, respectively. Figure 8.4(c) shows that the threat stays outside of the *CDZ* and *CAZ* during the whole simulation run. The *S&A* algorithm optimisation time is displayed in fig. 8.4(d). It depicts only the period in which the conflict risk resolution is in progress. The figure also shows that this time is close to a maximum of 0.05 s for just few seconds after conflict risk detection. Its value is smaller than the threshold of 0.01 s for the rest of the simulation time.

Figure 8.4(e) and fig. 8.4(f) show the evolution of computed safe heading, computed safe altitude ranges and position of the threat. This position is displayed in terms of bearing and vertical distance, respectively, in respect with the ownship. The threat position is plotted just for the time range of conflict risk resolution is in progress. The parameter displayed in the horizontal axis is the distance to the final manoeuvre's point. It replaces the simulation time to show directly how the command evolves while ownship approaches the potential collision point.

8.2.3 Climbing Threat

The climbing threat scenario shows results quite similar to the previous one. In this case, the threat starts from the initial position with latitude 53.025° N, longitude 0.017° W and altitude 40 m. It moves with an airspeed of 15 m s^{-1} and initially heads Southwards. The results of the simulation are plotted in figs. 8.5 and 8.6.

Ownship's and threat's trajectories in three dimensional space are displayed in fig. 8.5(a). The projection of these trajectories on horizontal and vertical planes are shown in fig. 8.5(b) and fig. 8.5(c), respectively. Also in this case the threat initially tries to catch the ownship with both an horizontal and a vertical manoeuvre to follow the ownship during the avoidance manoeuvre. These are a climb and a left turn. In the meanwhile, the ownship avoid the conflict risk by executing a left turn. This manoeuvre is effective on keeping the threat far from the *CDZ* and, therefore, does not require the *S&A* algorithm to update the resolution manoeuvre. Once again, when conflict risk is resolved, the ownship heads back to the assigned waypoint and continues performing the predefined flight plan.

Figures 8.6(a) and 8.6(b) displays the evolution of horizontal and vertical separation distances during the simulation, respectively. Figure 8.6(c) shows that also in this case the threat keeps outside the *CDZ* during the whole simulation run. The optimisation time used by the algorithm to perform the evaluation of the *S&A* operations during the simulation is plotted in fig. 8.6(d). It is displayed only the period in which the conflict risk resolution is in progress. The optimisation time value exceeds the threshold of 0.04 s just for some seconds immediately after the conflict risk detection. After that,

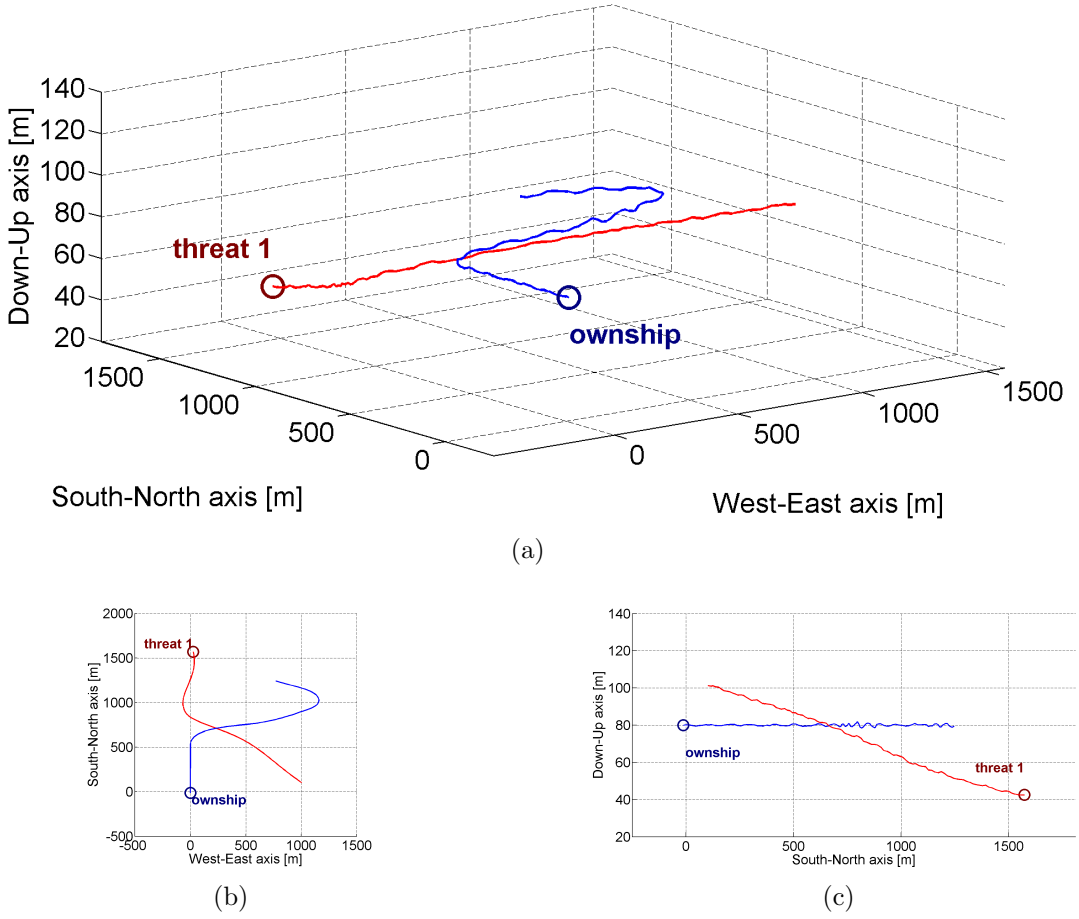

Figure 8.5: simulation graphs of climbing threat scenario (part I): (a) 3D trajectories of ownship and threat, (b) horizontal view of ownship and threat trajectories, (c) vertical view of ownship and threat trajectories

it maintains a value smaller than 0.01 s.

Figure 8.6(e) and fig. 8.6(f) show the evolution of the computed safe heading and altitude ranges, and the threat's position. This is displayed in terms of bearing and vertical distance, respectively, in respect with the ownship. The threat position is plotted just for the time range in which the conflict risk resolution is in progress. The parameter displayed in the horizontal axis is the distance to the point in which the manoeuvre is concluded. It replaces the simulation time to show directly how the command evolves while the ownship approaches the potential collision point.

8.2.4 Threat Approaching from Left

Some scenarios were also selected to show the capabilities of the algorithm for threats starting from the same altitude of the ownship. A scenario considering a threat ap-

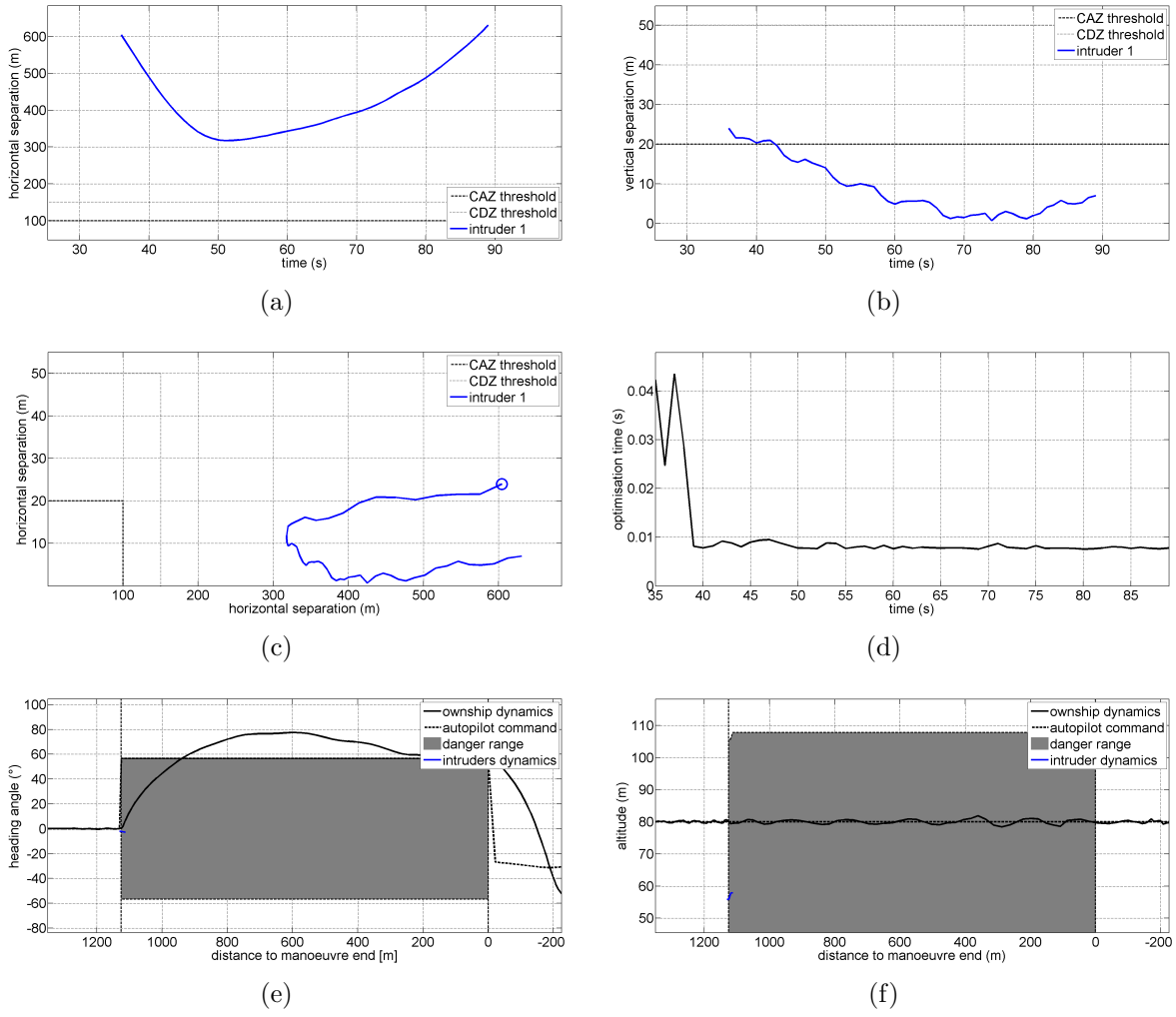

Figure 8.6: simulation graphs of climbing threat scenario (part II): (a) evolution of the horizontal separation distance between ownship and threat and comparison with the *CDZ* and *CAZ* thresholds, (b) evolution of the vertical separation distance between ownship and threat and comparison with the *CDZ* and *CAZ* thresholds, (c) horizontal/vertical separation between ownship and threat plot, (d) computational time needed by the algorithm to update advisories, (e) evolution of ownship heading angle, autopilot command and computed safe range during simulation and comparison with threat bearing in those time ranges in which a conflict risk is detected, (f) evolution of ownship altitude, autopilot command and computed safe range during simulation and comparison with threat vertical position in those time ranges in which a conflict risk is detected

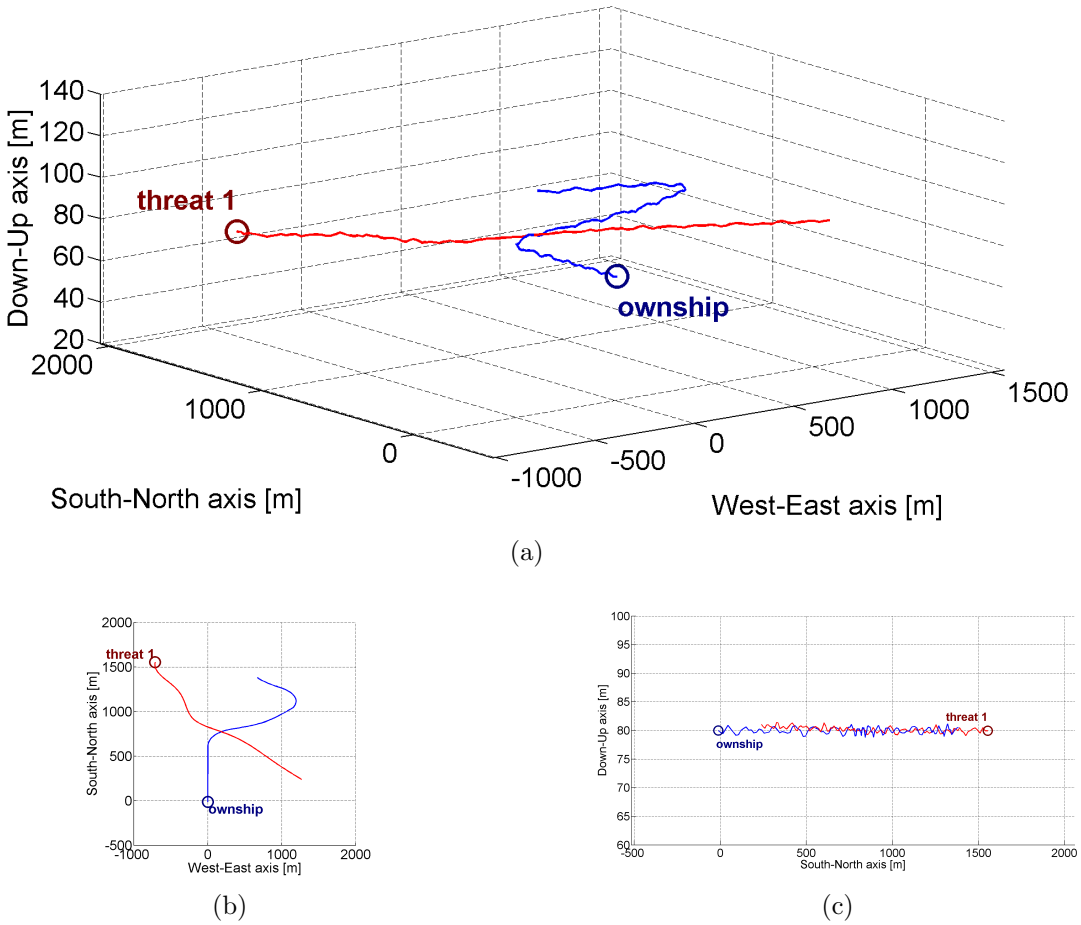

Figure 8.7: graphs of the simulation with threat approaching from left (part I): (a) 3D trajectories of ownship and threat, (b) horizontal view of ownship and threat trajectories, (c) vertical view of ownship and threat trajectories

proaching from the left side is here presented. The threat starts from the initial position with latitude 53.025° N, longitude 0.022° W and altitude 80 m. It moves with an airspeed of 15 m s^{-1} and an initial heading of 240° from North. The results of the simulation are plotted in figs. 8.7 and 8.8.

The trajectories of ownship and threat in three dimensional space are displayed in fig. 8.7(a). The projection of these trajectories on horizontal and vertical planes are shown in fig. 8.7(b) and fig. 8.7(c), respectively. Some initial oscillations in the threat horizontal trajectory are noticeable. This is due to the fact that the threat tries to catch the ownship. No altitude change is noticeable because the ownship does not change its altitude. According to the *Right of Way* rules, a right-turn is chosen by the algorithm as avoidance maneuvre. The ownship changes then its motion direction to the assigned waypoint once that the conflict risk is resolved.

Figures 8.8(a) and 8.8(b) display the evolution of horizontal and vertical separa-

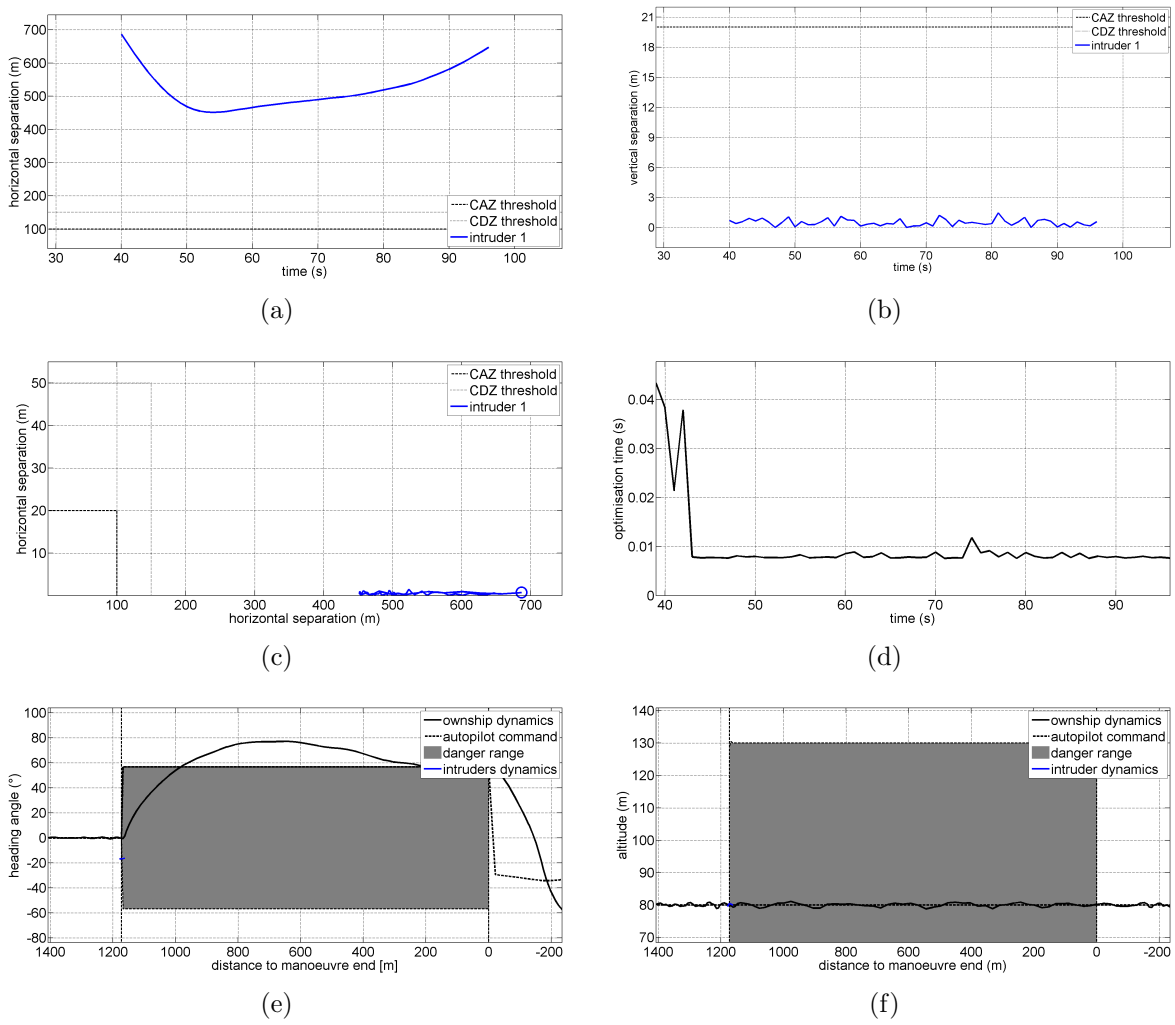

Figure 8.8: graphs of the simulation with threat approaching from left (part II): (a) evolution of the horizontal separation distance between ownship and threat and comparison with the *CDZ* and *CAZ* thresholds, (b) evolution of the vertical separation distance between ownship and threat and comparison with the *CDZ* and *CAZ* thresholds, (c) horizontal/vertical separation between ownship and threat plot, (d) computational time employed by the algorithm for the advisories update, (e) evolution of ownship heading angle, autopilot command and computed safe range during simulation and comparison with threat bearing in those time ranges in which a conflict risk is detected, (f) evolution of ownship altitude, autopilot command and computed safe range during simulation and comparison with threat vertical position in those time ranges in which a conflict risk is detected

tion distances during the simulation. Figure 8.8(c) shows that the threat is safely kept outside the *CDZ* during all the simulation. The optimisation time used by the algorithm to perform the *S&A* operations evaluation during the simulation is plotted in fig. 8.8(d). It is displayed only the period in which the conflict risk resolution is in progress. From the graph it is clear that the optimisation time is costantly under 0.01 s except for an initial peak exceeding 0.04 s.

Figure 8.8(e) and fig. 8.8(f) show the evolution of computed safe heading and altitude ranges, and the position of threat. This position is displayed in terms of bearing and vertical distance, respectively, in respect with the ownship. The threat position is plotted just for the time range where the conflict risk resolution is in progress. The parameter displayed in the horizontal axis is the distance to the point in which the manoeuvre is concluded. It substitutes the simulation time to show directly how the command evolves while the ownship approaches the potential collision point.

8.2.5 Threat Approaching from Right

Another case in the horizontal plane is the simulation of a threat coming from right. The initial position of threat is at latitude 53.025° N, longitude 0.011° W and altitude 80 m. The aircraft is supposed to move with an airspeed of $15\,\mathrm{m\,s^{-1}}$ and an initial heading of 150° from North. The results of simulation are plotted in figs. 8.9 and 8.10.

Trajectories of ownship and threat in three dimensional space are displayed in fig. 8.9(a). The projection of these trajectories on horizontal and vertical planes are shown in fig. 8.9(b) and fig. 8.9(c), respectively. Similarly to the previous case the threat try to catch the ownship in the horizontal plane and initially obscillate to get the proper heading to reach it. In the meanwhile, the ownship initially try a vertical maneouvre. Then, some seconds after the threat starts climbing, it change its strategy by trying a right turn. Once the conflict is resolved, it heads back to the assigned waypoint.

Figures 8.10(a) and 8.10(b) displays the evolution of horizontal and vertical separation distances during the simulation. Once again, fig. 8.10(c) shows that the constraints about *CDZ* and *CAZ* are respected during the whole simulation run. The optimisation time used by the algorithm to perform the evaluation of the *S&A* operations during the simulation is plotted in fig. 8.12(d). It displays only the period in which the conflict risk resolution is in progress. The optimisation time has a more complex profile in this case, despite it never reach the threshold of 0.05 s.

Figure 8.10(e) and fig. 8.10(f) show the evolution of computed safe heading and altitude ranges, and threat's position. This position is displayed in terms of bearing and vertical distance, respectively, in respect with the ownship. The threat position is plotted for the limited time range where the conflict risk resolution is in progress. The parameter displayed in the horizontal axis is the distance to the point in which the manoeuvre is performed. It substitutes the simulation time to show directly how the command evolves while the ownship reaches the potential collision point.

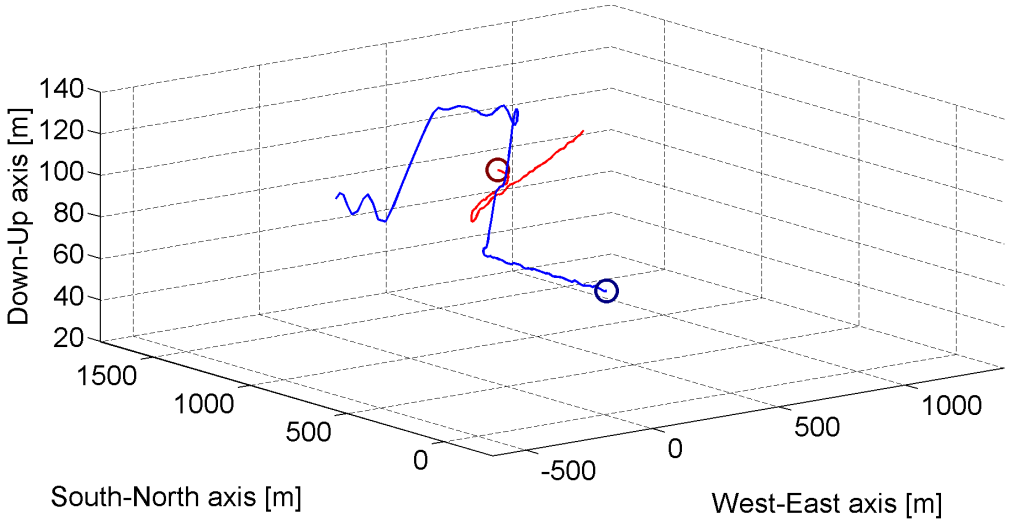

(a)

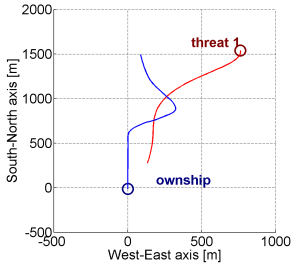

(b)

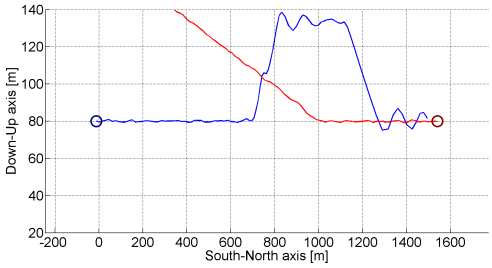

(c)

Figure 8.9: graphs of the simulation with threat approaching from right (part I): (a) 3D trajectories of ownship and threat, (b) horizontal view of ownship and threat trajectories, (c) vertical view of ownship and threat trajectories

8.2.6 Threat Descending from Left

Another interesting case, cause of the presence of a long pursuit final phase, is that of a descending threat from the left of the ownship. The initial condition considers a threat starting from the initial position with latitude 53.025° N, longitude 0.022° W and altitude 120 m. It moves with an airspeed of 15 m s^{-1} and an initial heading of 240° from North. The results of simulation are plotted in figs. 8.11 and 8.12.

The trajectories of ownship and threat in three dimensional space are displayed in fig. 8.11(a). The projection of these trajectories on horizontal and vertical planes are shown in fig. 8.11(b) and fig. 8.11(c). In this case also, some oscillations are necessary to threat to settle on the motion condition suitable to intercept the ownship. Finally a long pursuit takes place before the threat stops following the ownship. This time, the manoeuvre chosen by the ownship is a right-turn, once again according to the *Right of Way* rules. When the conflict risk is resolved, the ownship changes its motion

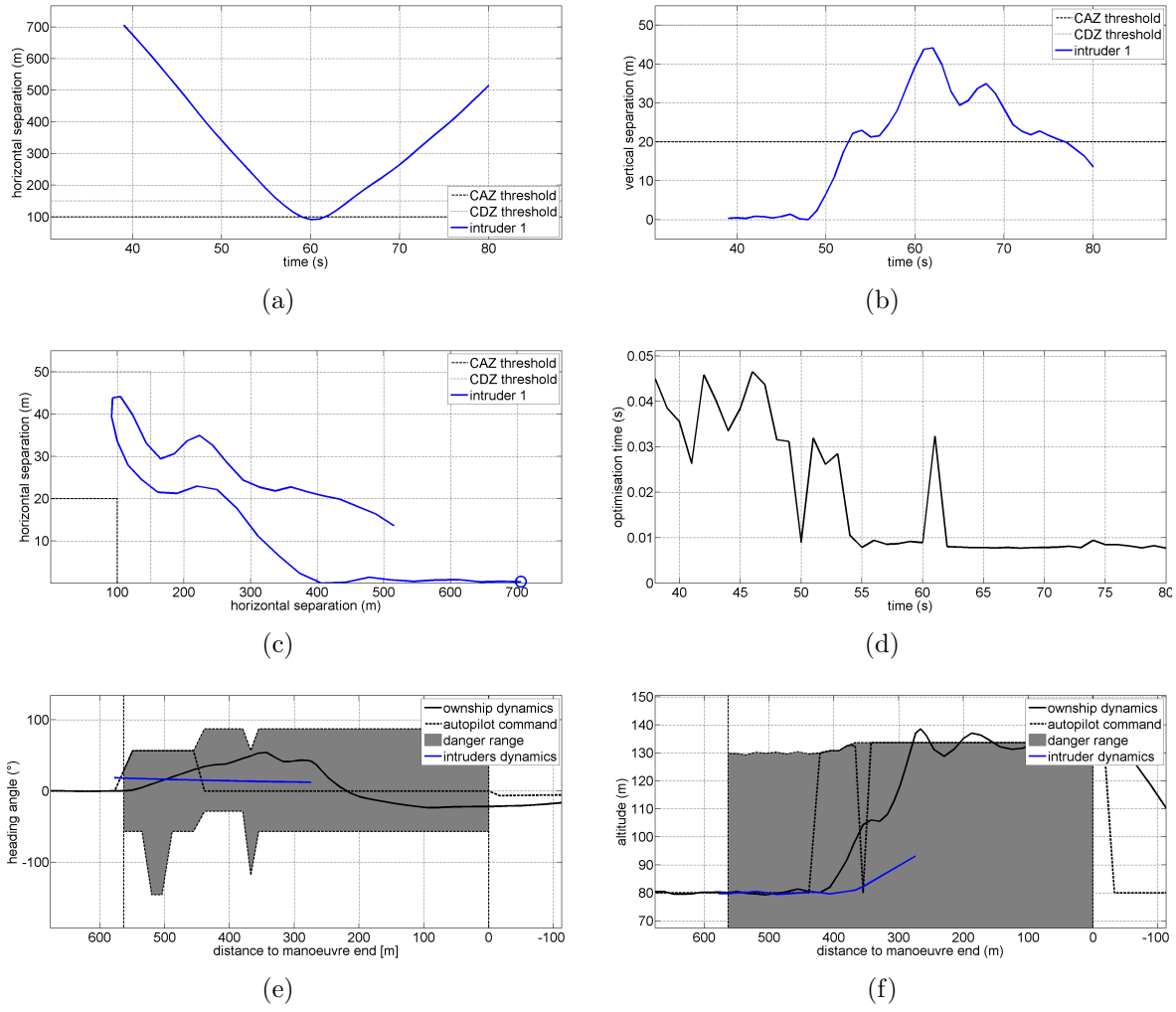

Figure 8.10: graphs of the simulation with threat approaching from right (part II): (a) evolution of horizontal separation distance between ownship and threat and comparison with *CDZ* and *CAZ* thresholds, (b) evolution of the vertical separation distance between ownship and threat and comparison with the *CDZ* and *CAZ* thresholds, (c) horizontal/vertical separation between ownship and threat plot, (d) computational time needed by the algorithm to update the advisories, (e) evolution of ownship heading angle, autopilot command and computed safe range during simulation and comparison with threat bearing in those time ranges in which a conflict risk is detected, (f) evolution of ownship altitude, autopilot command and computed safe range during simulation and comparison with threat vertical position in those time ranges in which a conflict risk is detected

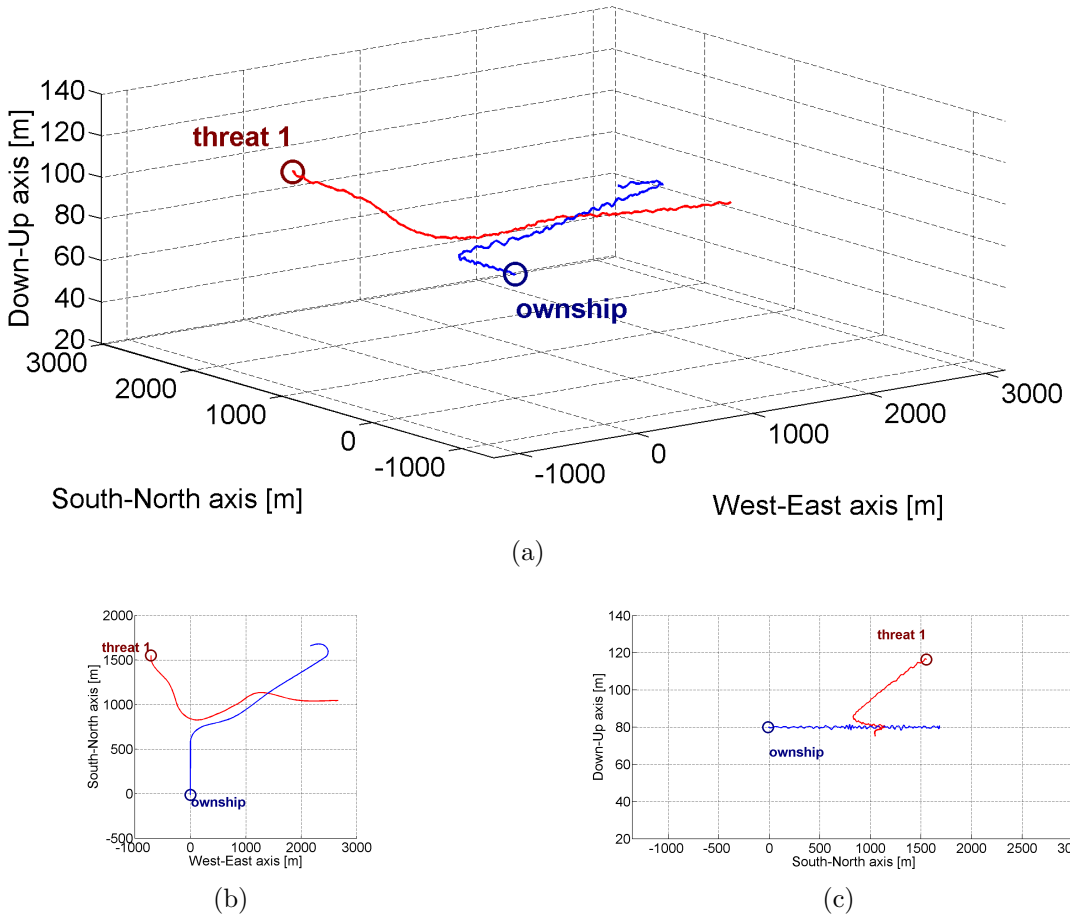

Figure 8.11: graphs of the simulation with threat descending from left (part I): (a) 3D trajectories of ownship and threat, (b) horizontal view of ownship and threat trajectories, (c) vertical view of ownship and threat trajectories

direction in order to point to the assigned waypoint.

Figures 8.12(a) and 8.12(b) display the evolution of horizontal and vertical separation distances during the simulation. Figure 8.12(c) demonstrates that the threat never enters the *CDZ*. The optimisation time used by the algorithm to perform evaluation of the *S&A* operations during the simulation is plotted in fig. 8.12(d). It is displayed only the period in which the conflict risk resolution is in progress. The optimisation time is smaller than 0.01 s in fig. 8.12(d), despite some peaks reaching a maximum value smaller than 0.045 s.

Figure 8.12(e) and fig. 8.12(f) show the evolution of computed safe heading and altitude ranges, and the threat's position. This position is displayed in terms of bearing and vertical distance, respectively, in respect with the ownship. The threat position is plotted just for the time range where the conflict risk resolution is in progress. The parameter displayed in horizontal axis is the distance to the point in which the

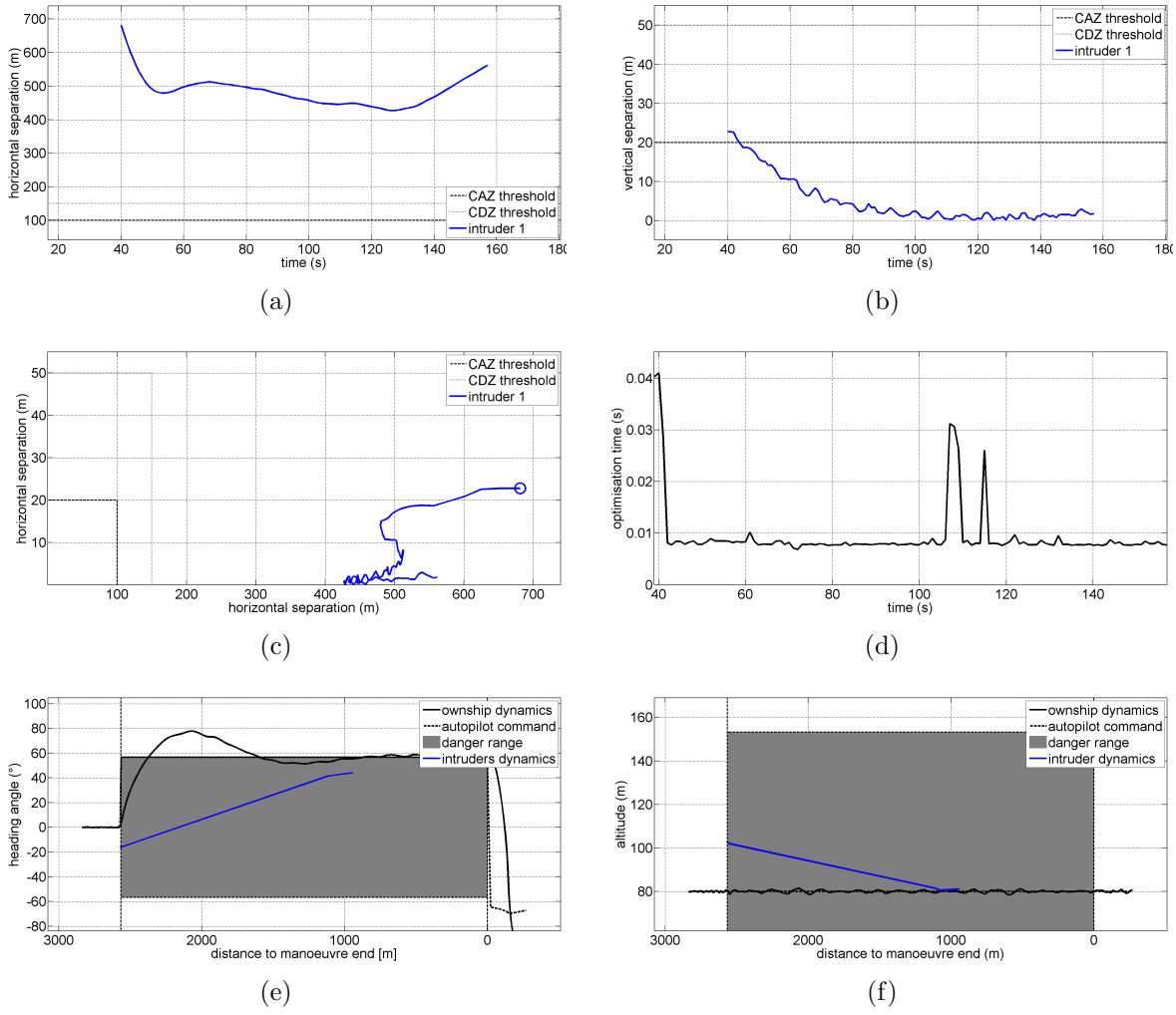

Figure 8.12: graphs of the simulation with threat descending from left (part II): (a) evolution of the horizontal separation distance between ownship and threat and comparison with *CDZ* and *CAZ* thresholds, (b) evolution of the vertical separation distance between ownship and threat and comparison with *CDZ* and *CAZ* thresholds, (c) horizontal/vertical separation between ownship and threat plot, (d) computational time employed by the algorithm for the advisories update, (e) evolution of ownship heading angle, autopilot command and computed safe range during simulation and comparison with threat bearing in those time ranges in which a conflict risk is detected, (f) evolution of ownship altitude, autopilot command and computed safe range during simulation and comparison with threat's vertical position in those time ranges in which a conflict risk is detected

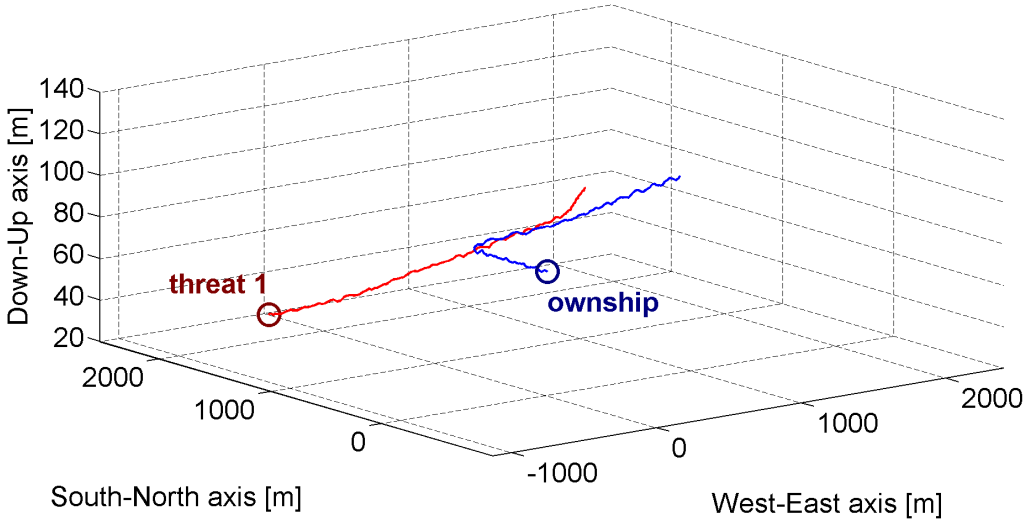

(a)

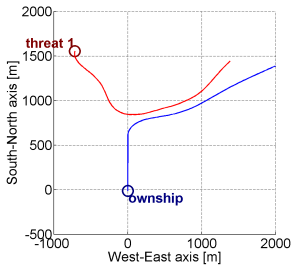

(b)

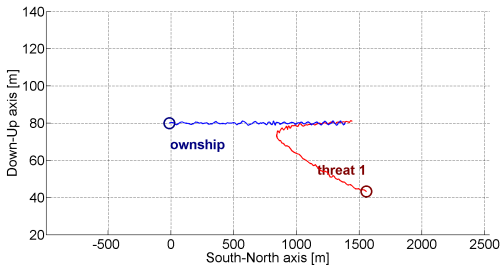

(c)

Figure 8.13: graphs of the simulation with threat climbing from left (part I): (a) 3D trajectories of ownship and threat, (b) horizontal view of ownship and threat trajectories, (c) vertical view of ownship and threat trajectories

manoeuvre is performed. It substitutes the simulation time to show directly how the command evolves while the ownship approaches the potential collision point.

8.2.7 Threat Climbing from Left

Another case characterised by a long pursuit is that of a climbing threat from the left of ownship. Here, the initial condition considers a threat starting from the initial position with latitude 53.025° N, longitude 0.022° W and altitude 40 m. It moves with an airspeed of 15 m s^{-1} and an initial heading of 240° from North. The results of simulation are plotted in figs. 8.13 and 8.14.

The ownship's and threat's trajectories in three dimensional space are displayed in fig. 8.13(a). Projections on horizontal and vertical planes are shown in fig. 8.13(b) and fig. 8.13(c), respectively. The threat trajectory's oscillations are due to the attempt

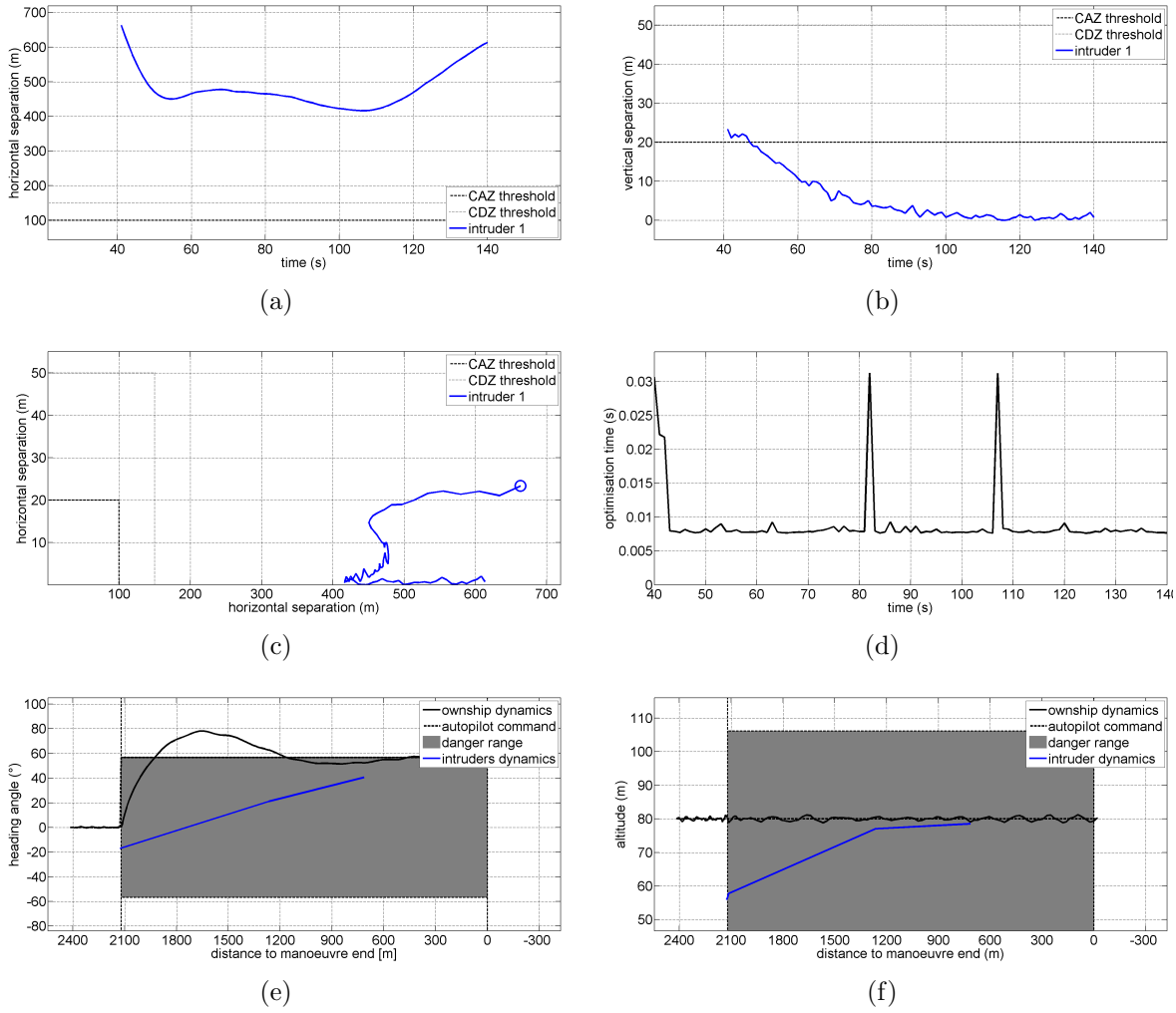

Figure 8.14: graphs of the simulation with threat climbing from left (part II): (a) evolution of the horizontal separation distance between ownship and threat and comparison with the *CDZ* and *CAZ* thresholds, (b) evolution of the vertical separation distance between ownship and threat and comparison with the *CDZ* and *CAZ* thresholds, (c) horizontal/vertical separation between ownship and threat plot, (d) computational time employed by the algorithm for advisories update, (e) evolution of ownship heading angle, autopilot command and computed safe range during simulation and comparison with threat bearing in those time ranges in which a conflict risk is detected, (f) evolution of ownship altitude, autopilot command and computed safe range during simulation and comparison with threat vertical position in those time ranges in which a conflict risk is detected

of threat to catch the ownship both in horizontal and vertical plane. It changes its heading in order to follow the ownship during the resolution manouevre. In the meanwhile, the ownship keeps on following the computed resolution manoeuvre. The suggested resolution manoeuvre does not change with time. This is due to the fact that *CDZ* is wide enough to take into account the threat's change of trajectory. When the conflict risk is resolved, the ownship changes its motion direction in order to point to the assigned waypoint.

Figures 8.14(a) and 8.14(b) display the evolution of horizontal and vertical separation distances during the simulation. Figure 8.14(c) shows that the distance between the two aircraft is greater than both the *CDZ* and *CAZ* during the whole simulation run. The optimisation time spent by algorithm to perform the evaluation of the *S&A* operations during the simulation is plotted in fig. 8.14(d). It is displayed only the period in which the conflict risk resolution is in progress. This figure shows that this parameter assumes a value smaller than 0.05 s.

Figure 8.14(e) and fig. 8.14(f) show the evolution of computed safe heading and altitude ranges, and the threat's position. This position is displayed in terms of bearing and vertical distance, respectively, in respect with the ownship. The threat position is plotted just for the time range where the conflict risk resolution is in progress. The parameter displayed in the horizontal axis is the distance to the point in which the manoeuvre is performed. It substitutes the simulation time to show directly how the command evolves while the ownship approaches the potential collision point.

8.2.8 Threat Descending from Right

Another case characterised by oscillations in the horizontal plane is that of the descening threat from the right of the ownship. The initial condition considers a threat starting from the initial position with latitude 53.025° N, longitude 0.011° W and altitude 120 m. It moves with an airspeed of 15 m s^{-1} and an initial heading of 240° from North. The results of the simulation are plotted in figs. 8.15 and 8.16.

The trajectories of ownship and threat on the three dimensional space are displayed in fig. 8.15(a). The projection of the trajectories in the horizontal and vertical planes are shown in fig. 8.15(b) and fig. 8.15(c), respectively. The threat trajectory's oscillations are due to the fact that the threat tries to catch the ownship both in the horizontal and vertical plane. In particular, it changes the heading in order to follow the ownship during the resolution manouevre. In the meanwhile, the ownship keeps on following the computed resolution manoeuvre. The suggested resolution manoeuvre does not change with time. This is due to the fact that *CDZ* is enough wide to take into account the threat's change of trajectory. When the conflict risk is resolved, the ownship changes its direction of motion in order to point to next waypoint.

Figures 8.16(a) and 8.16(b) displays the evolution of horizontal and vertical separation distances during the simulation, respectively. Figure 8.16(c) shows that the distance between the two aircraft is greater both than the *CDZ* and *CAZ* during the

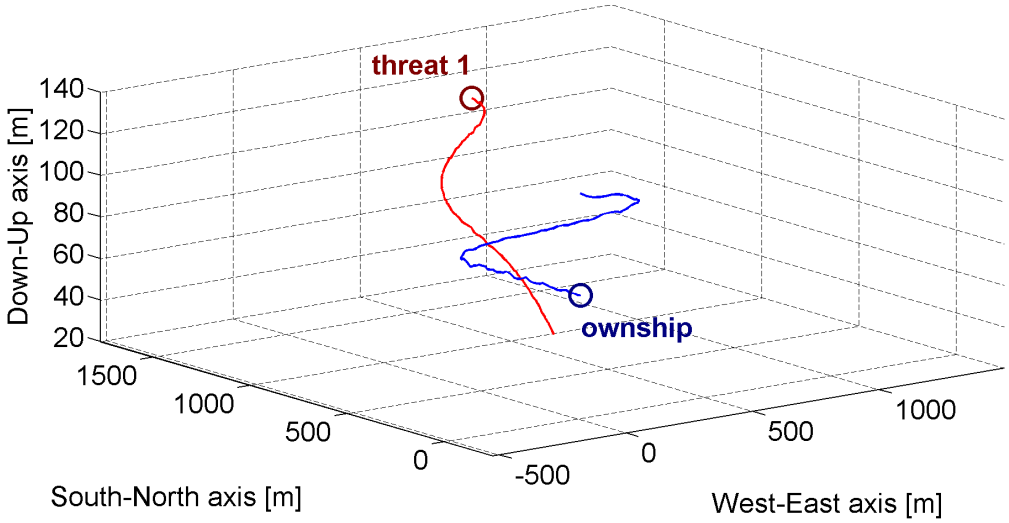

(a)

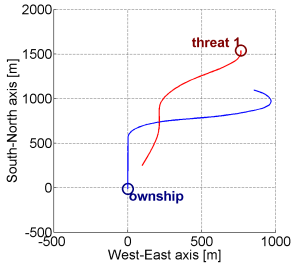

(b)

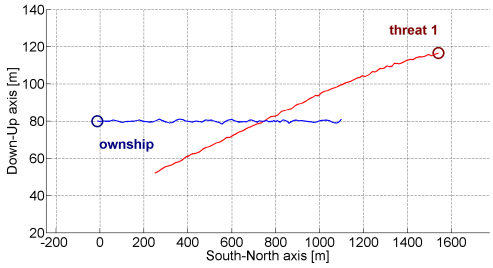

(c)

Figure 8.15: graphs of the simulation with threat descending from right (part I): (a) 3D trajectories of ownship and threat, (b) horizontal view of ownship and threat's trajectories, (c) vertical view of ownship and threat's trajectories

whole simulation run. The optimisation time used by the algorithm to perform the evaluation of *S&A* operations during the simulation is plotted in fig. 8.16(d). It is displayed only the period in which the conflict risk resolution is in progress. This figure shows that this parameter is smaller than 0.05 s.

Figure 8.16(e) and fig. 8.16(f) show the evolution of computed safe heading and altitude ranges, and the threat's position. This position is displayed in terms of bearing and vertical distance, respectively, in respect with the ownship. The threat's position is plotted just for the time range where the conflict risk resolution is in progress. The parameter displayed in the horizontal axis is the distance to the point in which the manoeuvre is concluded. It substitutes the simulation time to show directly how the command evolves while ownship approaches the potential collision point.

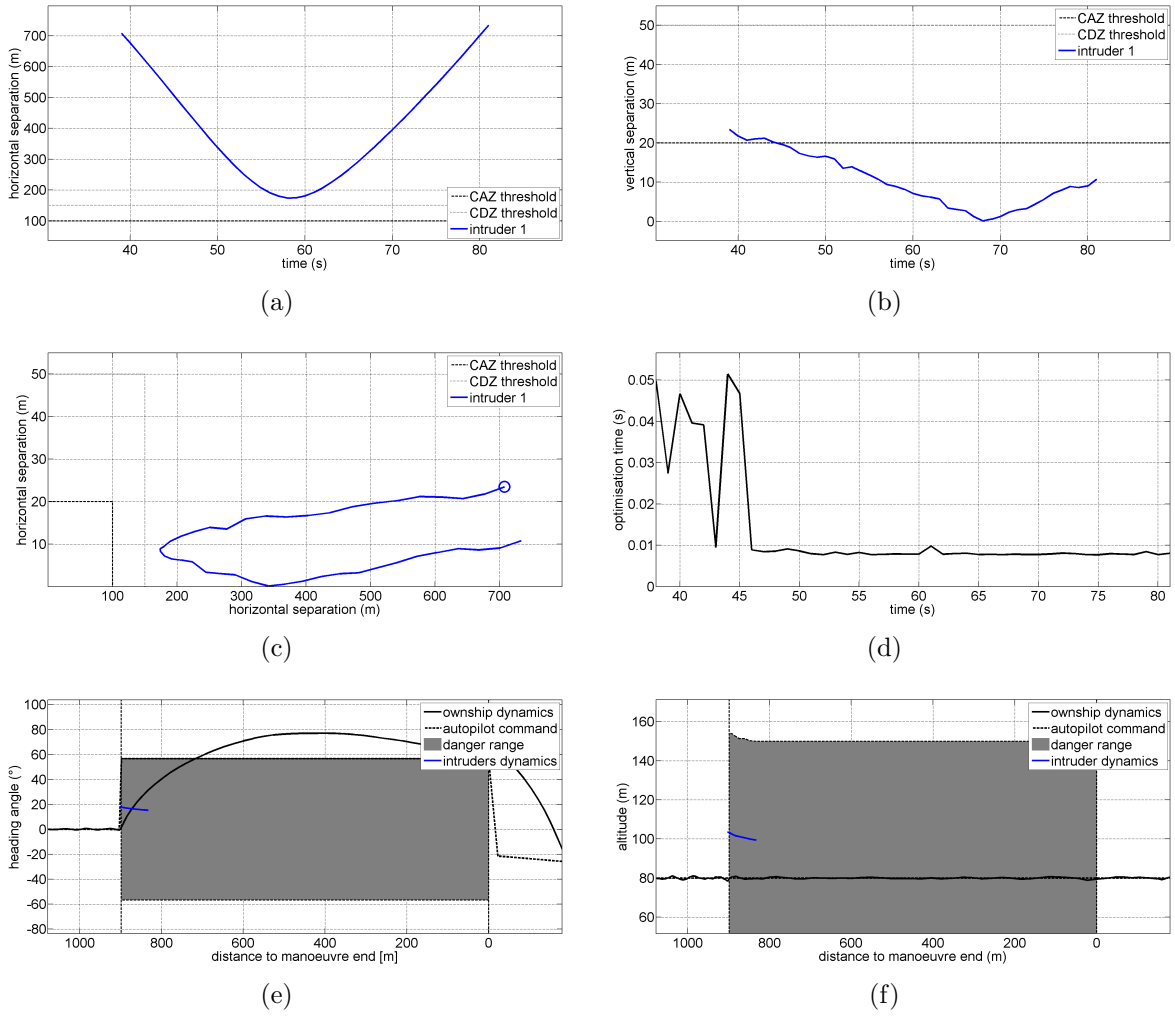

Figure 8.16: graphs of the simulation with threat descending from right (part II): (a) evolution of the horizontal separation distance between ownship and threat and comparison with *CDZ* and *CAZ* thresholds, (b) evolution of the vertical separation distance between ownship and threat and comparison with the *CDZ* and *CAZ* thresholds, (c) horizontal/vertical separation between ownship and threat plot, (d) computational time employed by the algorithm for the advisories update, (e) evolution of ownship heading angle, autopilot command and computed safe range during simulation and comparison with threat bearing in those time ranges in which a conflict risk is detected, (f) evolution of ownship altitude, autopilot command and computed safe range during simulation and comparison with threat vertical position in those time ranges in which a conflict risk is detected

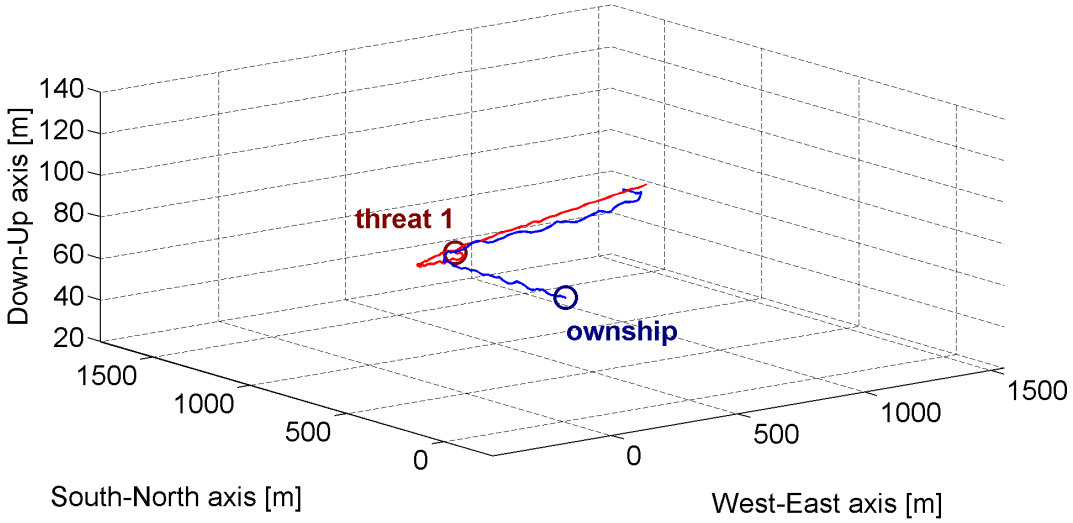

(a)

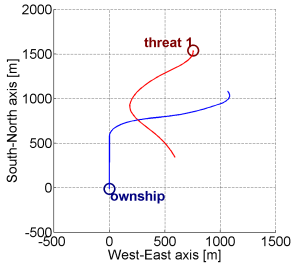

(b)

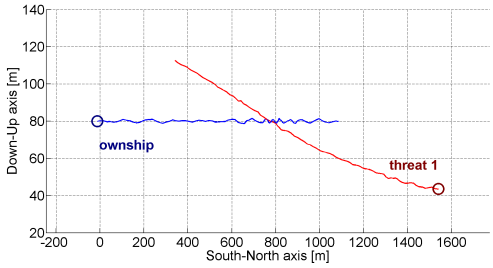

(c)

Figure 8.17: graphs of the simulation with threat climbing from right (part I): (a) 3D trajectories of ownship and threat, (b) horizontal view of ownship and threat trajectories, (c) vertical view of ownship and threat trajectories

8.2.9 Threat Climbing from Right

Finally, for completeness, it is presented also a simulation considering a threat starting from the initial position with latitude 53.025° N, longitude 0.011° W and altitude 40 m. It moves with an airspeed of 15 m s^{-1} and initial heading of 240° from North. The simulation's results are plotted in figs. 8.17 and 8.18.

The trajectories of ownship and threat on the three dimensional space are displayed in fig. 8.17(a). The projection of these trajectories in the horizontal and vertical planes are shown in fig. 8.17(b) and fig. 8.17(c), respectively. The oscillations in threat's trajectory are due to the fact that the threat try to catch the ownship both in the horizontal and vertical plane. In particular, it changes the heading in order to follow the ownship during the resolution manouevre. In the meanwhile, the ownship keeps on following the computed resolution manoeuvre. The suggested resolution manoeuvre does not change with time. This is due to the fact that the *CDZ* is wide enough to

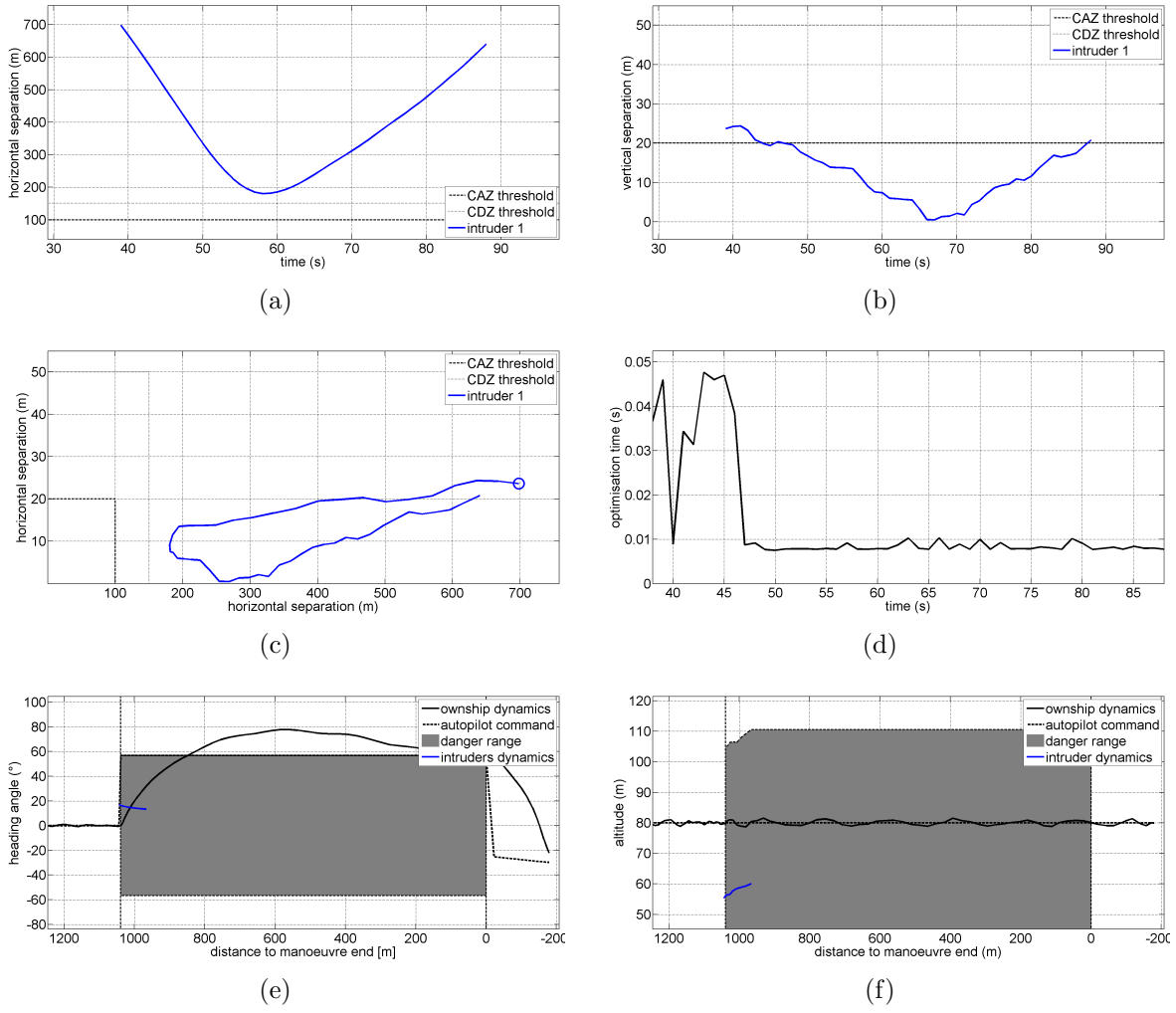

Figure 8.18: graphs of the simulation with threat climbing from right (part II): (a) evolution of the horizontal separation distance between ownship and threat and comparison with *CDZ* and *CAZ* thresholds, (b) evolution of the vertical separation distance between ownship and threat and comparison with *CDZ* and *CAZ* thresholds, (c) horizontal/vertical separation between ownship and threat plot, (d) computational time employed by the algorithm for the advisories update, (e) evolution of ownship heading angle, autopilot command and computed safe range during simulation and comparison with threat bearing in those time ranges in which a conflict risk is detected, (f) evolution of ownship altitude, autopilot command and computed safe range during simulation and comparison with threat vertical position in those time ranges in which a conflict risk is detected

take into account the change of trajectory of the threat. When the conflict risk is resolved, the ownship changes its direction of motion in order to point to the assigned waypoint.

Figures 8.18(a) and 8.18(b) display the evolution of the horizontal and vertical separation distances during the simulation, respectively. Figure 8.18(c) shows that the distance between the two aircraft is greater both than the *CDZ* and *CAZ* during the whole simulation run. The optimisation time used by the algorithm to perform the evaluation of the *S&A* operations during the simulation is plotted in fig. 8.18(d). It is displayed just the period in which the conflict risk resolution is in progress. This figure shows that this parameter is smaller than 0.05 s.

Figure 8.18(e) and fig. 8.18(f) show the evolution of computed safe heading and altitude ranges, and the threat's position. This position is displayed in terms of bearing and vertical distance, respectively, in respect with the ownship. The threat position is plotted just for the time range where the conflict risk resolution is in progress. The parameter displayed in the horizontal axis is the distance to the point in which the manoeuvre is concluded. It substitutes the simulation time to show directly how the command evolves while the ownship approaches the potential collision point.

8.3 Multiple Threats Scenario in *P/F* Mode

This scenario is characterised by the presence of two flying threats moving on a straight trajectory and a ground relief placed on the ownship flight route. The ownship's and the threats' initial conditions are defined in Table 8.2. The ownship is supposed to be controlled in the *P/F* mode with *A/R* switched on. It is routed to the waypoint defined by latitude 53.021° N, longitude 0.030° W and altitude 80 m. The dimensions chosen for the zones introduced in section 6.2 and the prescribed ground separation are the same chosen in section 8.2. The simulation's results are plotted in figs. 8.19 and 8.20.

The ownship's and threats' trajectories in three dimensional space are displayed in fig. 8.19(a). The projection of these trajectories on horizontal and vertical planes are shown in fig. 8.19(b) and fig. 8.19(c), respectively. In this case both the threats move on a straight levelled trajectory. In all this plots the local ground elevation map is displayed to provide the information about the separation with the ground.

Table 8.2: Data of the aircraft involved in the multiple threats scenario in *P/F* mode: *A/S* is the airspeed, ψ the heading, h the altitude

aircraft	**latitude**	**longitude**	A/S [m s^{-1}]	ψ [° from North]	h [m]
ownship	53.021° N	0.001° W	15	270	80
intr. 1	53.025° N	0.014° W	15	150	80
intr. 2	53.017° N	0.015° W	15	30	80

Figure 8.20(a) and fig. 8.20(b) display

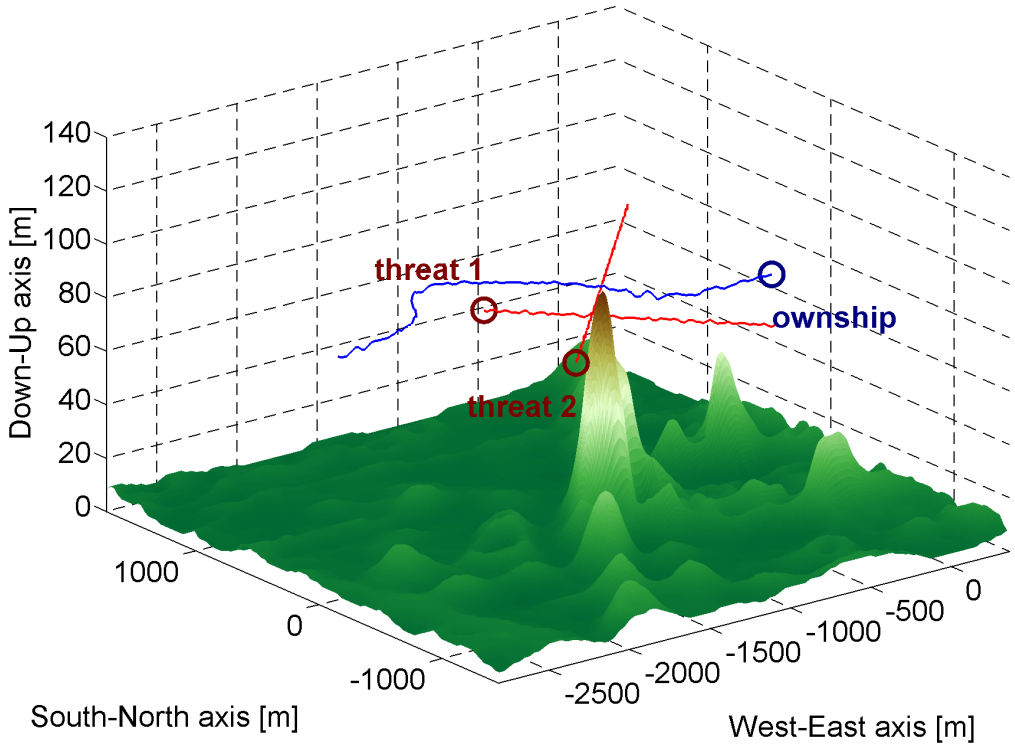

(a)

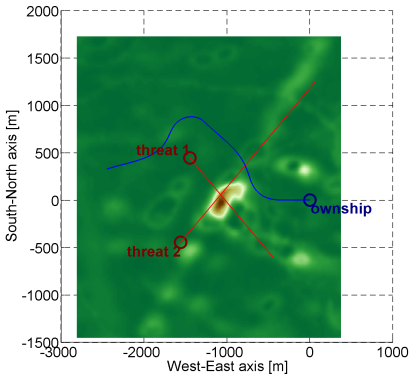

(b)

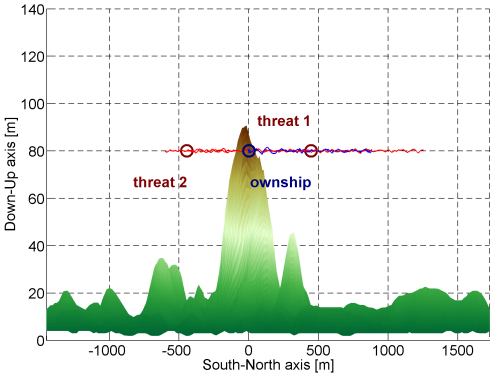

(c)

Figure 8.19: simulation graphs of the multiple threats scenario in P/F mode (part I): (a) 3D trajectories of ownship and threat, (b) horizontal view of ownship and threats trajectories, (c) vertical view of ownship and threats trajectories

Table 8.4: Data of the aircraft involved in the last-resort scenario

aircraft	latitude	longitude	airspeed [m s^{-1}]	heading [° from North]	altitude
ownship	53.012° *N*	0.012° *W*	15	10	cruising at 80 m
intr. 1	53.021° *N*	0.014° *W*	14	140	cruising at 70 m
intr. 2	53.040° *N*	0.030° *W*	14	190	descent after 8 s (150 m-50 m)

the evolution of horizontal and vertical separation distances between ownship and flying threats during the simulation, respectively. Figure 8.20(c) shows that the distance between ownship and threats is greater both than *CDZ* and *CAZ* during the whole simulation run. The optimisation time used by the algorithm to perform the *S&A* operations evaluation during the simulation is plotted in fig. 8.18(d). Here is displayed just the period in which the conflict risk resolution is in progress. This figure shows that this parameter is smaller than 0.05 s.

Figure 8.20(e) and fig. 8.20(f) show evolution of the computed safe heading and altitude ranges, and the threats' position. This position is displayed in terms of bearing and vertical distance, respectively, in respect with the ownship. Figure 8.20(f) plots also the local elevation. The ground obstacle bearing is not displayed in fig. 8.20(e) because it is close to zero. In fact, the obstacle is in front of the ownship in its direction of motion. The threats position is plotted just for the time range where the conflict risk resolution is in progress. The parameter displayed in the horizontal axis is the distance to the point in which the manoeuvre is concluded. It substitutes the simulation time to show directly that the command evolves while the ownship approaches the potential collision point.

8.4 Last-Resort Scenario

Table 8.3: Dimensions of the *CDZ*, *SZ* and *PUZ* considered in the last-resort scenario

zone	radius [m]	half-height [m]
CDZ	500	50
SZ	150	35
PUZ	100	25

For the last-resort simulation it was decided to consider the simulations presented in [163]. These include the same conflict geometry used for a simulation with *UAS* in *MAN* mode and another one in the *P/F* mode in order to compare the algorithm performances. Both simulations consider the *A/R* function switched 'ON'. In the first case it is assumed that the *UAV* operator does not react to the detected collision risk and the resolution manoeuvre is therefore autonomously executed. The scenario considers an head-on encounter with two flying threats as per the conditions listed in Table 8.4 and a ground obstacles. The dimensions chosen for the zones introduced in section 6.2 are set as in Table 8.3. The waypoints used in the *P/F* are tabulated in Table 8.5.

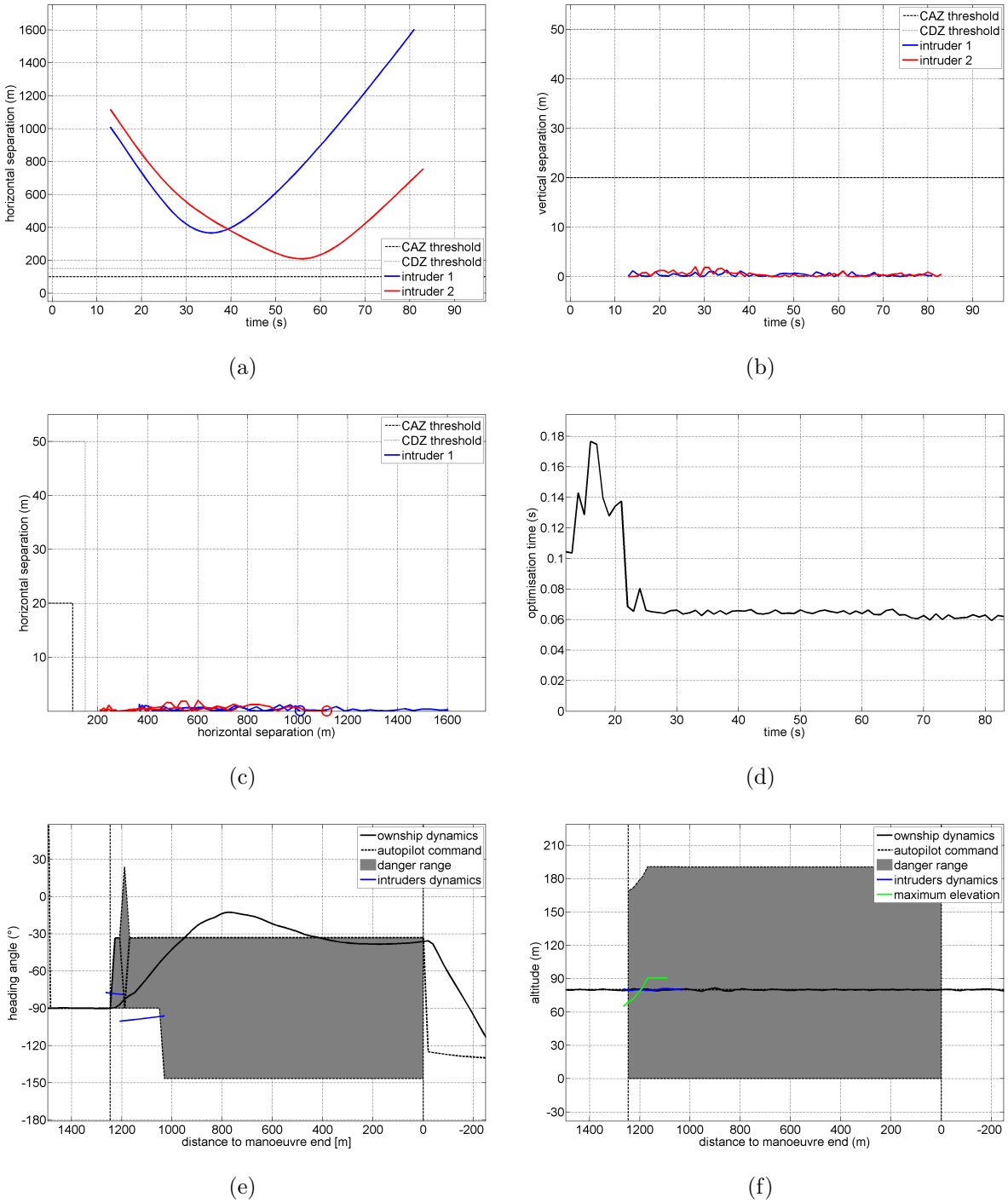

Figure 8.20: simulation graphs of the multiple threats scenario in P/F mode (part II): (a) evolution of the horizontal separation distance between ownship and threats and comparison with *CDZ* and *CAZ* thresholds, (b) evolution of the vertical separation distance between ownship and threats and comparison with the *CDZ* and *CAZ* thresholds, (c) horizontal/vertical separation between ownship and threats plot, (d) computational time employed by the algorithm for the advisories update, (e) evolution of ownship heading angle, autopilot command and computed safe range during simulation and comparison with threats bearing in those time ranges in which a conflict risk is detected, (f) evolution of ownship altitude, autopilot command and computed safe range during simulation and comparison with threats vertical position in those time ranges in which a conflict risk is detected

Simulations results for the *ANS* in *MAN* and *P/F* mode are shown in figs. 8.21 and 8.22, respectively. The altitude and heading profiles are compared with their estimation by the algorithm and the autopilot command during the avoidance manoeuvre in the same figures. In particular, figs. 8.21(a) and 8.22(a) refer to the altitude and figs. 8.21(c) and 8.22(c) to the heading angle. Moreover, it is shown in figs. 8.21(d) and 8.22(d) the comparison between:

Table 8.5: Data of the *WPs* considered in the *P/F* simulation of the last-resort scenario

WP	**latitude**	**longitude**	**altitude**	**airspeed**
1	$53.030° N$	$0.002° E$	80 m	$15\,\mathrm{m\,s^{-1}}$
2	$53.040° N$	$0.030° W$	150 m	$15\,\mathrm{m\,s^{-1}}$

- the dynamics profile,
- the ranges $\Delta\Psi_{\mathrm{res}}$ and ΔH_{res},
- the chosen autopilot command,
- the position of flying threats and the closest impact point.

More precisely, figs. 8.21(b) and 8.22(b) refer to the altitude and figs. 8.21(d) and 8.22(d) to the heading angle. These plots show on the horizontal axis the distance from the ground threats position. The ground obstacle heading in figs. 8.21(d) and 8.22(d) is not reported because it is close to zero. In fact, the obstacle is in front of the ownship in its direction of motion. The horizontal and vertical separation and the diagram of the function of these two variables are reported in Figs. 8.21(e), 8.21(f) and 8.21(g) and Figs. 8.22(e), 8.22(f) and 8.22(g) for *MAN* and *P/F* mode, respectively. Finally, figs. 8.21(h) and 8.22(h) show the trajectories of ownship, threats and the local elevation map.

As can be noticed in figs. 8.21(h) and 8.22(h) the chosen manoeuvre is a turn in both cases. Therefore it is noticeable a limited variation with a maximum amplitude of 0.8 m for the altitude value close to the trim value cause of the altitude autopilot action. In figs. 8.21(c) and 8.22(c), the heading angle profile estimation is conservative for the first value of the heading angle command, because slower than the real dynamics. It is moreover important to observe that the forbidden manoeuvre ranges reported in figs. 8.21(b), 8.21(d), 8.22(b) and 8.22(d) include the positions of threats and ground obstacle in the forbidden range. Finally, as illustrated in figs. 8.21(g) and 8.22(g), in both cases the horizontal and vertical separation profiles keep outside the boundaries defined by the *PUZ*. Despite this, some violation is noticeable for the *SZ*, that is the reason why this zone is considered in the algorithm.

8.5 Simulation Tests Operators Selection

The big differences between manned aviation and *UASs* in terms of human factors, highlighted in section 1.4, are related also with the different skills required to pilots and *UAV* operators. On the other hand, as stated in section 1.5, *UAV* operators have

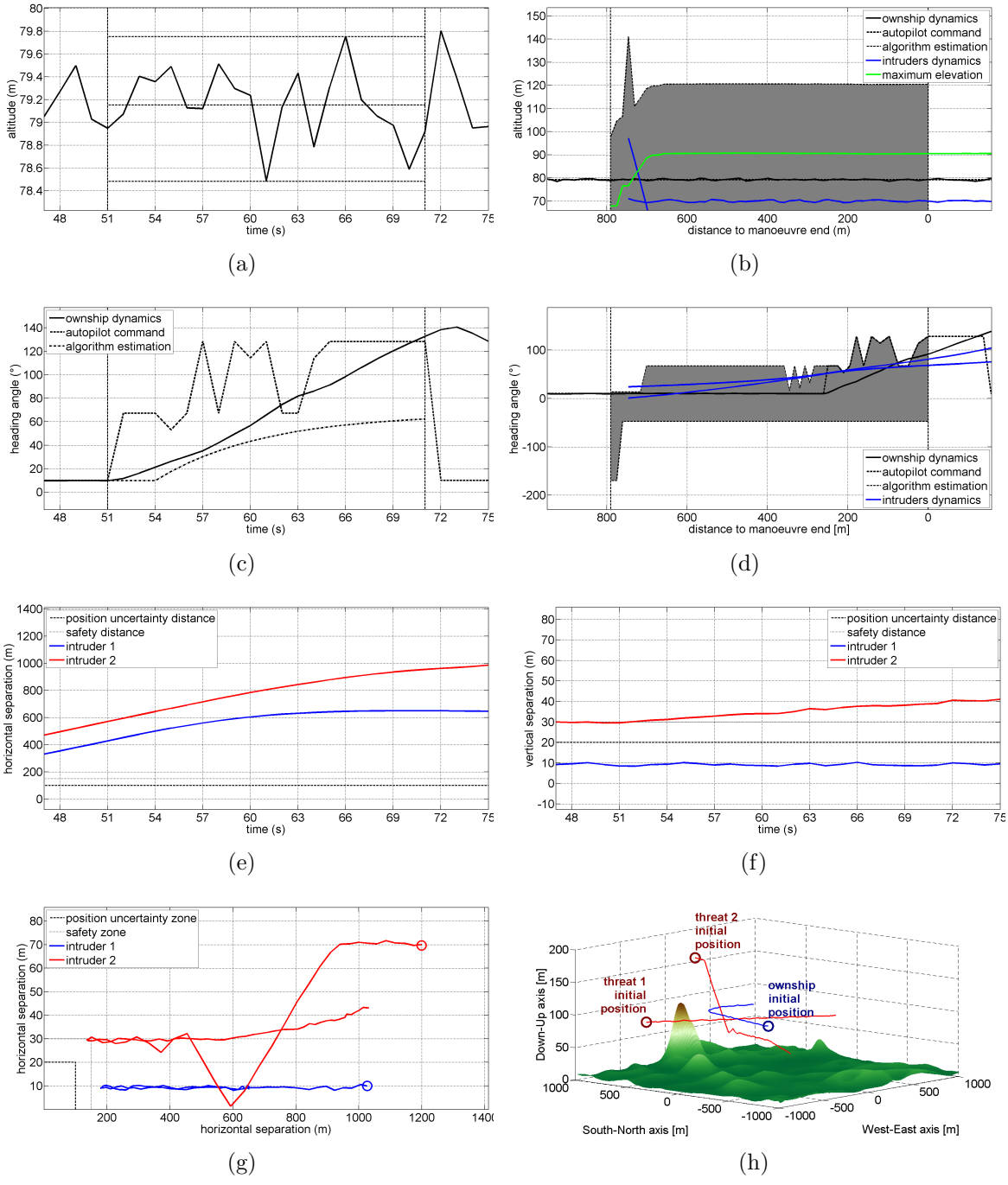

Figure 8.21: simulation graphs of the last-resort scenario in *MAN* mode: (a) altitude dynamics profile, (b) altitude command profile and safe manoeuvres ranges, (e) horizontal separation between threats and ownship, (f) vertical separation between threats and ownship, (g) horizontal/vertical separation diagram between threats and ownship, (h) ownship and threats trajectories and local elevation map of the simulation

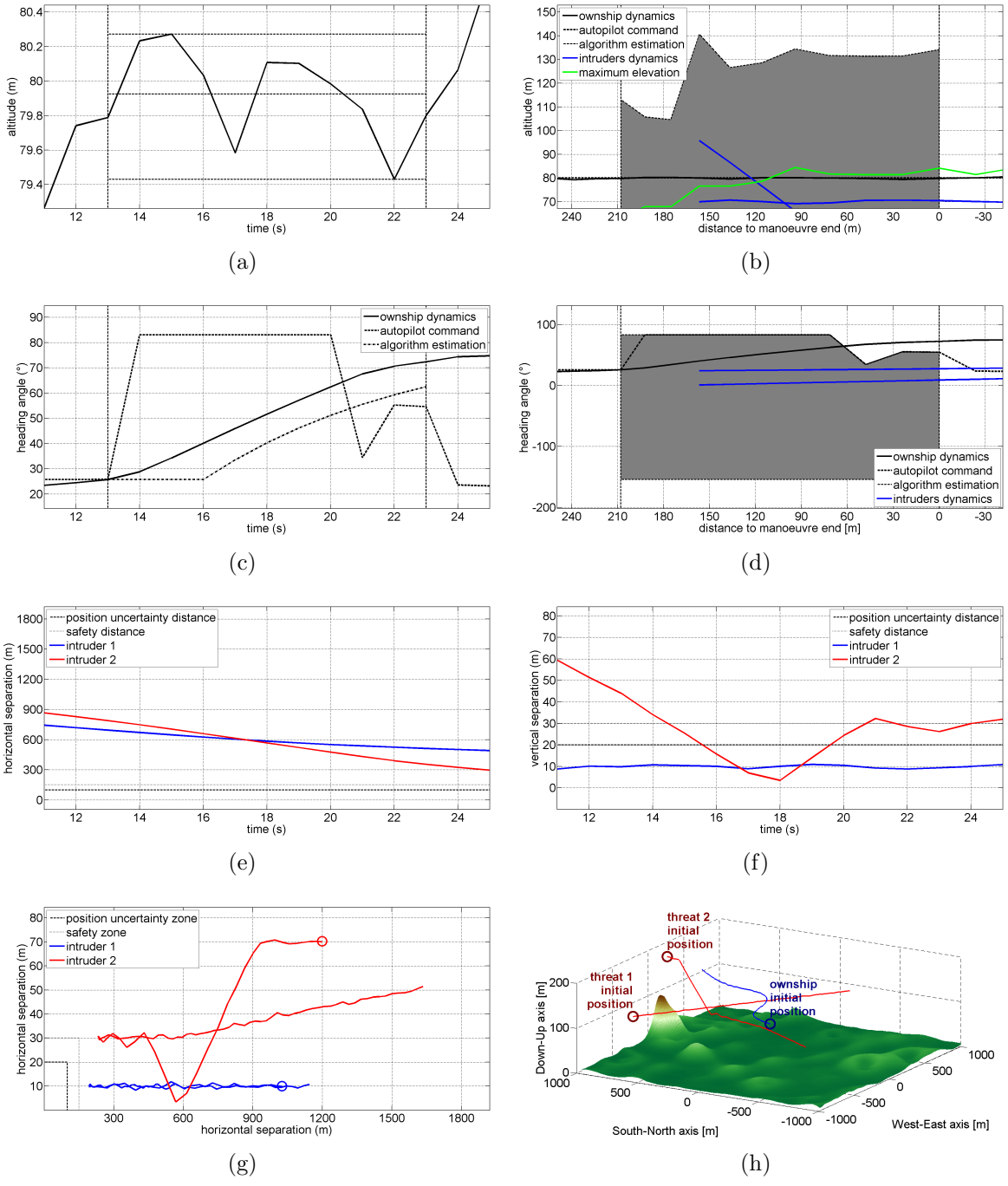

Figure 8.22: simulation graphs of the last-resort scenario in *P/F* mode simulation: (a) altitude dynamics profile, (b) altitude command profile and safe manoeuvres ranges, (e) horizontal separation between threats and ownship, (f) vertical separation between threats and ownship, (g) horizontal/vertical separation diagram between threats and ownship, (h) ownship and threats trajectories and local elevation map of the simulation

to operate their vehicles at an *ELOS* with manned aircraft. This implies that they have to be aware and use the same rules defined for flight safety in order to make the *UAV*'s behaviour predictable for manned aviation pilots and therefore interoperable with manned aircraft. Moreover the *UAV* operator is expected to share some of the qualifications requirements of manned aviation pilot.

For this reason, it was decided to use for these experiments a selection of pilots operating in Cranfield University airport. The selected pilots have different levels of flight experience. This characteristic was useful in order to obtain feedbacks derived from different levels of experience. The pilots interviewed were 11. In this sample, the following classes were identified:

novice pilot including 5 pilots with less than 500 hours of flight;
medium experience instructors including the 3 pilots with a maximum number of flight hours of 3000 hours;
expert pilots including 3 test pilots with a number of flight hours between 4500 and 17900 hours.

8.6 Simulation Tests Methodology

The tests were designed in order to collect the maximum amount of feedbacks from pilots and maximise their effectiveness. This analisys considered in particular the *PFD* concept described in section 7.6. It included the following six phases:

Phase 1: description to pilots of the *GCS* mock-up,
Phase 2: simulation of a free flight,
Phase 3: interview on the general layout of the *PFD*,
Phase 4: simulation with a test scenario,
Phase 5: interview on the effectiveness of the advisory scheme,
Phase 6: interview about the previous flight experience.

This procedure was repeated for every pilot. At first the pilot was briefed regarding the aim of the experiment. The *HMI* layout chosen for the *GCS* and the mock-up structure described in section 7.3 were moreover illustrated.

In the following simulation, the pilot was requested to perform a free flight in the *MAN* mode. The simulation started from a cruise condition (altitude 80 m, airspeed $12\,\mathrm{m\,s^{-1}}$, heading North). None conflict risks was simulated during this phase. This phase aimed to get the pilot used with aircraft dynamics and simulation environment. This simulated flight phase went on till pilot's request to stop it.

This simulation was followed by an interview in which the pilot was asked to communicate his/her first impressions about the proposed *PFD* layout. Then he was asked to give an evaluation about the following design solutions used on the *PFD*:

- heading indicator layout,

- altimeter layout,
- vertical speed indicator layout,
- airspeed indicator layout,
- angle of attack indicator layout,
- visualisation of the safety range in the indicators.

In the fourth phase the pilot was requested to perform a flight starting from the same cruise condition of the previous simulation. In this case, the pilot was instructed to fly the *UAV* in order to detect and follow a car, the black and yellow *Citroën 2CV (Deux Chevaux)* displayed in fig. 8.23, moving on the ground. During the same simulation, another *Piper J3 Cub 40 UAV* coming from North-East was moving on a collision route with the *UAV* flown by the operator. In this simulation phase the *A/R* switch defined in section 7.6 was set in OFF position. The pilot was not preliminary informed about the presence of another aircraft. This was done in order to avoid the reaction to be influenced from the preliminary knowledge about this conflict risk. The simulation was stopped in the middle of the conflict resolution in order to avoid the pilot forgetting his/her immediate feedback about the *S&A* system advisories during the most critical phase, *i. e.* the conflict detection and immediate resolution management.

Figure 8.23: *Citroën 2CV (Deux Chevaux)* model avilable in *FlightGear*

Similarly to the previous simulation test an interview followed this phase. In this case, the pilot was requested a general preliminary impression about the advisory scheme and an evaluation of the effectiveness of the following design solutions:

- *CDTI* polar grid and range indication,
- indication of flying threats trajectory on the *CDTI*,
- indication of the collision distance of the detected conflict risks on the *CDTI*,
- aural alerts sequence,
- resolution indication on the indicators,
- indication of the resolution manoeuvre on the *HUD*,

Finally the pilot was asked to summarise its previous flight experience in terms of flight hours and aircraft flown. This interview was done at the end of the test in order to avoid the influence of this information on test supervisor's judgement regarding pilot's feedback and on the evolution of discussion.

8.7 Simulation Tests Results

This section summarises the pilot feedbacks and try to identify some guidelines for future developments of the project. These concepts are classified according to the related *GCS* design factor.

General *PFD* Layout A novice suggested to differentiate the linear displays by graphical means (e.g. shape and color). He recommended moreover to increase the separation between these displays in order to avoid confusion.

Linear Gauge Instruments Instructors and expert pilots highlighted their lack of acquaintance with this concept applied to the airspeed and altitude indicators. For this reason, the expert pilots repeated the free flight simulation twice and continued it for a quite long time. A general conclusion was however that such a concept would require an adequate training, if the operator is a manned aviation pilot, in order to get him/her used to it.

Some instructors observed that, differently with conventional altitude indicators of manned aviation *PFDs*, such an indicator could require a bigger workload to manned aviation pilot. It requires the operator to search the current airspeed or altitude value in all indicator's extension. This is related with the fact that, as described in section 7.6.1 the box with the magnified altitude value is moving. On the other hand, one of the instructors stated that the airspeed indicator was quite effective in communicating to the operator the airspeed value changes cause of the limited range of variation. Differently this result was not obtained for the altitude indicator cause of the wider range.

The reaction of novices was quite uniform with a general appreciation for the idea of the sliding value on the range. They stated more precisely that it is effective in communicating to the operator its position on the range of allowed airspeeds or altitudes.

The angle of attack indicator received a general appreciation both regarding the idea to integrate it into the display, both regarding the layout used. It was in fact acknowledged as an useful tool to detect and signal the stall conditions. The only exception was a novice who considered it unuseful. Also the vertical speed indicator layout was appreciated, despite none detailed comment was collected on it.

Safety Ranges on Indicators The idea to depict the safety limitations of the flight envelope on the indicators with red and green bands was generally appreciated. Only a novice observed that he was disturbed by the constant presence of red color shapes on the display. On the other hand, an instructor suggested to add also an intermediate level yellow or orange strip on the instruments to warn the operator when approaching the unsafe values range. Moreover, an expert pilot suggested to display the increases in the minimum flight altitude. More precisely, it was suggested to display a yellow

strip extending from the previous minimum flight altitude to the new one, as soon as the aircraft approaches a different airspace zone.

Resolution Indication on the Indicators This indicator is another feature receiving positive comments by all the expert pilots and two of the novices. However, one of the expert pilots suggested to remove this visualisation from the altitude indicator. He asserted that it could cause wrong behaviours on the operator by making him/her indefinitely increase the climb or descent angle cause of the much slower altitude's dynamics. Another one recommended instead to avoid the visualisation of the resolution heading on the attitude indicator to avoid confusion. Regarding the graphical representation, one of the novices proposed to use an arrow instead of the blue line to get more noticeable indications. The only exception to these positive comments was the fact that one of the instructors did not appreciated the idea to display the resolution indication on the instruments: he judged it confusing.

CDTI A general appreciation was shown for the *CDTI* layout by the novices, despite with the following comments. One of them suggested to move the label displaying the size of the the *CDTI* range (2NM) outside the *CDTI*. This recommandation was done in order to avoid the superposition with the symbols displaying presence of other aircraft or ground obstacles. The grid displayed was not appreciated by two instructors and two novices that simply suggested to remove it from the *CDTI*. Another novice suggested to increase the step of the radial grid in order to declutter it, particularly when a big amount of traffic is displayed on the display. Regarding the visualisation of the intruder trajectory on the *CDTI*, the reactions were very different. All the expert pilots and four novices appreciated it, while one novice and two instructors found it unnecessary. Not a lot of feedbacks were collected on intruder collision distance's depiction. Positive appreciation were expressed by an expert pilot and an intruder. One of the instructors judged it unrelevant for safe operations and cause of unnecessary cluttering on display.

Indication of the resolution manoeuvre on the *HUD* All expert pilots and three novices appreciated the depiction of the suggested resolution manoeuvre on the *HUD*. One of them recommended the integration of information on the detected conflict risks and threats, a part the suggested avoidance manoeuvre, on the *HUD*. It was moreover suggested by the same pilot to include the angle of attack indicator on the *HUD*. Another comment requested the inclusion of the suggested new altitude on the displayed message. Also one of the instructors really appreciated the idea to display the resolution indication on the *HUD*. One of the instructors suggested to integrate the resolution indication as text message in the *PFD*, maybe on the attitude indicator.

Aural Alerts Sequence All the expert pilots, two instructors and three novices appreciated the idea of aural alerts. One of the expert pilots, one of the instructors and two of the novices suggested moreover to add a preliminary level of advisories issuing a message like "Traffic traffic" in the aural alerts sequence. Another suggestion was to make the indication of the resolution manoeuvre being preceded by a preliminary advisory of detected conflict risk.

8.8 Chapter Summary

This chapter illustrates a set of simulations aiming to show capabilities in critical conditions of the *S&A* algorithm described in chapter 6. Further simulations are then used to collect feedbacks from potential *UAS* operators about their impressions on *GCS* mock-up described in chapter 7. The simulations presented for the validation of the *S&A* algorithm show the performances in terms of *strategic conflict management*, *conflict resolution advisory*, *autonomous resolution*. More precisely, they deal with the algorithm's capability to monitor the conflict geometry evolution and accordingly update the resolution manoeuvre.

Firstly it is considered a set of simulations where a flying threat comes from different directions and tries to follow the ownship manoeuvres causing a conflict. In these simulations, the *UAS* is controlled in the *P/F* mode defined in section 7.6 with *A/R* switched on. This set of tests investigates the algorithm performance regarding *strategic conflict management* and *conflict resolution advisory*.

Then it is simulated a conflict geometry including two flying threats and a ground obstacle. These entities cause conflict risks detected by the *S&A* system in different simulation time steps. The *UAS* is controlled in the *P/F* mode defined in section 7.6 with *A/R* switched on. This simulation tests the algorithm's performances in terms of *strategic conflict management* and *conflict resolution advisory*.

Finally, section 8.4 presents a similar situation with two flying threats and a ground obstacle. In this case, it is supposed the *UAS* operating in the *MAN* mode defined in section 7.6 with *A/R* switched on. The *S&A* system starts resolution manoeuvre autonomously at the *minimum safe time before impact* while moving on straight levelled trajectory without reaction from *UAS* operator. It considers therefore the *strategic conflict management* and *autonomous resolution* performances for multiple threats scenarios.

The experiments on the *GCS* mock-up effectiveness were made with a selection of pilots with different levels of flight experience. This tests are based on the following procedure. At first the pilot is briefed regarding the aim of the experiment. The *HMI* layout chosen for the partial *GCS* mock-up are moreover illustrated. Then, the pilot is requested to perform a free flight in the *MAN* mode. This is followed by an interview in which the pilot communicates his/her first impressions about the proposed *PFD* layout. The pilot is finally instructed to fly the *UAV* in order to detect and follow a car moving on the ground. In the meanwhile, a conflict risk with another aircraft is

produced. The test is then concluded with the request to the pilot to give his general impression about the advisory scheme and an evaluation of the effectiveness of the *HMI* included in the partial *GCS* mock-up.

CHAPTER 9

Conclusions and Future Works

This chapter concludes the thesis with the conclusions and the future works suggested for the project. The project aims were the development of a *S&A* algorithm and the implementation of its *HMI* on *GCS*, designed to provide an effective system advisories communication to the operator. The solutions used for both *S&A* algorithm and *GCS* partial mock-up and the conclusions derived by preliminary tests are shortly recalled in section 9.1. The suggested future developments are then identified in section 9.2.

9.1 Conclusions

The *S&A* algorithm was designed for scenarios including multiple non-cooperative flying threats and ground obstacles. It is based on the hypothesis of a threat moving on a straight trajectory in order to get a fast evaluation of the advisories about the suggested resolution manoeuvre. The advisories are however updated with a very short time step (1 s) to constantly track the conflict geometry evolution. The resolution manoeuvres are step changes in heading or altitude autopilots commands, generating simple horizontal or vertical manoeuvre, respectively. They are evaluated in order to minimise the deviation from predefined trajectory. The value of these commands are optimised in order to maintain a minimum horizontal and vertical separation between ownship and every threat detected during the resolution manoeuvre. The separation is computed considering a prediction of the future ownship and threats trajectories. This estimation is based on a aircraft performances model based on fitting relationships. The algorithm chooses horizontal manoeuvres for the conflict resolution when the required heading variation is inferior to a predefined threshold, otherwise vertical manoeuvres are used to avoid the conflict. Resolution manoeuvres are autonomously executed by the system by switching on heading and altitude autopilots, when they are disabled, and applying the evaluated step command.

From the design point of view the *S&A* algorithm proposed was designed for multiple threats scenarios including both air and ground threats. The resulting solution is a system integrating both the *ACAS* and *TAWS* system for *UAVs* accordingly to the guidelines defined in section 4.5 and with the advantages defined in section 6.8 in respect with main solutions proposed in literature. The algorithm takes into account vehicle manoeuvring capabilities and right of way rules.

From the point of view of the performances, the simulations showed moreover that the typical times necessary for the *S&A* algorithm to update the advisories are largely

less than 1 s. More precisely, they are less than 0.05 and therefore smaller by almost two orders of magnitude compared to the prescribed update frequency of 1 Hz.This verifies that the algorithm allows to update conflict risks and resolution manoeuvres advisories at a constant rate of 1 Hz. This gives the possibility to take into account sudden trajectory changes of dynamic threats. The proposed algorithm is therefore potentially able to provide better results than more complex projection approaches cause of its lower computational resources.

The simulations of chapter 8 showed moreover that the algorithm produces reliable results for both manual (*MAN*) and autonomous (*P/F*) navigation modes. More precisely, as shown in section 8.2, the algorithm in *PF* mode exhibited good performances in non-cooperative collision scenarios, considering in particular the critical case of intruders mirroring the ownship manoeuvre. Section 8.3 showed the algorithm's capability to manage complex scenarios including multiple threats once more in *P/F*. According to the simulations described in section 8.4, the algorithm is able to generate safe last-resorts resolutions and integrating effectively the human operator involvement in the *MAN* mode. This implies that the proposed algorithm is particularly suitable both for *RPV* as a safety pilot support tool and also to be integrated with an autonomous navigation algorithm, such that described in this work.

Regarding the *GCS* mock-up, the proposed integration of the *S&A* algorithm is based on an innovative *PFD* layout integrated in the *GCS*. The choice of location on display and layout of instruments are inspired by the configuration used in manned aviation *PFD*. The *PFD* concept presented here is designed to provide in an effective way the information about flight parameters, navigation and *S&A* advisories in the new *PFD* concept proposed. Among the novelty introduced, it is noticeable the use of an original concept of digital displays for airspeed, altitude, vertical speed and angle of attack indicators. This concept is characterised by the presence of the parameter value moving on a linear range integrating red and green bands. These bands identify the allowed or forbidden zones of the flight envelope according to the current condition in terms of conflict risk detected, aerodynamics performances and structural limitations. Some other original solutions are the presence on the display of buttons allowing pilot to select the autopilot mode and the choice to integrate the controls for autopilots settings directly on the flight parameters indicators.

The *GCS* mock-up here proposed was tested by pilots. The tests aimed to get feedbacks mainly regarding the *PFD* concept, the *HUD* layer and the aural advisories scheme. Regarding the *PFD*, pilots showed a general acceptance for the layout despite some refinements were proposed to avoid confusion between the instruments. The linear gauges concept showed a better acceptance by novice pilots instead of expert ones when applied to airspeed and altitude indicators. However, a general positive judgement was shown for vertical speed indicator and angle of attack indicator. The idea of integrating safety ranges through green/red bands on the instruments was also generally appreciated. The same judgement was given to the resolution indication depiction on instruments, despite some refinements were proposed regarding its graphical form. Plenty of suggestions were given by pilots regarding *CDTI* decluttering. The visuali-

sation by textual messages of the resolution advisories on the *HUD* was appreciated. However, it was suggested to enhance the *S&A* system *HMI* layout on the *HUD* with *TA* replication. A similar comment was made on the aural alerts sequence with the suggestion to include a preliminary *TA* before the phase where the *RA* is issued.

9.2 Future Works

The presented *ANS* algorithm showed quite good results in the simulations illustrated. However, further works could be suggested to go on with its development. Regarding the *S&A* algorithm, the potential conflict geometries, the *UAV* dynamics and the effects of wind disturbances should be analysed in order to identify critical conditions regarding the definition of *SZ* dimensions and the values to be considered in order to get safe flight operations. Further validation of the algorithm should be done considering more complex conflict geometries including also converging and overtaking encounter geometries. It could moreover be interesting to test this *S&A* algorithm with non-cooperative sensors, as these are defined in section 3.8.1, such as radars and cameras.

Regarding the *GCS* mock-up, the pilots feedbacks, particularly on advisories syntax and sequences in aural alerts and messages displayed on *HUD*, should be taken into account to improve the current layout of the *GCS* mock-up. Moreover, it could be worthy to go on with pilots tests defining a set of further test scenario that are critical for the *GCS* layout design. In particular, it could be interesting to validate by simulations the autopilots interface described in section 7.6.3. Finally, the *ND* described in section 7.5 should be developed in order to include all the information and functions necessary to support the pilot in the tactical navigation task.

Regarding the complete *ANS*, the autonomous navigation capabilities of the developed system could then be enhanced by substituting the *PF* algorithm with a more refined optimal waypoint navigation system based on stochastic filtering techniques (e.g. Kalman filter). From the point of view of the complete system, it could be interesting to test the integration of other hazard layers, such as no-fly zones and weather hazards in the *S&A* algorithm and the *GCS PFD*.

Bibliography

[1] Valerie J. Gawron. Human factors issues in the development, evaluation, and operation of uninhabited aerial vehicles. In *AUVSI '98: Proceedings of the Association for Unmanned Vehicle Systems International*, pages 431–438, Huntsville, AL, 1998.

[2] Alan Hobbs. Limitations of the see-and-avoid principle. Technical report, Australian Transport Safety Bureau, PO Box 967, Civic Square ACT 2608, November 2004. Reprint.

[3] Andrew D. Zeitlin. Developing requirements for the unmanned aircraft sense & avoid function. In *AIAA Infotech@Aerospace Conference*, number 2009-1924, Seattle, WA, 2009.

[4] CAA Directorate of Airspace Policy. Cap-722: Unmanned aircraft system operation in UK airspace - guidance. Technical report, CAA, Norwich, UK, 2009.

[5] Ben Zimmer. The flight of 'drone' from bees to planes. *The Wall Street Journal*, 2013. URL http://online.wsj.com/news/articles/SB10001424127887324110404578625803736954968. Accessed 24th October 2013.

[6] Al Savvaris. Introduction to UAV operations & technology integration. In *UAV Operations & Technology Integration*, Cranfield University, UK, 2010. Short course.

[7] J. W. Ramsey. UAVs: Out of uniform. *Avionics Magazine*, 2004. URL http://www.aviationtoday.com/av/categories/bga/UAVs-Out-of-Uniform_779.html. Accessed 25th September 2010.

[8] NOAA website. Bridging the gap between earth and space: First-of-its-kind unmanned aerial vehicle demonstration, 2005. URL http://www.noaanews.noaa.gov/stories2005/s2421.htm. Accessed 25th September 2010.

[9] R. P. Petcoff. Global Hawk collects reconnaissance data during Haiti relief efforts. *The Official Web Site of the US Airforce*, 2010. URL http://www.af.mil/news/story.asp?id=123185754. Accessed 25th September 2010.

[10] Thomson Reuters Foundation. An Israeli Aerostar UAV loaned to the Chilean Air Force is prepared for a flight over the coastal region of Chile to survey earthquake damage in Conception. *AlertNet:Alerting humanitarians to emergencies*,

2008. URL http://www.alertnet.org/thenews/pictures/CHL104.htm. Accessed 25th September 2010).

[11] Monroe Conner. Altair Predator B image gallery. *Armstrong Flight Research Center web-site*, 2006. URL http://www.nasa.gov/centers/dryden/multimedia/imagegallery/Altair_PredatorB/index.html. Accessed 12th June 2013.

[12] Ullrich Neumann. KOLIBRI Geo Services website, 2008. URL http://www.geokolibri.com/index.php. Accessed 25th September 2010.

[13] G. Muscato. La robotica al servizio della vulcanologia (Robotics in the service of vulcanology). *Bollettino D'Ateneo - Università degli Studi di Catania*, 2008. URL http://www.bda.unict.it/Pagina/It/La_Rivista/0/2008/03/01/1615_.aspx.

[14] ICAO Secretariat. Progress report on Unmanned Aerial Vehicle (UAV) work. Technical report, ICAO, Kigali, Rwanda, 2007.

[15] Mark Okrent. Civil UAV activity within the framework of European Commission research. In *Proc. of AIAA 3rd Unmanned Unlimited Technical Conference, AIAA*, volume 6329, pages 1–12, 2004.

[16] EASA Rulemaking Directorate. Policy statement airworthiness certification of Unmanned Aircraft Systems (UAS). Technical Report E.Y013-01, EASA, 2009.

[17] WG-73: Unmanned aircraft systems. A concept for UAS airworthiness certification and operational approval - Volume 2: UAS operations. Technical report, EUROCAE, Malakoff, France, 2010.

[18] T. Hutchings, S. Jeffreys, and S.J. Farmer. Design and evaluation for situation awareness enhancement. In *Autonomous Systems, 2007 Institution of Engineering and Technology Conference on*, pages 1–8, 2007.

[19] Jason S. McCarley and Christopher D. Wickens. Human factors implications of UAVs in the national airspace. Technical Report AHFD-05-05/FAA-05-1, University of Illinois, Aviation Human Factors Division, Savoy, IL, 2005.

[20] Mica R. Endsley. Measurement of situation awareness in dynamic systems. *Human Factors: The Journal of the Human Factors and Ergonomics Society*, 37(1): 65–84, 1995. doi: 10.1518/001872095779049499. URL http://hfs.sagepub.com/content/37/1/65.abstract.

[21] Mica R. Endsley. Level of automation effects on performance, situation awareness and workload in a dynamic control task. *Ergonomics*, 42(3):462–492, 1999. doi: 10.1080/001401399185595. URL http://www.tandfonline.com/doi/abs/10.1080/001401399185595.

[22] C. J. Arback, N. Swarrz, and G. Kuperman. Evaluating the panoramic cockpit controls and displays system. In *Proceedings of the Fourth International Symposium on Aviation Psychology*, pages 30–36, Columbus, OH, 1987.

[23] J. Tadema and E. Theunissen. Feasibility of using synthetic vision technology for UAV operator support. In *Digital Avionics Systems Conference, 2003. DASC '03. The 22nd*, volume 2, pages 8.B.1 –81–13 vol.2, oct. 2003. doi: 10.1109/DASC.2003.1245895.

[24] Jill L. Drury, Laurel Riek, and Nathan Rackliffe. A decomposition of uav-related situation awareness. In *Proceedings of the 1st ACM SIGCHI/SIGART Conference on Human-robot Interaction*, HRI '06, pages 88–94, New York, NY, USA, 2006. ACM. ISBN 1-59593-294-1. doi: 10.1145/1121241.1121258. URL http://doi.acm.org/10.1145/1121241.1121258.

[25] T. Hutchings and S.J. Farmer. Human factors of sense and avoid systems. Unpublished.

[26] Russell Naughton. HARGRAVE, aviation and aeromodelling - Interdependent evolution and histories, 2003. URL http://www.ctie.monash.edu.au/hargrave/rpav_home.html. Accessed 28th November 2013.

[27] Jim Garamone. From U.S. civil war to afghanistan: A short history of UAVs. *U.S. Department of Defense website*, 2002. URL http://www.defense.gov/News/NewsArticle.aspx?ID=44164. Accessed 24th October 2013.

[28] P.W. Singer. Drones don't die - A history of military robotics. *Weider History Group - HISTORYnet.com website*, 2011. URL http://www.historynet.com/drones-dont-die-a-history-of-military-robotics.htm. Accessed 24th October 2013.

[29] Nesta. Drones: a history of flying robots. *Nesta website*, 2013. URL http://www.nesta.org.uk/events/hot_topics/assets/features/drones_a_history_of_flying_robots. Accessed 24th October 2013.

[30] J.W.R. Taylor and K. Munson. *Jane's pocket book of remotely piloted vehicles: robot aircraft today*. Collier Books, 1977. URL http://books.google.it/books?id=8o9TAAAAMAAJ.

[31] Lee Pearson. Developing the flying bomb. *Naval History & Heritage Command website*. URL http://www.history.navy.mil/download/ww1-10.pdf. Accessed 25th October 2013.

[32] The Worlds of David Darling. Kettering Bug. *Encyclopedia of Science*. URL http://www.daviddarling.info/encyclopedia/K/Kettering_Bug.html.

[33] J. VanDomelen. Target practice drones. *Mentor Graphics website*, 2012. URL http://blogs.mentor.com/jvandomelen/blog/tag/hewitt-sperry-automatic-airplane/. Accessed 27th November 2013.

[34] Wikipedia. History of unmanned aerial vehicles, 2010. URL http://en.wikipedia.org/wiki/History_of_unmanned_aerial_vehicles. Accessed 10th November 2013.

[35] Experimental Aircraft Association, Inc. EAA chapter 231 website, 2011. URL http://www.231.eaachapter.org/index.htm. Accessed 28th November 2013.

[36] Ingo Warnecke. Aircraft A8529 Photo - A8529, 1929 Curtiss N2C-2 Fledgling, C/N: 4. *Airport-Data.com website*, 2004. URL http://www.airport-data.com/aircraft/photo/000322867.html. accessed 27th November 2013.

[37] Kris Davies. Fairey Queen & robot seaplanes. *the Reborn Technology Blog*, 2008. URL http://reborn-technology.blogspot.it/2008/03/fairey-queen-robot-seaplanes.html. Accessed 28th November 2013.

[38] Mike Bajcar. Picture of the De Havilland DH-82B Queen Bee aircraft. *airliners.net website*, 2011. URL http://www.airliners.net/photo/De-Havilland-DH-82B/2219120/. Accessed 27th November 2013.

[39] Andreas Parsch. PQ-8/TDC. *Directory of U.S. Military Rockets and Missiles*, 2006. URL http://www.designation-systems.net/dusrm/app1/pq-8.html. Accessed 28th November 2013.

[40] L.S. Howeth. *History of Communications-Electronics in the United States Navy*, chapter 40. For sale by the Superintendent of Documents, U.S. Govt. Print. Off., 1963.

[41] Delmar S. Fahrney. The birth of guided missiles. In *United States Naval Institute Proceedings*, 1980.

[42] Scott Rose and the Warbirds Resource Group. Fieseler Fi 103 Reichenberg IV. *Luftwaffe Resource Center - A Warbirds Resource Center Group Site*, 2013. URL http://www.warbirdsresourcegroup.org/LRG/fi103.html. Accessed 29th November 2013.

[43] Wehrmacht History. V-2 rocket - Aggregat 4 (A-4) - Vergeltungswaffe 2 - surface-to-surface missile. *Wehrmacht History 1935 to 1945 - Technical Database*, 2013. URL http://www.wehrmacht-history.com/heer/missiles/v-2-rocket.htm. Accessed 29th November 2013.

[44] K. O. Eckland. Naval aircraft factory (naf). *Aerofiles*, 2008. URL http://www.aerofiles.com/_naf.html. Accessed 29th November 2013.

[45] Angela Mongelluzzo. Dollars for drones - Should the U.S. invest in drone technology?, 2012. URL https://sites.lafayette.edu/egrs451-sp12-uav/. Accessed 27th November 2013.

[46] Walter J. Boyne. The remote control bombers. *Air Force Magazine - Online Journal of the Air Force Association*, 93(11), 2010.

[47] Andreas Parsch. VB series. *Directory of U.S. Military Rockets and Missiles*, 2003. URL http://www.designation-systems.net/dusrm/app1/vb.html. Accessed 29th November 2013.

[48] UAV Universe website. 1930s & 1940s. URL https://sites.google.com/site/uavuni/1920s-1930s. Accessed 29th November 2013.

[49] Andreas Parsch. KD2C/KD3C. *Directory of U.S. Military Rockets and Missiles*, 2003. URL http://www.designation-systems.net/dusrm/app1/kd2c.html. Accessed 29th November 2013.

[50] Andreas Parsch. MQM-57. *Directory of U.S. Military Rockets and Missiles*, 2007. URL http://www.designation-systems.net/dusrm/m-57.html. Accessed 29th November 2013.

[51] Andreas Parsch. GAM-67. *Directory of U.S. Military Rockets and Missiles*, Accessed 29th November 2013. URL http://www.designation-systems.net/dusrm/app1/gam-67.html.

[52] Andreas Parsch. ADM-20. *Directory of U.S. Military Rockets and Missiles*, 2002. URL http://www.designation-systems.net/dusrm/m-20.html. Accessed 29th November 2013.

[53] Andreas Parsch. AQM-35. *Directory of U.S. Military Rockets and Missiles*, 2003. URL http://www.designation-systems.net/dusrm/m-35.html. Accessed 29th November 2013.

[54] Andreas Parsch. AQM/BQM/MQM/BGM-34. *Directory of U.S. Military Rockets and Missiles*, 2003. URL http://www.designation-systems.net/dusrm/m-34.html. Accessed 29th November 2013.

[55] Andreas Parsch. BQM-155. *Directory of U.S. Military Rockets and Missiles*, 2005. URL http://www.designation-systems.net/dusrm/m-155.html. Accessed 29th November 2013.

[56] Andreas Parsch. RQ-2. *Directory of U.S. Military Rockets and Missiles*, 2007. URL http://www.designation-systems.net/dusrm/app2/q-2.html. Accessed 29th November 2013.

[57] Andreas Parsch. D-21. *Directory of U.S. Military Rockets and Missiles*, 2004. URL http://www.designation-systems.net/dusrm/app4/d-21.html. Accessed 29th November 2013.

[58] Andreas Parsch. RQ-11. *Directory of U.S. Military Rockets and Missiles*, 2006. URL http://www.designation-systems.net/dusrm/app2/q-11.html. Accessed 29th November 2013.

[59] Andreas Parsch. RQ-4. *Directory of U.S. Military Rockets and Missiles*, 2008. URL http://www.designation-systems.net/dusrm/app2/q-4.html. Accessed 29th November 2013.

[60] Andreas Parsch. Wasp. *Directory of U.S. Military Rockets and Missiles*, 2007. URL http://www.designation-systems.net/dusrm/app4/wasp.html. Accessed 29th November 2013.

[61] Andreas Parsch. RQ/MQ-1. *Directory of U.S. Military Rockets and Missiles*, 2006. URL http://www.designation-systems.net/dusrm/app2/q-1.html. Accessed 29th November 2013.

[62] M.F.L. de Vries, G.J.M. Koeners, F.D. Roefs, H.T.A. van Ginkel, and E. Theunissen. Operator support for time-critical situations: Design and evaluation. In *25th Digital Avionics Systems Conference, 2006 IEEE/AIAA*, pages 1 –14, oct. 2006. doi: 10.1109/DASC.2006.313773.

[63] Jochum Tadema, Joris Koeners, and Erik Theunissen. Synthetic vision to augment sensor-based vision for remotely piloted vehicles. In *Defense and Security Symposium*, pages 62260D–62260D. International Society for Optics and Photonics, 2006.

[64] M. Quigley, M.A. Goodrich, and R.W. Beard. Semi-autonomous human-UAV interfaces for fixed-wing mini-UAVs. In *Intelligent Robots and Systems, 2004. (IROS 2004). Proceedings. 2004 IEEE/RSJ International Conference on*, volume 3, pages 2457 – 2462 vol.3, sept.-2 oct. 2004. doi: 10.1109/IROS.2004.1389777.

[65] W.A. Olson and M.G. Wuennenberg. Autonomy based human-vehicle interface standards for remotely operated aircraft. In *Digital Avionics Systems, 2001. DASC. 20th Conference*, volume 2, pages 7D3/1–7D3/9 vol.2, 2001. doi: 10.1109/DASC.2001.964199.

[66] Schutte Paul C. and Trujillo Anna C. Flight crew task management in non-normal situations. Technical report, NASA Langley Research Center, 1996. URL http://www.ncstrl.org:8900/ncstrl/servlet/search?formname=detail&id=oai%3ALTRS%3ANASA-96-40hfes-pcs.

[67] Terrence Fong and Charles Thorpe. Vehicle teleoperation interfaces. *Auton. Robots*, 11(1):9–18, July 2001. ISSN 0929-5593. doi: 10.1023/A:1011295826834. URL http://dx.doi.org/10.1023/A:1011295826834.

[68] Kevin J. Gruenwald. Defense.gov news photos. *U.S. Department of Defense website*, 2005. URL http://www.defense.gov/photos/newsphoto.aspx?newsphotoid=6487. Accessed 13th June 2013.

[69] I. Maza, F. Caballero, R. Molina, N. Peña, and A. Ollero. Multimodal interface technologies for uav ground control stations. *J. Intell. Robotics Syst.*, 57(1-4):

371–391, January 2010. ISSN 0921-0296. doi: 10.1007/s10846-009-9351-9. URL http://dx.doi.org/10.1007/s10846-009-9351-9.

[70] Smart Information Flow technologies (SIFT) website. Testbed for uav supervisory control (tusc). URL http://www.sift.net/projects/playbook/tusc. Accessed 13th June 2013.

[71] Asaf Degani, Everett A. Palmer, and Kristin G. Bauersfeld. soft controls for hard displays: Still a challenge. *Proceedings of the Human Factors and Ergonomics Society Annual Meeting*, 36(1):52–56, 1992. doi: 10.1177/154193129203600114. URL http://pro.sagepub.com/content/36/1/52.abstract.

[72] Mark Draper, Gloria Calhoun, Heath Ruff, David Williamson, and Timothy Barry. Manual versus speech input for unmanned aerial vehicle control station operations. *Proceedings of the Human Factors and Ergonomics Society Annual Meeting*, 47(1):109–113, 2003. doi: 10.1177/154193120304700123. URL http://pro.sagepub.com/content/47/1/109.abstract.

[73] T. Henley. Insertion of unmanned aircraft into unsegregated airspace. In *UAV Operations & Technology Integration*, Cranfield University, UK, 2010. Short course.

[74] Dennis M. Coulter. UAS integration into the national airspace system: Modeling the sense and avoid challenge. In *AIAA Infotech@Aerospace Conference*, number 2009-1926, Seattle, WA, 2009.

[75] B.M. Albaker and N.A. Rahim. A survey of collision avoidance approaches for unmanned aerial vehicles. In *Technical Postgraduates (TECHPOS), 2009 International Conference for*, pages 1 –7, dec. 2009. doi: 10.1109/TECHPOS.2009.5412074.

[76] E. Rantanen, C. D. Wickens, and X. Xu. Estimation of conflict risk using cockpit displays of traffic information. Technical report, University of Illinois, 2007.

[77] Xidong Xu, Christopher D. Wickens, and Esa Rantanen. Imperfect conflict alerting systems for the cockpit display of traffic information. Technical Report AHFD-04-8/NASA-04-2, University of Illinois, Aviation Human Factors Division, Savoy, IL, 2004.

[78] International Civil Aviation Organization ICAO. Rules of the air - Annex 2 to the conventionon international civil aviation. Technical report, ICAO, 1990.

[79] Recreational Aircraft Association of New Zealand. Law, 2011. URL http://www.raanz.org.nz/wiki/pmwiki.php?n=TM.Law. Accessed 31st July 2013.

[80] J. Tadema and E. Theunissen. Design of an integrated traffic, terrain and energy awareness display concept for uavs. In *AIAA Infotech@Aerospace 2009*, number AIAA 2009-5980, Chicago, Illinois, 2009.

[81] J. Tadema and E. Theunissen. A concept for UAV operator involvement in airborne conflict detection and resolution. In *Digital Avionics Systems Conference, 2008. DASC 2008. IEEE/AIAA 27th*, pages 4.C.1–1–4.C.1–12, 2008. doi: 10.1109/DASC.2008.4702829.

[82] E Theunissen and J Tadema. A simulation approach for evaluating operator-in-the-loop DSA concepts. In *Proceedings of the AIAA Modeling and Simulation Technologies Conference*, 2008.

[83] EUROCONTROL website. Airborne Collision Avoidance System (ACAS), 2008. URL http://www.eurocontrol.int/msa/public/standard_page/ACAS_Startpage.html. Accessed 5th October 2010.

[84] EUROCONTROL website. Mode S homepage, 2010. URL http://www.eurocontrol.int/msa/public/standard_page/nv_modes_homepage.html. Accessed 5th October 2010.

[85] A. A. Lambregts, J. Tadema, R.M. Rademaker, and E. Theunissen. Defining maximum safe maneuvering authority in 3D space required for autonomous integrated conflict resolution. In *Digital Avionics Systems Conference, 2009. DASC '09. IEEE/AIAA 28th*, pages 5.C.1–1–5.C.1–17, 2009. doi: 10.1109/DASC.2009.5347465.

[86] SKYbrary. Terrain awareness and warning system, 2010. URL http://www.skybrary.aero/index.php/Terrain_Awareness_and_Warning_System. Accessed 5th October 2010.

[87] *ACAS II Guide - Airborne Collision Avoidance System II (incorporating version 7.1)*. EUROCONTROL, January 2012.

[88] Wing David J, Adams Richard J, Duley Jacqueline A, Legan Brain M, Barmore Bryan E, and Moses Donald. Airborne use of traffic intent information in a distributed air-ground traffic management concept: Experiment design and preliminary results. Technical report, NASA Langley Technical Report Server, 2001.

[89] Richard Barhydt, Dr. Todd, M. Eischeid, Michael T. Palmer, and David J. Wing. Use of a prototype airborne separation assurance system for resolving near-term conflicts during autonomous aircraft operations, 2003.

[90] T.W. Rand and M.S. Eby. Algorithms for airborne conflict detection, prevention, and resolution. In *Digital Avionics Systems Conference, 2004. DASC 04. The 23rd*, volume 1, pages –31–17 Vol.1, 2004. doi: 10.1109/DASC.2004.1391290.

[91] Florent Martel, Richard R. Schultz, William H. Semke, Ziming Wang, and Mariusz Czarnomski. Unmanned aircraft systems sense and avoid avionics utilizing ADS-B transceiver. In *AIAA Infotech@Aerospace Conference*, number 2009-1923, Seattle, WA, 2009.

[92] Y.K. Kwang and Y.H. Kwang. Performance simulation of radar sensor based obstacle detection and collision avoidance for smart UAV. In *Digital Avionics Systems Conference, 2005. DASC 2005. The 24th*, volume 2, pages 10 pp. Vol. 2–, Oct 2005. doi: 10.1109/DASC.2005.1563413.

[93] S. Kemkemian, M. Nouvel-Fiani, P. Cornic, and P. Garrec. MIMO radar for sense and avoid for UAV. In *Phased Array Systems and Technology (ARRAY), 2010 IEEE International Symposium on*, pages 573–580, Oct 2010. doi: 10.1109/ARRAY.2010.5613309.

[94] Paul Freeman and Pete Moosbrugger. A low cost phased array solution for uav collision avoidance. In *PAIAA Infotech@Aerospace 2010*, number AIAA 2010-3439, Atlanta, Georgia, 2010.

[95] Syed Irtiza Ali Shah and Eric N. Johnson. 3D obstacle detection using a single camera. In *AIAA Guidance, Navigation, and Control Conference*, number AIAA 2009-5678, Chicago, IL, 2009.

[96] Brandon Call, Randy Beard, Clark Taylor, and Blake Barber. Obstacle avoidance for unmanned air vehicles using image feature tracking. In *AIAA Guidance, Navigation, and Control Conference and Exhibit*, number AIAA 2006-6541, Keystone, CO, 2006.

[97] Ryan Carnie, Rodney Walker, and Peter Corke. Image processing algorithms for UAV sense and avoid. In *Proceedings of the 2006 IEEE International Conference on Robotics and Automation*, pages 2848–2853, Orlando, FL, 2006.

[98] A. Dennis, J. Archibald, B. Edwards, and D.J. Lee. On-board vision-based sense-and-avoid for small UAVs. In *AIAA Guidance, Navigation and Control Conference and Exhibit*, number AIAA 2008-7322, Honolulu, HI, 2008.

[99] Yoko Watanabe, Anthony J. Calisey, and Eric N. Johnson. Vision-based obstacle avoidance for UAVs. In *AIAA Guidance, Navigation and Control Conference and Exhibit*, number AIAA 2007-6829, Hilton Head, SC, 2007.

[100] Giancarmine Fasano, Lidia Forlenza, Domenico Accardo, and Antonio Moccia. Integrated obstacle detection system based on radar and optical sensors. In *AIAA Infotech@Aerospace 2010*, number AIAA 2010-3421, Atlanta, GA, 2010.

[101] Hyo-Sang Shin, Antonios Tsourdos, Brian A. White, Madhavan Shanmugavel, and Min-Jea Tahk. UAV conflict detection and resolution for static and dynamic obstacles. In *AIAA Guidance, Navigation and Control Conference and Exhibit*, number 2008-6521, Honolulu, HI, 2008.

[102] Anurag Gangul and Sharath Avadhanam. On the limits of collision detection performance of a sense-and-avoid system for non-cooperative air traffic. In *AIAA Infotech@Aerospace 2010*, number 2010-3339, Atlanta, GA, 2010.

[103] Mykel J. Kochenderfer, J. Daniel Griffith, and James K. Kuchar. Hazard alerting using line-of-sight rate. In *AIAA Guidance, Navigation and Control Conference and Exhibit*, number 2008-6630, Honolulu, HI, 2008.

[104] Mykel J. Kochenderfer, Leo P. Espindle, James K. Kuchar, and J. Daniel Griffith. A bayesian approach to aircraft encounter modeling. In *AIAA Guidance, Navigation and Control Conference and Exhibit*, number 2008-6629, Honolulu, HI, 2008.

[105] James P. Chryssanthacopoulos, Mykel J. Kochenderfer, and Richard E. Williams. Improved Monte Carlo sampling for conflict probability estimation. In *51st AIAA/ASME/ASCE/AHS/ASC Structures, Structural Dynamics, and Materials Conference*, number 2010-3012, Orlando, FL, 2010.

[106] J. Tadema, E. Theunissen, and K. M. Kirk. Self separation support for UAS. In *AIAA Infotech@Aerospace 2010*, number AIAA 2010-3460, Atlanta, GA, 2010.

[107] Donald E. Swihart, Bertil Brännström, Edward Griffin, Ragnar Rosengren, and Paul Doane. Autonomous collision avoidance system for air-to-air operations. In *AIAA/ICAS International Air and Space Symposium and Exposition: The Next 100 Years*, number 2003-2755, Dayton, OH, 2003.

[108] D. Sislak, P. Volf, A. Komenda, J. Samek, and M. Pechoucek. Agent-based multi-layer collision avoidance to unmanned aerial vehicles. In *Integration of Knowledge Intensive Multi-Agent Systems, 2007. KIMAS 2007. International Conference on*, pages 365 –370, 30 2007-may 3 2007.

[109] P. Volf, D. Sislak, M. Pechoucek, and M. Prokopova. Convergence of peer-to-peer collision avoidance among unmanned aerial vehicles. In *Intelligent Agent Technology, 2007. IAT '07. IEEE/WIC/ACM International Conference on*, pages 377 –383, nov. 2007.

[110] J. Samek, D. Sislak, P. Volf, and M. Pechoucek. Multi-party collision avoidance among unmanned aerial vehicles. In *Intelligent Agent Technology, 2007. IAT '07. IEEE/WIC/ACM International Conference on*, pages 403 –406, nov. 2007.

[111] S.A.N. Magill and P.A. Platt. A fast-time simulation study of shared aircraft intent information. In *Digital Avionics Systems Conference, 2002. Proceedings. The 21st*, volume 1, pages 2A4–1 – 2A4–10 vol.1, 2002. doi: 10.1109/DASC.2002.1067911.

[112] Surya U. Shandy and John Valasek. Intelligent agent for aircraft collision avoidance. In *AIAA Guidance, Navigation, and Control Conference and Exhibit*, number 2001-4055, Montreal, Canada, 2001.

[113] Stephane Mondoloni, Sheila Conway, and Ph. D. An airborne conflict resolution approach using a genetic algorithm, 2001.

[114] M.S. Eby and III Kelly, W.E. Free flight separation assurance using distributed algorithms. In *Aerospace Conference, 1999. Proceedings. 1999 IEEE*, volume 2, pages 429 –441 vol.2, 1999. doi: 10.1109/AERO.1999.793186.

[115] W Kelly and M Eby. Advances in force field conflict resolution algorithms. In *AIAA guidance, navigation, and control conference and exhibit*, 2000.

[116] Gilles. Dowek, Cesar. Muõz, Alfons. Geser, Institute for Computer Applications in Science, and Engineering. *Tactical conflict detection and resolution in a 3-D airspace [microform] / Gilles Dowek, Cesar Muñoz and Alfons Geser ; [prepared ... under contract NAS1-97046].* ICASE, National Aeronautics and Space Administration, Langley Research Center ; Available from NASA Center for Aerospace Information, Hampton, VA : Hanover, MD :, 2001.

[117] Rob C.J. Ruigrok and Jacco M. Hoekstra. Human factors evaluations of free flight: Issues solved and issues remaining. *Applied Ergonomics*, 38(4): 437 – 455, 2007. ISSN 0003-6870. doi: http://dx.doi.org/10.1016/j.apergo.2007.01.006. URL http://www.sciencedirect.com/science/article/pii/S000368700700018X. ¡ce:title¿Flightdeck of the Future¡/ce:title¿.

[118] A.A. Kandil, A. Wagner, A. Gotta, and E. Badreddin. Collision avoidance in a recursive nested behaviour control structure for unmanned aerial vehicles. In *Systems Man and Cybernetics (SMC), 2010 IEEE International Conference on*, pages 4276 –4281, oct. 2010. doi: 10.1109/ICSMC.2010.5642396.

[119] C. Tomlin, G.J. Pappas, and S. Sastry. Conflict resolution for air traffic management: a study in multiagent hybrid systems. *Automatic Control, IEEE Transactions on*, 43(4):509 –521, apr 1998. ISSN 0018-9286. doi: 10.1109/9.664154.

[120] A.A.H.E. Goossens. Development and evaluation of level 3 situation awareness support functions for a UAV operator station. In *Digital Avionics Systems Conference, 2004. DASC 04. The 23rd*, volume 2, pages 12.D.4 – 12.1–8 Vol.2, oct. 2004. doi: 10.1109/DASC.2004.1390839.

[121] UAV Task-Force. UAV task-force final report. Technical report, JAA/EUROCONTROL, 2004.

[122] Jason S McCarley and Christopher D Wickens. Human factors concerns in UAV flight. *University of Illinois at Urbana-Champaign Institute of Aviation, Aviation Human Factors Division*, 2004.

[123] S.R. Dixon. *Imperfect Automation in Unmanned Aerial Vehicle Flight Control.* University of Illinois at Urbana-Champaign, 2003. URL http://books.google.co.uk/books?id=JMPsNwAACAAJ.

[124] Aeronautics website. GCS C4I system, 2007. URL http://www.aeronautics-sys.com/?CategoryID=256&ArticleID=176. Accessed 11th December 2013.

[125] Flight Standards Service. *Advanced Avionics Handbook*, chapter 2. Federal Aviation Administration, 2009. URL http://www.faa.gov/regulations_policies/handbooks_manuals/aviation/advanced_avionics_handbook/media/aah_ch02.pdf. Accessed 24th January 2014.

[126] M.C. Dorneich, P.M. Ververs, and M.D. Good. Design and evaluation of an integrated avionics alerting system. In *Digital Avionics Systems, 2001. DASC. 20th Conference*, volume 1, pages 5D1/1 –5D1/12 vol.1, oct 2001.

[127] CD Wickens, J Goh, J Helleberg, and DA Talleur. Modality differences in advanced cockpit displays: Comparing auditory vision and redundancy for navigational communications and traffic awareness. Technical Report ARL-02-8/NASA-02-6, Savoy, IL: University of Illinois, Aviation Research Laboratory, 2002.

[128] Maia B. Cook and Harvey S. Smallman. When plans change: Task analysis with Navy UAV operators, display requirements, and UAV re-routing taxonomy. Technical report, Pacific Science & Engineering Group, Inc., San Diego, CA, 2008.

[129] E. Theunissen. Spatial terrain displays: promises and potential pitfalls. In *Digital Avionics Systems Conference, 1998. Proceedings., 17th DASC. The AIAA/IEEE/SAE*, volume 1, pages E46/1–E46/8 vol.1, 1998. doi: 10.1109/DASC.1998.741583.

[130] Amy L. Alexander and Christopher D. Wickens. 3D navigation and integrated hazard display in advanced avionics: Performance, situation awareness, and workload. Technical Report AHFD-05-10/NASA-05-2, University of Illinois, Aviation Human Factors Division, Savoy, IL, 2005.

[131] Christopher D. Wickens, John Helleberg, Paul Kroft, Donald A. Talleur, and Xidong Xu. Mid air target detection: What makes it difficult? application of attention and situation awareness model, 2001.

[132] Christopher D. Wickens, John Hellenberg, and Xidong Xu. Pilot maneuver choice and workload in free flight. *Human Factors: The Journal of the Human Factors and Ergonomics Society*, 44(2):171–188, 2002. doi: 10.1518/0018720024497943. URL http://hfs.sagepub.com/content/44/2/171.abstract.

[133] J. Tadema and E. Theunissen. Design and evaluation of a GUI for operator involvement in airborne conflict detection and resolution. In *Digital Avionics Systems Conference, 2008. DASC 2008. IEEE/AIAA 27th*, pages 5.A.2–1–5.A.2–12, 2008. doi: 10.1109/DASC.2008.4702842.

[134] H. Von Viebahn. The 4D-display. In *Digital Avionics Systems Conference, 1998. Proceedings., 17th DASC. The AIAA/IEEE/SAE*, volume 1, pages E54/1–E54/7 vol.1, 1998. doi: 10.1109/DASC.1998.741592.

[135] Mohammad Takallu Lockheed, Louis J. Glaab, and Mohammad A. Takallu. Preliminary effect of synthetic vision systems displays to reduce low-visibility loss of control and controlled flight into terrain accidents. Technical report, NASA Langley Research Center, 2002.

[136] Christopher D. Wickens, I. Haskell, and K. Harte. Perspective flight path displays: Application of ergonomically driven display design principles. In *Systems, Man, and Cybernetics, 1988. Proceedings of the 1988 IEEE International Conference on*, volume 1, pages 506–509, 1988. doi: 10.1109/ICSMC.1988.754349.

[137] W.J. Kubbat, P.M. Lenhart, and H. Von Viebahn. 4D flight guidance displays, a gate to gate solution. In *Digital Avionics Systems Conference, 1998. Proceedings., 17th DASC. The AIAA/IEEE/SAE*, volume 1, pages E55/1–E55/8 vol.1, 1998. doi: 10.1109/DASC.1998.741594.

[138] E. Theunissen, R.M. Rademaker, and T.J. Etherington. Synthetic vision: a prototype display concept for commercial aircraft. *Aerospace and Electronic Systems Magazine, IEEE*, 17(10):13–18, 2002. ISSN 0885-8985. doi: 10.1109/MAES.2002.1044511.

[139] J Raymond Comstock, Lou J Glaab, Lance J Prinzel, and Dawn M Elliot. Can effective synthetic vision system displays be implemented on limited size display spaces. In *Proceedings of the Eleventh International Symposium on Aviation Psychology*. Citeseer, 2001.

[140] Lisa C Thomas and Christopher D Wickens. Eye-tracking and individual differences in off-normal event detection when flying with a synthetic vision system display. In *Proceedings of the Human Factors and Ergonomics Society Annual Meeting*, volume 48, pages 223–227. SAGE Publications, 2004.

[141] Amy L. Alexander and Christopher D. Wickens. Does workload modulate the difference between cockpit traffic display formats? *Proceedings of the Human Factors and Ergonomics Society Annual Meeting*, 46(1):1–5, 2002. doi: 10.1177/154193120204600101. URL http://pro.sagepub.com/content/46/1/1.abstract.

[142] Amy L Alexander and Christopher D Wickens. Cockpit display of traffic information: The effects of traffic load, dimensionality, and vertical profile orientation. In *Proceedings of the Human Factors and Ergonomics Society Annual Meeting*, volume 45, pages 105–109. SAGE Publications, 2001.

[143] SKYbrary. Head-up display. URL http://www.skybrary.aero/index.php/Head_Up_Display. Accessed 28th August 2013.

[144] Aviation Glossary. Hud head up display system. URL http://aviationglossary.com/hud-head-up-display-system/. Accessed 28th August 2013.

[145] Stephen J.H. Vronneau, Roger Ayotte, Jim McMenemy, and Mauro Gomez Peralta. Prevention of controlled flight into terrain in general aviation operations. Technical report, Federal Aviation Administration, 2004. URL http://www.atlasaviation.com/AviationLibrary/CFIT/prevention_of_controlled_flight_into_terrain.htm. Accessed 28th August 2013.

[146] Flight Safety Foundation. Head-up guidance system technology - a powerful tool for accident prevention. *Flight Safety Digest*, 1991. URL http://flightsafety.org/fsd/fsd_sep91.pdf. Accessed 28th August 2013.

[147] Steven Fadden, Patricia May Ververs, and Christopher D. Wickens. Pathway HUDs: Are they viable? *Human Factors: The Journal of the Human Factors and Ergonomics Society*, 43(2):173–193, 2001. doi: 10.1518/001872001775900841. URL http://hfs.sagepub.com/content/43/2/173.abstract.

[148] Strike Fighter Consulting Voice of the Warfighter. Taking a look at the heads-up display. 2011. URL http://strikefighterconsultinginc.com/blog/taking-a-look-at-the-heads-up-display/. Accessed 28th April 2013.

[149] Christopher D. Wickens, S. Fadden, D. Merwin, and P.M. Ververs. Cognitive factors in aviation display design. In *Digital Avionics Systems Conference, 1998. Proceedings., 17th DASC. The AIAA/IEEE/SAE*, volume 1, pages E32/1–E32/8 vol.1, 1998. doi: 10.1109/DASC.1998.741568.

[150] Gloria L. Calhoun, Mark H. Draper, Michael F. Abernathy, Michael Patzek, and Francisco Delgado. Synthetic vision system for improving unmanned aerial vehicle operator situation awareness. *Enhanced and Synthetic Vision 2005*, pages 219–230, 2005. doi: 10.1117/12.603421. URL +http://dx.doi.org/10.1117/12.603421.

[151] Mladjan Jovanovic, Dusan Starcevic, and Zeljko Obrenovic. Designing aircraft cockpit displays: Borrowing from multimodal user interfaces. In Marina L. Gavrilova and C. J. Tan, editors, *Transactions on Computational Science III*, pages 55–65. Springer-Verlag, Berlin, Heidelberg, 2009. ISBN 978-3-642-00211-3. doi: 10.1007/978-3-642-00212-0_3. URL http://dx.doi.org/10.1007/978-3-642-00212-0_3.

[152] Christopher D. Wickens, Stephen Dixon, and Bobbie Seppelt. In vehicle displays and control task interference: The effects of display location and modality. Technical Report AHFD-02-7/NASA-02-5/GM-02-1, University of Illinois, Aviation Human Factors Division, Savoy, IL, 2002.

[153] W.D. Byblow. Effects of redundancy in the comparison of speech and pictorial displays in the cockpit environment. *Applied Ergonomics*, 21(2):121 – 128, 1990. ISSN 0003-6870. doi: 10.1016/0003-6870(90)90134-J. URL http://www.sciencedirect.com/science/article/pii/000368709090134J.

[154] S. Moghimi. Navigation and control systems design for piper uav - towards implementation. Technical report, Cranfield University, Bedfordshire, UK, 2010.

[155] Flightgear flight simulator, 2010. URL http://www.flightgear.org/. Accessed 19th August 2013.

[156] Earth Remote Sensing Data Analysis Center. Aster global digital elevation model, 2009. URL http://www.gdem.aster.ersdac.or.jp/index.jsp. Accessed 29th October 2010.

[157] Marco Melega, Samuel Lazarus, Mudassir Lone, and Al Savvaris. Autonomous sense & avoid capabilities based on aircraft performances estimation. *Proceedings of the Institution of Mechanical Engineers, Part G: Journal of Aerospace Engineering*, 2013. doi: 10.1177/0954410012472603.

[158] Ordnance survey. URL http://www.ordnancesurvey.co.uk/about/. Accessed 13th August 2013.

[159] NASA Ames Research Center Color Usage Research Lab website. Using color in information display graphics. URL http://colorusage.arc.nasa.gov/index.php. Accessed 19th August 2013.

[160] Falcon gauge website, 2008. URL http://www.falcongauge.com/. Accessed 14th August 2013.

[161] Belite aircraft website. URL http://www.beliteaircraft.com/. Accessed 5th May 2014.

[162] Chris Brady. Flight instruments. 1999. URL http://www.b737.org.uk/flightinsts.htm. Accessed 21th August 2013.

[163] M. Melega, S. Lazarus, A. Savvaris, and A. Tsourdos. Multiple threats sense and avoid algorithm for static and dynamic obstacles. *paper under submission*, 2014.

Index